THE UNIVERSITY OF GENOVA

SCUOLA POLITECNICA

DIME

Department of Mechanical, Energy, Management and Transportation Engineering

Doctoral Thesis in Mechanical, Energy and Management Engineering (IMEG-Curricula Technical Physics, Applied Thermodynamics, Heat Transfer and Acoustics) A. Y. 2022-23

Modeling and analyses of thermal response tests in real and reduced-scale experiments for geothermal applications involving deep boreholes

Supervisor:

Prof. Ing. Marco Fossa, DIME

Ph.D. Student:

Ing. Stefano Morchio, DIME

March 2023

Modeling and analyses of thermal response tests in real and reduced-scale experiments for geothermal applications involving deep boreholes

Abstract

This Ph.D. dissertation is aimed at developing models and defining innovative experimental strategies for performing and analyzing Thermal Response Tests (TRTs) for Ground Coupled Heat Pump (GCHP) applications. Three finite difference numerical models related to coaxial, single and double U Borehole Heat Exchangers (BHEs) have been developed starting from literature contributions and coupled with the Fast Fourier Transform (FFT) spectral method. The models have been implemented in three in-house Fortran90 codes that have been optimized to cope with variable longitudinal and radial mesh distribution for simulating the BHE configurations at given geothermal gradients, resembling both standard conditions and geothermal anomalies. The models have been extensively validated through the comparison of the numerical results with experimental measurements. Different ground properties and geothermal gradients along the ground depth can be handled by the models and set as initial and boundary conditions of the problem. The FFT method has been implemented in a dedicated Fortran90 code to exploit the advantage of handling different boundary conditions in terms of the heat transfer rate injected or extracted in a TRT without the need to perform the numerical simulation from scratch. The spectral analysis related to the FFT method has been also useful to highlight the importance of the numerical (that is also real) effect related to the geothermal gradient on simulated and real TRTs. The present Ph.D. study is aimed at the analysis of the BHE behavior in the early period, say for Fourier numbers typical of TRT measurements. The numerical results are addressed to the comprehension of the applicability of standard TRT analysis methods (essentially based on the Infinite Line Source model, ILS) when applied to shallow and deep BHEs (DBHEs) that may involve thermal conditions of "crossing temperatures" between ground and heat carrier fluid. The study has been carried out for single and multiple ground layers of equal thickness with different thermal conductivities along the depth. The heat transfer rate per unit length perfectly uniform with depth is the main hypothesis on which the ILS model is essentially based. On the other hand, the

unavoidable variation of the distribution of the heat transfer rate per unit length along the borehole depth violates the assumption of uniform temperature at the borehole wall at each time. The developed models described in the present Ph.D. thesis take into account this aspect providing simulations closer to reality. Therefore these models and related simulation results can serve as useful numerical references for other models and approaches. The present Ph.D. study demonstrates also that the thermal conditions of "crossing temperatures" between ground and heat carrier fluid in BHE (especially for DBHE) are related to the “natural” heat rate made available by the geothermal gradient that in some cases can override the external heat input rate injected (or extracted) by the TRT machine. This affects the ground thermal conductivity estimations based on standard TRT methods. This effect is incorporated into the q_{ratio} parameter introduced by the present Ph.D. study and a specific dimensionless g-transfer function called g_0. Both q_{ratio} and the g_0 function incorporate the geothermal gradient. The q_{ratio} is expected to be relevant to future TRT guidelines at national and international levels. Error analyses on the BHE and ground properties estimations from the ILS model are reported in the present thesis.

Besides the numerical work, the present Ph.D. thesis is aimed to present the experimental setup related to a suitable reduced-scale prototype of the real BHE and the surrounding ground for innovative TRT experiments. The scaled ground volume is realized with a slate block. The scaled heat exchanger, inserted into the slate block, is equipped with a central electrical heater along its entire depth and with temperature sensors at different radial distances and depths for the Electric Depth Distributed Thermal Response Test, EDDTRT. The measurements collected during the Ph.D. work highlight the possibility of performing reliable TRT experiments and estimating the grout/ground thermal conductivity by exploiting a central electric heater and cheap digital one-wire sensors distributed along the depth instead of the expensive optical fibers. It has to be specified that for the reduced scale experiment the digital one-wire sensors have been necessarily replaced by thermocouples. Measurement error analyses are reported in the thesis. The all-in-one BHE equipped with the central electrical heater and with temperature sensors for the EDDTRT assures continuous BHE performance monitoring, test for correct grouting, and test for aquifer presence.

A Geothermal Heat Pump Portal and Online Designer for Ground Heat Exchanger Fields has been realized during the Ph.D. study (see https://en.geosensingdesign.org/). The present website offers the first worldwide ever (and completely Free) web calculation tool for the design of BHE fields based on a modified version of the Ashrae Method, also employed in the corresponding UNI Italian standard.

Keywords: borehole heat exchanger, modeling, spectral method, ground thermal conductivity, thermal response test, geothermal gradient, scale prototype, BHE fields sizing

Acknowledgments

This work wouldn't have been possible without the support I received from numerous people along this journey.

Firstly, I would like to deeply acknowledge Prof. Marco Fossa and their collaborators and colleagues (Prof. Antonella Priarone, Prof. Giovanni Tanda, Prof. Francesco Devia …) for allowing me to conduct my Ph.D. study within his research group at the Dime Department of Mechanical, Energy, Management and Transportation Engineering, at The University of Genova.

Thanks also to Prof. Marco Fossa for being the main supervisor of my work and supporting me with his guidance during all of this work. Thanks for allowing me to engage in interesting projects and collaborations with other research groups.

I am deeply grateful also to José Acuña, Richard A. Beier and Philippe Pasquier. This achievement is also yours!

Thanks to Prof. Richard A. Beier for being the research advisor of my Ph.D. study, sharing with me his knowledge about ground heat exchangers and his valuable discussions.

I would also like to express my deep gratitude to Prof. Philippe Pasquier. Thank you for hosting me as a visiting researcher at Polytechnique Montréal. Thanks for allowing me to work with you and your research group.

I would like to deeply acknowledge José Acuña for allowing me to conduct my first international experience before the start of my Ph.D. study within his research group at the Division of Applied Thermodynamics in the Energy Department at KTH.

Thanks also to Prof. Louis Lamarche, Prof. Michel Bernier, and Prof. Hanane Dagdougui I met at ETS and Polytechnique Montréal respectively. Thank you for the interesting discussions, presentations, lectures and research ideas sharing.

I deeply thank my family, colleagues and friends.

Contents

NOMENCLATURE

A	ratio related to the finite difference discretization [-]/ Area [m^2]
A_{D1}	ratio of areas in coaxial borehole [-]
$A_{D1,U}$	ratio of areas in U-pipe borehole [-]
A_{D2}	ratio of areas in coaxial borehole [-]
B	ratio related to the finite difference discretization [-] / borehole separating distance [m]
b	constant [K]
C	grout thermal capacitance assigned to each grout node [J/(mK)]
C_r	ratio of volumetric heat capacities of fluid to ground [-]
c	specific heat [J/kg K]
COP	coefficient of performance [-]
Co	Courant number, $Co = \frac{w\Delta\tau}{\Delta z}$ [-]
d	diameter [m]
$deltaprecision$	Temperature difference related to the spacing between two radial coordinates according to the ILS solution [K]
E_1	exponential integral in ILS model [-]
$\varepsilon_{i\%}$	relative percentage error [-]
FD	Finite Difference
Fo	Fourier number, $Fo = \frac{\alpha\tau}{x^2}$ [-]
FFT	Fast Fourier Transform
f	external excitation function [°C]
G	temperature transfer function [-]
g	dimensionless (multi BHE) temperature transfer function [-]
H	active depth of the BHE [m]
H_{gr}	depth of the ground volume in calculation domain [m]
h	convective heat transfer coefficient [$W/m^2 \cdot K$]
k	thermal conductivity [W/(m·K)]
L	overall length of borehole heat exchangers [m]
m	slope [K/cycles]
$\dot{m}$	mass flow rate [kg/s]
n_t	number of elements of the solution related to the temporal discretization
N_1	net transfer unit corresponding to short-circuit heat transfer (coaxial) [-]
N_2	net transfer unit corresponding to heat transfer between fluid and ground (coaxial) [-]
N_g	net transfer unit corresponding to heat transfer between fluid and ground (U-pipe) [-]

N_{12}	net transfer unit corresponding to short-circuit heat transfer (U-pipe) [-]
N_{gr}	dimensionless conductance of ground [-]
Nu	Nusselt number, $Nu = \frac{hx}{k}$ [-]
$\dot{Q}$	heat transfer rate [W]
$\dot{Q}'$	heat transfer rate per unit length [W/m]
q_{ratio}	ratio of external heat input rate per unit length to an idealized (natural) heat rate, equation (91) [-]
R	thermal resistance [m·K/W]
Re	Reynolds number, $Re = \frac{\rho w x}{\mu}$ [-]
r	radial coordinate [m]
s	shank spacing [m]
S	temperature profiles from numerical solution (or experimental measurements) [°C]
T	temperature [K]
T_p	temperature penalty [°C]
T_{p1}	auxiliary excess temperature in Ashrae method [°C]
V	Volume [m^3]
w	velocity [m/s]
X	grout thermal capacitance weighting factor [-]
Y	grout thermal resistance weighting factor [-]
z	vertical coordinate [m]

Greek letters

α	thermal diffusivity, $\alpha=k/(\rho c)$ [m^2/s]
β	dimensionalization constant of the spectral method [°C]
γ	Euler constant, γ=0.5772 [-]
ρ	density [kg/m^3]
Δ	finite increment in a variable [-]
φ	opening angle denoting an infinitesimal arc in axisymmetric cylindrical geometry
π	pi constant [-]
σ	standard deviation (%)
τ	time [s]
θ_D	dimensionless temperature difference [-]
θ_8	excess temperature, equation (127) [°C]

Subscripts

a	annular pipe
A	Ashrae Method
ave	average
b	borehole
bhe	borehole heat exchanger
c	center pipe
D	dimensionless
eq	equivalent

ESU	equivalent single U
ext	external
f	heat carrier fluid
fb	fluid-borehole
fg	fluid-grout
f1	heat carrier fluid in the annular pipe/ in the inlet pipe (U-pipe case)
f2	heat carrier fluid in the center pipe/ in the outlet pipe (U-pipe case)
gb	grout-borehole
geo	geothermal
gg	grout-grout
gr	of the ground medium, of the ground domain
gt	of the grout medium, of the grout domain
h	hydraulic / six hour period
H	based on depth H
i	index, spatial discretization (radial)
in	inner dimension/inlet
innovative	*TRT* related to the measurement method
j	index, spatial discretization (vertical)
m	membrane (outer pipe) / one month period
max	maximum
meter	related to the measurement method
n	index, temporal discretization
N	ten years + one month + six hours
out	outlet dimension/outlet
p	pipe
pg	pipe-grout
pp	pipe-pipe
ref	reference
total	overall property
w	water
y	ten year period
∞	far field and initial condition
0	initial condition
12	short circuit (pipe-pipe)
2U	double U-BHE
8	Tp8 Method

Superscripts

n	index, temporal discretization
*	effective

1. Introduction

The present chapter is about the general aspects related to ground-coupled heat pump technology for the exploitation of the geothermal source. The main aspects faced by the present dissertation have been clearly stated in the present section. The list of publications produced during the Ph.D. work that serves as the main references and the thesis structure are reported at the end of this chapter.

1.1 Ground-coupled heat pump applications and modeling

The heat pump coupled with the ground through multiple vertical or horizontal borehole heat exchangers (BHEs) constitutes the Ground Coupled Heat Pump (GCHP) closed-loop system. Typically, vertical BHEs are the most frequently adopted solution with coaxial, single, or double U-pipe configurations. The impact of the GCHP on the market related to residential and industrial building heating, ventilation and air conditioning has increased over the last decade thanks to the environmental and economic benefits related to the intrinsic high energy efficiency potential of these systems. The efficiencies achieved from the use of GCHP are higher than those from the conventional air heat pump because the lower source temperature of the related thermodynamic cycle (the ground temperature) is on average higher than the one exploited by the air source heat pumps (the external air temperature). The market related to the GCHP involves about one million installations in Europe, while more than half of GCHP in the world are installed in the United States. According to the International Energy Agency (IEA, 2020), Sweden and Germany are the two main European markets, with 20,000 up to 30,000 new installations every year in each country. The extended use of GCHP can confer an important gain in reducing CO_2 emissions since these systems could supply more than 90% of air and water heating than the condensing gas boiler technology (92–95% efficiency), taking also into account the primary carbon intensity of electricity consumption.

The conventional depth of vertical BHE is frequently 200 m or less, while the typical limit depth for air drilling is 350 m. BHEs deeper than 350 m are referred to as Deep Borehole Heat Exchangers (DBHEs). The great advantage of drilling at such a large depth (even more than 800–1000 m) is the capability to exploit higher temperature levels, especially if the ground has a significant geothermal gradient. The DBHEs represent the better choice for supplying heat to an entire urban district since the surface extension for drilling is reduced together with the total pipe length. As reported in the present thesis work, DBHEs represent a suitable solution in densely populated and cold urban areas, especially for buildings requiring high heat loads. The benefits that can be obtained by adopting this solution are many (in terms of better BHE performance and a higher heat rate effectively extracted from the ground, especially for areas where lack of land is a constraint), while typical higher costs (and technical complications) associated with drilling at such depths must be necessarily considered.

The optimization of GCHP systems employing conventional BHEs or DBHEs has become important over the years. In particular, the modeling of the BHE is one of the key challenges for predicting the performance and the ground thermal response for the correct ground thermal conductivity estimation. In this sense, in terms of the efficiency and also sizing of the whole system, the short-term response of the BHE gets the same importance as the long-term response. The knowledge of the ground thermal properties (first of all the ground thermal conductivity) is the key element for the correct sizing of the GCHP systems and their energy and economic sustainability. Ground thermal conductivity k_{gr} and the effective BHE thermal resistance R_b^* are typically evaluated through the Thermal Response Test (TRT). The TRT is an experimental procedure first proposed by (Mogensen, 1983) and it is based on the Infinite Line Source model (ILS, Carslaw and Jaeger, 1947, Ingersoll et al., 1955). The main assumptions of the ILS model involve pure heat conduction in an infinite medium, constant heat transfer rate in time and space from a linear source, and uniform ground thermal properties.

The TRT experiment is based on constantly heating (or cooling) the heat carrier fluid flowing through an already installed BHE while continuously measuring the temperatures of the fluid entering and leaving the TRT machine (or the BHE). The effective k_{gr} and the R_b^* can be estimated from the slope and the intercept of the average fluid temperature profile on a semilogarithmic time scale. These estimations represent the key factor for obtaining the correct and reliable sizing of the BHE field.

1.2 Research objectives

The present research activity embraced different aspects related to geothermal heat exchanger modeling, from new algorithms for coaxial and U-pipe systems applied to Thermal Response Test analysis to measurements applied to reduced scale geothermal units, to the implementation of a web-based calculation tool for geothermal heat pump design.

TRTs involving shallow and DBHEs of different geometries with a geothermal gradient in cases of single and multiple ground layers along the depth represent the main topic faced by the present Ph.D. thesis.

As it is easy to deduce, the need to reconstruct numerical TRTs using simulation tools capable of reproducing in a reliable way the thermal transient related to coaxial, single and double U pipes while employing reasonably short computational times has assumed increasing relevance becoming a research topic of great interest in the geothermal field during recent years. The main focus of the present work is on how the ILS model can effectively confer the correct ground thermal conductivity estimation when coaxial, single and double U BHE penetrate a single or multiple ground layers with different geothermal gradients along the depth. To this aim three Fortran90 programs implementing the finite-difference (FD) models related to coaxial, single and double U BHEs presented by (Morchio and Fossa, 2019, Morchio and Fossa, 2020) have been exploited for evaluating

the influence of specific TRT parameters on the ground thermal conductivity estimation when the ILS model is applied in TRT analysis. These models have been proved and validated against available literature TRT measurements, showing very accurate thermal profiles which overlap those related to the experimental data as reported in (Morchio and Fossa, 2019, Morchio and Fossa, 2020). The simulated cases reported in the present thesis work are addressed to evaluate the influence of these parameters for shallow and DBHEs penetrating single or multiple ground layers with different geothermal gradients along the depth. Among the different parameters investigated, the present work introduce the q_{ratio} parameter, which is defined as the ratio between the absolute value of the external heat transfer rate $\dot{Q}'$ (per unit length) and the "natural" heat rate $\dot{Q}'_{geo}$ corresponding to the geothermal gradient within the BHE length. Especially in DBHEs the influence of the heat injected/extracted rate on the estimated value of the ground thermal conductivity from an ILS-based TRT analysis can occur through the interaction between the injected/extracted heat rate and the natural heat rate related to the geothermal gradient. This interaction can affect the ILS-based k_{gr} estimated values when q_{ratio} is far from the condition q_{ratio}>>1. The simulations' results reported in the present study highlight how q_{ratio} is the dominant parameter that indicates when the ILS-based k_{gr} estimated value departs from the weighted-thickness average.

The present study is aimed to highlight how the effect of the q_{ratio} parameter on the TRT analyses is also related to a specific dimensionless g-transfer function called g_0 that is obtained by performing a complete circulation test of the same duration of the TRT without conferring any heat input rate. The three Fortran90 programs implementing the FD Models related to coaxial, single and double U-BHE geometries are exploited to evaluate the $g_j(\tau)$ and $g_{0,j}(\tau)$ functions related to each j_{th} node of fluid volume. A dedicated Fortran90 program, whose results have been successfully cross-checked with those provided by an independent Matlab solver, implements the routine for performing the Fast Fourier Transform (FFT) computation in the spectral domain used to reconstruct the $T_{f,j}(\tau)$ temperature profiles from the FD Models. The g_0 function incorporates the geothermal gradient and in general, the disturbance effect (particularly prominent for DBHEs) related to the undisturbed ground temperature profile during the TRT. In the present thesis work it has been demonstrated that when q_{ratio} is lower than 1 the $g_{0,j}(\tau)$ function is able to modify the slope of the general solution $T_{f,j}(\tau)$ for each fluid node.

The thermal conductivity of both the ground and the backfilling material (also known as grout) must be estimated (i.e. the couple k_{gr} and the R_b^*) since they constitute important input parameters for the BHE field sizing methods. In this sense, a reduced-scale experimental apparatus has been designed, realized and reported in the present study. The reduced-scale experimental apparatus is aimed to perform and analyze an innovative TRT based on electric heating at the BHE axis, monitoring the BHE probes along the depth relying on a solution cheaper than the one represented by the conventional TRT and DTRT methods. The reference sizing method of a BHE field is the Ashrae method improved with the Tp8 approach (Fossa and Rolando, 2015, Fossa, 2017). A Geothermal Heat Pump Portal and Online Designer for Ground Heat Exchanger Fields has been realized during the Ph.D. study (see https://en.geosensingdesign.org/). The present website offers the first worldwide ever (and completely Free) web calculation tool for the design of BHE fields based on a modified version of the Ashrae Method, also employed in the corresponding

UNI Italian standard.

The specific objectives of the present doctoral thesis have been summarized:

i. Analyses of how the ILS model can effectively confer the correct ground thermal conductivity estimation when coaxial, single and double U BHE penetrate a single or multiple ground layers with different geothermal gradients along the depth.
ii. Among the different parameters investigated, the present work introduces the q_{ratio} parameter. The ILS-based k_{gr} estimated values are affected by the effect related to the geothermal gradient when q_{ratio} is far from the condition $q_{ratio}>>1$.
iii. The simulations' results highlight how q_{ratio} is the dominant parameter that indicates when the ILS-based k_{gr} estimated value departs from the weighted-thickness average.
iv. Highlight how the effect of the q_{ratio} parameter on the TRT analyses is also related to a specific dimensionless g-transfer function called g_0 that is obtained by performing a complete circulation test of the same duration of the TRT without conferring any heat input rate.
v. It has been demonstrated that when q_{ratio} is lower than 1 the $g_{0,j}(\tau)$ function is able to modify the slope of the general solution $T_{f,j}(\tau)$ for each fluid node.
vi. Present the Italian and Canadian patent related to the all-in-one BHE equipped with the central electrical heater and with digital temperature sensors placed at different radial positions and depths for innovative Electric Depth Distributed Thermal Response Test (EDDTRT) experiments. This innovative concept assures continuous BHE performance monitoring, testing for correct grouting, and testing for aquifer presence.
vii. Present the experimental setup related to the suitable reduced-scale prototype of the real all-in-one BHE and the surrounding ground for the EDDTRT.
viii. Demonstrate that the measurements collected highlight the possibility of performing reliable TRT experiments and estimating the grout and ground thermal conductivity through the innovative all-in-one vertical ground heat exchanger.
ix. Realize a Geothermal Heat Pump Portal and Online Designer for the design of BHE fields based on a modified version of the Ashrae Method, also employed in the corresponding UNI Italian standard (see https://en.geosensingdesign.org/).

1.3 Structure of the present Ph.D. Thesis and related papers

The present Ph.D. is organized into six main chapters. The present first chapter serves as an introduction to the overall context of the research topic, presenting the objectives of the dissertation and its structure. The second chapter is dedicated to the explanations of the FD Models developed during the present Ph.D. study for the performance analyses of coaxial, single and double U BHEs. The second chapter presents also the first investigations on the ILS-based k_{gr} estimations in TRT with coaxial BHE and

DBHE with the related error analyses. The third chapter constitutes the core of the work since reports the main investigations and explanations on how the ILS model can effectively confer the correct ground thermal conductivity estimation when coaxial, single and double U BHE penetrate a single or multiple ground layers with different geothermal gradients along the depth. The third chapter of the present thesis explains how the ILS-based k_{gr} estimations in TRT analysis can be affected by the q_{ratio} parameter introduced in the present work. The q_{ratio} affects the TRT analysis for single and multiple ground layers of equal thickness with different ground thermal conductivities along the depth. The q_{ratio} is also related to the g_0-transfer function evaluated for the FFT related to the spectral analysis method. Error analyses on the BHE and ground properties estimations from the ILS model are reported in the third chapter. The experimental setup related to a suitable reduced-scale prototype of the real BHE and the surrounding ground for innovative EDDTRT experiments is reported in the fourth chapter of the thesis. Measurement error analyses in estimating the grout and ground thermal conductivity are reported in the study. The thermal conductivity estimations of both the ground and grout constitute important input parameters for the BHE field sizing methods. Indeed, the fifth chapter is dedicated to presenting the main input parameters and references related to the web calculation tool for the design of BHE fields based on a modified version of the Ashrae Method, also employed in the corresponding UNI Italian standard (see https://en.geosensingdesign.org/). General conclusions, discussion and future work are presented in the final sixth chapter.

The publications that serve as the main references for the present thesis in the related chapters are listed below.

CHAPTER 2:

1. S. Morchio, M. Fossa, "*Thermal Modeling of Deep Borehole heat exchangers for geothermal applications in densely populated urban areas"*, Thermal Science and Engineering Progress (TSEP), 2019. https://doi.org/10.1016/j.tsep.2019.100363

2. S. Morchio, M. Fossa, "*On the ground thermal conductivity estimation with coaxial borehole heat exchangers according to different undisturbed ground temperature profiles"*, Applied Thermal Engineering, 2020. https://doi.org/10.1016/j.applthermaleng.2020.115198

3. S. Morchio, M. Fossa, Corrigendum to "*On the ground thermal conductivity estimation with coaxial borehole heat exchangers according to different undisturbed ground temperature profiles*", Applied Thermal Engineering, 2021, https://doi.org/10.1016/j.applthermaleng.2021.116981

4. S. Morchio, M. Fossa, *"Modelling and Validation of a New Hybrid Scheme for Predicting the Performance of U-pipe Borehole Heat Exchangers during Distributed Thermal Response Test Experiments"*, Applied Thermal Engineering, 2020. https://doi.org/10.1016/j.applthermaleng.2020.116514

CHAPTER 3:

5. S. Morchio, M. Fossa, R. A. Beier, *"Study on the best heat transfer rate in Thermal Response Test experiments with coaxial and U-pipe Borehole Heat*

Exchangers", Applied Thermal Engineering, 2022, 200, 117621. https://doi.org/10.1016/j.applthermaleng.2021.117621

6. S. Morchio, P. Pasquier, M. Fossa, R. A. Beier, *"A spectral method aimed to explain q_{ratio} as the dominant parameter when the Infinite Line Source model is applied to interpret the Thermal Response Test data"*, Under Review, 2022.

CHAPTER 4:

7. S. Morchio, M. Fossa, A. Priarone, A. Boccalatte, *"Reduced Scale Experimental Modelling of Distributed Thermal Response Tests for the Estimation of the Ground Thermal Conductivity".* Energies. 2021; 14(21):6955. https://doi.org/10.3390/en14216955

CHAPTER 5:

8. M. Fossa, S. Memme, S. Morchio, M. Parenti, A. Priarone, *"Una WebApp di Università di Genova per il dimensionamento dei campi sonda geotermici per applicazioni a pompa di calore"*, Aicarr Journal, 2022.

During this doctoral work, the author worked actively in the following supporting publications:

a. R. A. Beier, M. Fossa, S. Morchio, "Models of thermal response tests on deep coaxial borehole heat exchangers through multiple ground layers", Applied Thermal Engineering, 2020, 116241, ISSN 1359-4311, https://doi.org/10.1016/j.applthermaleng.2020.116241
b. R. A. Beier, S. Morchio, M. Fossa, "Thermal response tests on deep boreholes through multiple ground layers ", Geothermics, 2022, https://doi.org/10.1016/j.geothermics.2022.102371
c. S. Morchio, "The flow of sound pathways through the music network: introduction and analysis of music connections", International Journal of Advanced Engineering Research and Science 8(10), 263-290. https://dx.doi.org/10.22161/ijaers.810.30
d. S. Morchio, "The harmonic and melodic connection numbers involving the mutual inclusions among the generic groups of notes arbitrarily emitted", International Journal of Advanced Engineering Research and Science 8(12), 205-233. https://dx.doi.org/10.22161/ijaers.812.21

2. The Finite Difference Models developed for the performance analyses and k_{gr} estimations in TRT with coaxial, single and double U-pipe BHEs

The FD Models developed during the present Ph.D. study are explained in the present chapter with the three main published papers as the main references. These papers are aimed at the performance analyses of coaxial, single and double U BHEs. This chapter includes also the first investigations on the ILS-based k_{gr} estimations in TRT with coaxial BHE and DBHE with the related error analyses.

2.1 The FD Model for the performance analyses of coaxial BHE and DBHE

A detailed analysis of deep boreholes for GCHP application is reported in the present section. The method is applied to study the behavior of coaxial pipes to be employed in densely populated and cold urban areas. Validation is performed to assess model accuracy and reliability, offering contributions to previous papers on the subject.
Several models for the analysis of the thermal behavior of coaxial vertical heat exchangers have been developed in recent years. They have been employed in heat pump geothermal applications (GCHP) as well as for the analysis of experimental data in TRT measurements. Coaxial heat exchangers are triggering great interest in the Scandinavian countries (e.g. the Swedish Effsys program, Mazzotti et al., 2018) for a variety of positive features. These vertical coaxial exchangers can be also installed at depths larger than the conventional BHE and are referred to as Deep BHE (DBHE). Drilling at very high depths (even 800-1000m) has the great advantage of exploiting higher ground temperature levels and thus more favorable temperatures at the heat pump and even better long term heat transfer conditions. For instance, it has been proven that an 800-meter-long DBHE is capable of achieving the heat transfer guaranteed by 6 or more *U* conventional heat exchangers, each having a length of 300 meters (Holmberg et al., 2016). In such a way the surface extension for drilling is reduced together with the total pipe length. These aspects make the deep boreholes particularly suitable to be employed in those areas where lack of land is a constraint, as in towns where there is a high density of buildings associated with a high level of heat demand. These towns can be characterized by vast surfaces already occupied by geothermal low/medium-length traditional installations, as happens in many suburbs of large Swedish cities. The high thermal load assured by a single DBHE together with the high coefficient of performance (COP) and the limited CO_2 emissions make this type of application a valid energy solution for many cold, densely populated regions.
To summarize, DBHEs exploit the favorable temperatures of ground at high depths and help reduce land use at the surface.

The use of the DBHEs in the Geothermal Heat Pump industry can contribute to energy savings and emission reduction in densely populated areas like, for example, many Chinese regions. Regarding the specific case of China, geothermal heat pumps had a great development in this Country and in recent years GCHP installations had a progressive

annual increase rate of over 27%; Ground Source Heat Pump (GSHP) application has reached 330 million m^2 in China in 2014 (Zheng et al., 2015). Cities like Beijing, Tianjin and Shenyang have established a series of GSHP systems, which led to a massive reduction of CO_2 emissions of 19.87×10^6 tons (Zhang and Hu, 2018).

BHEs and their deep counterparts can be also employed as an interface for seasonal solar thermal energy storage. (Gao et al., 2015) reviewed the studies on borehole seasonal solar thermal energy storage. They considered analytical and numerical models for ground thermal recharge and carried out system simulations. They showed that in the specific case of China, there are still some special problems for the development of borehole seasonal solar thermal storage related to the lack of land and quite slow development in building integrated solar collectors.

The effective use of GCHPs is mainly related to the correct modeling and simulation of ground heat exchangers and their surrounding ground volume. This is particularly important for deep BHEs and coaxial ones. The typical approaches for predicting the heat exchanger behavior are of three types and they can be classified into semi-analytical models, thermal resistance and capacitance models, and finite difference (or volumes) methods.

Semi-analytical models are described in the next section and they refer to the base analytical solutions of the Fourier conduction equation. (Carslaw and Jaeger, 1947) contributed to the solution of the cylindrical heat source, (Ingersoll et al., 1955) presented the Infinite line source problem, (Eskilson, 1987) first solved the problem of the thermal response of a system of linear sources arranged in a given geometry. More recent contributions are those by (Cimmino and Bernier, 2014) that solved the Eskilson problem by applying analytical solutions to segments of the linear source and by (Priarone and Fossa, 2015) that compared the single line source response at different boundary conditions. Capacity Resistance Models (CRM) solve a system where unknowns are ground and BHE thermal capacitances and resistances and they are particularly suitable for short to medium term simulations (De Carli et al., 2010, Bauer et al., 2011, Zarrella et al., 2011).

In the present investigation, a hybrid method based on both the concept of thermal resistances and finite difference has been developed and applied for simulating long coaxial BHEs according to the approach recently proposed by (Holmberg et al., 2016). The study reported in the present chapter is stressing some issues related to model validation and proper spatial and temporal discretization and it is applied to demonstrate how hydraulic optimization and heat transfer from the ground can be properly simulated for short to medium-time analyses.

2.1.1 Theoretical background on modeling the ground heat exchangers

BHE models often refer to heat conduction. The ground transient behavior is accounted for, in terms of a “transient” thermal resistance. The inner BHE contribution is modeled as the resistance R_b^* (in the present work denoted as the effective borehole thermal resistance, see Eqs. (27) and (31) in Section 2.2). The ground contribution is modeled as the resistance R_{ground}. The R_b^* term can be reasonably considered as a constant resistance (steady since the long time scale proper of the ground thermal transient) while

the R_{ground} (τ) is a time-dependent resistance. The present approach constitutes the two thermal resistances model for GCHP simulation, synthetically represented by Figure 1.

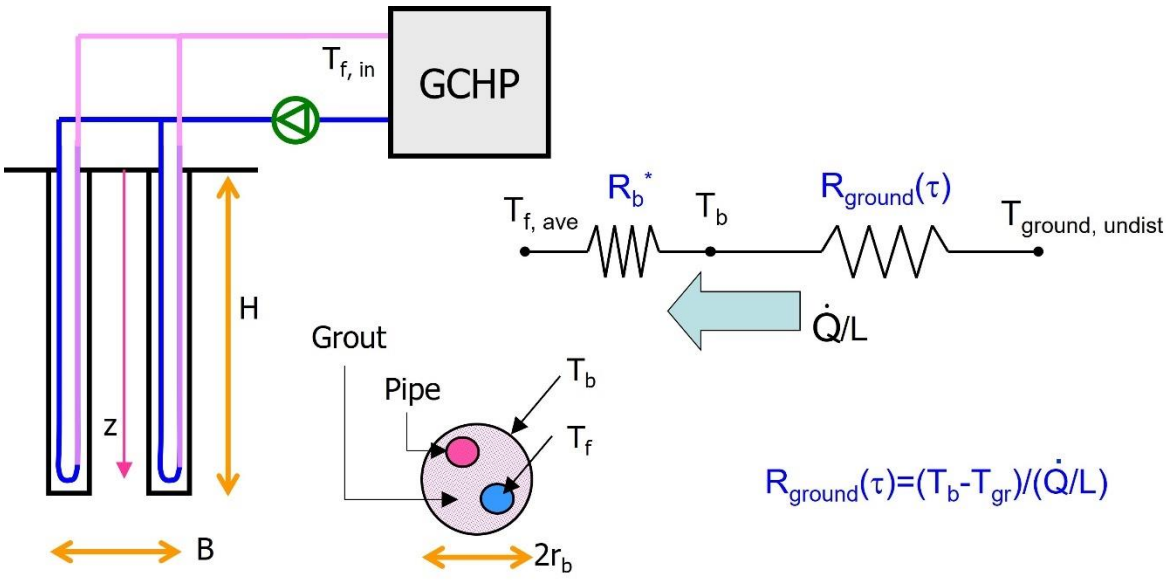

Figure 1 The two thermal resistances model for GCHP simulation.

In order to correctly describe the ground thermal transient behavior, it is possible to refer to analytical models (namely the categories related to the Infinite Line Source, ILS, Infinite Cylindrical Source Model, ICS, Finite Line Source, FLS, more in general denoted as Temperature Response Factors Γ, see Eq. (6.1)) to obtain a reasonable determination of the R_{ground} (τ) term. In addition to these models, numerical models based on Finite Difference (FD) methods (like the one presented in this thesis work) or Finite Volumes methods can be employed and coupled with those related to the thermal resistance and capacitance (TRCM) schemes to numerically describe the inner BHE (R_b*) and the ground (R_{ground} (τ)) thermal transient behaviors in a complete form.
Thermal conduction in the ground is one of the fundamental hypotheses used in thermal response models for geothermal heat exchangers' analysis. (Carslaw and Jaeger, 1947) first provided the ground theoretical response of single heat sources pertaining to the Infinite Line Source (ILS) category. This infinite linear source does not have a dimension in the radial direction and it extends in an infinite medium. The main assumptions related to the ILS model used to interpret thermal response test data are constant and uniform heat transfer rate from a linear source; pure radial heat conduction in an infinite medium with a uniform initial temperature; constant, homogeneous and isotropic ground thermophysical properties; no effects related to the groundwater flow. The temperature variation at a point located at a distance r of an infinite linear source that injects (or absorbs) a constant heat transfer rate per unit length $\dot{Q}'$ into an infinite medium in which is embedded is given by:

$$T(r,\tau) - T_{gr,\infty} = \frac{\dot{Q}'}{4\pi k_{gr}} \int_x^{\infty} \frac{e^{-\beta}}{\beta} d\beta = \frac{\dot{Q}'}{4\pi k_{gr}} E_1(x) \qquad (1)$$

The ILS model provides the ground temperature $T(r,\tau)$ as a function of the radial distance and time. Here k_{gr} is the ground thermal conductivity, $T_{gr,\infty}$ is the undisturbed ground

temperature that is assumed to be the mean value along the BHE active depth *H* of the undisturbed ground temperature, $Fo_r = \frac{\alpha_{gr}\tau}{r^2}$ is the radius based on the Fourier number and finally E_1 is the exponential integral function, which has a very useful expression as expansion series:

$$E_1(x) = -\gamma - \ln(x) - \sum_{n=1}^{m} \frac{(-1)^n x^n}{n\, n!} \tag{2}$$

Here $\dot{Q}' = \frac{\dot{Q}}{H}$, x= $\frac{1}{4Fo_r}$ and γ is the Euler constant (γ ≈ 0.5772). E_1 can also be approximated by the Abramowitz and Stegun formulas (1964):

$$0 \le x \le 1$$
$$E_1(x) = a_0 - \ln(x) + a_1 x + a_2 x^2 + a_3 x^3 + a_4 x^4 + a_5 x^5 + \varepsilon(x) \tag{3}$$
$$|\varepsilon(x)| < 2 * 10^{-7}$$

$$a_0 = -0.57721566 \qquad a_1 = 0.99999193 \qquad a_2 = -0.24991055$$

$$a_3 = 0.05519968 \qquad a_4 = -0.00976004 \qquad a_5 = 0.00107857$$

$$1 \le x < \infty$$
$$E_1(x) = (x^2 + b_1 x + b_2)/[x e^x (x^2 + b_3 x + b_4)] + \varepsilon(x) \tag{4}$$
$$|\varepsilon(x)| < 5 * 10^{-5}$$

$$b_1 = 2.334733 \qquad b_2 = 0.250621 \qquad b_3 = 3.330657$$

$$b_4 = 1.681534$$

It can be demonstrated that Eq.(3) is also accurate within 1% at Fo_r higher than 0.145 (Fossa, 2016) and both Eqs (3) and (4) are much more accurate than the typical E_1 approximation employed since Mogensen's pioneering work (1983).

Another one-dimensional model (and solution) available for the infinite ground medium is the Infinite Cylindrical Source (ICS) model, by (Ingersoll et al., 1955). Compared to the ILS model, the specific heat transfer rate (per unit source length) is applied to the surface of a hollow infinite cylinder of a given radius. The solution is described by a rather complex analytical function that was named the "*G*" one, whose values are often available in tabular form:

$$T(r,\tau) - T_{gr,\infty} = \frac{\dot{Q}'}{k_{gr}} G\left(Fo_{rb}, p = \frac{r}{r_b}\right) =$$
$$= \frac{1}{\pi^2} \int_0^{\infty} \frac{e^{-\beta^2 \cdot Fo_{rb}} - 1}{J_1^2(\beta) + Y_1^2(\beta)} [J_0(p\beta) Y_1(\beta) - J_1(\beta) Y_0(p\beta)] \frac{1}{\beta^2} d\beta \tag{5}$$

where J_0, J_1, Y_0, Y_1 are Bessel functions of the zeroth and first order, respectively.

More recent semi-analytical models have been developed to better describe a real ground heat exchanger located in a semi-finite volume. These models belong to the family of the

Finite Line Source (FLS) and the main contribution are by (Eskilson, 1987, Spitler and Yavuzturk, 1999, Zeng, 2002, Lamarche and Beauchamp, 2007, Claesson and Javed, 2011, Cimmino et al., 2013).
Numerical models assume great importance in solving the heat conduction equation in a finite domain. (Eskilson, 1987) defined new temperature transfer functions (Temperature Response Factor) known as *g*-functions:

$$T_{ave}(r_b) - T_{gr,\infty} = \frac{\dot{Q}'_{ave}}{2\pi k_{gr}} g(ln(9Fo_H), r_b/H, B/H, borefield\ geometry) \qquad (6)$$

The *g*-function is calculated by using numerical or semi-analytical methods (according to different boundary conditions as discussed by Cimmino and Bernier, 2014, and Priarone and Fossa, 2015). Often *g*-functions are available graphically (as reported in Eskilson Doctoral Thesis, 1987). The dimensionless g-solutions provide the performance of a borehole for various borefield geometries. The above temperature response factors are not defined in the same way; to be compared to one another a conversion constant has to be applied. Taking as a reference the ICS convention one can introduce a general temperature transfer function Γ as:

$$T(r_b) - T_{gr,\infty} = \frac{\dot{Q}'}{k_{gr}}\Gamma \qquad \Gamma_G = G \qquad \Gamma_{ILS} = \frac{E_1}{4\pi} \qquad \Gamma_g = \frac{g}{2\pi} \qquad (6.1)$$

Line and cylindrical source models, briefly discussed above, do not describe the pipe geometry of the BHE and further inner BHE models have been proposed for this aim. (Hellstrom, 2002) suggested that the coaxial geometry may have some advantages in reducing borehole thermal resistance. (Beier et al., 2013) focused on the coaxial design, in particular on the pipe-in-pipe geometry. (Zanchini et al., 2010) studied a coaxial design in which the stainless steel outer pipe is in direct contact with the surrounding ground. (Acuña and Palm, 2011) described a coaxial pipe in which an external flexible tube filled with water pushes the conduit against the borehole wall. Beyond this, (Acuña, 2010) measured the fluid and borehole wall vertical temperature profile in a coaxial heat exchanger during a Distributed TRT (DTRT experiment). It has been demonstrated by (Acuña, 2013) that coaxial exchangers exhibit better thermal performance when compared to traditional *U* pipes. From the hydrodynamic point of view, at the same operating conditions and the same drilling dimension, the coaxial heat exchanger has a reduced total pressure loss when compared to *U* pipes because of its larger hydraulic diameter.
(De Carli et al., 2010) proposed a model based on electric analogy (Capacity Resistance Model, CaRM) for vertical heat exchangers (Coaxial pipe, single U-pipe, double U-pipe). (Bauer et al., 2011) developed two-dimensional thermal resistance and capacity models (TRCM) for different types of BHE (coaxial included); these models consider the thermal capacity of the grouting material. Furthermore, the coaxial geometry is used to correctly locate the center of the grout thermal capacity for single-U and double-U geometries. A similar model configuration can also be found in (Beier and Smith, 2003). (Beier et al.,

2013) developed an analytical model to predict vertical temperature profiles of the circulating fluid in a coaxial heat exchanger (pipe-in-pipe geometry). This model handles an arbitrary vertical temperature profile in the undisturbed ground; the heat transfer between the fluid within the BHE and the surrounding ground is represented by using a thermal resistance model.
(Holmberg et al., 2016) developed a numerical model that employs both thermal resistances and the finite difference scheme in the ground medium for simulating coaxial BHE response and assessing the overall performance in terms of total COP, including the energy requirements in the circulation pumps.
(Iry and Rafee, 2018), have performed numerical simulations with a commercial CFD code changing the ratio between the diameters of a coaxial BHE having a length of up to 165 meters. (Fang et al., 2018) have stated that the operation of DBHEs combined with heat pumps seems more appropriate and economically sustainable for building heating. They also studied the effect of central pipe insulation. Their studies indicate that an insulated inner pipe makes a significant difference in DBHE performance due to its mitigation of thermal short-circuiting between the upward and downward-flowing fluids.

2.1.2 Present model for the coaxial ground heat exchanger

Studies related to the coaxial DBHE, able to cope with non-constant ground properties and possibly with peculiar ground temperature profiles are a quite new research activity. The present approach to a detailed description of the behavior of a long coaxial heat exchanger is made by developing a two-dimensional axisymmetric model based on the finite difference approach coupled with a thermal resistance description of the pipe wall effects. This numerical model solves the transient conduction and convection problem inside the heat exchanger and in the surrounding ground by imposing a given (constant or not) heat transfer rate to the carried fluid at the top inlet section of the heat exchanger. A Fortran90 program has been built and it is an evolution of the model proposed by (Holmberg et al., 2016). In the present model, the mesh describing the thermal volumes is variable along the radial as well as the longitudinal direction. The contributions to Holmberg et al. model are several: they include an analysis of Courant number effects, a proposed criterion for selecting the correct radial mesh spacing and distribution based on the ILS analytical solution, further comparisons and parametric analyses.
The ground thermo-physical properties, as well as the geothermal gradient (i.e. the undisturbed ground temperature profile), can change along the vertical z-axis and non-conventional temperature distributions can be taken into account. Worth noticing, for deep heat exchangers it is quite likely that such anomalous ground temperature distributions can be found in real installations and their anomalies can affect the overall performance of the heat pump. This aspect can hardly be accounted for using an analytical model (e.g. the ILS or FLS ones).
Time step, heat load, fluid mass flow rate, and heat load variation in time can be set depending on the simulation targets. The numerical problem solution may be obtained using two different far-field boundary conditions, namely an undisturbed temperature profile (as a function of z) or an adiabatic boundary condition (BC). By comparing the numerical results from both BCs it is possible to establish the correct dominion extension,

and this is an additional contribution due to the present study on this problem. The present model has been validated by using experimental measurements, theoretical data, and temperature profiles related to a 490 m DBHE coaxial heat exchanger. Further simulations then are here performed by both changing the diameters of the coaxial pipes as well as the undisturbed ground temperatures.

2.1.3 Model assumptions and equation data set

Based on the two thermal resistances model for GCHP simulation presented in Figure 1, the electro-thermal analogy has been conveniently used to describe the inner pipe and fluid heat transfer through proper thermal resistances (Figure 1.1) of the specific geometry related to the coaxial BHE. The numerical grid (Figure 2) implements a two-dimensional axial-symmetric model in cylindrical geometry. An upwind energy balance is applied to fluid volumes and the finite difference discretization of the Fourier equation is applied to the ground volume. The thermal inertia of pipes is neglected.
The total thermal resistance R_1 between the geothermal fluid in the central pipe and the fluid in the annular pipe at the same depth is expressed by the following equation:

$$R_1 = \frac{1}{2\pi r_{in,c} h_c} + \frac{\ln\left(\frac{r_{out,c}}{r_{in,c}}\right)}{2\pi k_c} + \frac{1}{2\pi r_{out,c} h_a} \qquad (7)$$

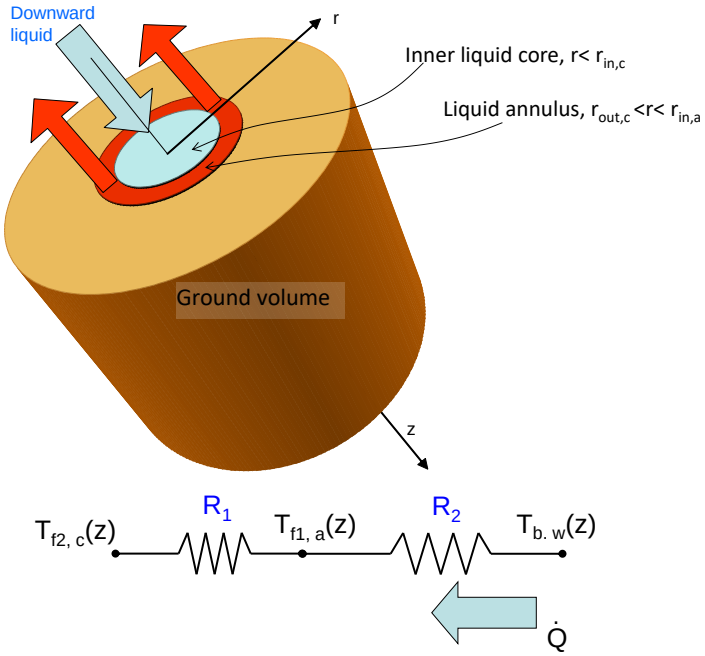

Figure 2.1 Axisymmetric geometry and the thermal resistance network.
Fluid direction can be also reverted with respect to the above representation. Pipe thickness is not present in the sketch.

The first term on the right-hand side of Eq. (7) is the resistance of the convective film on the inside of the center-pipe wall, while the second term is the resistance of the pipe wall. The third term is the convective film resistance on the outside of the center-pipe wall.

Similarly, the total thermal resistance R_2 between the carrier fluid in the annular conduit and the borehole wall surface at the same depth is expressed by the following equation:

$$R_2 = \frac{1}{2\pi r_{in,a} h_a} + \frac{\ln\left(\frac{r_{out,a}}{r_{in,a}}\right)}{2\pi k_a} + \frac{\ln\left(\frac{r_b}{r_{out,a}}\right)}{2\pi k_w} \quad (8)$$

The first term on the right-hand side of Eq. (8) corresponds to the thermal resistance of the convective film on the inside of the annular pipe. The second and third terms are respectively the resistances of the external pipe wall and the thin ring of water between the annular pipe and borehole wall. The above equation considers the possibility that a thin (quiet) water film (k_w conductivity) is present in between the outer pipe and the rock medium; in such a way any different contact resistance can be taken into account. The convective heat transfer coefficients h_a, h_c are calculated based on the mass flow rate and the related Reynolds numbers, Re_{d_h}. In case of Re_{d_h}<2300, the typical equations of the internal forced convection in the laminar flow regime are used to compute the Nusselt number Nu_{d_h}. More likely, when the fluid flow regime is turbulent (Re_{d_h}≥2300), Nu_{d_h} and the related convective heat transfer coefficients are calculated using the Petukhov correlation as modified by (Gnielinski, 1976). The convective heat transfer coefficient inside the annular duct is assumed to be the same on both the outer and inner walls since it is expected that their maximum difference is within 5% (Kays et al., 2005). The bulk fluid velocity w is calculated by the mass flow rate and pipe diameters assumed as inputs for the problem solution. In this way, R_1 and R_2 can be calculated given the pipe geometry and the material properties.

The thermal conduction in the ground surrounding the borehole is expressed by the Fourier law in cylindrical coordinates, in the absence of internal heat generation:

$$\frac{1}{r}\frac{\partial}{\partial r}\left(r k_g \frac{\partial T}{\partial r}\right) + \frac{\partial}{\partial z}\left(k_g \frac{\partial T}{\partial z}\right) = \rho c \frac{\partial T}{\partial \tau} \quad (9)$$

Equation (9) is discretized by introducing a numerical grid based on finite differences. It consists of nodes along the radial direction r (indexed with the letter i) and along the axial direction z (indexed with the letter j). In general, a variable internodal spacing along r and along the z directions can be assumed. Variable thermo-physical properties along z can be considered and set and for this reason, the ground thermal diffusivity α_j and the ground thermal conductivity k_j are here indexed with the letter j.

By applying the transient energy conservation law to each control volume, it is possible to write the finite difference formulation of the two-dimensional thermal conduction equation for each ground node as follows:

$$\frac{T_{i,j}^{n+1} - T_{i,j}^{n}}{\Delta\tau} = \left(\frac{2\alpha_j}{r_i \Delta r_i}\right)\left[A T_{i+1,j}^{n+1} - (A+B) T_{i,j}^{n+1} + T_{i-1,j}^{n+1} B\right] + \frac{(2\alpha_{j+1})}{\Delta z_j}\frac{(T_{i,j+1}^{n+1} - T_{i,j}^{n+1})}{\Delta z_j + \Delta z_{j+1}} -$$

$$\frac{(2\alpha_j)}{\Delta z_j}\frac{(T_{i,j}^{n+1}-T_{i,j-1}^{n+1})}{\Delta z_j+\Delta z_{j-1}} \quad (10)$$

The terms A and B group the following quantities:

$$A=\frac{(r_i+\frac{\Delta r_i}{2})}{\Delta r_i+\Delta r_{i+1}} \quad (11)$$

$$B=\frac{(r_i-\frac{\Delta r_i}{2})}{\Delta r_i+\Delta r_{i-1}} \quad (12)$$

The expression (10) follows an implicit scheme. It is also possible (depending on the choices made by the user) to maintain an evenly spaced grid along *z* and/or *r*. Present simulations have been carried out with a non-constant radial grid, while depth distances have been uniformly spaced.

Proper *z* spacing has been chosen by comparing the fluid temperature results in the first 10 hours (the most affected by grid issues) by doubling the finite volumes in the depth direction with respect to the reference grid (100 partitions along *z*). The maximum fluid temperature difference resulted in 0.2 K (for any instant and volume position) and the average one less than 0.02 K.

Interdistances between radial nodes have been selected following the "intrinsic log" nature of the heat diffusion as suggested by the ILS analytical solution. For this reason, the following radial distribution law has been applied:

$$r_{i+1}=r_i e^{deltaprecision\left(\frac{2\pi k_{gr}}{\dot{Q}'}\right)} \quad (13)$$

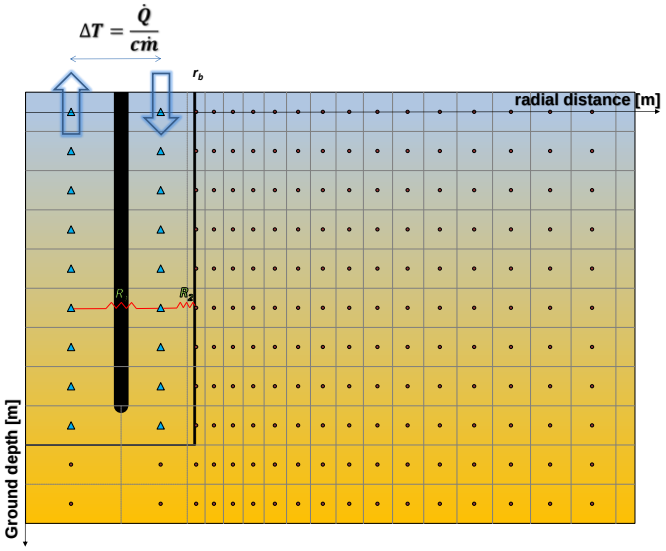

Figure 2 Node distribution along the radial and vertical directions for a given portion of the calculation domain. Nodes left of solid lines represent liquid volumes.

This law has been here derived from the ILS analytical equation (it has been considered the expansion series of the exponential integral function truncated at the second term) where *deltaprecision* is to some extent related to the temperature difference between two adjacent nodes. This parameter can be selected as an input as a tradeoff between reduced round-off errors and node overall number. The presence of the $k_{gr}/\dot{Q}'$ ratio comes from the ILS solution itself and it is related to the temperature gradients in the radial direction, to be properly managed with a suitable radial mesh.
Figure 2 shows the node distribution along *z* and *r*, where each node is identified by its coordinates. The solid lines identify the cylindrical axisymmetric surfaces of pipes.
The following energy balance equations describe the thermal transient of each fluid control volume within the BHE. In the equations below, ΔT is the carrier fluid temperature difference at the pipe top inlet and outlet.
In the following, the discretization schemes in the annular pipe, center pipe, inlet and outlet top nodes outside the ground, respectively, are provided.

$$\frac{\left(T_{f1,j}{}^{n+1}-T_{f1,j}{}^{n}\right)}{\Delta\tau}=\frac{w_{f1}\left(T_{f1,j-1}{}^{n+1}-T_{f1,j}{}^{n+1}\right)}{\Delta z_j}+\frac{\left(T_{1,j}{}^{n+1}-T_{f1,j}{}^{n+1}\right)}{\rho c\pi\left(r_{in,a}{}^{2}-r_{out,c}{}^{2}\right)R_2}+\frac{\left(T_{f2,j}{}^{n+1}-T_{f1,j}{}^{n+1}\right)}{\rho c\pi\left(r_{in,a}{}^{2}-r_{out,c}{}^{2}\right)R_1} \quad (14)$$

$$\frac{\left(T_{f2,j}{}^{n+1}-T_{f2,j}{}^{n}\right)}{\Delta\tau}=\frac{w_{f2}\left(T_{f2,j+1}{}^{n+1}-T_{f2,j}{}^{n+1}\right)}{\Delta z_j}+\frac{\left(T_{f1,j}{}^{n+1}-T_{f2,j}{}^{n+1}\right)}{\rho c\pi r_{in,c}{}^{2}R_1} \quad (15)$$

$$\frac{\left(T_{f1,j}{}^{n+1}-T_{f1,j}{}^{n}\right)}{\Delta\tau}=\frac{w_{f1}\left(T_{f2,j}{}^{n+1}+\Delta T-T_{f1,j}{}^{n+1}\right)}{\Delta z_j} \quad (16)$$

$$\Delta T=\frac{\dot{Q}}{\dot{m}c} \quad (17)$$

$$\frac{\left(T_{f2,j}{}^{n+1}-T_{f2,j}{}^{n}\right)}{\Delta\tau}=\frac{w_{f2}\left(T_{f2,j+1}{}^{n+1}-T_{f2,j}{}^{n+1}\right)}{\Delta z_j} \quad (18)$$

Similar equations have been written for the case when the fluid enters from the top of the central pipe (descending fluid in the central pipe).

The conductive heat transfer in the ground equals the one transferred through the overall thermal resistance R_2 of the BHE:

$$\left(T_{f1,j}-T_{b,j}\right)\frac{\Delta z_j}{R_2}=-\frac{k_j 2\pi r_b\Delta z_j\left(T_{2,j}-T_{0,j}\right)}{\left(\Delta r_1+\frac{\Delta r_0}{2}+\frac{\Delta r_2}{2}\right)} \quad (19)$$

From equation (19) it is possible to write the following equation (20), valid for the borehole wall nodes:

$$\frac{T_{b,j}^{n+1}-T_{b,j}^{n}}{\Delta\tau}=\left(\frac{2\alpha_j}{r_b\Delta r_1}\right)\left[(A+B)T_{2,j}^{n+1}-(A+B)T_{1,j}^{n+1}+\left({T_{f1,j}}^{n+1}-{T_{b,j}}^{n+1}\right)\frac{(\Delta r_1+\frac{\Delta r_0}{2}+\frac{\Delta r_2}{2})}{R_2 k_j 2\pi r_b}B\right]+$$
$$\frac{(2\alpha_{j+1})}{\Delta z_j}\frac{(T_{b,j+1}^{n+1}-T_{b,j}^{n+1})}{\Delta z_j+\Delta z_{j+1}}-\frac{(2\alpha_j)}{\Delta z_j}\frac{(T_{b,j}^{n+1}-T_{b,j-1}^{n+1})}{\Delta z_j+\Delta z_{j-1}} \quad (20)$$

The following equation is used to calculate the specific heat transfer rate distribution along the borehole length considering the thermal resistance network of the coaxial geometry:

$$\dot{Q}'(z)=\frac{T_{b,w}(z)-T_{f1,a}(z)}{R_2}\ \forall\ 0<z\le H_b \quad (21)$$

Where:

- $T_{b,w}(z)$ is the computed borehole wall temperature distribution along the *z*-direction.
- $T_{f1,a}(z)$ is the computed fluid temperature distribution along the *z*-direction in the annular pipe.

Far-field boundary conditions can be applied with either a given temperature $T_{gr}(z)$ profile or adiabatic modes. Proper grid sizing and dominion extension can be checked by applying both the boundary conditions (BCs) and cross-checking the numerical results.

Initial condition: $\tau=0;\quad T(r,z,0)=T_{gr}(z)$ (22)

Boundary condition (type 1)
$$\begin{cases} T(r,0,\tau)=T_{gr}(0)\ \forall\ r\ge r_b \\ T(r_{max},z,\tau)=T_{gr}(z) \\ \left.\frac{\partial T(r,z,\tau)}{\partial z}\right|_{z=z_{max}}=0 \end{cases} \quad (23)$$

Boundary condition (type 2)
$$\begin{cases} T(r,0,\tau)=T_{gr}(0)\ \forall\ r\ge r_b \\ \left.\frac{\partial T(r,z,\tau)}{\partial r}\right|_{r=r_{max}}=0 \\ \left.\frac{\partial T(r,z,\tau)}{\partial z}\right|_{z=z_{max}}=0 \end{cases} \quad (24)$$

Equations (10) to (24) constitute a system that can be written in matrix form which has been here solved by applying an iterative Gauss-Seidel algorithm.
Grid spacing and time steps have been carefully evaluated by assessing the effects of different Courant numbers *Co* on the results of the simulations.

$$Co=\frac{w\Delta\tau}{\Delta z} \quad (25)$$

The *Co* analysis has been carried out for a specific test case described by Table 1 data.
A constant ground temperature gradient has been considered, as can be found for example in Italian lithologies, even for deep boreholes (e.g. Della Vedova et al., 2015). Courant

numbers have been changed in the 0.2 to 1 range, until fluid temperatures (especially in the first 10 hours of simulation) did not differ as an average for more than 0.1°C and as a maximum difference for more than 0.2°C. Figure 3 shows as an example the effects of the different Courant numbers in the very early period (τ=0.46 and 0.92 hours) and in the late one (τ=92 hours). The present analysis suggested that a Courant number equal to 0.4 seems suitable for assuring accuracy while saving at most computational time. Figure 4 shows the effects of *Co* on the fluid temperature predictions. The results refer to the fluid maximum temperature differences as calculated along the whole BHE depth.

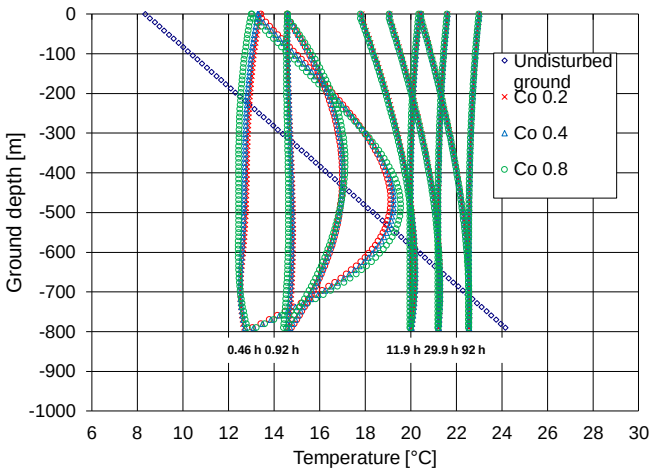

Figure 3 Fluid temperature profiles for a long BHE (800m) as a function of time and different Courant numbers when the undisturbed ground temperature profile is linear with depth.

The effects of the ground volume depth H_{gr} on the fluid temperature solution have been investigated. Two different H_{gr}/H ratios (H_{gr}/H=1.05 and H_{gr}/H=1.3) have been compared

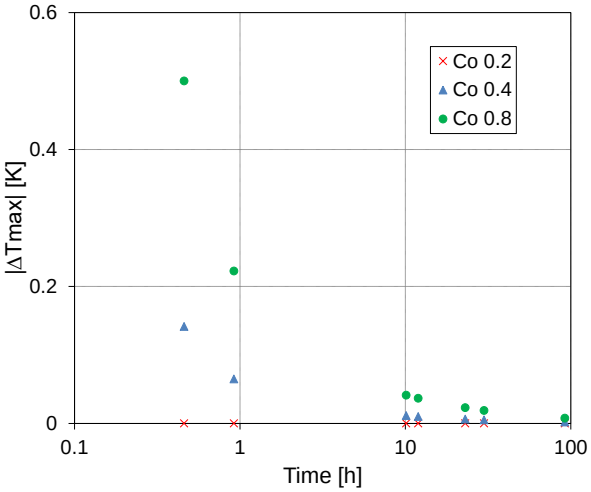

Figure 4 Maximum fluid temperature difference with respect to Co=0.2 results as a function of time and different Courant numbers for a long BHE (800 m).

in terms of fluid maximum temperature differences as calculated along the whole 800 m BHE depth. From this comparison, it turns out that the two temperature solutions are coincident. Therefore H_{gr}/H=1.05 is the value employed in all numerical simulations reported in the following sections since the same fluid temperature solution is achieved through a lower number of partitions along the z-direction preserving the same Δz which is in turn related to the Co=0.4 value.

2.1.4 Model validation against theoretical solutions

A preliminary series of calculations (with BC types 1 and 2) have been carried out with reference to a DBHE 800 m long. The length of the BHE has been selected for both stressing the model's capability to cope with very deep heat exchangers and to simulate conditions like the ones related to the ILS model. In such a way, even if the simulation is carried out by considering the fluid circulation, the ground temperature distribution (at mid-BHE depth, where end effects are expected to be negligible) can be compared with ILS 1D predictions. The geometry and operating conditions of this first reference case are provided in Table 1.

Table 1 Model validation: BHE geometry and operating conditions for 800m BHE

Borehole length	800 m
Borehole diameter	0.140 m
Center pipe diameter	0.09 m
Center pipe thickness	0.008 m
Annular pipe diameter	0.139 m
Annular pipe thickness	0.0004 m
Mass flow rate	3 kg/s
Heat load	32000 W
Fluid inlet pipe	Inner pipe
Ground thermal conductivity	3 W/mK
Ground thermal diffusivity	10^{-6} m^2/s
Geothermal gradient	0.02 K/m

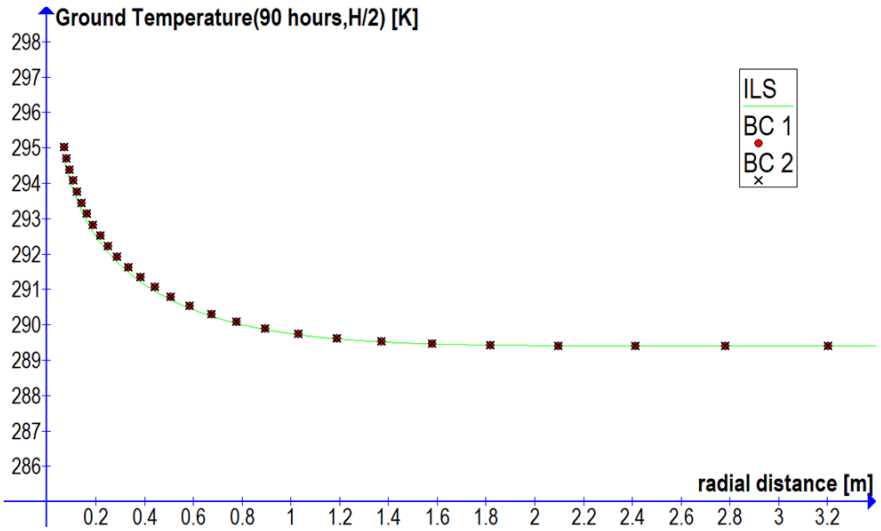

Figure 5 Radial temperature in the ground medium at mid BHE depth after 90 hours of heat injection and comparison with ILS predictions at same Fo number. Different BC conditions at external radius are applied.

Two BC conditions (the adiabatic or given temperature at the outer ground radius) have been applied for checking that the overall ground volume is large enough for describing the far-field persistency of the initial temperature profile. The two solutions (at different BC)

show an excellent agreement and are coincident up to the thousandth of a degree. More important, they show a trend at the end time (T(r) traced for $r_b \leq r \leq r_{max}$ and for $z = H/2$ at 90 hours) that follows the trend predicted by the ILS model using the Abramowitz and Stegun formulas, as shown by Figure 5.

Further simulations have been carried out for retracing some operating conditions considered in (Holmberg et al., 2016) paper. Table 2 describes this specific case and the related geometry. The BHE is 490m long and the time span is 50 hours, simulating a TRT in heat extraction mode (or a winter operating condition for a heat pump).

Table 2 Model comparison with literature data: BHE geometry and operating conditions for 490m BHE

Borehole length	490 m
Borehole diameter	0.140 m
Center pipe diameter	0.05 m
Center pipe thickness	0.0046 m
Annular pipe diameter	0.139 m
Annular pipe thickness	0.0004 m
Mass flow rate	1 kg/s
Heat load	-19600 W
Fluid inlet pipe	Annular pipe
Ground thermal conductivity	3.53 W/mK
Ground thermal diffusivity	10^{-6} m^2/s

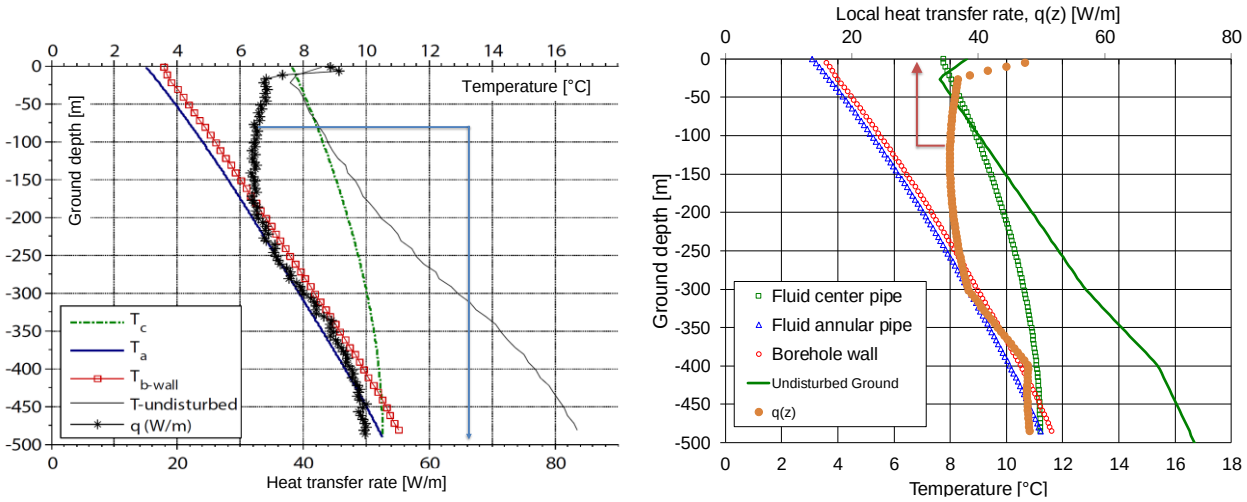

(a) (b)

Figure 6 Fluid and BHE temperatures along the z-axis (depth) as reported in (Holmberg et al., 2016) paper (left) and as calculated with the present model (right). Time is 50h.

Figure 6a shows the literature temperature profiles while Figure 6b shows the present model predictions in terms of fluid temperatures (inner pipe and annular one) and BHE wall. In both figures the undisturbed ground temperature profile (input of simulation) is reported together with the calculated local heat transfer rate (per unit length). As can be observed the agreement is good and the present model is able to replicate well the reference data.

2.1.5 Model validation against experimental measurements

Available literature data related to measurements with coaxial heat exchangers in both time and space are scarce. To the Authors' knowledge, the only recent experiments on DBHE refer to Swedish research (Mazzotti et al., 2018), where unfortunately a complete dataset of measurements is not provided. On the other hand, measurements in time and space (along the BHE depth) have been presented in (Acuña, 2013, Acuña and Palm, 2013) and they concern a 190m deep coaxial borehole. Measurements employ special optical fiber temperature sensors, providing both the fluid temperature (inner and annular pipes) and the interface temperature (annular external wall in contact with the ground). The simulations have been carried out by setting the fluid flow rate, the heat transfer rate and the ground thermal conductivity at the average values provided by (Acuña and Palm, 2013), namely 0.58 liters/s, 6.5 kW and 3.53 W/mK, respectively. Worth noticing the simulations have been carried out while maintaining the flow rate and heat rate constant in time, despite the measurements show daily oscillations of the above quantities. The upper "non-active length" described by (Acuña and Palm, 2013) has been applied in the present model too. The initial temperature of both ground and fluid has been set equal to the measured values

provided by the Authors, which show a peculiar non-linear trend along the depth. Figure 7a represents both the original measured data and the corresponding temperature profile employed as the initial and far-field boundary condition in the present numerical model.
The numerical results have been obtained both in terms of time and space. Very interesting is probably Figure 7b, where the experimental fluid and BHE temperatures are presented as a function of the depth at 91.1 hours after the beginning experiment. The present data are superposed to the original year 2013 Figure. The agreement is very good for fluid profiles, while BHE wall data differ by some 0.2°C from the measured values, especially in the upper part of the ground volume. Figure 8 shows the average fluid temperature (measured and estimated off-ground at TRT machine ports) as a function of time along 98 hours of the experiment. Simulations are presented as superposed profiles onto the original figure by (Acuña and Palm, 2013). It is apparent from figure inspection that the present model is able to well reproduce the experimental data, even if the constant heat rate condition at the simulation level does not allow the real temperature fluctuations to be properly described.

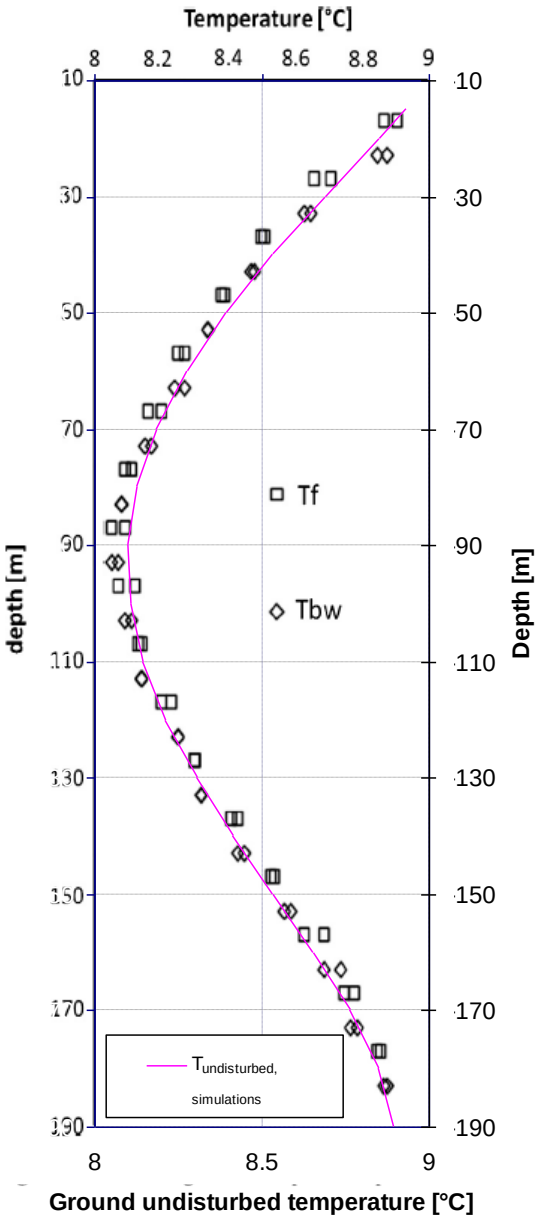

(a)

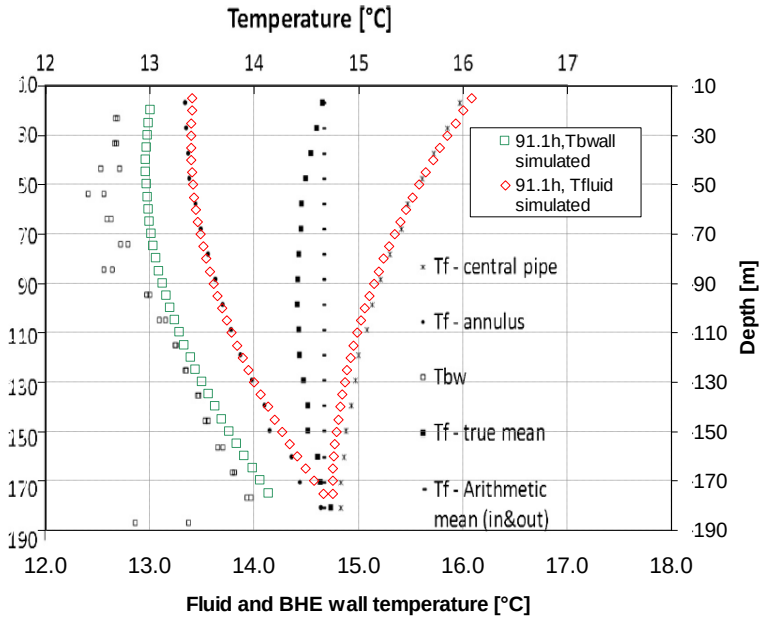

(b)

Figure 7 Validation of the present model against (Acuña and Palm, 2013) measurements. (a) Undisturbed ground temperature profile: continuous line is model Initial Condition. (b) Fluid and BHE wall temperatures at 91.1 hours from fluid circulation start.

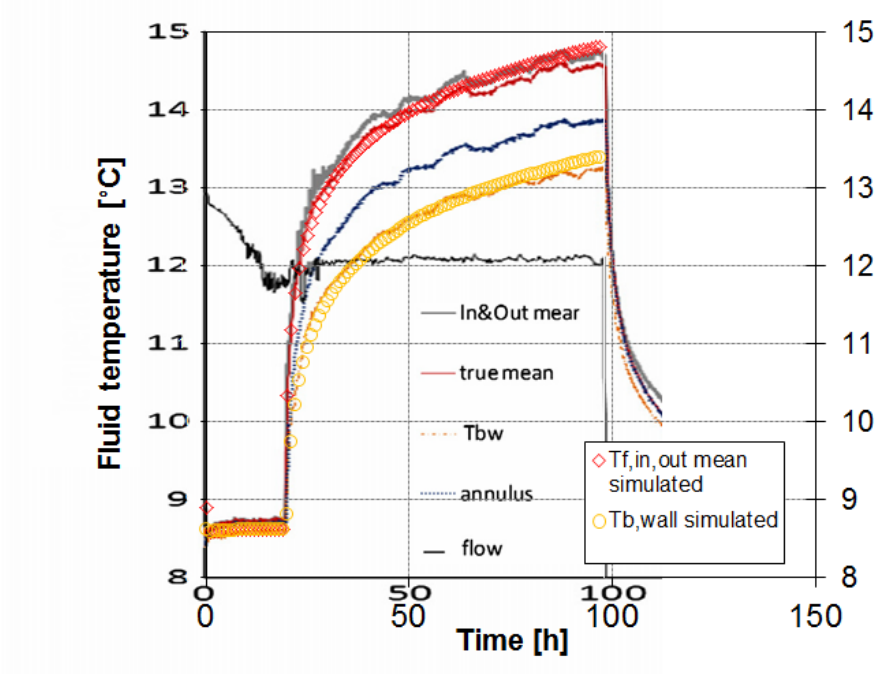

Figure 8 Validation of the present model against (Acuña and Palm, 2013) measurements. Average fluid (in &out) and BHE wall temperatures as a function of time.

2.1.6 Results and discussion

One of the objectives of the present investigation was to obtain indications on the hydrodynamic and thermal performance of such DBHES for general design purposes. Attention is paid to the temperature of the fluid exiting the borehole and to the pressure losses experienced by the fluid inside pipes at a given mass flow rate. Different simulations have been carried out while changing the diameter ratios of the coaxial exchanger. Simulations refer to 9 geometries at a time horizon of about 100 hours. Even if the model can be applied for longer time windows (tuning the ground outer diameter accordingly), the above duration has been considered suitable for both describing the hydraulic issues related to coaxial boreholes and obtaining useful information related to thermal effects during the heat load peak periods, ranging from a fraction of hours to few days. It is worth noticing, the 100-hour range is also suitable for describing the on/off cycles of the heat pump in order to apply, by superposition techniques, the present short-term DBHE response to the long-term one, as calculated from *g*-function models. DBHE dimensions are those described in Table 1 and just the diameter ratios have been changed according to Table 3 parameters. The mass flow rate of the carrier fluid is increased for test #8 and test # 9, while the center pipe wall thickness is reduced compared to the other tests.

Table 3 Parametric analysis data: pipe geometry and flow rates

Test Case #	Center Pipe inner diameter [m]	Mass flow rate [kg/s]	Center Pipe wall thickness [m]
1	0.05	3	0.008

2	0.075	3	0.008
3	0.085	3	0.008
4	0.09	3	0.008
5	0.1	3	0.008
6	0.105	3	0.008
7	0.08	3	0.008
8	0.08	3.5	0.006
9	0.08	3.5	0.002

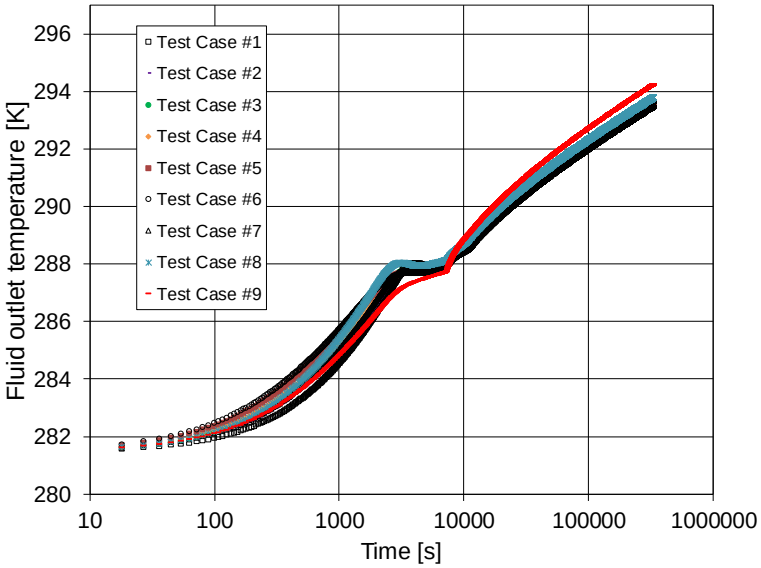

Figure 9 Temperature of the fluid leaving the BHE over time, for different coaxial pipe geometries

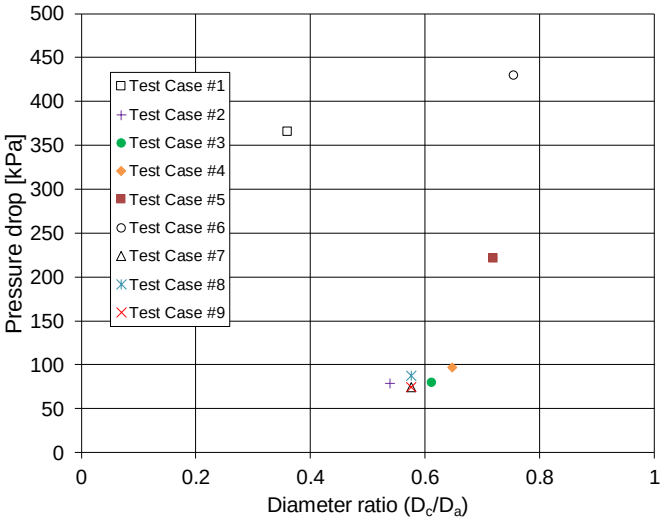

Figure 10 Pressure drop in coaxial pipes for Table 3 operating conditions as a function of the inner to annular pipe diameter ratios

Figure 9 shows the exit fluid temperature from BHE and the pipe geometry is the parameter. Worth noticing, the lower the exit temperature the better the heat exchanger performance. The first 7 tests (which differ only for the different diameters of the central pipe) involve temperatures at the outlet of BHE, which remain all within about 0.15 K. There is an initial thermal transient related to the first two hours of circulation of the flow without supplying heat. Test #8 differs on average by about 0.30 K in terms of BHE outlet temperature compared to Test #1. Test #9 has slightly larger temperature differences (0.65 K) compared to case #1. The lowest outlet temperature, all along time, is obtained by

geometry #1 having a diameter of central pipe equal to 0.05 m (the diameter of the annular pipe for all nine cases is set at 0.139 m).
Figure 10 refers to pressure losses due to pipe friction and shows an interesting profile passing through a minimum at a diameter ratio (Center pipe over annular one) located at about 0.55-0.60. This result is in close agreement with the findings by (Iry and Rafee, 2018), according to whom the minimum pumping power in a 165 m coaxial BHE can be achieved at a diameter ratio of 0.65. The above diameter ratio range thus seems to represent the optimum choice for reducing the pumping power at a given flow rate.
In the present investigation, also taking into account the similar thermal performance of all BHEs, geometries #7 to #9 seem to be the best ones from both thermal and hydrodynamic points of view.
A final series of simulations have been carried out by imposing the overall pressure drop related to geometry #7 (about 75 kPa) to all the other heat exchangers by varying their mass flow rates. In such a way the new flow rates range from 1.0 kg/s (geometry #6) to 3.0 kg/s (geometry #7). It can be noticed that imposing pressure loss is equivalent to

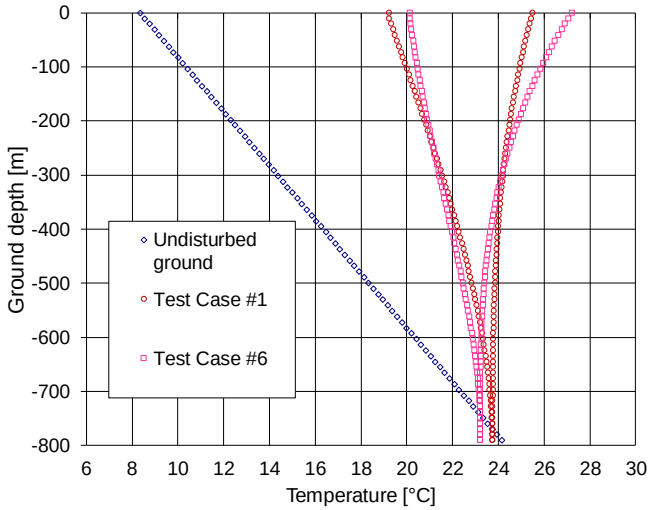

Figure 11 Fluid and ground temperature profiles at the end of a 92h period of constant heat injection in the ground. Mass flow rate is tuned for yielding the same pressure drop in the different pipe geometries. Cases #1 and #6 are considered as extreme conditions.

working with a pump at a given head.
Figure 11 shows the fluid temperatures along the DBHE at the final instant of the simulations (92 hours) for different coaxial pipe diameter ratios. Figure 11 also shows the far field (and initial) ground temperature which varies linearly (as an assumption for these simulations) with depth due to a constant geothermal gradient.
It can be noticed that, at a common heat transfer rate for all geometries, the inlet/outlet temperature difference $\Delta T_{in/out}$ changes with the mass flow rate. Consequently, the increase of $\Delta T_{in/out}$ moves the fluid temperatures near the heat exchanger bottom in the direction of the undisturbed (initial) temperature, thus producing a “temperature inversion” between fluid and ground. In addition to “temperature inversion” effects, the different pipe

geometry plays the role of controlling the "thermal short-circuiting" between the descending liquid in the inner pipe and the rising liquid inside the annulus. The comparison for example of cases #6 and #1 having more or less the same mass flow rate but a larger inner pipe diameter for case #6, is particularly interesting. Cases #1 and #6 are here selected and represented in Figure 8 since they represent the two extreme conditions among the geometries here considered. Geometry #6 has a higher heat transfer area (pipe to pipe) with respect to case #1 and this situation enhances the short-circuiting, carrying the descending fluid #6 (inside the inner pipe) to a lower temperature at BHE bottom with respect to fluid in pipe #1. On the other hand, the rising #1 fluid can be better cooled by the surrounding ground without being heated too much by its descending counterpart, thus gaining an outlet temperature at the BHE top section lower than case #6.

2.2 The ILS-based k_{gr} estimations in TRT with coaxial BHE and DBHE and the related error analyses

The first-ever demonstration of fluid direction influence on TRT accuracy is reported in the present section. The effects of the undisturbed ground temperature profile on TRT results are included in the analysis. Comprehensive parametric analyses on TRT estimations at different BHE lengths are reported. In particular, this section is aimed at the analysis of the BHE behavior in the early period, say for Fourier numbers typical of the TRT measurements. The novelty of the present numerical results is related to the applicability of standard TRT methods when applied to DBHEs and different geothermal gradients can be found. The application of the present finite difference model to coaxial BHEs is related to the assessment of the effects of the undisturbed ground temperature profile and the direction of the carrier fluid on the ground thermal conductivity estimation in TRT experiments. It is here demonstrated that different BHE depths (ranging from 150 to 800m) and different undisturbed temperature profiles (including zero and positive geothermal gradients) can severely affect the TRT ground conductivity estimation (errors up to 25%) if the flow direction is based on the annular pipe or the central pipe inlets. The BHE field design requires a series of input information, among which the ground thermal conductivity (k_{gr}) is the most important one. The TRT is the experimental technique first proposed by (P. Mogensen, 1983) for estimating k_{gr} by measuring the carrier fluid temperatures in a pilot BHE and applying the ILS solution (Carslaw and Jaeger, 1947, Ingersoll et al., 1955). After Mogensen, many researchers applied his standard TRT method in a variety of applications but mainly related to U-pipe BHEs and to "conventional" BHE depths, namely from 100 to 300m. Literature examples of conventional depth BHEs are those related to the early studies by (Gehlin, 2002, Austin, 1998, Pahud and Matthey, 2001, Acuña et al., 2009).
More recently (Acuña and Palm, 2010) reported a detailed description of the 189 m length coaxial borehole heat exchanger during a Distributed TRT experiment. (Gordon et al., 2017) consider the coaxial geometry and BHE depth ranges between 80 and 200 meters. In their work, a semi-analytical model is proposed and used to produce accurate predictions of the fluid temperature during a TRT experiment. (Zarrella et al., 2017) studied a 96 m BHE and estimated the ground properties by applying their capacitance-resistive thermal model. (Bae et al., 2019) investigated the TRT response of both coaxial and U-pipe in a

series of 150 m deep BHEs and they found differences in k_{gr} estimations made with U-pipe and coaxial BHEs.
(Holmberg et al., 2018) presented data from temperature profile measurements performed in boreholes before (undisturbed temperature) and after TRT experiments on boreholes ranging between 50 and 500 m. They showed for a large set of locations in Norway that very different ground temperature profiles can be found, and that the constant positive geothermal gradient is not the rule anywhere, and "thermal anomalies" are common in urban areas due to heat island effects.
(Fang et al., 2018) developed a numerical model for the coaxial DBHE based on the Finite Difference Method (FDM). They showed that different hydraulic configurations can affect the DBHE performance and that the geothermal gradient plays an important role in the DBHE thermal transient behavior.
The above literature analysis shows that some "secondary" parameters (fluid direction, geothermal gradient, BHE length) can affect the BHE thermal performance, but comprehensive studies on the influence of such parameters on ground property estimations from TRT measurements seem to be lacking in the literature.
The aim of this study is hence to investigate how the ground thermal conductivity estimation is influenced by different ground temperature profiles during a TRT experiment and the role of the BHE length in mitigating (and amplifying) the effects of the geothermal gradient on the estimation of the ground conductivity from standard TRT analysis.
Due to their rising interest, coaxial BHEs are here considered with depth up to 800 m and whose flow direction can be changed. The analysis is carried out by using a two-dimensional transient model in axial-symmetrical cylindrical geometry developed by the Authors (Morchio and Fossa, 2019) and similar to the one proposed by (Holmberg et al., 2016). The numerical investigation is carried out by imposing the ground conductivity in the numerical domain and by applying different undisturbed temperature profiles, including those related to the constant positive and nil geothermal gradients. The two flow directions (i.e. outer pipe downward and upward) have been applied in all simulations and the resulting fluid temperature records (as predicted at the ground surface) have been used for performing standard TRT analysis based on the ILS model.
The results showed that when considering deep BHE, temperature inversions (fluid to ground) can occur near the bottom end of the heat exchanger as an effect of the geothermal gradient values. The results also showed that the ground conductivity estimation, through the ILS analysis, is affected (in terms of accuracy) by the BHE depth and even by the selected flow direction, which must be properly selected based on the knowledge of the undisturbed ground temperature profile.

2.2.1 Theoretical background on thermal response test

The ground thermal conductivity k_{gr} strongly depends on the site lithology ($1<k_{gr}<5$ [W/mK], typical). A higher ground thermal conductivity k_{gr} leads to a better BHE thermal behavior, resulting in higher GSHP plant performance or shorter BHE length at the same expected COP (coefficient of performance). It is therefore a priority to correctly estimate the ground thermal conductivity (Li et al., 2019), especially in the design process (ASHRAE, 2015). The ground's thermal properties can be estimated together with the

effective borehole thermal resistance by performing the TRT on-site (Spitler and Gehlin, 2015). The TRT is an efficient measurement technique first proposed by (P. Mogensen, 1983) and it typically lasts from 50 to 100 hours. The TRT analysis is based on the assumption that the heat diffusion problem in the ground is a time-dependent one-dimensional phenomenon. For short periods of the heat exchanger's continuous work, the thermal field is essentially radial. Due to this reason the one-dimensional ILS (Infinite Line Source) model (Thomson (Lord Kelvin), 1882, Carslaw and Jaeger, 1947, Ingersoll et al., 1955), and ICS (Infinite Cylindrical Source) model (Carslaw and Jaeger, 1947, Ingersoll et al., 1955) model are very well suited to represent the solution $T(r,\tau)$ of the TRT conduction problem. When the Fourier number based on BHE radius Fo_r is lower than 10^3 ILS and ICS are completely equivalent to the FLS (Finite Line Source) solution (Eskilson, 1987, Zeng et al., 2002, Lamarche and Beauchamp, 2007, Claesson and Javed, 2011, Yavuzturk and Spitler, 1999, Cimmino et al., 2013), as demonstrated by (Fossa, 2017).

The classic TRT analysis is based on the ILS solution and on the approximation of its exponential integral function $E_1(Fo_r)$ through a truncated series just including the Euler constant γ and the logarithm of Fo_r.

The experimental test consists of circulating hot (or cold) water inside a pilot BHE that has been installed in the BHE field area. A constant heat transfer rate is provided to the heat carrier fluid, typically via an electric heater. The constant thermal power is transferred to the liquid flow rate, then to the ground surrounding the borehole. It is also assumed that the constant heat transfer rate provided on the top to the fluid, is uniformly distributed along the ground depth. This is a major hypothesis within the ILS model since in a real case there is a distribution of the specific heat transfer along the BHE depth which relates to a certain fluid temperature distribution along the vertical *z*-direction and to the ground undisturbed ground temperature profile along *z*.

The TRT and its standard analysis interpretation method are therefore based on four fundamental hypotheses:

- One-dimensional and time-dependent thermal conduction mechanism in the ground.

- ILS time-dependent model (based on a constant heat transfer rate in time and space from a linear source, pure heat conduction in an infinite medium, and uniform ground thermal properties) to analyze the temperature transient values of the carrier fluid and approximation of the E_1 solution with a truncated series at the logarithmic term.

- The specific heat transfer rate $\dot{Q}'$ [W/m] is assumed to be constant in time and uniform along the ground heat source.

- The effective borehole thermal resistance R_b* is almost constant in time (the thermal transient related to the volumetric capacity inner to the BHE characterizing the initial phase of the TRT is ignored to estimate the k_{gr}).

In the TRT analysis, the medium is represented by the ground while k_{gr} and α_{gr} are the ground thermal conductivity and diffusivity respectively, τ is the time coordinate. Among the different series expansions to approximate $E_1(x)$, the expression as truncated at the logarithmic term is the most common:

$$E_1(x) \approx -\gamma - \ln(x) \quad (26)$$

where γ is the Euler constant, γ ≈ 0.5772.

Assuming a 2-resistances model (ground and borehole thermal resistances in series) by introducing the effective borehole resistance, R^*_b, to the right-hand side of Eq. (1) and exploiting the approximation in Eq. (26), it can be easily demonstrated that the time-varying average fluid temperature (as computed at the inlet and outlet section of the TRT-machine), $T_{f,ave}$, is:

$$T_{f,ave}(\tau) = T_{gr,\infty} + \dot{Q}' \left[R^*_b + \frac{1}{4\pi k_{gr}} E_1\left(\frac{1}{4Fo_{rb}}\right)\right] = T_{gr,\infty} + \dot{Q}' \left\{R^*_b + \frac{1}{4\pi k_{gr}}\left[-\gamma - ln\left(\frac{1}{4Fo_{rb}}\right)\right]\right\} \quad (27)$$

where:

$$T_{f,ave}(\tau) = \frac{[T_{f,in}(\tau) + T_{f,out}(\tau)]}{2} \quad (28)$$

The initial part of the experiment (few hours) is usually devoted to fluid circulation without any heat transfer rate, in order to reach a thermal equilibrium between the fluid and the surrounding ground along the BHE depth. The thermal equilibrium temperature $T_{gr,\infty}$ between the fluid and the surrounding ground reached at the end of the circulation period prior to the start of heat injection (or extraction) of a TRT, according to the ILS model, is assumed to be the mean value along the BHE active depth *H* of the undisturbed ground temperature.

It can be easily demonstrated that Eq. (27) can be rearranged assuming the linear form in a semilogarithmic time scale expressed by Eq. (30). In this form, Eq. (29) is referred to as the simplified line-source model (First Order Approximation, FOA, of the ILS model):

$$T_{f,ave}(\tau) = mln(\tau) + b \quad (29)$$

where *m* is the logarithmic slope and the constant *b* contains R^*_b. The analysis of TRT experimental $T_{f,\,ave}$ profiles shows that a linear trend on a semilogarithmic time scale appears after a transient of the order of Fo_{rb}=10 (according to Eskilson, 1987). The k_{gr} value is estimated by computing the slope *m* inside an appropriate Fo_{rb} window ($Fo_{rb} \geq 10$):

$$k_{gr} = \frac{\dot{Q}'}{4\pi m} \quad (30)$$

In a TRT analysis with the ILS method, the effective borehole thermal resistance R^*_b (in turn related to k_{gr}) is usually calculated after the k_{gr} has been estimated according to the following expression:

$$R^*_b(\tau) = \frac{[T_{f,ave}(\tau) - T_{gr,\infty}]}{\dot{Q}'} - \frac{1}{4\pi k_{gr}}\left[-\gamma - ln\left(\frac{1}{4Fo_{r_b}}\right)\right] \quad (31)$$

The TRT has become a standard procedure in real GSHP applications for the BHE field correct design. The (Bae et al., 2019) study is of particular interest since they investigated the TRT response of both coaxial and U-pipe in a series of 150 m deep BHEs, and they found differences in k_{gr} estimations made with U-pipe and coaxial BHEs. (Acuña, 2013) and (Hellstrom, 2002) reported that the coaxial BHEs are more efficient than U-type BHEs because of their intrinsic lower BHE thermal resistance (R^*_b). This is implied by larger hydraulic diameters than the U-pipe BHE for the same borehole radius r_b. (Le Lous et al., 2015) developed a numerical model of a DBHE with coaxial collector.

(Morchio and Fossa, 2020) explained that for the coaxial BHE the borehole length and the geothermal gradient can influence the thermal performance as well as the ground thermal conductivity estimation. They found that in some cases (mainly related to DBHEs) different ground thermal conductivity estimates can be achieved by adopting the annular and the center inlet hydraulic configurations. On this line of research, (Fang et al., 2018) showed that different hydraulic configurations can affect the DBHE performance and that the geothermal gradient plays an important role in the DBHE thermal transient behavior (Fang et al., 2018).

2.2.2 Model assumptions and input data settings

The numerical simulations reported in the present section concern a TRT 94 hours long. Each numerical simulation has been performed using the in-house built Fortran code which implements the 2D numerical transient model developed by the Authors.

In particular, each numerical simulation is focused on the ground thermal conductivity k_{gr} estimation. The procedure is based on the numerical simulation of the fluid temperature in time as a function of different undisturbed ground temperature profiles. For TRT analysis purposes, the off-ground fluid average temperature $T_{f,ave}$ is calculated and used for FOA-ILS-based TRT estimations of the ground thermal conductivity. The investigation is aimed at inferring the error between the k_{gr} estimations and their input values at the model level. Estimations are obtained through the classic approach based on the analysis of the fluid temperature evolution as a function of the logarithm of time (Eq. 29). The comparison between the conductivity estimate and its input value in numerical simulations leads to the determination of the percentage errors to be analyzed for assessing the influence of the undisturbed ground temperature profiles and the flow direction on the k_{gr} predictions. All the numerical simulations are focused on the early period (100 hours) of heat exchanger response, typical for TRT experiments and important for describing the on/off cycles of the heat pump and its peak working conditions.

The performed simulations have been carried out with a non-constant radial grid, while depth distances have been uniformly spaced. Constant thermo-physical properties along z have been assumed in each simulation, even if the model is able to account for variable ground properties in space.

Eighteen numerical TRT simulations have been performed. A constant fluid temperature difference is applied (in terms of proper heat transfer rate) at the ground top surface. The first 4 out of 94 hours TRT simulation are devoted to fluid circulation inside the pipes without heat rate, as in real TRTs. Three different coaxial borehole lengths are considered (H_b=150, 400 and 800 m) for assessing the borehole length influence on the BHE performance and conductivity back estimation. The three coaxial borehole heat exchangers have different working conditions as reported in Table 4. This choice aim to have the same fluid temperature difference on the ground top and the same heat transfer rate per unit length injected into the ground (namely 40 W/m) during the TRT numerical experiments (cases 150/40, 400/40, 800/40 in Table 4). Three different undisturbed ground temperature profile types are considered. They are graphically shown in Figure 12. A constant 0.02 K/m ground temperature gradient has been considered, that can be found for example in Italian lithologies, even for deep boreholes (e.g. Della Vedova et al., 2015). Further simulations have been performed considering a 0.03 K/m and a 0 K/m geothermal gradient to study its influence on the numerical solutions. The nil geothermal gradient is a rather realistic value as it can be found for example in Norwegian lithologies which are characterized by such vertical ground temperature profile, even for deep boreholes (e.g. Holmberg et al., 2018). Nine of the eighteen simulations have been performed considering the inner pipe as the fluid inlet pipe. The remaining nine simulations have been performed considering the annular pipe as the fluid inlet pipe. This is to study the hydraulic configuration influence on the predicted fluid temperatures. In particular, it is of interest to investigate if the direction of the carrier fluid could influence the TRT ground thermal conductivity estimation adopting the ILS interpretative model.

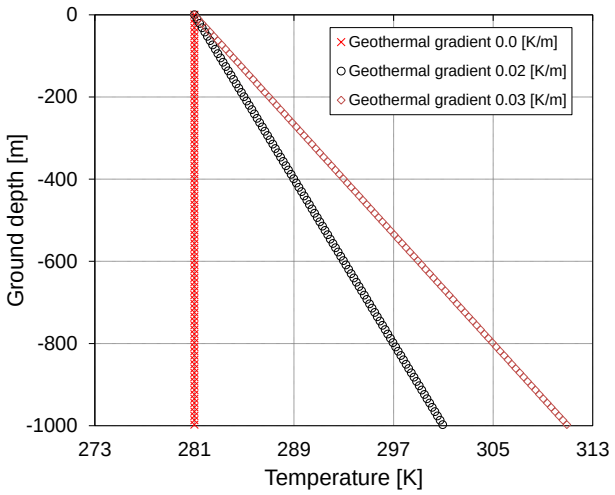

Figure 12 The three undisturbed ground temperature profile types considered for the numerical simulations.

Table 4 Geometry and operating conditions for 150m, 400m and 800m coaxial BHE

Input data	Case 150/40	Case 400/40	Case 800/40
Borehole length	150 m	400 m	800 m
Borehole diameter	0.140 m	0.140 m	0.140 m
Center pipe inner	0.09 m	0.09 m	0.09 m

diameter			
Center pipe wall thickness	0.008 m	0.008 m	0.008 m
Annular pipe inner diameter	0.139 m	0.139 m	0.139 m
Annular pipe wall thickness	0.0004 m	0.0004 m	0.0004 m
Center pipe thermal conductivity	0.42 W/mK	0.42 W/mK	0.42 W/mK
Annular pipe thermal conductivity	0.42 W/mK	0.42 W/mK	0.42 W/mK
Fluid temperature difference on the top	3 K	3 K	3 K
Heat load	6000 W	16000 W	32000 W
Ground thermal conductivity	3 W/mK	3 W/mK	3 W/mK
Ground thermal diffusivity	10^{-6} m^2/s	10^{-6} m^2/s	10^{-6} m^2/s

It is worth noticing that the section area (center and annulus) of the coaxial BHEs has a dimension that guarantees the same fluid mean velocity in each pipe (consequently the same *Co* in each pipe).
The grid properties and the numerical domain extension for each simulation type have been reported in Table 5.

Table 5 Grid meshing properties characterizing the numerical simulations

Grid data	**150 m BHE data**	**400 m BHE data**	**800 m DBHE data**
Domain end radial r-coordinate	3.2 m	3.2 m	3.2 m
Domain end axial z-coordinate	157.5 m	420 m	840 m
Number of partitions along the radial direction	30	30	30
Finite increment Δz	1.97 m	5.25 m	10.5 m
Time step $\Delta\tau$	10.51 s	10.51 s	10.51 s

The domain extension has been chosen to ensure that the overall ground volume is large enough for describing the far field persistency of the initial temperature profile, as discussed in (Morchio and Fossa, 2019).

2.2.3 Results and discussion

For all the TRT numerical simulations of the present study, it has been investigated the applicability of the ILS model to estimate the k_{gr} ground thermal conductivity value set in the program input file. The parametric analysis has been done for three length types by varying the geothermal gradient of the undisturbed ground temperature profile. The

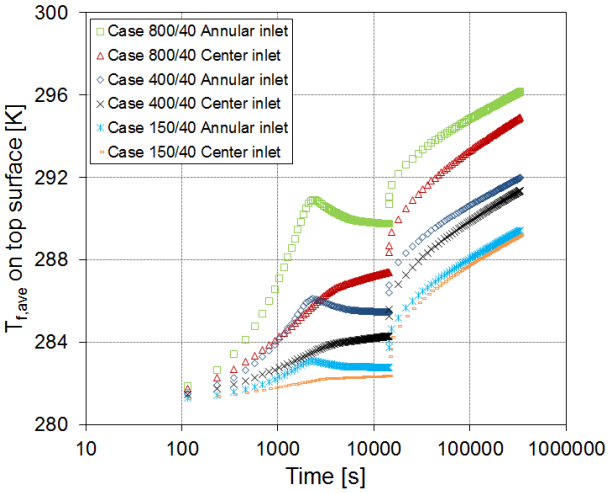

Figure 13 Fluid mean temperature computed on the top during time for cases 800/40, 400/40, 150/40 considering the two different hydraulic configurations.

logarithmic trend line of the computed $T_{f,\,ave}$ profiles has been obtained ignoring the time relating to the initial thermal transient of the order of Fo_{rb}=10. Its slope is used to derive the ground thermal conductivity k_{gr} (Eq. 30). This procedure has been implemented to investigate if the ILS model is a suitable TRT approach also for the coaxial DBHEs. In such a way it is possible to deduce the borehole length influence and the effect operated by the different hydraulic configurations (the annular inlet versus the center inlet) on the performance of the coaxial BHE from simulations results.

2.2.4 The borehole length and the hydraulic configuration influence

The linear undisturbed ground temperature profile type related to the constant and positive geothermal gradient of 0.02 K/m is considered and set as the initial condition of the problem.

Figure 13 refers to different BHE lengths and all simulations have been carried out with the same initial period during which the fluid is circulated without heating and the remaining period at a constant heat transfer rate. The sudden increase in temperature is associated with the beginning of the heat injection in the fluid (and into the ground). By

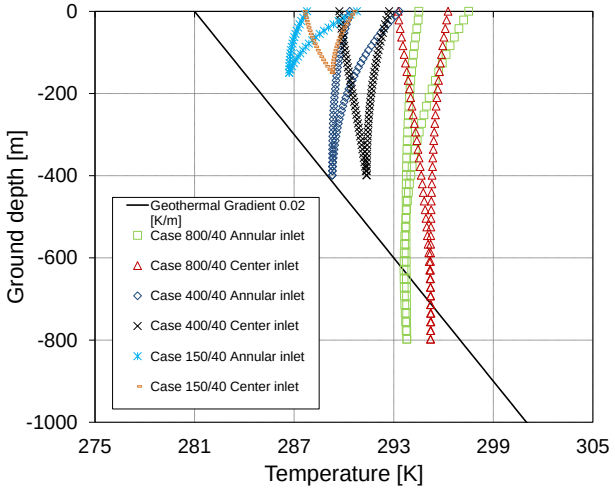

Figure 14 Fluid temperature profiles along the z direction at the end of the TRT (90 hours of heat injection into the ground) adopting two different hydraulic configurations for cases 800/40, 400/40, 150/40.

observing Figure 13 it is possible to notice that the fluid temperature trends of the 150 m BHE exhibit similar values for both the hydraulic configurations while differences arise for the 400 and 800 m DBHEs. Focusing on the 400 and 800 m DBHE, the fluid mean temperature difference between the two hydraulic configurations is higher than that of the 150 m BHE at the end of the circulation phase (without any heat transfer rate conferred to the carrier fluid). This means that for the coaxial DBHE the choice of the hydraulic configuration is more relevant than in the case of the conventional 150 m coaxial BHE since it determines a better thermal working condition, as stressed also by (Holmberg et al., 2016) and (Fang et al., 2018).

If the general goal is heat extraction from the ground it is more suitable to use the annular inlet hydraulic configuration for the coaxial DBHE because of the higher fluid outlet temperatures. Viceversa, if the general aim is the heat injection to the ground it is

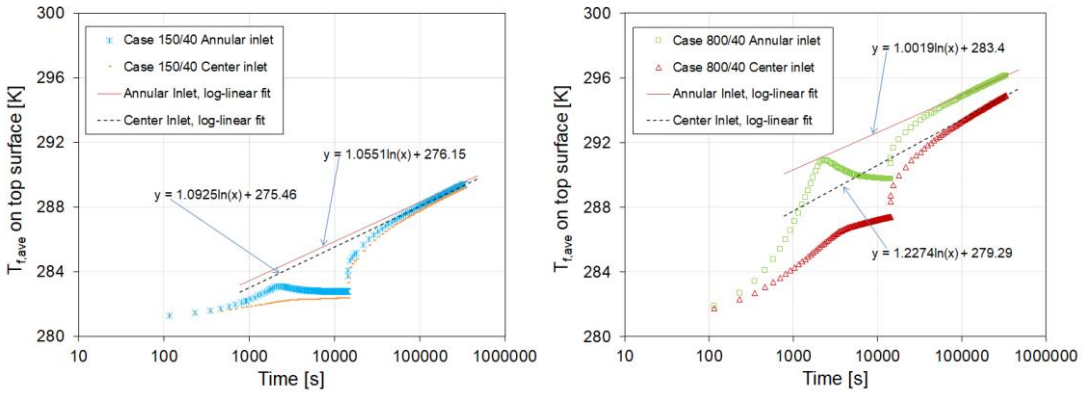

(a) (b)

Figure 15 Ground thermal conductivity estimation for cases 150/40 (left) and 800/40 (right) in two different hydraulic configurations.

preferable to adopt the center inlet hydraulic configuration for the coaxial DBHE since the fluid outlet temperature is lower. Figure 14 shows the different fluid temperature distributions along the *z*-direction in each pipe at the end of the TRT and the different outlet temperature value of both hydraulic configurations. It is apparent from Figure 14 inspection that for deep BHEs (400 and 800m) the fluid temperature can cross the undisturbed temperature profile, causing some heat rate inversion at the bottom end of the heat exchanger, since the fluid itself is no longer warmer than the (undisturbed) ground when the geothermal gradient is positive and the BHE sufficiently deep.

By applying the ILS model it is possible to derive the k_{gr} value considering the fluid mean temperature on the top surface during time after the initial thermal transient of the order of Fo_{rb}=10. The k_{gr} value estimation procedure applying the ILS model is shown in Figure 15 for cases 150/40 and 800/40. Figure 15 shows immediately that the average fluid temperature (as estimated off-ground) exhibits different slopes when represented as a function of the logarithm of time. This is immediately a clue for different possible k_{gr} estimations based on different sets of fluid temperatures related to different hydraulic configurations. The reason for the different temperature slopes and profiles is related to the fluid direction since in coaxial BHEs the ground interacts with the annular leg only and annular fluid temperature depends on the fluid direction.

For all the cases the comparison between the estimated k_{gr} values and the percentage errors are reported in Table 6.

Table 6 Ground thermal conductivity values estimated using two different hydraulic configurations compared to the k_{gr} value in the program input file

Test Case	k_{gr} (input value)	k_{gr} (Center inlet)	% Error	k_{gr} (Annular inlet)	% Error
150/40	3.0 [W/mK]	2.91 [W/mK]	-2.9 %	3.02 [W/mK]	+0.6 %
400/40	3.0 [W/mK]	2.82 [W/mK]	-6.0 %	3.12 [W/mK]	+4.2 %
800/40	3.0 [W/mK]	2.59 [W/mK]	-13.5 %	3.18 [W/mK]	+5.9 %

For each test case, the percentage error in the k_{gr} estimation adopting the center inlet is greater than that of the annular inlet configuration. It has to be noted that as the borehole length increases the percentage error in the k_{gr} estimation increases for both hydraulic configurations. For the 800 m coaxial DBHE it is possible to obtain the correct k_{gr} value estimation only by adopting the annular inlet hydraulic configuration (case 800/40).
Another issue related to any TRT experiment is the choice of the proper duration of the experiment and the time window according to which to apply the ILS model. Here below are presented a series of results related to the selection of different time ranges for ILS data reduction applied to the 800/40 case.
Table 7 reports the ILS approach results on k_{gr} estimations by selecting different time windows for best-fit analyses devoted to temperature slope estimation (Eq. 30). Worth noticing, the time intervals in Table 7 do not necessarily have the same ending point (the 94^{th} hours).
Table 7 reveals that for any time window the Annular Inlet condition assures the best k_{gr} estimation in any case and that a reasonable error can be obtained also for shorter (and probably less expensive) experiments up to 54 hours.

Table 7 Ground thermal conductivity values estimated for different time intervals using two different hydraulic configurations compared to the k_{gr} value in the program input file

Time interval	k_{gr} (Center inlet)	% Error	k_{gr} (Annular inlet)	% Error
17.6-94 hours	2.59 [W/mK]	-13.5 %	3.18 [W/mK]	+5.9 %
17.6-50 hours	2.59 [W/mK]	-13.5 %	3.22 [W/mK]	+7.5 %
30-94 hours	2.62 [W/mK]	-12.6 %	3.18 [W/mK]	+5.9 %
50-94 hours	2.64 [W/mK]	-12.1 %	3.16 [W/mK]	+5.4 %
74-94 hours	2.65 [W/mK]	-11.7 %	3.15 [W/mK]	+5.1 %
54-74 hours	2.63 [W/mK]	-12.3 %	3.17 [W/mK]	+5.6 %
34-54 hours	2.61 [W/mK]	-13.1 %	3.19 [W/mK]	+6.4 %
14-34 hours	2.59 [W/mK]	-13.5 %	3.26 [W/mK]	+8.8 %

Another interesting evidence from Table 7 analysis is that the center inlet and annular inlet show the same trends in error distribution as a function of the time window, namely when percentage error on the k_{gr} estimation is minimum for one hydraulic configuration, the same happens for its counterpart.

The next section further investigates the results presented so far by inserting a new variable in the problem which is the undisturbed ground temperature profile, represented by its geothermal gradient.

2.2.5 The geothermal gradient influence on the DBHE thermal behavior

In this sub-section, two different undisturbed ground temperature profiles are taken into account. The 0 K/m and the 0.03 K/m geothermal gradients have been assigned to the undisturbed ground temperature profile. The 0.03 K/m case is characterized by temperature profiles very similar to the previous 0.02 K/m case.

Very interesting are the evidence related to the condition when the undisturbed temperature is constant in depth (0 K/m gradient). Figure 16 shows the fluid temperature profiles as available off-ground for the 3 different BHE depths. It can be noticed that no substantial

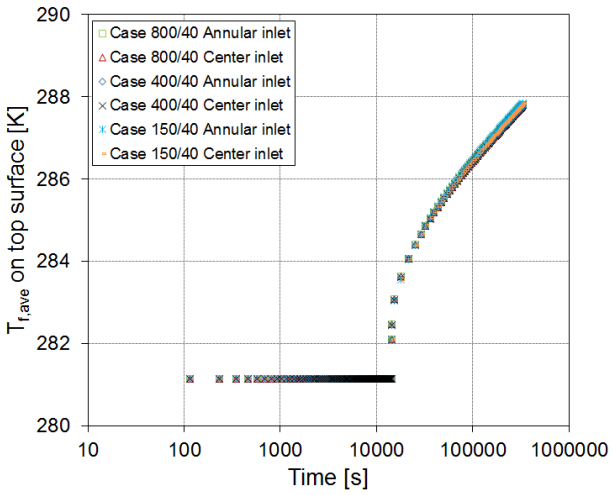

Figure 16 Fluid mean temperature computed on the top during time for cases 800/40, 400/40, 150/40 considering a 0 K/m geothermal gradient temperature initial profile and two different hydraulic configurations.

difference appears in fluid temperatures even if the BHE length and hydraulic configuration are changed. Both hydraulic configurations produce almost the same fluid mean temperature solutions for all BHE lengths. As a consequence of this fact also the k_{gr} values (as again estimated by the ILS approach) are not affected by the choice of the hydraulic configuration (Table 8).

The k_{gr} value estimation procedure applying the ILS model and the comparison between the related k_{gr} values and the percentage error is reported in Table 8 for all the cases. The two different geothermal gradient initial profiles (the 0 and the 0.03 K/m gradients) have been considered, representing those gradients as the limiting cases of the present investigation. The ILS model is here used with a time window starting from Fo_{rb}=10 to the end of the 94 hours experiment.

Table 8 Ground thermal conductivity values estimated using two different hydraulic configurations compared to the k_{gr} value in the program input file.

Test Case	Geothermal gradient	k_{gr} (input value)	k_{gr} (Center inlet)	% Error	k_{gr} (Annular inlet)	% Error

150/40	0.0 K/m	3.0 [W/mK]	3.04 [W/mK]	+1.5 %	3.04 [W/mK]	+1.5 %
400/40	0.0 K/m	3.0 [W/mK]	3.05 [W/mK]	+1.6 %	3.05 [W/mK]	+1.7 %
800/40	0.0 K/m	3.0 [W/mK]	3.05 [W/mK]	+1.7 %	3.05 [W/mK]	+1.7 %
150/40	0.03 K/m	3.0 [W/mK]	2.92 [W/mK]	-2.6 %	3.09 [W/mK]	+3.0 %
400/40	0.03 K/m	3.0 [W/mK]	2.72 [W/mK]	-9.5 %	3.16 [W/mK]	+5.4 %
800/40	0.03 K/m	3.0 [W/mK]	2.44 [W/mK]	-18.8 %	3.27 [W/mK]	+9.0 %

It is apparent from Table 8 inspection that the k_{gr} value estimation is not affected by the hydraulic configuration when the geothermal gradient is set to 0 K/m. As seen in the previous Section, when the geothermal gradient is constant and positive, k_{gr} estimations change as the borehole length increases. The percentage error in the k_{gr} estimation adopting the center inlet is greater than that of the annular inlet configuration in presence of a constant and positive geothermal gradient. It has to be noted that the highest percentage error on the k_{gr} estimation is for the center inlet of the 800/40 case, while the lowest is for the annular inlet configuration of the 150/40 case as the gradient is set to 0.02 K/m. As final information, the maximum error in k_{gr} estimation for gradient set to 0.02 K/m has been found again for the 800/40 center inlet case and resulted to be - 13.5 % for the same time window.

2.3 The FD Models for the performance analyses of single and double U-pipe BHE and DBHE

A new hybrid model for the analysis of U-pipe thermal behavior has been proposed and presented in the present section. The model calculates transient temperature profiles in single and double U-BHEs. The model is validated against real TRTs data, numerical and analytical models. New thermal weighting factors have been introduced for describing the U-BHE types. The uncertainty related to the grout volumetric heat capacity has been studied.

In many applications related to the GCHP, the short-term response of the BHE gets the same importance as the long-term response in terms of the efficiency of the whole system. The need to reconstruct numerical TRTs using simulation tools capable of reproducing in a reliable way the thermal transient of single and double U pipes while employing reasonably short computational times has been a research topic in the geothermal field during recent years. Therefore, several analytical and numerical models have been developed in recent years to study the thermal transient behavior of U-BHE. The accurate modeling and simulation of the complex transient 3D transport phenomena of U-tube BHEs is a complicated and intricate procedure. To this aim, it is possible to refer to fully discretized BHE models that use design tools based on finite element or finite volume programs often implemented in commercial software packages. The fully discretized models (FEM) lead to extensive computation times while precise and accurate results are achieved. Through the FEM models, a complete representation of the real 3D heat transfer problem related to the U-BHE can be obtained as presented in recent studies by (Signorelli et al., 2007, Clausen, 2008, He et al., 2009, Lamarche et al., 2010, Fossa et al., 2013). FEM models are also favorably adopted and implemented in commercial software (Comsol, Ansys Multiphysics) since allow to easily build non-mapped meshes. On the contrary, the FD models require only mapped meshes and usually a 2D geometry when the BHE

analysis is performed. Other models follow a two-dimensional (2D) horizontal description of the borehole (Yavuzturk et al., 1999, Austin et al., 2000). Analytical models are simpler and attractive since they involve reduced computation times, but they neglect the short-time thermal behavior related to the convective energy transport of the carrier fluid in the borehole. Among the analytical models, the ILS model first proposed by (Ingersoll et al., 1955), provides the simplest 1D solution of the heat conduction problem that characterizes the ground surrounding the borehole, while the main advantage is that the knowledge of the real BHE geometry is not needed. The same model can be applied by adding the effective borehole resistance introduced (by Mogensen, 1983) and (Hellstrom, 1991) to the ILS expression resulting in the most complete and effective model to analyze also the carrier fluid thermal transient behavior during the TRT, as presented in the study of (Bae et al., 2011). (Beier, 2014) proposed an analytical model to calculate the transient vertical temperature profiles in U-tube borehole heat exchanger and the temperature distribution in the ground. Several Authors referred to semi-analytical models based on the Delta-circuit thermal resistance network, like those of (Hellstrom, 1991) and (Zeng et al., 2003). The steady-state description of the Delta-circuit models is not valid for variations on a dimensionless time window below $Fo_{rb}=5$ (Eskilson, 1988) as also clarified more recently by (Fossa, 2011). A first step to extend the range of validity to shorter Fo_{rb} windows is represented by the RC models that take into account the capacity of the grouting material. In this way, the carrier fluid thermal transient behavior related to shorter times can be better detected by RC models, like the CaRM model by (Zarrella et al., 2011). Other examples of RC models found in literature are those presented by (Minaei and Maerefat, 2017) and (Calvo et al., 2015). Also the different U-pipe locations into the borehole assume an important role in the thermal performance of U-BHE, as discussed and analyzed by (Zhang et al., 2019). The RC model proposed by (Bauer et al., 2011) uses an explicit finite difference approach as presented in (Bauer et al., 2011). The approach of the present model is similar to the one presented by (Bauer et al., 2011), but an implicit finite difference scheme is adopted. In this study, a new hybrid FD/RC model aimed to analyze the thermal transient behavior of the single and double U-BHE has been developed and presented. The FD models combined with the RC models represent according to the present Authors a powerful approach to combine the advantages of both types of models, in order to ensure the good accuracy of the results also for very short times. The simplified hypotheses related to the hybrid models (FD/RC) lead to computational times shorter than those of the FEM models ones. Although the hybrid models are not suitable to completely detect the physics of the real 3D thermal transient behavior inside and around the BHE, they allow to obtain sufficiently precise fluid, grout and ground temperature profiles along time as well as depth. As demonstrated by the present study, the problem-solution related to the present hybrid model developed by the Authors shows a very good agreement with the fully discretized FEM models and also with data sets from real TRT experiments. The new hybrid model for the single and double U-BHE together with the one developed for the Coaxial BHE and described in a couple of recent papers by the present Authors (Morchio and Fossa, 2019, Morchio and Fossa, 2020) provide a more complete view for modeling the geothermal system in GCHP applications.

Suitable criteria related to a new hybrid RC scheme have been employed in the present FD-2D model to describe the thermal transient behavior of the U-pipe BHE as well as that of the surrounding ground. A detailed description of these criteria is provided by the present study as an original contribution to the existing literature. The above literature analysis shows that the grout thermal properties and the U-pipe locations into the borehole

assume an important role in the thermal performance of the U-BHE, but comprehensive and systematic studies on the influence of such parameters on predictions of TRT measurements seem to be lacking in literature. One of the aims of this study is hence to investigate how the uncertainty related to the knowledge of the grout thermal properties can affect the good accuracy of the numerical results. In particular, a new thermal weighting factor has been specifically introduced, as the first step of the analysis provided by the present study, to analyze the influence of the uncertainty related to the grout volumetric heat capacity $(\rho c)_{gt}$ value. The new thermal weighting factor is used to compensate for the uncertainty source related to the knowledge of the exact $(\rho c)_{gt}$ value in order to provide very close agreement among predictions and measurements also for very short times of the TRT.

The model solves the 2D Fourier equation in the ground domain by discretizing the differential equations. The FD scheme has been employed for each volume of the ground domain which assumes a two-dimensional cylindrical axisymmetric geometry. The BHE-domain (that is composed of the fluid, grout, borehole wall nodes, and the related volumes) is described by the RC scheme coupled with the FD description of the vertical energy transfers (of conduction for the borehole wall and grout volumes and convection for the fluid volumes) between adjacent nodes. The present model can be employed also to calculate the transient vertical temperature profiles in U-BHE (fluid, grout and borehole wall) and the temperature distribution in the ground.

The numerical simulations are devoted to analyzing the thermal and hydrodynamic behavior of the single and double-U tube types for different borehole lengths and different operating conditions. The results are validated by comparison with real experimental TRT measurements as well as against the analytical U-pipe model by (Beier, 2014). Additional validations (not reported in the present dissertation for the sake of brevity) are constituted by those obtained against the numerical ANSYS reference simulations and against the RC model by (Bauer et al., 2011).

A brief analysis aimed at the correct placement of the grout thermal capacitance in terms of the local temperature node, to be located somewhere in between the pipe surface and the BHE periphery, is reported in the present study. It also describes how to choose these allocations by varying appropriate weighting factors specifically introduced in the FD/RC model.

2.3.1 Modelling the outer ground and the single and double U-pipe heat exchanger

The present model has been developed by the Authors for describing the thermal transient of the fluid (and grout) as well as that of the ground surrounding the single and double U-pipe BHE. A two- dimensional finite difference discretization of the Fourier equation is applied to the ground volume, with an implicit scheme under the assumption of a two-dimensional cylindrical axial-symmetric geometry.

The inner borehole is here described through a combination of one-dimensional balance equations, including the discretization of the differential form of the energy equation for the fluid and grout volumes and a network of thermal resistance and capacitances for describing the radial heat flow inside the solid volume represented by the plastic pipe and grout volumes. An upwind energy balance is applied to the fluid volumes in order to model the convective energy transport of the carrier fluid. The FD discretization is hence coupled with a thermal resistance and capacitance (RC) network, thus leading to a hybrid FD/RC approach. Figure 17 shows the fluid, grout and ground nodes placed in the (r,z) plane. Up to $r=r_b$ the thermal resistance/capacitance model applies. The surrounding ground is

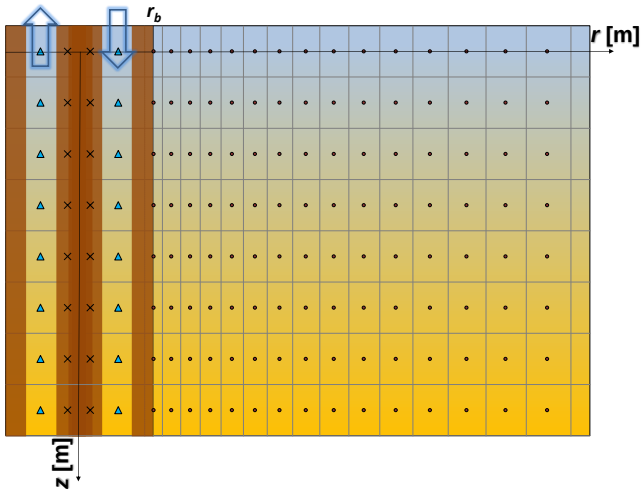

Figure 17 BHE and ground domains.

described as an axisymmetric domain where the Fourier equation is solved with the finite difference approach. The dotted points (ground nodes) denote the ground domain area characterized by the FD scheme calculation, while the triangular and cross-shaped symbols (the fluid and grout nodes respectively) denote the BHE-domain area where the thermal resistance and capacitance network model is applied. It has to be noted that the inner BHE nodes do not have any radial coordinate since the real cylindrical axisymmetric geometry concerns the surrounding ground (borehole wall included).

Far-field boundary conditions (namely BC1 and BC2), ground and pipe meshing, and Courant number, *Co*, have been varied for enhancing the accuracy in predicting the fluid temperature evolution, as described in detail in (Morchio and Fossa, 2019, Morchio and Fossa, 2020, Beier et al. 2020).

$$\text{BC1:} \begin{cases} T(r,0,\tau) = T_{gr}(0) \;\forall\; r \geq r_b \\ T(r_{max},z,\tau) = T_{gr}(z) \\ \left.\frac{\partial T(r,z,\tau)}{\partial z}\right|_{z=z_{max}} = 0 \end{cases} \tag{32}$$

$$\text{BC2:}\begin{cases} T(r,0,\tau) = T_{gr}(0)\ \forall\ r \geq r_b \\ \left.\frac{\partial T(r,z,\tau)}{\partial r}\right|_{r=r_{max}} = 0 \\ \left.\frac{\partial T(r,z,\tau)}{\partial z}\right|_{z=z_{max}} = 0 \end{cases} \quad (33)$$

$$Co = \frac{w_f \Delta\tau}{\Delta z} \quad (34)$$

The initial undisturbed ground temperature profile *T(r,z,0)* can be imposed constant and uniform (along the *z*-direction), as well as different geothermal gradients or any type of function $T_{gr}(z)$ (or user-defined point series), can be applied as the initial condition for all the calculation domain.

Initial condition: $\tau = 0; \quad T(r,z,0) = T_{gr}(z)$ (35)

2.3.2 The outer ground as a finite difference scheme of the Fourier Equation

The ground domain volume, the related geometry and discretization, as well as all the general functions solved by the Fortran program, are the same ones employed in the Coaxial model reported in recent papers by the present Authors (Morchio and Fossa, 2019, Morchio and Fossa, 2020, Beier et al. 2020) and that demonstrated to be robust and very accurate with respect to available literature TRT measurements.

The transient 2-D Fourier heat conduction equation in cylindrical axisymmetric geometry is written in an implicit form for each volume of the ground domain. This leads to writing, as finite difference form:

$$\frac{T_{i,j}^{n+1} - T_{i,j}^{n}}{\Delta\tau} = \left(\frac{2\alpha_{gr,j}}{r_i \Delta r_i}\right)\left[B_1 T_{i+1,j}^{n+1} - (B_1 + B_2) T_{i,j}^{n+1} + T_{i-1,j}^{n+1} B_2\right] + \frac{(2\alpha_{gr,j+1})}{\Delta z_j}\frac{(T_{i,j+1}^{n+1} - T_{i,j}^{n+1})}{\Delta z_j + \Delta z_{j+1}} - \frac{(2\alpha_{gr,j})}{\Delta z_j}\frac{(T_{i,j}^{n+1} - T_{i,j-1}^{n+1})}{\Delta z_j + \Delta z_{j-1}} \quad (36)$$

Where:

$$B_1 = \frac{(r_i + \frac{\Delta r_i}{2})}{\Delta r_i + \Delta r_{i+1}} \quad (37)$$

$$B_2 = \frac{(r_i - \frac{\Delta r_i}{2})}{\Delta r_i + \Delta r_{i-1}} \quad (38)$$

The B_1 and B_2 terms in Eq. (36), (37) and (38) turn out from writing the transient energy balance equation for each ground volume and represent the ratio related to the finite difference discretization of the 2-D Fourier heat conduction equation along the radial direction. Variable (along the *z*-direction) ground thermal properties have been taken into account by Eq.(36) to represent the real heterogeneous lithology as well as groundwater seepage conditions.

The in-house-developed Fortran code has been built and validated to cope with variable *z*-

longitudinal and *r*-radial mesh distributions in the ground domain. The r_i-z_j coordinates of each node can follow user-defined patterns (specific functions or point series) and are linked to the related finite increment Δr_i and Δz_j as reported hereafter:

$$r_{i+1} = r_i e^{deltaprecision\left(\frac{2\pi H_b k_{gr}}{\dot{Q}}\right)} \quad (39)$$

$$r_i - r_{i-1} = \frac{\Delta r_i}{2} + \frac{\Delta r_{i-1}}{2} \quad (40)$$

$$z_j - z_{j-1} = \frac{\Delta z_j}{2} + \frac{\Delta z_{j-1}}{2} \quad (41)$$

$$r_{i+1} - r_i = \frac{\Delta r_i}{2} + \frac{\Delta r_{i+1}}{2} \quad (42)$$

$$z_{j+1} - z_j = \frac{\Delta z_j}{2} + \frac{\Delta z_{j+1}}{2} \quad (43)$$

The ILS analytical solution suggests that the heat diffusion in the ground has an "intrinsic log" nature. In this sense, the inter-distances between radial nodes are identified by the ILS-derived radial distribution law shown in Eq. (39). The expansion series of the exponential integral function truncated at the second term (Eq. 26) has been considered for the ILS analytical equation. The $H_b k_{gr}/\dot{Q}$ ratio comes from the ILS solution itself; k_{gr}, H_b and $\dot{Q}$ are inputs of the model. The parameter *deltaprecision* is an input of the present model and represents the temperature difference between two adjacent nodes as a tradeoff between reduced round-off errors and the node overall number.

2.3.3 The thermal resistance/capacitance scheme

An innovative approach in locating the thermal capacities of the grout nodes has been developed by the Authors. This constitutes an original contribution and the proposed method can be compared in terms of accuracy with the existent thermal resistance and capacities models. The present model has been extensively validated against analytical solutions and literature data, including those related to real TRT experiments, as described in the following sections of this study. The FD scheme used for each grout and fluid volume of the BHE-domain discretization is coupled with a thermal resistance/capacitance network. The "delta" configuration of the thermal resistance network inside the BHE has been adopted and the grout thermal capacitance has been taken into account for modeling the thermal transient of the single and double U-pipe configuration. The present modeling configuration is aimed at obtaining a very close description of the fluid temperature as distributed along the BHE depth in the very first hours from the start of the TRT experiment, included the pre-circulation phase (the adiabatic part).

Figure 18 schematically shows the horizontal section of the single and double U-pipe BHE,

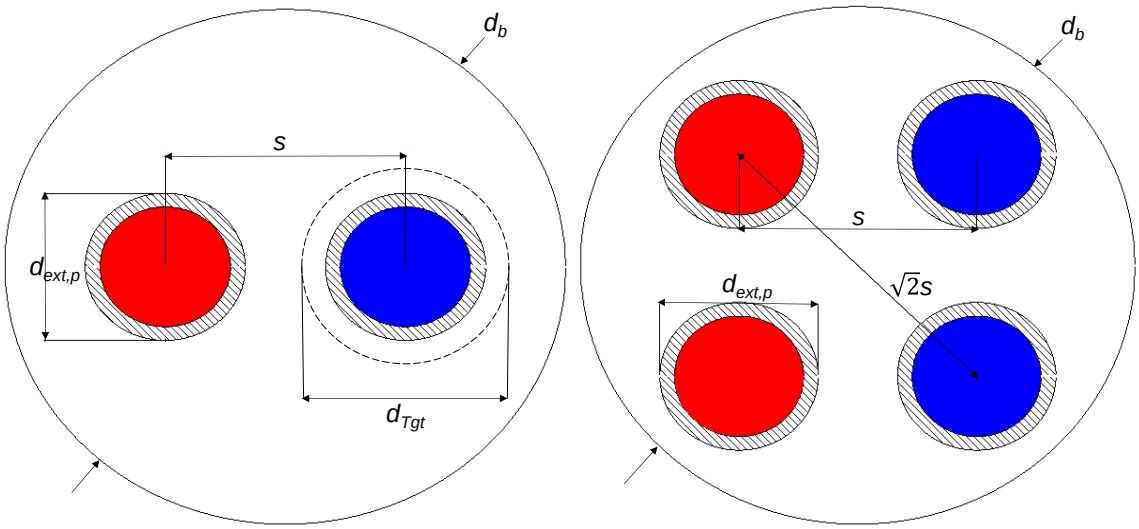

Figure 18 Cross section of the single and double U-pipe BHE, including the diameters and the shank spacing *s* definitions.

including the definition of the diameters and the shank spacing *s* (center-to-center inter-distance). Diameters d_b and $d_{ext,p}$ are related to real BHE geometries while diameter d_{Tgt} is a thermal parameter described in Eq. (79).

2.3.4 Single U-BHE modeling of borehole thermal resistance R_{bhe}

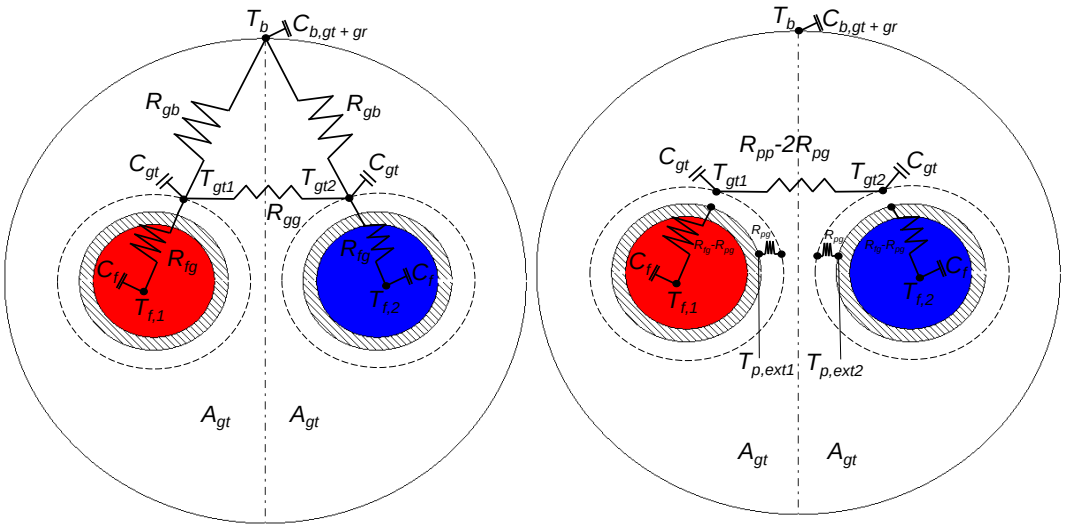

Figure 19 Electro-thermal analogy circuit employed in the present FD/RC model (a). Nodes T_{gt1} and T_{gt2} are located somewhere outside the pipe external wall according to the value assumed by the variable *Y* (Eq. 49). Auxiliary temperature nodes and resistances R_{pg} and R_{pp} (b).

In the case of single U-pipe, each BHE horizontal section (at each depth) is represented by

five nodes (two for the fluid domain volumes, three for the thermal capacitance of the grout material) connected by the thermal resistance network of the electro-thermal analogy (similar to the one proposed by Bauer et al., 2011). These nodes are represented in the related electro-thermal circuit shown in Figure 19a. It is worth noticing that in the present model, a thermal capacity (grout and ground) is also assigned to the node at the BHE wall. Another original contribution introduced by this model is the weighting factor X that handles the fraction of the total grout thermal capacitance assigned to each of the two internal nodes, the one outside the pipe wall and the one at the BHE periphery. In particular, C_{gt} accounts for the former node above, through the weight X that distributes the grout thermal mass on those nodes according to Eqs. (44) to (46).

$$A_{gt,tot} = \frac{\pi {d^2}_b}{4} - \frac{2\pi {d^2}_{ext,p}}{4} = \frac{\pi}{4}\left[d_b^2 - 2d_{ext,p}^2\right] \tag{44}$$

$$A_{gt} = \frac{A_{gt,tot}}{2} \tag{45}$$

$$C_{gt} = \rho_{gt} c_{gt} A_{gt,tot} X = \rho_{gt} c_{gt} \frac{\pi}{4}\left[d_b^2 - 2d_{ext,p}^2\right] X \tag{46}$$

The $A_{gt,tot}$ term represents the total grout area inherent to each horizontal section of the single U-BHE that is the BHE circumference area minus the two pipe circumference areas. The section A_{gt} that concerns each of the two grout nodes/volumes is used as the representative area of the heat transfer rate of conduction along the z-direction between adjacent grout nodes for both T_{gt1} and T_{gt2} (see section 2.3.7, Eq.(82) and (83)). Therefore, X can assume the following range of values: $0 \leq X \leq 0.5$. Specifically, $X=0.5$ means that nodes T_{gt1} and T_{gt2} equally share the whole grout thermal mass and no grout capacitance is applied to the BHE wall node. Worth noticing that $X=0.5$ is also the default value adopted in the RC model by (Bauer et al., 2011), even if that set of equations is written without introducing the variable X. When X is lower than 0.5 means that a fraction (or the total amount) of the total grout thermal capacitance is also assigned to each borehole wall node (identified by T_b) which generally "carries" the following thermal capacity:

$$C_{b,gt+gr} = [\rho_{gt} c_{gt} A_{gt,tot}(1 - 2X) + (\rho c)_{gr} r_b \Delta r_b \Delta\varphi] \tag{47}$$

X can be set in the input file of the present model. It has to be specified that all the simulation cases reported in the present study have been performed by assuming $X=0.5$.
Figure 19b shows the auxiliary temperature nodes $T_{p,ext1}$ and $T_{p,ext2}$ and the auxiliary resistances R_{pg} and R_{pp}. In particular, R_{pg} is the grout shell thermal resistance included inside the R_{fg} term, while R_{pp} is the equivalent thermal resistance between the outer walls of the two pipes. The definitions of the thermal resistances R_{fg}, R_{gb} and R_{gg} of the single U-BHE thermal capacitance circuit are reported hereafter:

$$R_{fg} = \frac{1}{2\pi r_{in,p} h} + \frac{\ln\left(\frac{r_{ext,p}}{r_{in,p}}\right)}{2\pi k_p} + Y R_{gt,total} \tag{48}$$

Where Y is the grout thermal resistance weighting factor introduced by the present model. Y is an input value of the present model used to derive the grout shell thermal resistance R_{pg} to be included inside the R_{fg} term:

$$Y = \frac{\ln\left(\frac{d_{gt}}{d_{eq}}\right)\frac{1}{2\pi k_{gt}}}{\ln\left(\frac{d_b}{d_{eq}}\right)\frac{1}{2\pi k_{gt}}} \tag{49}$$

It has to be specified that the d_{gt} diametral position does not correspond to the d_{Tgt} of Figure 18. The Y definition in Eq.(49) correctly denotes the ratio between the two conduction thermal resistances in cylindrical geometry. As a consequence, d_{gt} identifies the generic diametral position computed from the reference BHE axis of symmetry. The real equivalent grout and pipe area is taken into account through the d_{eq} concept. The value assumed by d_{gt} depends on the Y input value. The same Y ratio is used to derive the R_{pg} term as a Y fraction of $R_{gt,total}$ as represented by the last right-hand term of Eq.(48) that is related to the real U-pipe geometry. Thus the d_{Tgt} previously introduced in Figure 18 identifies the real diameter locations of the T_{gt1} and T_{gt2} nodes into the real BHE cross-section. The d_{Tgt} value depends on the same Y input value. In particular, Y can assume the following range of values: $0 \leq Y \leq 1$. Consequently, the d_{gt} diametral position which is evaluated from the BHE axis can assume (depending on the value assumed by Y) a value between $d_{eq} \leq d_{gt} \leq d_b$. Finally, Y is used to express the d_{Tgt} position assumed by each of the two grout nodes into the real single-U geometry and evaluated from the axis of each plastic pipe, as shown in Figures 18, 19a and 19b. More details will be given in sub-section 2.3.4 of the present study.

For the single-U BHE configuration, the equivalent diameter d_{eq} is evaluated according to the (Bauer et al., 2011) model suggestions:

$$d_{eq} = \sqrt{2} d_{ext,p} \tag{50}$$

The Y ratio is used to determine how much of the overall grout thermal resistance $R_{gt,total}$ is shared between resistances R_{fg} and R_{gb}. $R_{gt,total}$ on the other hand is the overall grout thermal resistance that many Authors, starting from (Hellstrom, 1991) and (Zeng et al., 2003), have proposed in a series of correlations based on BHE geometry and grout thermal conductivity. In the present study the following correlation (Bauer et al., 2011) is employed (for the single U-BHE):

$$R_{gt,total} = \frac{arcosh\left[\frac{d_b^2 + d_{ext,p}^2 - s^2}{2 d_b d_{ext,p}}\right]}{2\pi k_{gt}} \left(1.601 - 0.888 \frac{s}{d_b}\right) \tag{51}$$

In general, the $R_{gt,total}$ empirical correlations for single and double U-BHE have been obtained by adding correction terms gained from numerical simulations to well-known two-dimensional heat conduction shape factors. It has to be noted that the present empirical

correlations for computing $R_{gt,total}$ could be replaced by other $R_{gt,total}$ literature correlations. Once the parameter Y is defined, it can be also used to calculate the grout shell thermal resistance R_{pg} located in between the auxiliary temperature nodes $T_{p,ext}$ and T_{gt} (see Figure 19b):

$$R_{pg} = YR_{gt,total} \tag{52}$$

As a consequence the counterpart thermal resistance R_{gb} between node T_{gt} and node T_b is calculated as follows (for the single U-BHE):

$$R_{gb} = R_{gt,total}(1 - Y) \tag{53}$$

A brief explanation of the mathematical passages necessary to derive R_{gg} is needed. Indeed, the thermal resistance R_{pp} between the outer walls of the two pipes (see Figure 19b) has to be introduced to derive R_{gg}. R_{pp} can be computed if the two-dimensional heat conduction shape factor for two parallel long cylinders in an infinite medium is applied (Incropera and DeWitt, 2002):

$$R_{pp} = \frac{arcosh\left[\frac{2s^2 - d_{ext,p}^2}{d_{ext,p}^2}\right]}{2\pi k_{gt}} \tag{54}$$

R_{gg} can be derived as a function of the above R_{pg} and R_{pp} parameters by taking into account the series/parallel configuration of this sub-network of thermal resistances (Figures 19a and 19b):

$$R_{pp} - 2R_{pg} = \left[\frac{1}{R_{gg}} + \frac{1}{2R_{gb}}\right]^{-1} \tag{55}$$

Hence,

$$R_{gg} = \frac{2R_{gb}(R_{pp} - 2R_{pg})}{2R_{gb} - R_{pp} + 2R_{pg}} = \frac{2R_{gt,total}(1-Y)(R_{pp} - 2YR_{gt,total})}{2R_{gt,total}(1-Y) - R_{pp} + 2YR_{gt,total}} \tag{56}$$

2.3.5 Double U-BHE modeling (parallel flow)

One of the main assumptions under the double U-BHE of the present model is that the twin U-pipes are hydraulically operating in parallel, i.e at any vertical position (including the inlet and outlet fluid sections) each couple of pipes is characterized by the same fluid temperatures. The thermal resistance-capacitance circuit and the thermal resistance and capacitance definitions are properly modified and adapted for the new "equivalent single U" configuration (ESU-pipe in the following), as shown in Figure 20. It has to be specified that the new thermal resistance and grout capacitance definitions employ the actual geometry values ($r_{in,p}$, $r_{ext,p}$, s) of each pipe of the double-U BHE for their computation. The convective heat transfer coefficient that concerns the fluid flowing in each pipe is

based on the real fluid velocity inside each leg of the real four pipes BHE. In such a way the double U-pipe geometry can be represented again by two pipes only and hence like a single U-pipe having the overall mass flow rate and fluid velocity equal to those of each pipe of the original double U-pipe configuration, as described by Eq.(57) and (58):

$$\dot{m}_{ESU} = \dot{m}_{2U} \tag{57}$$

$$\rho_f w_{f,2U} \pi r_{in,p,ESU}^2 = 2\rho_f w_{f,2U} \pi r_{in,p,2U}^2 \tag{58}$$

To this aim, the following Eq. (59) shows the pipe inner radius value employed in the energy balance equation for each fluid volume (the pipe wall thickness is the same as the original double-U pipe):

$$r_{in,p,ESU} = \sqrt{2} r_{in,p,2U} \tag{59}$$

The mass flow rate in the ESU pipe is the one flowing in the real double U-BHE in order to fulfill the energy conservation equation and the real heat transfer rate $\dot{Q}$ conferred (or extracted) to the carrier fluid on the top ground surface that is the same for both the double and single ESU pipes.

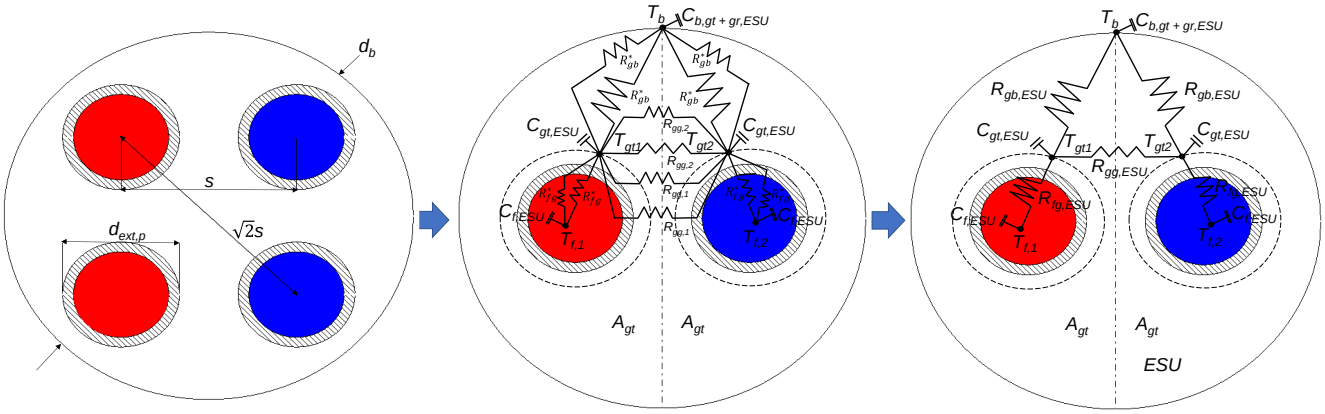

Figure 20 Temperature nodes, thermal resistances and capacitances employed in the double U pipe model and its ESU corresponding thermal network.

The grout thermal capacitance assigned to each of the two internal nodes $C_{gt,ESU}$ representing the grout inside the BHE, the $A_{gt,tot}$ term that represents the total grout area inherent to each horizontal section of the double U-BHE, the section A_{gt} that concerns each of the two grout nodes/volumes and used for computing the heat transfer rate of conduction along the *z*-direction between adjacent grout nodes for both T_{gt1} and T_{gt2} are expressed as follows:

$$A_{gt,tot} = \frac{\pi d^2{}_b}{4} - \frac{4\pi d^2{}_{ext,p}}{4} = \frac{\pi}{4}\left[d_b^2 - 4d_{ext,p}^2\right] \tag{60}$$

$$A_{gt} = \frac{A_{gt,tot}}{2} \tag{61}$$

$$C_{gt,ESU} = \rho_{gt} c_{gt} A_{gt,tot} X = \rho_{gt} c_{gt} \frac{\pi}{4} \left[d_b^2 - 4 d_{ext,p}^2 \right] X \tag{62}$$

X can assume values ranging from 0 to 0.5 and its physical meaning is the same as single U pipe case. Being the ESU-pipe configuration almost the same as the single U-BHE, the concepts and the related equations are also almost the same as the single U-BHE. The only adaptations with respect to the single U-BHE configuration are expressed by the following expressions:

$$d_{eq,ESU} = 2 d_{ext,p} \tag{63}$$

$$Y_{ESU} = \frac{\ln\left(\frac{dgt,ESU}{d_{eq,ESU}}\right)\frac{1}{2\pi k_{gt}}}{\ln\left(\frac{d_b}{d_{eq,ESU}}\right)\frac{1}{2\pi k_{gt}}} = \frac{\ln\left(\frac{dgt,ESU}{2 d_{ext,p}}\right)}{\ln\left(\frac{d_b}{2 d_{ext,p}}\right)} \tag{64}$$

$$R_{gt,total,ESU} = \frac{arcosh\left[\frac{d_b^2 + d_{ext,p}^2 - s^2}{2 d_b d_{ext,p}}\right]}{2\pi k_{gt}} \left(3.098 - 4.432 \frac{s}{d_b} + 2.364 \frac{s^2}{d_b^2} \right) \tag{65}$$

The last Eq.(65) is employed according to (Bauer et al., 2011) model suggestions. As in the case of the single U pipe, the Y_{ESU} definition in Eq.(64) correctly denotes the ratio between the two conduction thermal resistances in cylindrical geometry. As a consequence, $d_{gt,ESU}$ identifies the generic diametral position computed from the reference BHE axis of symmetry. The real equivalent grout and pipe area is taken into account through the $d_{eq,ESU}$ concept. The value assumed by $d_{gt,ESU}$ depends on the Y_{ESU} input value.
Although the shape factors for more than two isothermal surfaces are not available, the same Eq.(54) adopted for the single U-BHE has been employed also for computing the thermal resistances between the outer walls of two pipes $R_{pp,1}$ (side by side) in case of double U-BHE pipe. This is because in the present model the double U-pipe geometry has been collapsed into the above ESU configuration. The thermal resistance between the outer walls of the other two pipes $R_{pp,2}$ (crosswise) is based on the geometrical proportion related to the two different shank spacings characterizing the double U configuration:

$$R_{pp,2} = \sqrt{2} R_{pp,1} \tag{66}$$

The remaining equations of the double U-BHE model are reported in summary hereafter:

$$R_{pg,ESU} = Y_{ESU} R_{gt,total,ESU} \tag{67}$$

$$R_{fg}^* = \frac{1}{2\pi r_{in,p} h} + \frac{\ln\left(\frac{r_{ext,p}}{r_{in,p}}\right)}{2\pi k_p} + R_{pg,ESU} = \frac{1}{2\pi r_{in,p} h} + \frac{\ln\left(\frac{r_{ext,p}}{r_{in,p}}\right)}{2\pi k_p} + Y_{ESU} R_{gt,total,ESU} \tag{68}$$

The same Y_{ESU} ratio is used to derive the $R_{pg,ESU}$ term as a Y_{ESU} fraction of $R_{gt,total,ESU}$ as represented by Eq.(67) that is related to the real U-pipe geometry.

$$R_{fg,ESU} = \frac{R^*_{fg}}{2} \tag{69}$$

$$R^*_{gb} = R_{gt,total,ESU}(1 - Y_{ESU}) \tag{70}$$

$$R_{gb,ESU} = \frac{R^*_{gb}}{2} \tag{71}$$

Each pipe of the ESU configuration identifies the two pipes of each fluid column (hot or cold) of the real double-U BHE which are characterized by the same and univocal fluid temperature at each *z*-depth (main assumption of parallel flow). For this reason, there are only two (and not four) $R_{gg,1}$ thermal resistances side by side among the two couples of pipes pertaining to the two fluid columns (hot and cold).

$$R_{gg,1} = \frac{2R^*_{gb}\left(R_{pp,1} - 2R_{pg,ESU}\right)}{2R^*_{gb} - R_{pp,1} + 2R_{pg,ESU}} = \frac{2R_{gt,total,ESU}(1-Y_{ESU})\left(R_{pp,1} - 2Y_{ESU}R_{gt,total,ESU}\right)}{2R_{gt,total,ESU}(1-Y_{ESU}) - R_{pp,1} + 2Y_{ESU}R_{gt,total,ESU}} \tag{72}$$

$$R_{gg,2} = \frac{2R^*_{gb}\left(R_{pp,2} - 2R_{pg,ESU}\right)}{2R^*_{gb} - R_{pp,2} + 2R_{pg,ESU}} = \frac{2R_{gt,total,ESU}(1-Y_{ESU})\left(R_{pp,2} - 2Y_{ESU}R_{gt,total,ESU}\right)}{2R_{gt,total,ESU}(1-Y_{ESU}) - R_{pp,2} + 2Y_{ESU}R_{gt,total,ESU}} \tag{73}$$

$$R_{gg,ESU} = \left[\frac{2}{R_{gg,1}} + \frac{2}{R_{gg,2}}\right]^{-1} \tag{74}$$

Hence,

$$R_{gg,ESU} = \frac{R_{gg,1}R_{gg,2}}{2\left(R_{gg,1} + R_{gg,2}\right)} \tag{75}$$

2.3.6 The inner grout volumes locations (for the single and double U-BHE configurations)
It must be stressed that the exact position of the two inner grout nodes capacities in the real BHE physics is necessarily unknown and it depends for example on the real shank spacing of the real U pipe assembly. The approach followed by the present model to locate the grout nodes' capacities is described hereafter. The grout thermal resistance weighting factor *Y* has been proposed in the present model as an input (*Y* has already been introduced for the R_{fg}, R_{gb} and R_{gg} definitions) and represents the ratio between the thermal resistance of conduction from the equivalent pipe area (delimited by d_{eq}) to the generic d_{gt} diametral position and the one from the equivalent pipe area to the borehole wall.

$$Y = \frac{\ln\left(\frac{d_{gt}}{d_{eq}}\right)\frac{1}{2\pi k_{gt}}}{\ln\left(\frac{d_b}{d_{eq}}\right)\frac{1}{2\pi k_{gt}}} \tag{76}$$

This type of writing allows relating these two conduction thermal resistances in cylindrical geometry (and correctly computed from the same reference BHE axis of symmetry also taking into account the real equivalent grout and pipe area through the d_{eq}). The same Y ratio is represented by the following Eq.(77) which is used to derive the R_{pg} term as a Y fraction of $R_{gt,total}$, thus it is specifically related to the real U-BHE geometry and allows to identify the locations of the T_{gt1} and T_{gt2} nodes into the BHE cross-section.

$$Y = \frac{R_{pg}}{R_{gt,total}} \tag{77}$$

Thus, the same Y proportion between the two thermal resistances of conduction denoted by Eq.(76) is used to identify the locations of the T_{gt1} and T_{gt2} nodes into the real BHE geometry (around each plastic pipe axis) through the Eq.(77). It has to be specified that the numerator and denominator terms of the Eq.(76) and Eq.(77) are not mutually coincident but the same Y ratio is assured.
Y allows to determine the general d_{Tgt} position that can be assumed by each grout node inside the real BHE (around each plastic pipe axis) for the single and double U-BHE configurations, as shown in Figures 18, 19a and 19b.
In particular, Y can assume a value between $0 \leq Y \leq 1$. Consequently, d_{gt} can assume, depending on the value assumed by Y, the following range of values: $d_{eq} \leq d_{gt} \leq d_b$. The locations d_{Tgt} of the two inner T_{gt1} and T_{gt2} grout nodes into the real BHE geometry can consequently be easily derived by Eq.(78), as expressed by Eq.(79) that defines each grout shell whose thickness (d_{Tgt} - $d_{ext,p}$) assures the R_{pg} value:

$$R_{pg} = \frac{\ln\left(\frac{d_{T_{gt}}}{d_{ext,p}}\right)}{2\pi k_{gt}} = YR_{gt,total} \tag{78}$$

$$d_{T_{gt}} = d_{ext,p} e^{2\pi k_{gt} Y R_{gt,total}} \tag{79}$$

It has to be noted that if $Y=0$, then d_{gt} coincides with d_{eq} and the two grout nodes locations identified by d_{Tgt} are coincident with the $d_{ext,p}$ position attached to the outer wall of each plastic pipe into the real geometry of the BHE.
The Y input value can assume the specific value denoted by Y_{ref} that makes the generic d_{gt} coincident with the d_{ref} diametral position. For the single and double U-BHE configurations, d_{ref} is located between the d_{eq} and the d_b diametral positions. The d_{ref} diametral position is defined as follows according to (Bauer et al., 2011) model suggestions:

$$d_{ref} = \sqrt{\frac{d_b^2 + d_{eq}^2}{2}} \tag{80}$$

The following Y_{ref} factor represents the specific value assumed by Y that makes d_{gt}

coincident with d_{ref} and the two inner grout volumes locations d_{Tgt} placed at a specific diametral position (different from the $d_{ext,p}$ position attached to the outer wall of each plastic pipe).

$$Y_{ref} = \frac{\ln\left(\frac{d_{ref}}{d_{eq}}\right)\frac{1}{2\pi k_{gt}}}{\ln\left(\frac{d_b}{d_{eq}}\right)\frac{1}{2\pi k_{gt}}} = \frac{R_{pg}}{R_{gt,total}} \quad (81)$$

The value related to the Y_{ref} factor is considered as the starting default value assumed by the Y input weighting factor to perform numerical simulations involving the single and double U pipe of the present model.
The present study demonstrated that in most cases, for obtaining an accurate reproduction of experimental TRT data through the present model, it is preferable to place the two inner grout nodes at a different location from the one denoted by the Y_{ref} value. In this sense in most of the simulation cases, the Y input value has to be different from the Y_{ref} starting value in order to compensate for the uncertainty sources related to the exact knowledge of the k_{gt}, $(\rho c)_{gt}$, and s values. For the specific physical and geometrical conditions of each U-BHE, the optimum Y input value is the one that minimizes the root mean square error between the simulation results and the experimental measurements.

2.3.7 The inner U-BHE model equations

The FD discretization is also employed for the transient heat conduction equation coupled with the RC network concerning each grout nodes denoted by $T_{gt1,j}$ and $T_{gt2,j}$ temperatures (and the related finite volumes):

$$\frac{T_{gt1,j}^{n+1}-T_{gt1,j}^{n}}{\Delta\tau} = \frac{1}{C_{gt}}\left\{\left(\frac{T_{gt2,j}^{n+1}-T_{gt1,j}^{n+1}}{R_{gg}}\right)+\left(\frac{T_{f1,j}^{n+1}-T_{gt1,j}^{n+1}}{R_{fg}}\right)+\left(\frac{T_{b,j}^{n+1}-T_{gt1,j}^{n+1}}{R_{gb}}\right)+\frac{(k_{gt}A_{gt})}{\Delta z_j}\left[\left(\frac{T_{gt1,j+1}^{n+1}-T_{gt1,j}^{n+1}}{\frac{\Delta z_j+\Delta z_{j+1}}{2}}\right)+\left(\frac{T_{gt1,j-1}^{n+1}-T_{gt1,j}^{n+1}}{\frac{\Delta z_j+\Delta z_{j-1}}{2}}\right)\right]\right\} \quad (82)$$

$$\frac{T_{gt2,j}^{n+1}-T_{gt2,j}^{n}}{\Delta\tau} = \frac{1}{C_{gt}}\left\{\left(\frac{T_{gt1,j}^{n+1}-T_{gt2,j}^{n+1}}{R_{gg}}\right)+\left(\frac{T_{f2,j}^{n+1}-T_{gt2,j}^{n+1}}{R_{fg}}\right)+\left(\frac{T_{b,j}^{n+1}-T_{gt2,j}^{n+1}}{R_{gb}}\right)+\frac{(k_{gt}A_{gt})}{\Delta z_j}\left[\left(\frac{T_{gt2,j+1}^{n+1}-T_{gt2,j}^{n+1}}{\frac{\Delta z_j+\Delta z_{j+1}}{2}}\right)+\left(\frac{T_{gt2,j-1}^{n+1}-T_{gt2,j}^{n+1}}{\frac{\Delta z_j+\Delta z_{j-1}}{2}}\right)\right]\right\} \quad (83)$$

The upwind scheme employed for the fluid domain volumes is written in an implicit form to evaluate the vertical convective energy transport in the pipes. This last is coupled with the heat transfer rate contributions seen by each fluid volume through the thermal resistance network along with the z-depth positions. The (descending) carrier fluid equation for each node in the entering U-BHE leg is reported hereafter:

$$\frac{({T_{f1,j}}^{n+1}-{T_{f1,j}}^{n})}{\Delta\tau} = \frac{w_f({T_{f1,j-1}}^{n+1}-{T_{f1,j}}^{n+1})}{\Delta z_j} + \frac{({T_{gt1,j}}^{n+1}-{T_{f1,j}}^{n+1})}{(\rho c)_f\pi({r_{in,p}}^2)R_{fg}} \quad (84)$$

The (rising) carrier fluid equation for each node in the exiting U-BHE leg is reported here below:

$$\frac{\left({T_{f2,j}}^{n+1}-T_{f2,j}{}^{n}\right)}{\Delta\tau}=\frac{w_f\left({T_{f2,j+1}}^{n+1}-{T_{f2,j}}^{n+1}\right)}{\Delta z_j}+\frac{\left({T_{gt2,j}}^{n+1}-{T_{f2,j}}^{n+1}\right)}{(\rho c)_f\pi\left({r_{ext,p}}^{2}\right)R_{fg}} \quad (85)$$

Both the laminar (Re_{d_h}<2300) and the transitional-turbulent (Re_{d_h}≥2300) flow regime and the related convective heat transfer coefficients are managed by the model with proper correlations (as reported in Morchio and Fossa, 2019, Morchio and Fossa, 2020, Beier et al., 2020). The constant (or time-variable) fluid inlet temperature $T_{f,in}(s/2,0,\tau)$ or the constant (or time-variable) fluid inlet-outlet temperature difference ΔT calculation type can be processed. It has to be specified that:

$$\Delta T=\frac{\dot{Q}}{\dot{m}c_f} \quad (86)$$

The heat transfer rate $\dot{Q}$ conferred (or extracted) to the carrier fluid on the top ground surface can vary during the numerical experiment following a user-defined function (or a generic point series, possibly based on the experimental data) while the mass flow rate $\dot{m}$ and time step $\Delta\tau$ can assume a constant or different step-wise value.
In the following, the two-dimensional heat conduction equation for each borehole wall volume is reported. The 2-D heat transfer rate of conduction in the ground exchanged by each borehole wall node at each time step is coupled with the one exchanged by the BHE grout nodes located inside the thermal resistance network:

$$\frac{T_{b,j}^{n+1}-T_{b,j}^{n}}{\Delta\tau}=\left(\frac{2\alpha_{gr,j}}{r_b\Delta r_b}\right)\left[(B_1+B_2)T_{b+1,j}^{n+1}-(B_1+B_2)T_{b,j}^{n+1}+\left({T_{gt1,j}}^{n+1}-2{T_{b,j}}^{n+1}+{T_{gt2,j}}^{n+1}\right)\frac{(\Delta r_1+\frac{\Delta r_0}{2}+\frac{\Delta r_2}{2})}{R_{gb}k_{gr,j}2\pi r_b}B_2\right]+\frac{(2\alpha_{gr,j+1})}{\Delta z_j}\frac{(T_{b,j+1}^{n+1}-T_{b,j}^{n+1})}{\Delta z_j+\Delta z_{j+1}}-\frac{(2\alpha_{gr,j})}{\Delta z_j}\frac{(T_{b,j}^{n+1}-T_{b,j-1}^{n+1})}{\Delta z_j+\Delta z_{j-1}} \quad (87)$$

The 2-D heat conduction Eq.(56) implemented for each borehole wall volume represents another original contribution by the present model for U-pipes. Equations (32), (33), (35), (36), (82), (83), (84), (85), (87) constitute a linear system of equations that can be written in matrix form and iteratively solved.

2.3.8 Present model limitations

Negative values for the thermal resistances R_{gg} can be obtained with the presented methodology. This does not affect the second law of thermodynamics as long as the equivalent thermal resistance R_{eq} between the grout areas remains positive:

$$R_{eq}=\left[\frac{1}{R_{gg}}+\frac{1}{2R_{gb}}\right]^{-1}>0 \quad \text{for the single U-BHE} \quad (88)$$

$$R_{eq,1} = \left[\frac{1}{R_{gg,1}} + \frac{1}{2R^*_{gb}}\right]^{-1} > 0 \text{ and } R_{eq,2} = \left[\frac{1}{R_{gg,2}} + \frac{1}{2R^*_{gb}}\right]^{-1} > 0 \text{ for the double U-BHE (89)}$$

If Equations (88) and (89) are not satisfied, the value of *Y* has to be reduced until the conditions apply. Otherwise, it has been proved by the present study that the numerical solution cannot be achieved. It has to be noted that the value assumed by the *Y* weighting factor can be used also to compensate for the uncertainty sources related to the knowledge of the exact k_{gt}, $(\rho c)_{gt}$, and *s* values. While the grout thermal conductivity k_{gt} and the grout volumetric heat capacity $(\rho c)_{gt}$ representative values can be known, the real shank spacing (center to center) *s* value in the real BHE physics remains necessarily unknown. Another uncertainty source is related to the intrinsic 2D nature of the present model employing the hybrid FD/RC description of the problem. The FD/RC models that assume an axisymmetric cylindrical geometry of the ground domain are not suitable to completely describe the physics related to the real 3D transient behavior inside and around the BHE.

2.3.9 Model validation and results

The single and double U-BHE configurations of the present model have been validated against real TRTs field data as well as against analytical and numerical models. The discussion of the results is reported in this section and it is aimed to demonstrate the validity and the robustness of the present model. The solution accuracy is assured since the finite increment Δz, the time step interval $\Delta\tau$, the carrier-fluid velocity values determine a resulting *Co* (Courant) number within 0.46 in each pipe for each test (a detailed analysis concerning the Courant number has been reported in Morchio and Fossa, 2019, Morchio and Fossa, 2020). A sensitivity analysis of mesh spacing and domain extension has been conducted. An ILS-based log criterion (Morchio and Fossa, 2019, Morchio and Fossa, 2020) for enlarging the grid in the radial direction has been applied. The domain extension has been chosen to ensure that the BC1 and BC2 solutions overlap in time for any domain node.

The effect of the grout thermal resistance weighting factor *Y* on the inlet and outlet carrier fluid temperature profile in time is also reported. From the preliminary simulation results reported in the present section, it will be clarified that when the *Y* value has to be switched from the Y_{ref} value, this can be considered the first warning that one (or all) of the k_{gt}, $(\rho c)_{gt}$, and *s* values adopted in the model are too dissimilar from the ones characterizing the real installation. The discussion of the simulation results is conducted by assuming that the k_{gt} and *s* values adopted in the model are those of the real installation. This is not very realistic but it constitutes the main assumption to numerically study the influence of the uncertainty related to the $(\rho c)_{gt}$ value, as the first step of the analysis provided by the present study. Moreover, different $(\rho c)_{gt}$ values do not imply different effective borehole resistance in terms of intercept values (the $(\rho c)_{gt}$ value influences only the short-time of the TRT), as instead, it happens for different k_{gt} and *s* values.

2.3.10 Validation against literature data

Table 9 shows the grid properties adopted for each of the four validation cases reported. The main data concerning each simulation case are reported in Table 10. Some of the

simulation results reported in the following have been discussed by varying the input values related to the grout volumetric heat capacity and the grout thermal resistance weighting factor Y with respect to the ones of each base case in Table 10.

Table 9
Grid properties characterizing the numerical simulations

Input Type	Case#1	Case#2	Case#3	Case#4
Domain end radial r-coordinate	3 m	3 m	3 m	3.02 m
Domain end axial z-coordinate	203.17 m	157.5 m	168 m	260 m
Number of partitions along the r-direction	30	30	30	30
Number of partitions along the z-direction	43	50	50	50
Finite increment Δz	4.72 m	3.15 m	3.36 m	5.2 m
Time step $\Delta\tau$	3.6 s	2.57 s	1.8 s	3.6 s

Table 10
Main input data of each base case simulation performed

Input Type	Case#1	Case#2	Case#3	Case#4
Type of U pipe	single	single	double	single
Calculation type	$\Delta T_{in,out}$ assigned	$\Delta T_{in,out}$ assigned	$\Delta T_{in,out}$ assigned	$\Delta T_{in,out}$ assigned
Y_{ref}	0.756	0.7	0.65	0.7
X	0.5	0.5	0.5	0.5
Shank spacing s	0.1 m	0.06 m	0.06 m	0.075 m
Borehole length H_b	193.5 m	150 m	160 m	251.5 m
Borehole diameter d_b	0.2 m	0.14 m	0.152 m	0.14 m
Pipe inner radius $r_{in,p}$	0.0163 m	0.0163 m	0.0163 m	0.0176 m
Pipe wall thickness	0.0037 m	0.0037 m	0.0037 m	0.0024 m
Mass flow rate $\dot{m}$	0.45 kg/s	0.416 kg/s	0.717 kg/s	0.51 kg/s
Geothermal fluid conductivity k_f	0.64 W/(mK)	0.64 W/(mK)	0.6 W/(mK)	0.49 W/(mK)
Geothermal fluid density ρ_f	1000 kg/m^3	1000 kg/m^3	1000 kg/m^3	980 kg/m^3
Geothermal fluid specific heat capacity c_f	4180 J/(kgK)	4180 J/(kgK)	4180 J/(kgK)	4180 J/(kgK)
Geothermal fluid dynamic viscosity	0.001 kg/(ms)	0.001 kg/(ms)	0.001kg/(ms)	0.002 kg/(ms)
Pipe thermal conductivity k_p	0.38 W/(mK)	0.4 W/(mK)	0.4 W/(mK)	0.4 W/(mK)
Ground thermal conductivity k_{gr}	2.3 W/(mK)	6.25 W/(mK)	3 W/(mK)	3.08 W/(mK)
Ground volumetric heat capacity $(\rho c)_{gr}$	2.22MJ/(m^{3}K)	2.22MJ/(m^{3}K)	2.5 MJ/(m^{3}K)	2.24MJ/(m^{3}K)
Grout thermal conductivity k_{gt}	1.5 W/(mK)	1.2 W/(mK)	0.8 W/(mK)	1.67 W/(mK)
Grout volumetric heat	2.19MJ/(m^{3}K)	2.19MJ/(m^{3}K)	2 MJ/(m^{3}K)	4.2 MJ/(m^{3}K)

capacity $(\rho c)_{gt}$				
Heat input rate $\dot{Q}$	9645 W	7000 W	9000 W	9450 W
Average undisturbed ground temperature	285.03 K	289.59 K	283.69 K	282.25 K

2.3.11 Case#1

The first validation case (Case#1) concerns the comparison of the fluid inlet and outlet temperatures computed by the present model against the real TRT performed in Ravensburg (Germany) and reported in (Bauer et al., 2011), as shown by Figure 21 (a). According to the available data presented by (Bauer et al., 2011), the duration of the heat injection period is 90 hours. The mean value of the undisturbed ground temperature profile

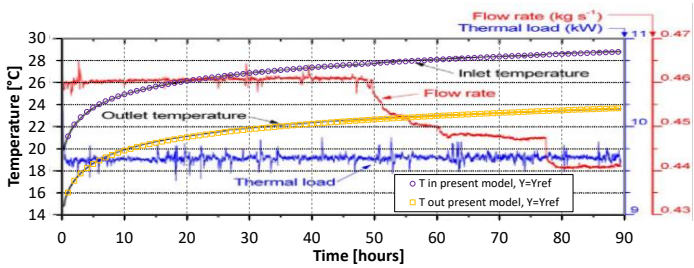

(a)

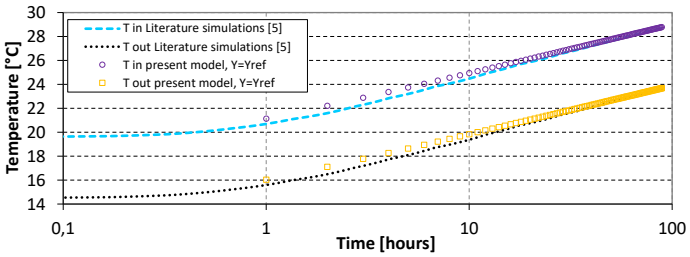

(b)

Figure 21 Numerical data by the present model compared with the Ravensburg TRT measurements (Bauer et al., 2011) (a) and the Comsol model (Fossa et al., 2013) (b). Present results are overlapped on original Figure (a).

along the *z*-direction reported in Table 10 has been assumed as the initial condition for all the temperature nodes of the numerical domain. The mean heat input rate and mass flow rate values reported in Table 10 have been assumed in the present Case#1, according to the available data presented in (Bauer et al., 2011). The simulation results are also compared with the ones computed by the Comsol model proposed in a previous investigation by the Authors (Fossa et al., 2013) and reported in Figure 21 (b). From Figure 21 inspection it is apparent that a good agreement between the real TRT data and the simulated ones by Fortran and Comsol models has been inferred when the $Y=Y_{ref}=0.756$ value is set.

2.3.12 Case#2

The second validation case (Case#2) is a comparison against real TRT measurements reported in (Fossa et al., 2018) and (Fossa et al., 2016). The experiment was carried out by researchers of the present research group at the University of Genova, Savona Campus. The related TRT machine (Figure 22) was developed on purpose to perform steady and

Figure 22 Pulsating TRT machine developed at the University of Genova and employed for the TRT experiment here described as Case#2.

pulsated heat flux experiments. As reported by (Fossa et al., 2018), no heat rate was applied during the first 7 hours (undisturbed temperature measurements) and a constant heat injection has been operated for the following 100 hours of the experiment. As stated by (Fossa et al., 2018), in the heating periods the heat transfer rate was set to 7000 W and the control was able to maintain a small 1.5% RMS variation irrespective of the daily supply voltage oscillations. The volumetric flow rate of water was maintained at 1500 liters/h, with 4 l/h RMS variation all along the test. The present model has been employed to reconstruct the experimental temperature profiles obtained during the 100 hours of constant heat injection rate. The first 7 hours of fluid circulation have not been considered and the numerical simulations start assuming the constant and depth-uniform average undisturbed ground temperature value (detected after the first 7 hours of the pre-circulation phase) for all the nodes of the numerical domain. In Figures 23(b) and 24(b) the first 50 hours of the numerical TRT performed by the present model are shown and compared to the real measurements reported by (Fossa et al., 2018) and (Fossa et al., 2016).

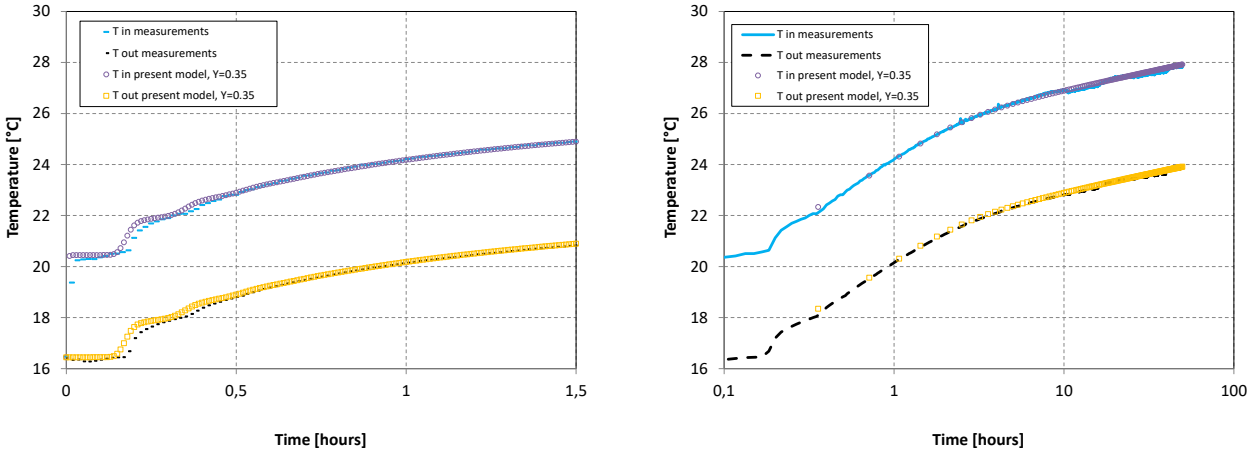

(a) (b)

Figure 23 Single U TRT experiment at Savona Campus $(\rho c)_{gt}=2.19$ [$MJ/(m^3K)$]. Comparison of measured and simulated fluid temperatures at the beginning of the experiment (a) and during the whole period (b).

The reconstructed profiles of the inlet and outlet fluid temperature have been obtained from simulations at different Y values and for different grout volumetric heat capacity values. The reason for such a parametric investigation is related to the fact that in real-world installations, it is quite common that the grout material thermal properties k_{gt} and $(\rho c)_{gt}$ given by the manufacturer are not those of the actual operating conditions, especially in the early period of BHE installation, as demonstrated by (Minchio et al., 2020). Figures 23 and 24 show the experimental and numerical profiles of fluid temperatures. The simulation profiles overlap with measurements for both the very early time (Figure 23 (a))

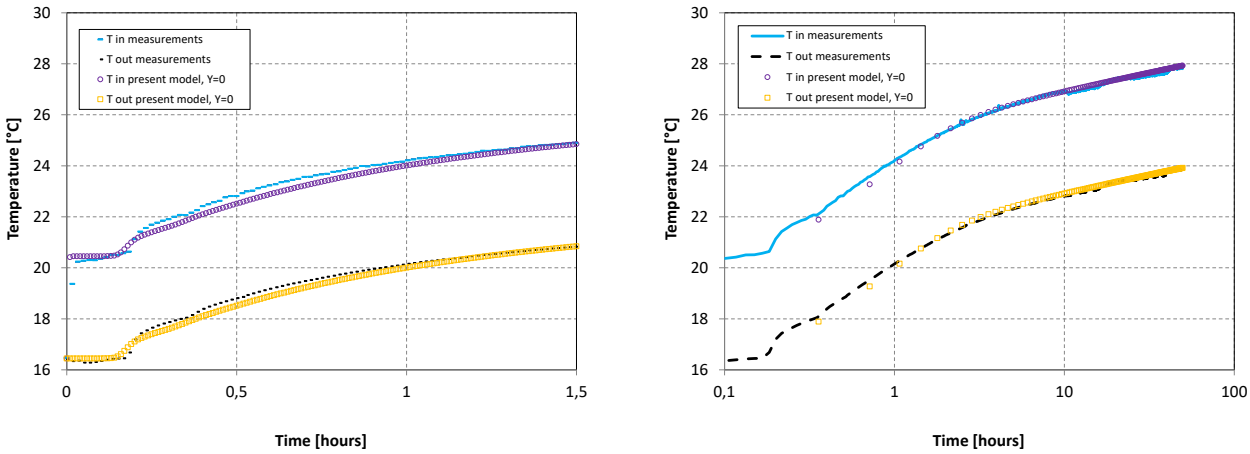

(a) (b)

Figure 24 Single U TRT experiment at Savona Campus $(\rho c)_{gt}=1.35$ [$MJ/(m^3K)$]. Comparison of measured and simulated fluid temperatures at the beginning of the experiment (a) and during the whole period (b).

as well as for the late regime of the TRT (Figure 23 (b)). It has to be specified that the results reported in Figure 23 have been obtained by setting $(\rho c)_{gt}$ to 2.19 [$MJ/(m^3K)$] which is the value that characterizes the grout material of the Ravensburg experiment (Case#1).

In this case, Y is set at 0.35, a value that allowed a very good description of the fluid temperature in the initial 2 hours of the experiment where temperature fluctuations occur as an effect of the initial stratification of temperatures in the stagnant fluid present in the pipes. Figure 24 shows the same simulation performed by setting the $(\rho c)_{gt}$ value to 1.35 $[MJ/(m^3K)]$ which was the value measured by the Authors on a sample of grout carried in their lab. The instrument employed was an Isomet thermal conductivity meter by Applied Precision company. In this case, a $Y=0$ value is needed to obtain a good agreement between measurements and simulations. From this example, it is apparent that the uncertainty related to the knowledge of the grout volumetric heat capacity $(\rho c)_{gt}$ has a similar influence on results as the value applied to the Y weighting factor. The compensation effect assured by the value adopted by the Y weighting factor influences the simulated thermal solution for the short-time of the numerical TRT while the long-time solution remains the same. Other sources of uncertainty (not investigated in the present study) on the correct reproduction of the experimental data that can be compensated by the value assumed by the Y weighting factor are represented by the knowledge of the real k_{gt} and s values. While the grout thermal properties can be estimated from manufacturer information or laboratory measurements, the real shank spacing remains necessarily unknown in a real installation.

2.3.13 Case#3

Case#3 concerns the validation of the double U-BHE configuration against the real TRT field data reported in (Signorelli et al., 2007). The inlet and outlet temperature profiles during time computed by the present model have been also compared with those obtained from the Comsol model proposed in a previous investigation by the Authors (Fossa et al., 2013). As reported by (Signorelli et al., 2007), the constant heating power of 9 kW was assumed throughout a 200 hours test. The first 17 hours of pre-circulation were employed to determine the average ground temperature before starting the thermal response test. As

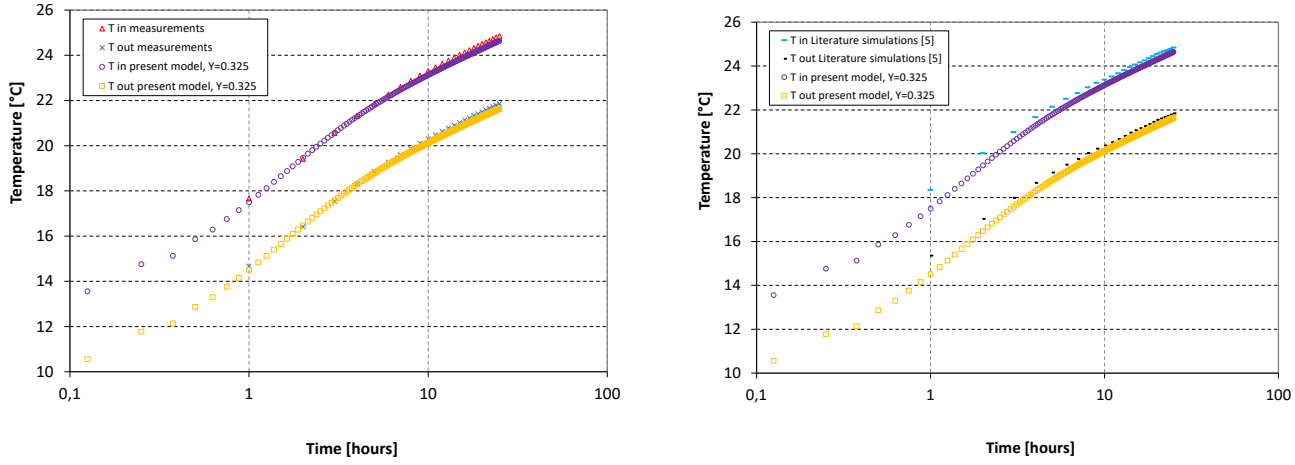

(a) (b)

Figure 25 Double U TRT experiment in Switzerland (Signorelli et al., 2007). The present model simulated fluid temperatures compared with the measurements (a) and the Comsol model (Fossa et al., 2013) (b).

stated by (Signorelli et al., 2007), the heat injection rate varied within about 5% of the

average, the variations being attributed to changes in grid voltage. The numerical simulations performed by the present model have been run by taking into account the average undisturbed ground temperature value detected after the first 17 hours of the real pre-circulation test and uniformly imposed as the initial condition for all the nodes of the numerical domain. The remaining data of Case#3 reported in Table 2 are set accordingly with those reported by (Signorelli et al., 2007) and (Fossa et al., 2013). In Figure 25(a) the first 25 hours of the numerical TRT performed by the present model are shown and compared to the real measurements reported by (Signorelli et al., 2007). In Figure 25(b) the present model inlet and outlet fluid temperatures are compared with those obtained through the literature Comsol model (Fossa et al., 2013). From Figure 25 inspection it is apparent that a good agreement between the real TRT data and the simulated ones by Fortran and Comsol models has been inferred when the *Y=0.325* value is set. This may denote that the grout thermal properties k_{gt} and $(\rho c)_{gt}$ given by the manufacturer or set as the input of the model together with the shank spacing *s* value are not those of the real BHE installation.

2.3.14 Case#4

The validation Case#4 is constituted by the comparison against the TRT measurements reported in (Beier, 2014), (Calvo et al., 2015), (Acuña, 2013), (Acuña et al., 2009), (Beier

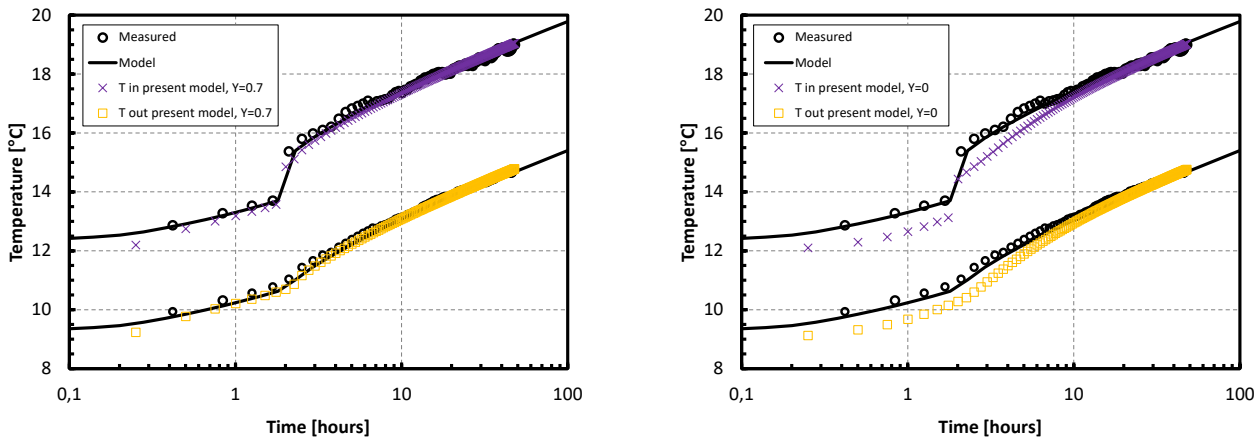

(a) (b)

Figure 26 Single U TRT in Stockholm (Sweden), present model validation against measured data and numerical results by (Beier, 2014) model for different values of the *Y* parameter. Present results are overlapped on original Figures.

et al., 2012). In particular, the simulation results can be discussed by varying the *Y* value (the adopted *Y* values are $Y= Y_{ref} =0.7$ and *Y=0*) and can be compared with those already obtained by the U-pipe analytical model of (Beier, 2014). The main data adopted for performing the numerical simulations are reported in Table 10 according to (Beier, 2014), (Calvo et al., 2015), (Beier et al., 2012). As explained by (Beier et al., 2012), the TRT lasted approximately 160 hours and consisted of four different phases (Acuña et al., 2009). It has to be specified that in the present study only the heat injection phase has been investigated and reproduced by the present model. In the real experiment, the fluid

circulated through the U-tube for 24 hours without any heating. The temperatures along the entire borehole length become nearly uniform due to the circulation, and approximately equal to the mean value of the undisturbed ground temperature profile along the *z*-direction (282.25 K, shown in Table 10). The heat injection period lasts about 48 hours, during which a nearly constant heat input rate to the circulating fluid was maintained. The heat input rate conferred to the fluid on the top surface before 2 hours is 6600 W while it is 9450 W after 2 hours, as explained in (Beier, 2014). It has to be specified that the grout's apparent thermal conductivity value of 1.675 W/(mK) reported in (Calvo et al., 2015) has been adopted in the present Case#4 since the borehole is filled with groundwater, which is a common practice in Sweden (Beier, 2014), while ensuring the perfect overlapping between the experimental, analytical and simulated data, as reported in Figure 26. The case characterized by the $Y = Y_{ref} = 0.7$ value guarantees the best agreement of the simulated values with the temperature measurements for the entire duration of the test, as can be seen in Figure 26. Once again, it has been proved that the *Y* value influences the simulated fluid temperature profiles only for the early time of the TRT. The thermal transient behavior of the late regime is not affected by the *Y* choice, as clarified in Figure 26. It is also possible to compare the simulated fluid temperature profiles along the ground-depth with those obtained from the DTRT Swedish measurements (Acuña, 2013), (Acuña et al., 2009), (Beier et al., 2012), as shown in Figure 27. For the last few hours, the deviation between the simulated and measured profiles is a few tenths of a degree, especially at the bottom of the BHE.

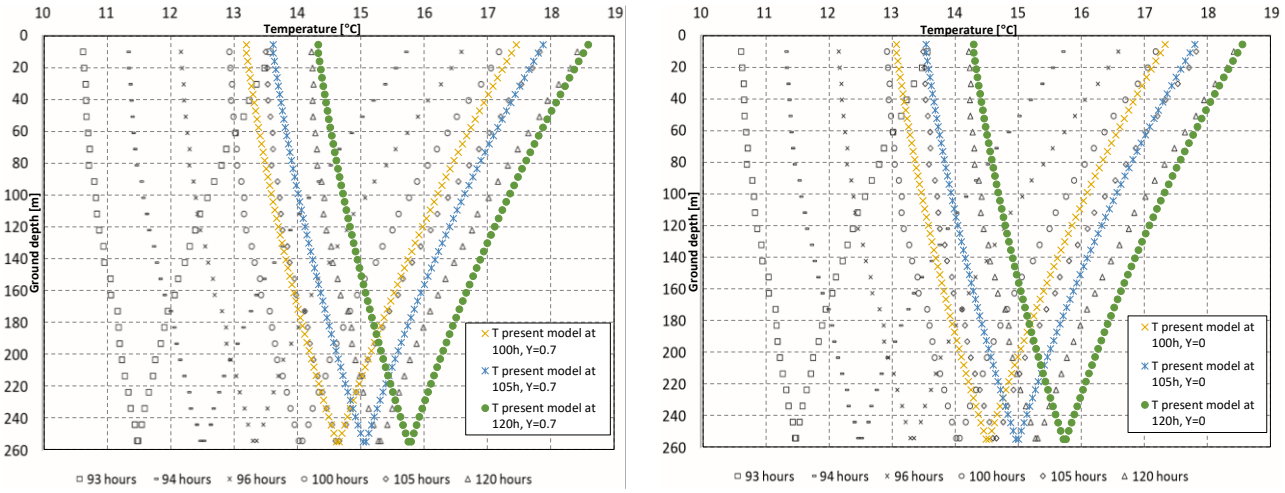

Figure 27 Single U TRT in Stockholm (Sweden), present model validation against DTRT measured data (Acuña, 2013) along the borehole depth for different values of the *Y* parameter. Present results are overlapped on original Figures.

2.3.15 Statistical analysis of the results

Differences between the results of both experimental and model data are presented in Table 11. Unfortunately, a complete dataset of measurements and simulated data is not provided for all the cases. The error deviations between the experimental and the simulated

data have been presented in terms of the root mean square error (*RMSE*), which is defined by the following equation:

$$RMSE = \sqrt{\frac{\sum_{n=1}^{N}(T_{Literature} - T_{FD/RC,comp})^2}{N-1}} \quad (90)$$

Where N is the total number of data points, $T_{Literature}$ are the inlet (or outlet) fluid temperatures available in literature and $T_{FD/RC,comp}$ are the inlet (or outlet) fluid temperatures computed by the present FD/RC model.

Table 11
Comparison between the temperatures computed by the present model and those available in literature

Case, related Figure	Compared data type	$RMSE_{Tinlet}$	$RMSE_{Toutlet}$
Case#1, Fig.21	Literature simulations	0.24 [°C]	0.24 [°C]
Case#2, Fig.23	Literature measurements	0.07 [°C]	0.08 [°C]
Case#2, Fig.24	Literature measurements	0.08 [°C]	0.09 [°C]
Case#3, Fig.25(a)	Literature measurements	0.17 [°C]	0.17 [°C]
Case#3, Fig.25(b)	Literature simulations	0.33 [°C]	0.33 [°C]
Case#4, Fig.26(a)	Literature measurements	0.13 [°C]	0.09 [°C]
Case#4, Fig.26(a)	Literature simulations	0.18 [°C]	0.12 [°C]
Case#4, Fig.26(b)	Literature measurements	0.28 [°C]	0.25 [°C]
Case#4, Fig.26(b)	Literature simulations	0.44 [°C]	0.36 [°C]

It has to be noted that the lowest values of *RMSE* have been obtained when the present FD/RC model data are compared with the real temperature measurements, like those provided by (Signorelli et al., 2007), (Beier, 2014), (Fossa et al., 2018), (Fossa et al., 2016). In this sense, the present FD/RC model proved to be robust, effective and reliable.

3. The ILS-based TRT analyses for the correct ground thermal conductivity estimation when coaxial, single and double U BHE involve a single or multiple ground layers with different geothermal gradients along the depth

The main investigations and explanations on how the ILS model can effectively confer the correct ground thermal conductivity estimation when coaxial, single and double U BHE involve a single or multiple ground layers with different geothermal gradients along the depth are reported in the present chapter. The present chapter explains how the ILS-based k_{gr} estimations in TRT analysis can be affected by the q_{ratio} parameter introduced in the present work. The q_{ratio} affects the TRT analysis for single and multiple ground layers of equal thickness with different ground thermal conductivities along the depth. The q_{ratio} is also related to the g_0-transfer function evaluated for the FFT spectral analysis method. Error analyses on the BHE and ground properties estimations from the ILS model have been carried out.

3.1 The influence of the external heat transfer rate on the ILS-based k_{gr} estimations in TRT with coaxial, single and double U BHE involving a single ground layer with geothermal gradient

The present section demonstrates that the external heat injection/extract rate can influence TRT analysis accuracy. Focus is devoted to the analyses of TRT simulations aimed at understanding the main factors that influence the ground thermal conductivity and the effective borehole thermal resistance estimations. The ILS model assumes the heat transfer rate per unit length injected (or extracted) into the surrounding ground is constant and uniform with depth. According to the ILS model, the ground thermal conductivity estimate should not be influenced by the magnitude (the absolute value) of the heat transfer rate per unit length applied in the test.

Comprehensive studies concerning the influence of the heat rate per unit length on the BHE/ground property evaluation seem to be lacking in literature, but some guidelines are available. In the United States, the (ASHRAE guidelines, 2015) for a TRT recommend a heat input rate between 45 and 75 W/m. This recommendation is based on a borehole with a U-tube of depth of about 100 m or less, which is the most common configuration in the US. The guidelines do not explicitly consider the coaxial configuration or deep boreholes. The TRT Italian standard (UNI 11466, 2012) recommends a heat input rate between 30 and 80 W/m in case the ILS model is applied to the TRT analysis.

The present study identifies another mechanism besides natural convection that can cause the selection of the heat injected/extracted rate to influence the estimated value of the ground thermal conductivity from a TRT. In DBHEs the influence can occur through the interaction between the injected/extracted heat rate and the geothermal gradient.

For this reason, the undisturbed ground temperature profile should be considered in the choice of the heat transfer rate applied to the carrier fluid during the TRT. The q_{ratio} parameter has been introduced and defined as the ratio between the absolute value of the external heat transfer rate $\dot{Q}'$ (per unit length) and the "natural" heat rate $\dot{Q}'_{geo}$ corresponding to the geothermal gradient. Since $\dot{Q}'$ is controlled during a TRT, the engineer has some control over q_{ratio}. External and "natural" heat transfer rates are linked by the q_{ratio} parameter. This study explores how changes in q_{ratio} affect the transient fluid inlet and outlet temperatures and the fluid vertical temperature profiles. Thermal profile inversions and errors in the TRT analyses have been found if q_{ratio} is lower than 1. Conventional TRT analysis with the ILS model fits the average transient fluid temperature to estimate the ground thermal conductivity k_{gr}. Thus, changes in the TRT response curves from changes in the parameter q_{ratio} may affect the estimate of k_{gr}. To explore the dependence, three different hybrid models recently presented by the Authors (Morchio and Fossa, 2019, Morchio and Fossa, 2020, Beier et al., 2020) have been employed to run parametric numerical TRT simulations for coaxial, single, and double U-pipe BHEs. These models have been validated against experimental results in the above papers by the Authors: the models proved to be robust and very accurate with respect to the available literature TRT measurements. The reader is directed to those papers for a complete model description.

The introduced parameter q_{ratio} is expected to be relevant to future TRT guidelines at national and international levels (Fossa, 2017), especially for DBHE. The conventional ILS model does not include any influence of the external heat transfer rate on the BHE/ground property evaluation. Analyses of numerically simulated TRTs show this omission can sometimes produce an error in the estimate of the ground thermal conductivity. The error may be between ±10% and ±22% for coaxial boreholes (800 m depth) if the ground has a significant geothermal gradient. On the other hand, for single and double U-pipe BHEs the error is less than ±5% under similar conditions. The parameter q_{ratio} is identified as an indicator of when the error is significant. This parameter is equal to the external heat rate (injection or extraction) divided by a natural heat rate that is related to the geothermal gradient. Errors greater than ±10% tend to occur for coaxial boreholes with a center-pipe fluid inlet when $|q_{ratio}|<1$. Under the same conditions but with the annulus as the fluid inlet, the error is less than ±6%.

3.1.1 Dimensionless parameter q_{ratio}

The ILS model assumes the heat flux across the borehole wall is uniform with depth. Consider the case when the ground has a geothermal gradient, which substantially increases the undisturbed ground temperature with depth. One would expect the uniform-flux assumption to eventually break down with increasing geothermal gradient and/or increasing borehole depth. In this case, the natural heat rate corresponding to the geothermal gradient can change the heat flux normally imposed by the external heat rate during a TRT. In some sense, the natural heat rate is competing with the external heat injection/extraction rate.

Consider the ratio of the external heat rate per unit length, $\dot{Q}/H$ over the natural heat rate written as

$$q_{ratio} = \frac{\frac{\dot{Q}}{H}}{k_{gr}H\frac{dT_{gr,\infty}}{dz}} \quad (91)$$

The denominator represents the natural heat corresponding to a constant geothermal gradient, $dT_{gr,\infty}/dz$. That is, the natural heat rate is given as

$$\dot{Q}'_{geo} = k_{gr}H\frac{dT_{gr,\infty}}{dz} \quad (92)$$

This expression for q_{ratio} can be obtained from the dimensionless conservation of energy equations for the circulating fluid in the borehole pipes. For example, the dimensionless equation for the annulus in a coaxial BHE reveals q_{ratio} is related to the last term in Eq. (93). The term acts as a source/sink of heat. The parameter q_{ratio} is related to a term in the dimensionless conservation of energy equation for the circulating fluid (Beier, 2020). The dimensionless energy balance on the fluid flowing through the annulus in a coaxial BHE is written as (Beier, 2020):

$$\frac{N_{gr}C_rA_{D2}}{2}\frac{\partial\theta_{D2}}{\partial\tau_D} + (-1)^m\frac{\partial\theta_{D2}}{\partial z_D} + N_1(\theta_{D2}-\theta_{D1}) + N_2(\theta_{D2}-\theta_{Db})_{r_D=1} + (-1)^m\frac{dT_{Dgr,\infty}}{dz_D} = 0, \quad 0 < z_D < 1, 0 < \tau_D \quad (93)$$

Here, the temperature difference, θ, is with respect to the undisturbed ground temperature profile, $T_{gr,\infty}(z)$, and

$$\theta(r,z,\tau) = T(r,z,\tau) - T_{gr,\infty}(z) \quad (94)$$

Subscript 1 in θ_{D1} represents the fluid in the center pipe while subscript 2 corresponds to the annulus.
Dimensionless time, τ_D, dimensionless radial coordinate, r_D and dimensionless depth, z_D, are defined in Table 12 along with the other dimensionless groups. The parameter *m* equals 1, when the fluid enters the center pipe where it flows downward and then travels upward through the annulus. The value of *m* equals 2, when the fluid enters the annulus where it flows downward.

The first term in Eq. (93) corresponds to the rate of energy change within the fluid at depth *z*. The second term represents the difference in the energy between the fluid entering the element of thickness *dz* and the fluid leaving the element during the differential time interval. The third term takes into account the energy transferred from the fluid in the inner pipe to the fluid within the annulus. The fourth term corresponds to the heat transfer between the annular fluid and the surrounding ground. The fifth term takes into account the geothermal gradient and behaves as a source/sink of heat. For simplification Eq. (93) is written for the coaxial BHE in this study without grout surrounding the external pipe. The case with grout is described by (Beier, 2020).

Table 12
Dimensionless groups in energy conservation Eq. (93).

Dimensionless groups	***Physical meaning***
$T_D = \frac{2\pi\, k_{gr} H\, T}{\dot{Q}}$	Dimensionless temperature
$\theta_D = \frac{2\pi\, k_{gr} H\, (T - T_{gr,\infty})}{\dot{Q}}$	Dimensionless temperature difference from undisturbed ground temperature at given depth
$\tau_D = Fo = \frac{k_{gr}\, \tau}{\rho_{gr}\, c_{gr}\, r_b^2}$	Dimensionless time or Fourier number
$r_D = \frac{r}{r_b}$	Dimensionless radius
$z_D = \frac{z}{H}$	Dimensionless depth
$N_1 = \frac{H}{\dot{m}\, c_f\, R_1}$	Net transfer unit corresponding to short-circuit heat transfer (coaxial)
$N_2 = \frac{H}{\dot{m}\, c_f\, R_2}$	Net transfer unit corresponding to heat transfer between fluid and ground (coaxial)
$N_{gr} = \frac{2\pi k_{gr} H}{\dot{m} c_f}$	Dimensionless conductance of ground
$q_{ratio} = \frac{\frac{\dot{Q}}{H}}{k_{gr} H \frac{dT_{gr,\infty}}{dz}}$	External heat input rate per unit length over an idealized (natural) heat rate added to the fluid due to the geothermal gradient
$C_r = \frac{\rho_f\, c_f}{\rho_{gr}\, c_{gr}}$	Ratio of volumetric heat capacities of fluid to ground
$A_{D1} = \frac{\pi {r_{in,c}}^2}{\pi\, r_b^2} = \frac{{r_{in,c}}^2}{r_b^2}$	Ratio of inside cross-sectional area of center pipe to circular area based on outer radius of external pipe
$A_{D2} = \frac{\pi\, ({r_{in,a}}^2 - {r_{out,c}}^2)}{\pi\, r_b^2} = \frac{{r_{in,a}}^2 - {r_{out,c}}^2}{r_b^2}$	Ratio of annular cross-sectional area to circular area based on outer radius of external pipe

The last term on the left-hand side of Eq. (93) can be rearranged in terms of the geothermal gradient, $\frac{dT_{gr,\infty}}{dz}$, using the definitions of T_D and z_D, as

$$(-1)^{m+1}\frac{dT_{Dgr,\infty}}{dz_D} = (-1)^{m+1}\frac{2\pi k_{gr}}{\frac{\dot{Q}}{H}}\frac{H\,dT_{gr,\infty}}{dz} = (-1)^{m+1}\frac{2\pi}{q_{ratio}} \quad (95)$$

Thus, this term is basically the reciprocal of q_{ratio} multiplied by 2π where

$$q_{ratio} = \frac{\frac{\dot{Q}}{H}}{k_{gr}H\frac{dT_{gr,\infty}}{dz}} \quad (96)$$

The term acts as a source/sink of heat in Eq. (93). The value of the term is uniform with depth if the undisturbed ground temperature is linear. A similar term appears in the conservation of energy equation (Eq. 97) for the fluid in the center pipe (which is Eq. (10) in Beier, 2020):

$$\frac{N_{gr}C_rA_{D1}}{2}\frac{\partial\theta_{D1}}{\partial\tau_D} + (-1)^{m+1}\frac{\partial\theta_{D1}}{\partial z_D} + N_1(\theta_{D1}-\theta_{D2}) + (-1)^{m+1}\frac{dT_{Dgr,\infty}}{dz_D} = 0,\ \ 0 < z_D < 1\ , 0 < \tau_D \quad (97)$$

Similar conservation equations apply to fluid flowing through the pipes in a U-pipe BHE. Again a term similar to the last term in Eq. (93) appears, which is related to parameter q_{ratio}. Thus, the parameter also applies to U-pipe BHE.

Picture an elemental volume in the annulus of thickness *dz*. If the flow is downward in the annulus, then the term in Eq. (93) acts as a heat sink, because the geothermal gradient tends to cause cooler fluid from above to enter the elemental volume. On the other hand, the term acts as a heat source under upward flow in the annulus, because the geothermal gradient tends to make warmer fluid enter the elemental volume from below. The geothermal gradient influences the borehole fluid through radial heat conduction in the ground. A similar interpretation of q_{ratio} applies to the fluid flowing through the center pipe or pipes in a U-pipe borehole. (Beier, 2020) writes a more complete description of the dimensionless equations and provides a semi-analytical solution for coaxial DBHEs.

3.1.2 Problem statement, assumptions and input data sets

The effect of q_{ratio} on the BHE thermal behavior and ground properties estimations has been investigated through TRT numerical simulations. Then, the applicability of the ILS model has been evaluated for estimating the ground thermal conductivity k_{gr}. The (almost) logarithmic trend line of the computed $T_{f,\,ave}$ profiles has been obtained ignoring the time relating to the initial transient lasting 10 Fo_{rb} units, according to (Eskilson, 1987). According to the classic ILS analysis of TRT measurements, the fluid temperature profile (i.e. the slope in a semilog diagram) is used to derive the ground thermal conductivity k_{gr}.

Specific parameters for each BHE type and the related numerical grids are reported in Table 13. The parametric analysis has been done for two borehole depths with the same geothermal gradient of the undisturbed ground temperature. The k_{gr} value is a typical value found by field tests such as those of (Acuña, 2013, Beier et al., 2012,

Signorelli et al., 2007, Minchio et al., 2020). The value is also consistent with laboratory measurements as reported in a specific rocks thermal property database (Dalla Santa et al., 2020).

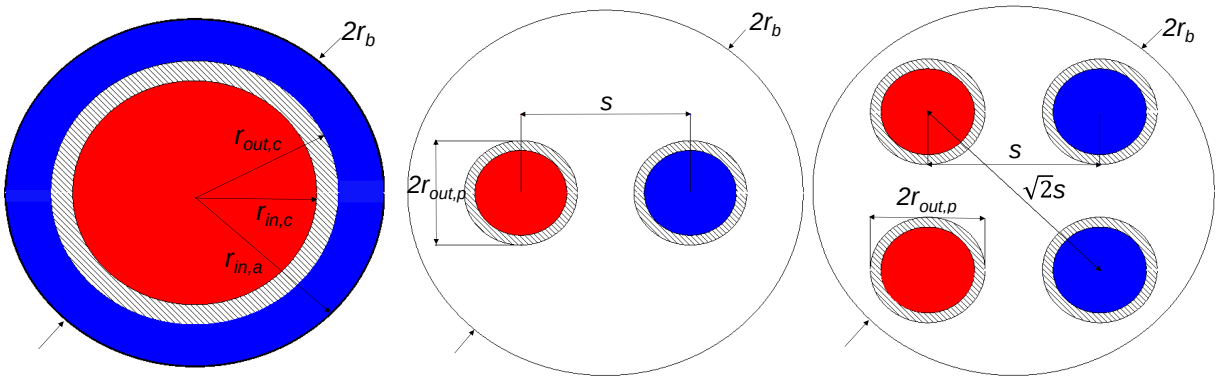

Figure 28 Cross section of the coaxial, single and double U-pipe BHE, including the diameters and the shank spacing *s* definitions.

The dimensions and properties assumed for the coaxial boreholes are typical of some boreholes installed in Sweden. These boreholes are drilled through granite, and the borehole diameter remains nearly the same along the borehole length. Very often these coaxial boreholes are installed without using backfilling material (also known as grout material), as reported by (Mazzotti et al., 2018) and (Holmberg et al., 2016). On the other hand, grout material is installed in single or double-U boreholes. For the double U-tube configuration, the fluid flow is parallel through the pair of U-tubes. Figure 28 shows the configurations of ground heat exchangers.

Four different heat input values have been considered (for both the heat injection and heat extraction modes): 1.12 kW, 6 kW, 32 kW and 170 kW. In some cases, especially those related to deep BHEs, the heat input rate values cannot be achieved in real-world TRT experiments. The heat injection/extraction rates from the TRT equipment are not realistic or feasible. These rates are used here in any case, to properly demonstrate the effect of q_{ratio} on the TRT temperature profiles and ILS estimate of k_{gr}. In a few cases, the borehole temperatures are sufficiently low to potentially induce freezing of the ground in the immediate vicinity of the borehole. Freezing of ground moisture is ignored in order to more clearly demonstrate the effect of q_{ratio}. Freezing effects in the case with the coldest borehole would mask the effects due to q_{ratio} in comparison to cases with warmer borehole temperatures.

The pipe diameters differ between the coaxial and U-pipe configurations to make the pipe sizes typical for each configuration. The pipe geometry dimensions related to the coaxial BHEs are the same employed for the simulations reported by (Morchio and Fossa, 2020). Properties of the grout are listed only for the U-tube configurations because the coaxial arrangement uses no grout.

Thirty-two simulations of a 94h TRT have been performed by using the three different models developed by the Authors for the coaxial and the single/double U pipes. The first 4 hours constitute the circulation phase of the experiment employed to make the

carrier fluid reach an almost steady temperature, which is related to the undisturbed ground temperature $T_{gr,\infty}$. Sixteen simulations concern the coaxial pipe of both the BHE lengths and the related heat input rate values. In particular, eight simulations have been performed employing the "annular inlet" hydraulic configuration (four in the "heat injection" and four in the "heat extraction" mode), while eight simulations have been performed employing the "center inlet" hydraulic configuration (four in "heat injection" and four in "heat extraction"). The remaining sixteen simulations concern the U-pipe of both the BHE lengths and the related heat input rate values. In particular, eight simulations are related to the single-U pipe (four in "heat injection" and four in "heat extraction"), while eight simulations are related to the double-U pipe (four in "heat injection" and four in "heat extraction").

Table 13
Main input data of each base case simulation performed.

Input Type	Coaxial 150m	Coaxial 800m	U pipe 150m	U pipe 800m
Calculation type	$\Delta T_{in,out}$ assigned	$\Delta T_{in,out}$ assigned	$\Delta T_{in,out}$ assigned	$\Delta T_{in,out}$ assigned
Domain end radial *r*-coordinate	3.2 m	3.85 m	3.2 m	3.85 m
Domain end axial *z*-coordinate	152.25 m	840 m	152.25 m	840 m
Number of partitions along the *r*-direction	30	30	30	30
Number of partitions along the *z*-direction	30	160	30	160
Finite increment Δz	5.25 m	5.25 m	5.25 m	5.25 m
Time step $\Delta\tau$	4.23 s	12.68 s	4.23 s	12.68 s
Grout thermal resistance weighting factor *Y*	-	-	0	0
Grout thermal capacitance weighting factor *X*	-	-	0.5	0.5
Shank spacing *s*	-	-	0.06 m	0.06 m
Borehole length	150 m	800 m	150 m	800 m
Borehole diameter	0.14 m	0.14 m	0.14 m	0.14 m
Pipe inner radius	0.045 m	0.045 m	0.0163 m	0.0163 m
Pipe wall thickness	0.008 m	0.008 m	0.0037 m	0.0037 m
Annular pipe inner radius	0.0695 m	0.0695 m	-	-
Annular pipe wall thickness	0.0004 m	0.0004 m	-	-
Mass flow rate	0.477 kg/s	2.548 kg/s	0.477 kg/s	2.548 kg/s
Geothermal fluid conductivity	0.6 W/mK	0.6 W/mK	0.6 W/mK	0.6 W/mK
Geothermal fluid density	1000 kg/m^3	1000 kg/m^3	1000 kg/m^3	1000 kg/m^3
Geothermal fluid specific heat capacity	4186 J/kgK	4186 J/kgK	4186 J/kgK	4186 J/kgK
Geothermal fluid dynamic viscosity	0.001 kg/ms	0.001 kg/ms	0.001 kg/ms	0.001 kg/ms
Pipe thermal conductivity	0.42 W/mK	0.42 W/mK	0.42 W/mK	0.42 W/mK
Ground thermal conductivity k_{gr}	3 W/mK	3 W/mK	3 W/mK	3 W/mK

Ground volumetric heat capacity $(\rho c)_{gr}$	3 MJ/m^{3}K	3 MJ/m^{3}K	3 MJ/m^{3}K	3 MJ/m^{3}K
Grout thermal conductivity k_{gt}	-	-	1.2 W/mK	1.2 W/mK
Grout volumetric heat capacity $(\rho c)_{gt}$	-	-	1.35 MJ/m^{3}K	1.35 MJ/m^{3}K
Heat input rate, $\lvert\dot{Q}\rvert$	1.12 kW; 6 kW	32 kW; 170 kW	1.12 kW; 6 kW	32 kW; 170 kW
Heat input rate per unit borehole length, $\lvert\dot{Q}'\rvert$	7.5 W/m; 40 W/m	40 W/m; 213.33 W/m	7.5 W/m; 40 W/m	40 W/m; 213.33 W/m
Ground surface temperature (z=0)	281.15 K	281.15 K	281.15 K	281.15 K
Geothermal gradient, $\frac{dT_{gr,\infty}}{dz}$	0.02 K/m	0.02 K/m	*0.02 K/m*	0.02 K/m

The heat transfer rate has been injected (or extracted) into the geothermal carrier fluid on the top surface between the inlet and outlet section of the BHE (TRT-machine) while maintaining a constant temperature difference at the carrier fluid (see Table 13, "Calculation Type"). The constant and positive natural geothermal gradient of 0.02 K/m has been assumed for the undisturbed ground temperature profile of the simulation cases. Therefore, it is possible to derive the specific heat transfer rate $\dot{Q}'_{geo}$ naturally available related to the geothermal gradient within a length of 150m and 800m respectively, as expressed by Eq. (92).
In such a way it is possible to evaluate the $|q_{ratio}|$ value for each case as reported in Table 14.

Table 14
Main parameters of each base case simulation performed.

Case	$\dot{Q}'_{geo}$	$\lvert q_{ratio}\rvert$
H =150 m; $\lvert\dot{Q}'\rvert$=7.5 W/m	9 W/m	$\lvert q_{ratio,150/7.5}\rvert$ =0.83
H =150 m; $\lvert\dot{Q}'\rvert$=40 W/m	9 W/m	$\lvert q_{ratio,150/40}\rvert$ =4.44
H =800 m; $\lvert\dot{Q}'\rvert$=40 W/m	48 W/m	$\lvert q_{ratio,800/40}\rvert$ =0.83
H =800 m; $\lvert\dot{Q}'\rvert$=213.33 W/m	48 W/m	$\lvert q_{ratio,800/213.33}\rvert$ =4.44

The 800m and 150m BHE cases are characterized by the same q_{ratio} since the heat input rate per unit borehole length values, $\lvert\dot{Q}'\rvert$, and the specific heat transfer rate $\dot{Q}'_{geo}$ values are changed by the same proportionality factor.

3.1.3 Results and discussion

For both the coaxial and the single/double U pipes numerical simulations below demonstrate that the thermal behaviors of the 150m BHE and 800m BHE are similar at the same q_{ratio}. Therefore, q_{ratio} can be considered an important parameter to characterize thermal transient behavior during a TRT. As a consequence, similar ground thermal conductivity k_{gr} and borehole thermal resistance R^*_b estimates are obtained according to the classic ILS approach. As it will be shown in the next sections, similar temperature profiles

arise for the cases characterized by the same q_{ratio} despite the different borehole lengths.

The focus is on the parameter q_{ratio}, because q_{ratio} is apparently the dominant parameter affecting the ILS estimate of k_{gr} among the dimensionless parameters listed in Table 12. The other parameters do affect the ILS model estimate, but their effects are typically less. For instance, 15 out of the 16 cases for a coaxial borehole listed in Tables 15 and 16 of (Beier, 2020), have a $|q_{ratio}|$of 1.1 or less. Other parameters were changed over typical ranges, but errors greater than ±10% were observed in the estimate of k_{gr} by a 1D radial model in 13 of the 16 cases. For the most part, changes in the other parameters did not override the effects of q_{ratio} on the estimate of k_{gr}.

3.1.4 Circulation period prior to heat injection/extraction

During the first period of a TRT, the fluid is typically circulated prior to heat injection/extraction. The average undisturbed ground temperature, $T_{gr,\infty}$, is estimated by the average of the inlet and outlet fluid temperatures. This estimated $T_{gr,\infty}$ after 4 hours of fluid circulation in the numerical simulations is reported in Table 15 and compared with the depth-averaged value of the undisturbed ground temperature profile. The 4-hour circulation period has been chosen as a sufficient time in order to reach stable inlet and outlet fluid temperatures. The given undisturbed ground temperature profile constitutes the initial condition of each numerical simulation.

Table 15

$T_{gr,\infty}$ values calculated as fluid averages at the ground top surface (after 4 hours of fluid circulation) and the corresponding values calculated as depth-averaged values from the initial ground temperature values along the heat exchanger.

Case	$T_{gr,\infty} = \frac{[T_{f,in}(4h) + T_{f,out}(4h)]}{2}$	$T_{gr,\infty} = \frac{1}{N}\sum_{i=1}^{N} T_{gr,i}$
150 m annular inlet	282.77 K	282.62 K
150 m center inlet	282.38 K	282.62 K
150 m single U-pipe	282.66 K	282.62 K
150 m double U-pipe	282.65 K	282.62 K
800 m annular inlet	289.70 K	289.13 K
800 m center inlet	287.33 K	289.13 K
800 m single U-pipe	289.21 K	289.13 K
800 m double U-pipe	289.04 K	289.13 K

For coaxial BHEs in Table 15 the value of $T_{gr,\infty}$ calculated as depth-averaged undisturbed ground temperature differs from the one inferred from the inlet and outlet fluid temperatures. The difference is less for the U-pipe type BHE. This difference is more accentuated as the BHE depth increases (the geothermal gradient is the same for all the cases), as shown by the 800 m cases, and this fact can be related to the heat sink/source effect as the fluid flows through the annular pipe. Since the R_1 value is greater than R_2, the carrier fluid is more capable of effectively maintaining its temperature as it flows up through the center pipe (heat sink effect related to the annular inlet configuration). The

opposite happens for the center inlet hydraulic configuration since the carrier fluid restores part of the heat transfer rate, that has already been extracted, to the surrounding ground through R_2 as it flows up through the annular pipe (heat source effect related to the center inlet configuration).

3.1.5 Heat injection/extraction period

Typically the TRT analysis based on the ILS model uses the average of the inlet and outlet fluid temperatures, $T_{f,ave}(\tau)$. The transient curves of $T_{f,ave}(\tau)$ during heat injection TRTs are

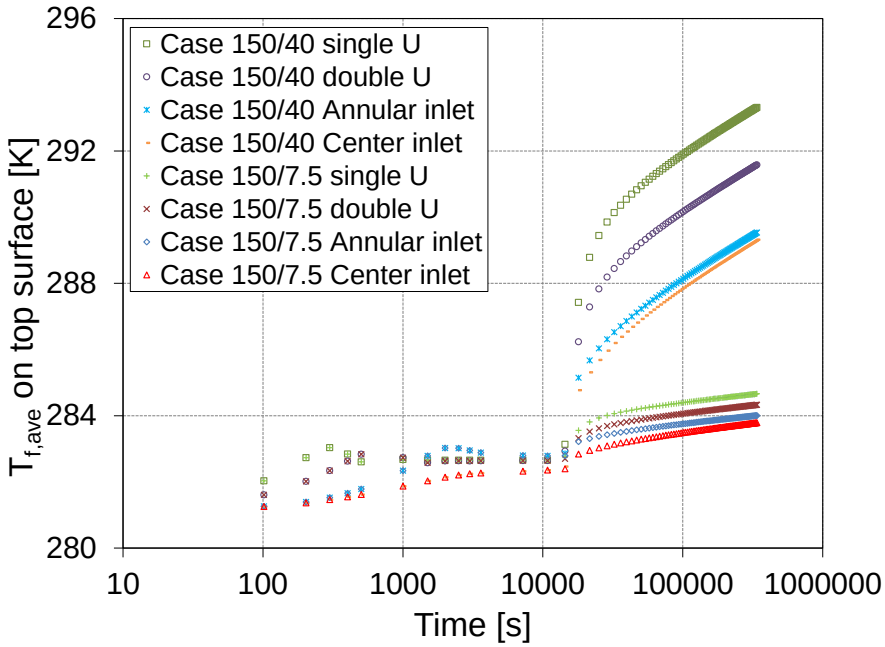

Figure 29 Fluid temperature (inlet/outlet average) as a function of time for different BHE geometries and heat transfer rates (heating mode). During the first 4 hours the fluid is circulated without heat transfer at inlet/outlet sections.

shown in Figure 29 for the 150m coaxial and single-double U BHEs for both q_{ratio} values (in $q_{ratio,150/40}$ and $q_{ratio,150/7.5}$ the first subscript is the depth in meters and the second number is the heat transfer rate per unit length, in W/m). Figure 30 shows the transient curves of $T_{f,ave}(\tau)$ during the heat extraction TRT for the 150m coaxial and single-double U BHEs for both the two different q_{ratio} values ($q_{ratio,150/(-40)}$ and $q_{ratio,150/(-7.5)}$). Figure 29 and Figure 30 show that at the same BHE length (150m) and the same geothermal gradient (0.02 K/m), the different BHE types and hydraulic configurations estimate different undisturbed ground temperatures $T_{gr,\infty}$. The estimate of $T_{gr,\infty}$ is the value of $T_{f,ave}(\tau)$ at the end of the 4 hours of circulation prior to heat injection/extraction. The rise $T_{f,ave}(\tau)$ is a consequence of the natural heat rate associated with geothermal gradient. The subsequent 90 hours of "heat injection" (or "heat extraction") demonstrate how different BHE types and hydraulic configurations determine different temperatures $T_{f,ave}(\tau)$ and, in some cases, also different $T_{f,ave}(\tau)$ slopes (in semi-log representations like the present ones).

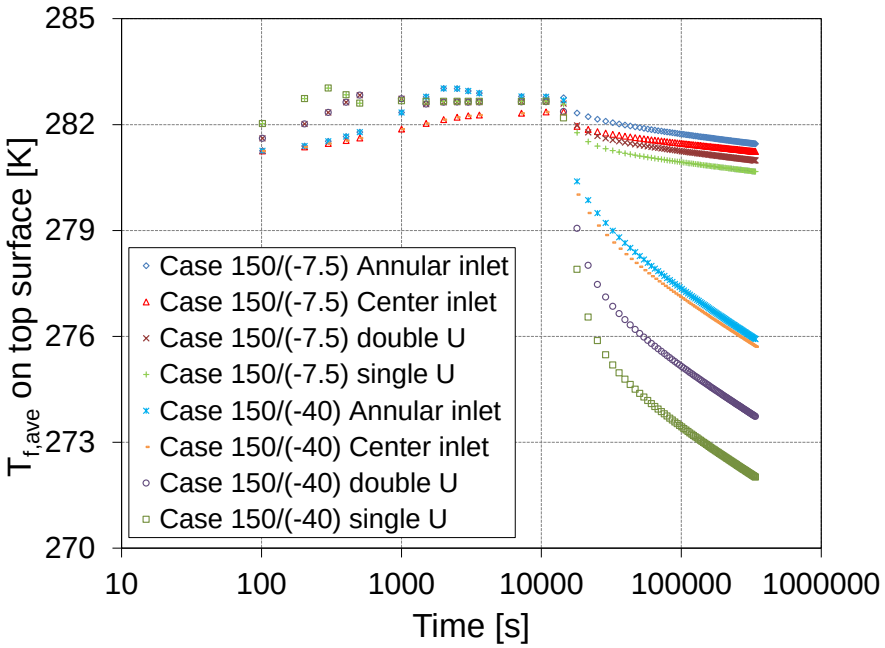

Figure 30 Fluid temperature (inlet/outlet average) as a function of time for different BHE geometries and heat transfer rates (heat extraction mode). During the first 4 hours the fluid is circulated without heat transfer at inlet/outlet sections.

For the cases in the heat injection mode at the same q_{ratio}, the coaxial BHE that adopts the hydraulic configuration "center inlet" is the best BHE in terms of performance (lowest $T_{f,ave}(\tau)$). On the other hand, the single-U BHE is characterized by the highest R^*_b and therefore the highest $T_{f,ave}(\tau)$. For the cases in the heat extraction mode at the same q_{ratio}, the coaxial BHE that adopts the hydraulic configuration "annular inlet" is the best BHE in terms of performance (highest $T_{f,ave}(\tau)$). The single-U BHE is characterized by the highest R^*_b and therefore the lowest $T_{f,ave}(\tau)$. All the cases at the same q_{ratio} are characterized by almost the same slope of the $T_{f,ave}(\tau)$ profile, except for those denoted by the $|q_{ratio,150/7.5}| = |q_{ratio,150/(-7.5)}| = 0.83$. As a consequence, a similar k_{gr} estimate (classic TRT analysis) can be obtained from all the cases except those denoted by $|q_{ratio,150/7.5}| = |q_{ratio,150/(-7.5)}|$. A detailed analysis will be presented in the next section.

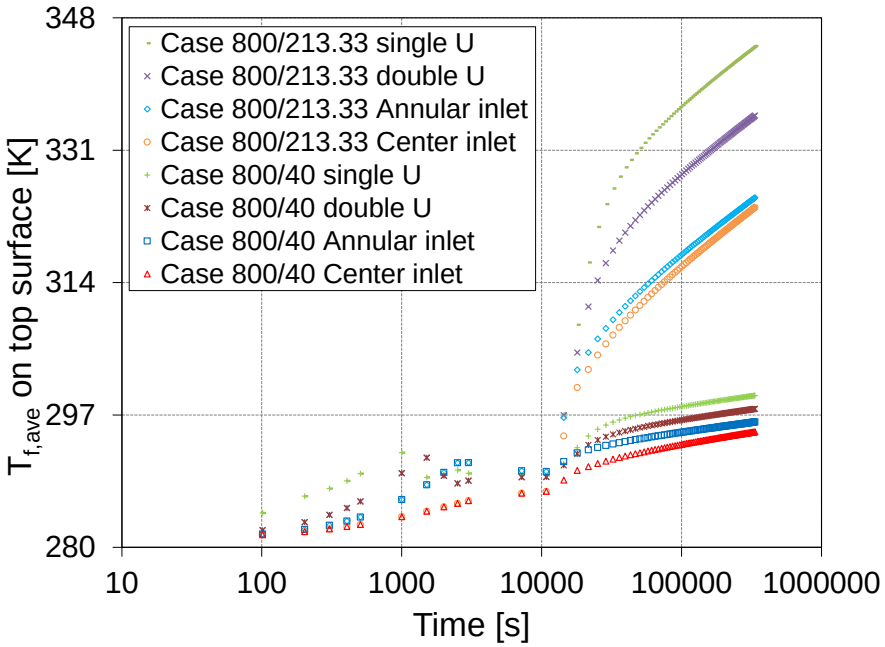

Figure 31 Fluid temperature (inlet/outlet average) as a function of time for different DBHE geometries and heat transfer rates (heating mode). During the first 4 hours the fluid is circulated without heat transfer at inlet/outlet sections.

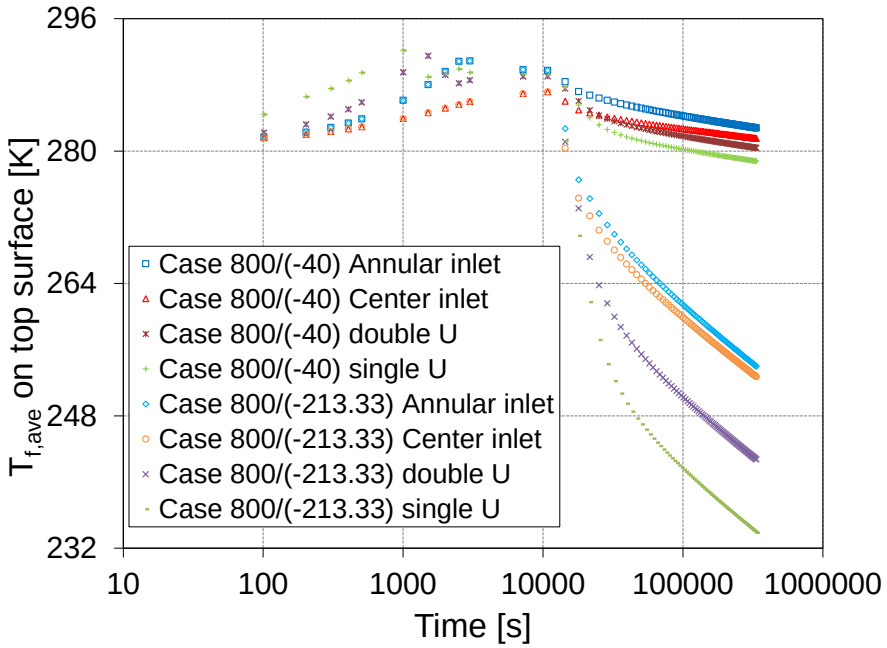

Figure 32 Fluid temperature (inlet/outlet average) as a function of time for different DBHE geometries and heat transfer rates (heat extraction mode). During the first 4 hours the fluid is circulated without heat transfer at inlet/outlet sections.

Similar considerations at the same q_{ratio} can be made for the 800m DBHE cases in the heat

injection (Figure 31) and in the heat extraction (Figure 32) mode. At first glance, the slope of the $T_{f,ave}(\tau)$ profiles denoted by $|q_{ratio,800/40}| = |q_{ratio,800/(-40)}|$ =0.83 and related to the center inlet configuration are different from the ones of the corresponding annular inlet configuration. As a consequence, a similar k_{gr} estimate can be obtained from all the 800m DBHE cases except those denoted by $|q_{ratio,800/40}| = |q_{ratio,800/(-40)}|$ (a detailed

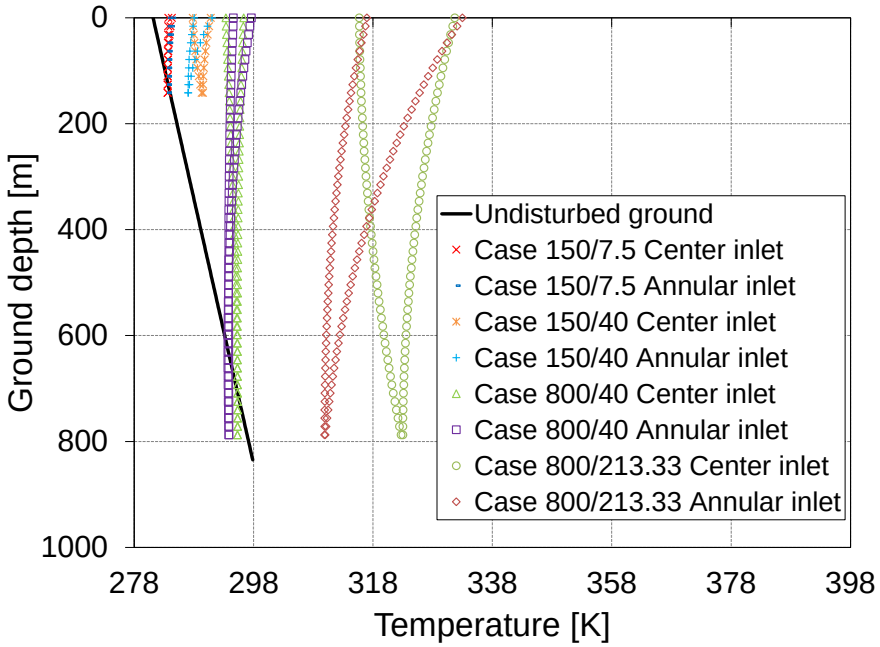

Figure 33 Fluid temperatures as a function of depth for different coaxial BHE configurations and heat transfer rates. Time is the 94th hour. Heat injection mode.

analysis will be presented in the next section).

The vertical temperature profiles of the cases characterized by the same q_{ratio} value are similar and mutually proportional in shape in Figures 33 through 36. For the same q_{ratio} lower than 1, a temperature inversion between the fluid and the undisturbed ground occurs over the same borehole section for different cases. See Figure 33 and Figure 34 with heat injection mode for the coaxial and U-pipe, respectively. Figure 35 and Figure 36 illustrate profiles for the heat extraction mode for the coaxial and U-pipe, respectively.

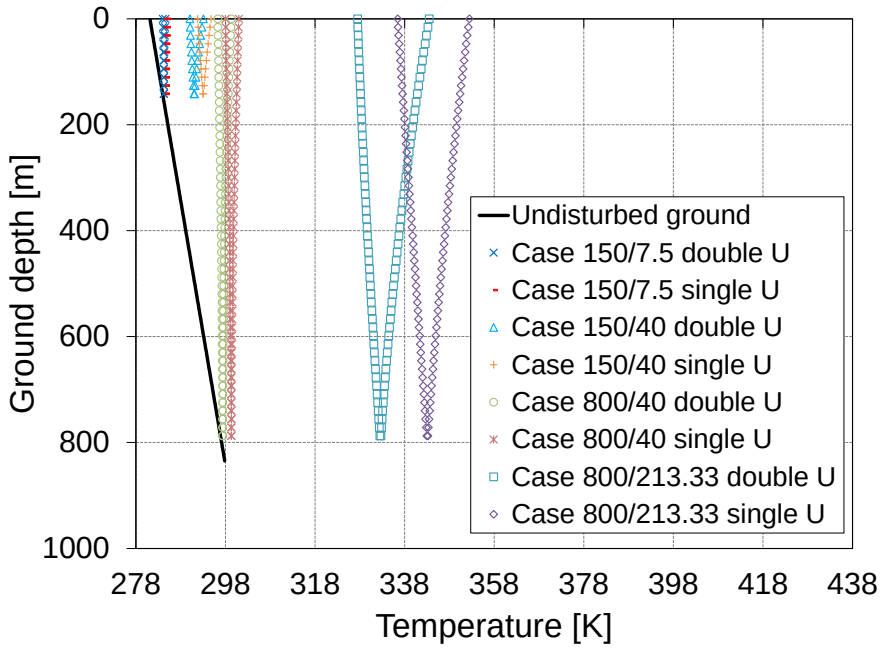

Figure 34 Fluid temperatures as a function of depth for different U-pipe configurations and heat transfer rates. Time is the 94th hour. Heat injection mode.

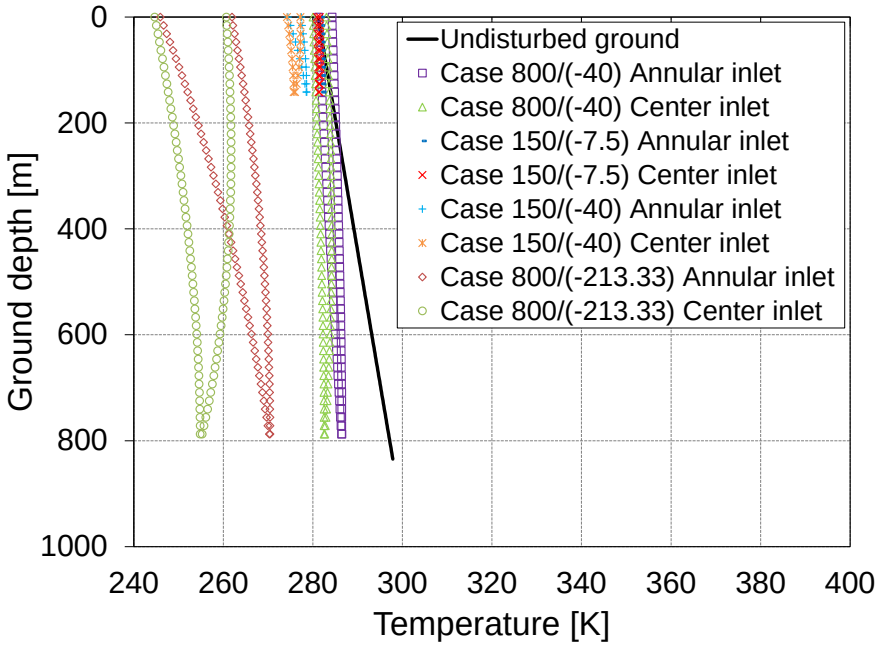

Figure 35 Fluid temperatures as a function of depth for different coaxial configurations and heat transfer rates. Time is the 94th hour. Heat extraction mode.

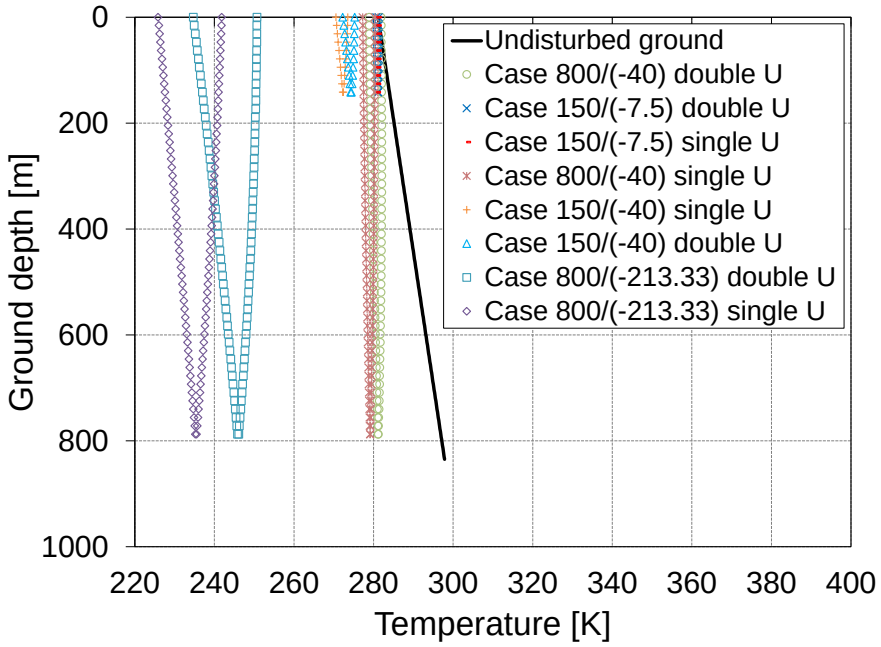

Figure 36 Fluid temperatures as a function of depth for different U-pipe configurations and heat transfer rates. Time is the 94th hour. Heat extraction mode.

Although temperature profiles are shown at only 94 h in Figures 33 to 36, it is useful to review the history of the fluid temperature profiles during the TRT. At time equals zero the fluid temperature profiles in the center pipe and annulus are the same as the geothermal gradient profile. After 4 h of circulation without any heat injection/extraction, the fluid temperature profiles cross the geothermal gradient profile in all cases. Circulation increases the temperature of the fluid at the top and reduces the fluid temperature at the bottom. After the start of heat injection (extraction), the fluid temperatures increase (decrease) and the overall profiles move to the right (left). The cumulative movement is larger at 94 h for the cases with a larger value of q_{ratio}.

At time 94 h some of the fluid temperature profiles cross the linear geothermal gradient profile in Figures 33 and 35 for the coaxial BHE. In these cases with $|q_{ratio}|$ lower than 1, the external heat transfer rate $\dot{Q}$ (for both the heat injection and extraction modes) is not sufficient to always override the radial heat transfer rate that the carrier fluid in the annular pipe exchanges with the surrounding ground. This inevitably leads to temperature inversions between the fluid and the surrounding (undisturbed) ground at 94 h. For cases with $|q_{ratio}|$ greater than 1 as listed in Table 14, the corresponding temperature profiles in Figures 33 to 36 do not have a temperature inversion. In these cases, the external heat transfer rate $\dot{Q}$ is large enough to move the fluid temperature profiles at 94 h completely away from the geothermal gradient profile. These temperature inversions are partially mitigated when the carrier fluid flows through the coaxial BHE according to the center inlet hydraulic configuration. When the $|q_{ratio}|$ is lower than 1 and the fluid flow is moving upward in the annulus, the heat source effect due to the geothermal gradient tends to dominate. Similarly, when the $|q_{ratio}|$ is lower than 1 and the fluid flow is downward

oriented in the annulus, the heat sink effect due to the geothermal gradient tends to dominate. As a consequence, for the heat injection mode, the fluid temperatures in the annular pipe in "Case 800/40 Center inlet" and "Case 150/7.5 Center inlet" are higher on the bottom part of the BHE (and lower in the BHE upper part) than those of the corresponding "Annular inlet" cases as shown by Figure 33. Equivalently, for the heat extraction mode, the temperature levels of the fluid in the annular pipe in "Case 800/(-40) Center inlet" and "Case 150/(-7.5) Center inlet" are lower on the bottom part of the BHE (and higher in the BHE upper part) than those of the corresponding "Annular inlet" cases as shown by Figure 35. The inversions between the fluid and the surrounding ground temperatures thus inevitably occur in the bottom part of the coaxial BHE of the "800/40" and "150/7.5" cases ($|q_{ratio}|<1$) for both the hydraulic configurations adopted.

As reported by several literature studies about deep BHEs (Holmberg et al., 2016, Wang et al., 2017, Zanchini et al., 2009) the flow inlet in the annulus is more beneficial for deep, coaxial BHEs in the heat extraction mode (because of the highest $T_{f,ave}(\tau)$ thanks to the favorable ground profile when the cold fluid is flowing down in the annular pipe). Equivalently, the flow inlet in the center pipe is more beneficial for deep, coaxial BHEs in the heat injection mode (because of the lowest $T_{f,ave}(\tau)$ thanks to the favorable ground profile when the hot fluid is rising in the annular column). This is more accentuated as the BHE depth increases (at the same geothermal gradient), as shown by the 800 m cases, and this fact can be attributed to the q_{ratio} effect as related to the heat sink/source effect as the fluid flows through the annular pipe.

When the geothermal gradient is constant and positive, the carrier fluid direction (upward or downward in the annular column) can determine also different $T_{gr,\infty}$ for the coaxial cases. This difference is more accentuated for the 800 m coaxial cases. The two $T_{f,ave}(\tau)$ profiles (related to the two hydraulic configurations for coaxial BHEs of the same length) tend to overlap and to reach a common temperature value at the end of the experiment when the $|q_{ratio}|$ is greater than 1, as shown by Figures 29 to 32. On the other hand, the $|q_{ratio}|$ lower than 1 tends to keep the $T_{f,ave}(\tau)$ profiles (center inlet vs annular inlet) farther apart from each other, as shown by Figures 29 to 32. In general, the $|q_{ratio}|$ influences the performance of the coaxial BHE of the same length since the $T_{f,ave}(\tau)$ related to the annular inlet hydraulic configuration tends to be more different from the one related to the center inlet when the $|q_{ratio}|$ is lower than 1.

Some studies (Holmberg et al., 2016, Beier et al., 2013, Beier, 2014) report that the flow direction has no significant influence for short boreholes (≈ 200 m). This is because in these cases the $|q_{ratio}|$ tends to be greater than 1 for the typical thermal powers at the TRT machine and the geothermal gradient values. No temperature inversions occur at 94 h when $|q_{ratio}|$ is greater than 1 as clearly shown in Fig. 32 and Fig. 34.

Note temperature inversions can still occur at earlier times during the TRT. The q_{ratio} has a lower effect on the temperature profiles of the U pipes. The temperature inversions between fluid and surrounding ground do not occur for the U pipes when $|q_{ratio}|<1$, since the thermal resistance of the grout material tends to lead the carrier fluid to higher temperature levels during the heat injection experiments. Indeed, for the U-pipes the "150/7.5 double U" and "800/40 double U" ($|q_{ratio}|<1$) are the only cases that show some temperature inversions in the bottom part of the BHE as shown in Fig. 33 and Fig. 35.

Additional simulations (not reported here for the sake of brevity) performed at the same geothermal gradient of 0.02 K/m, indicate that the temperature inversions for the U pipes can occur only for $|q_{ratio}|<<1$.

The vertical and horizontal coordinates in Figures 33, 34, 35, 36 can be scaled so that the vertical profiles for the two different borehole lengths almost overlap each other. That is, Eqs. (98) and (99) indicate the vertical coordinate z_D and the horizontal coordinate θ_D. These coordinates are rewritten as:

$$z_D = \frac{z}{H} \tag{98}$$

$$\theta_D = \frac{2\pi\, k_{gr} H\, (T - T_{gr,\infty})}{\dot{Q}} \tag{99}$$

Figures 37 and 38 show the new scaled profiles related to Figures 33 and 34 respectively that have been reported as an example.

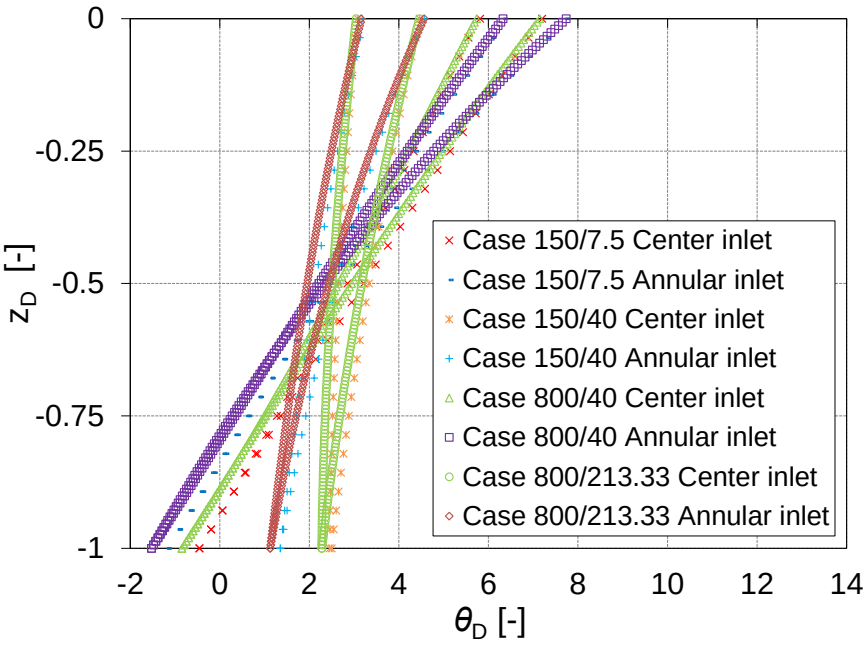

Figure 37 Non dimensional fluid temperatures as a function of non dimensional depth for different coaxial configurations and heat transfer rates. Time is the 94th hour. Heat injection mode.

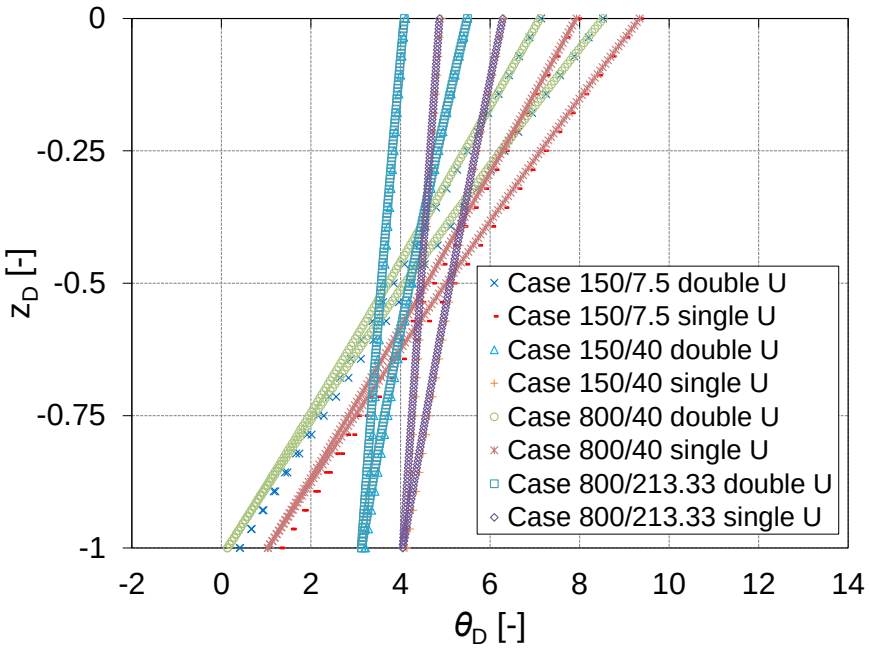

Figure 38 Non dimensional fluid temperatures as a function of non dimensional depth for different U-pipe configurations and heat transfer rates. Time is the 94th hour. Heat injection mode.

The negative values of θ_D denote the temperature inversions between the fluid and the surrounding ground and the related z_D positions. Perfect numerical agreement between the dimensionless profiles related to the 150/7.5, 800/40 and 150/40, 800/213.33 cases is not

achieved, especially in the bottom part of the BHE. This is due to the differences between the local thermal resistance R_1, R_2, R_{fb}, R_{12} values among the cases characterized by the same q_{ratio} which in turn imply different values for some dimensionless groups in Table 12 despite the same $\frac{H}{\dot{m}}$. The differences in the R_1, R_2, R_{fb}, R_{12} values among the cases characterized by the same q_{ratio} are due to the different convective heat transfer coefficients h_a, h_c. These values are calculated based on the fluid mean velocity inside the pipe and the related Reynolds numbers, Re_{d_h}, based on the hydraulic diameter d_h.

3.1.6 Estimates of k_{gr} and R^*_b

An analysis devoted to the k_{gr} estimation from the slope of the $T_{f,ave}(\tau)$ profile in a semi-logarithmic time scale has been done for all the simulation cases. The procedure has been implemented to investigate if the ILS approximation is a suitable TRT approach also for the DBHEs and analyze the q_{ratio} influence on the ILS-based estimations. The k_{gr} program input value of 3 *W/mK* has been imposed for all the cases. Since the borehole radius r_b and the ground thermal properties are the same for all the simulated cases, the Fo_{rb} number assumes the same values for all the cases. The analysis has been made for different Fo_{rb} intervals by varying the starting Fo_{rb} from 10 to 55 in increments of 5. The Fo_{rb} value of *66.12* at the end of the TRT remains fixed, which is related to the end of the 90-h period of heat injection/extraction. The k_{gr} values have been estimated for each Fo_{rb} window. The k_{gr} estimated values for all the simulated cases in the heat injection and extraction mode are reported in Table 16 where Fo_{rb} assumes the following range: $10 \leq Fo_{rb} \leq 66.12$. The results of the classic ILS-analysis on the k_{gr} estimate for all the Fo_{rb} windows are shown in Figure 39 (for the 150m BHEs) and in Figure 40 (for the 800m BHEs) for the heat injection cases. The results for all the Fo_{rb} windows are shown in Figure 41 (for the 150m BHEs) and in Figure 42 (for the 800m BHEs) for the heat extraction cases.

Table 16

Ground thermal conductivity estimated values considering the $10 \leq Fo_{rb} \leq 66.12$ interval compared to the k_{gr} value (3.0 W/(mK)) imposed in the program input file.

Case	k_{gr} (ILS-estimated value)	|% Error|
150/7.5 Center inlet	2.627 [W/mK]	12.43 %
150/7.5 Annular inlet	3.143 [W/mK]	4.76 %
150/7.5 single U	2.955 [W/mK]	1.49 %
150/7.5 double U	2.945 [W/mK]	1.84 %
150/40 Center inlet	2.914 [W/mK]	2.87 %
150/40 Annular inlet	3.017 [W/mK]	0.56 %
150/40 single U	2.963 [W/mK]	1.23 %
150/40 double U	2.968 [W/mK]	1.06 %
800/40 Center inlet	2.593 [W/mK]	13.55 %
800/40 Annular inlet	3.177 [W/mK]	5.90 %
800/40 single U	2.905 [W/mK]	3.16 %
800/40 double U	2.917 [W/mK]	2.77 %

800/213.33 Center inlet	2.937 [W/mK]	2.10 %
800/213.33 Annular inlet	3.058 [W/mK]	1.94 %
800/213.33 single U	2.904 [W/mK]	3.20 %
800/213.33 double U	2.941 [W/mK]	1.96 %
150/(-7.5) Center inlet	3.466 [W/mK]	15.54 %
150/(-7.5) Annular inlet	2.849 [W/mK]	5.02 %
150/(-7.5) single U	2.974 [W/mK]	0.85 %
150/(-7.5) double U	3.002 [W/mK]	0.09 %
150/(-40) Center inlet	3.068 [W/mK]	2.27 %
150/(-40) Annular inlet	2.962 [W/mK]	1.27 %
150/(-40) single U	2.966 [W/mK]	1.11 %
150/(-40) double U	2.979 [W/mK]	0.70 %
800/(-40) Center inlet	3.642 [W/mK]	21.41 %
800/(-40) Annular inlet	2.899 [W/mK]	3.33 %
800/(-40) single U	2.899 [W/mK]	3.33 %
800/(-40) double U	2.977 [W/mK]	0.76 %
800/(-213.33) Center inlet	3.128 [W/mK]	4.27 %
800/(-213.33) Annular inlet	3.006 [W/mK]	0.21 %
800/(-213.33) single U	2.903 [W/mK]	3.23 %
800/(-213.33) double U	2.952 [W/mK]	1.58 %

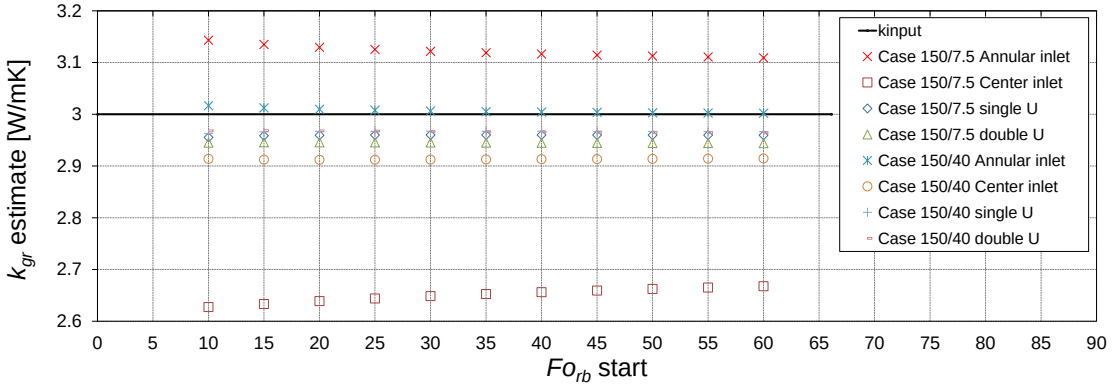

Figure 39 Ground conductivity estimates from classic TRT analysis as a function of the Fourier number window taken into consideration. BHE geometry and operating conditions are the parameters (heat injection cases related to the 150m BHEs).

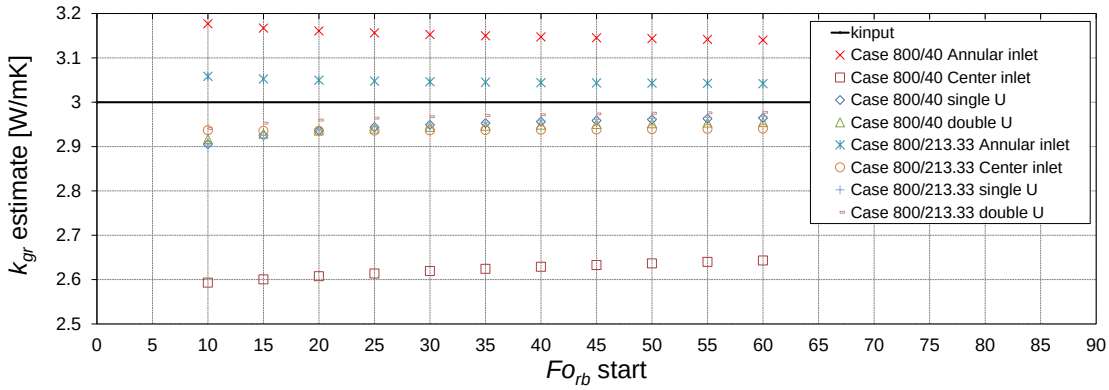

Figure 40 Ground conductivity estimates from classic TRT analysis as a function of the Fourier number window taken into consideration. BHE geometry and operating conditions are the parameters (heat injection cases related to the 800m DBHEs).

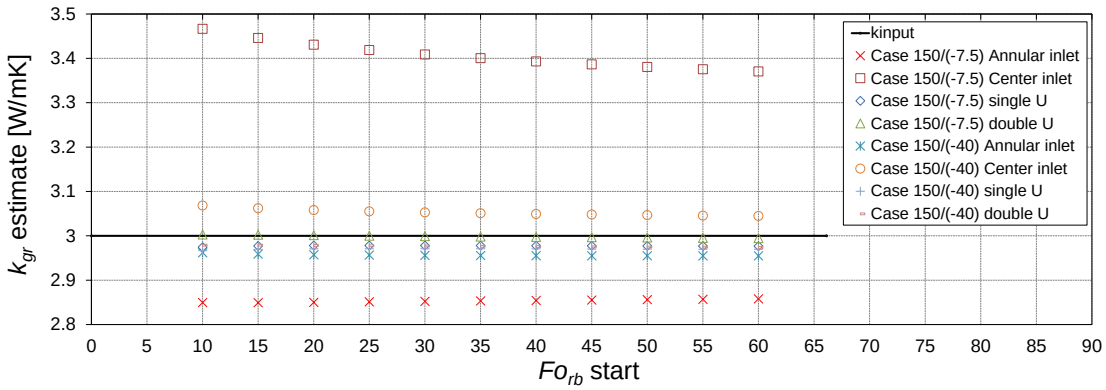

Figure 41 Ground conductivity estimates from classic TRT analysis as a function of the Fourier number window taken into consideration. BHE geometry and operating conditions are the parameters (heat extraction cases related to the 150m BHEs).

Table 16 and Figures 39 through 42 show that the error of the k_{gr} estimate (equal to 3 W/mK) is less than ±5% for the 150m and 800m U-pipe BHEs. For the coaxial BHE, the error is lower than ±5% for both the hydraulic configurations only if $|q_{ratio}|$ is greater than 1. See cases denoted by $\left|q_{ratio,800/213.33}\right| = \left|q_{ratio,800/(-213.33)}\right| = 4.44$ and $\left|q_{ratio,150/40}\right| = \left|q_{ratio,150/(-40)}\right| = 4.44$.

The error in the k_{gr} estimation can be higher than ±10% only for $|q_{ratio}|$<<1 in the case of U-pipes. Additional simulations (not plotted here for the sake of brevity) with $|q_{ratio}|$ equal to 0.052 show the error can be higher than ±15% in case of the double U-BHE. The $|q_{ratio}|$ of 0.052 corresponds to heat input rate values of the order of 70 W for the 150m U-BHE and 2 kW for the 800m U-DBHE. Such low thermal powers are not usually employed at the TRT machine in real-world TRT experiments. For this reason, the TRT analysis based on the classic ILS approach has not revealed limitations for the U pipes. Still, for deep coaxial boreholes, the influence of the magnitude of the heat transfer rate per unit length should be considered in terms of $|q_{ratio}|$ in future TRT guidelines at the national and

international level.

In Table 16 the estimated k_{gr} values related to the coaxial 150/40 and 800/40 cases are different from those related to the same cases reported in (Morchio and Fossa, 2020). The correct estimated values are those reported in Table 16 of the present thesis. The k_{gr} estimations reported in (Morchio and Fossa, 2020) were affected by a systematic error due to computational issues. A corrigendum (Morchio and Fossa, 2021) to the previous paper (Morchio and Fossa, 2020) has been prepared by the Authors for the Reader of both papers. The main conclusions in paper (Morchio and Fossa, 2020) remain unchanged with the corrected values.

The estimated R^*_b value is the intercept in the simplified line-source model for each Fo_{rb} window. Then, the ILS-based model has been applied for each Fo_{rb} window by employing the corresponding k_{gr} estimated value for the same Fo_{rb} intervals. Figures 43 and 44 show the results for the coaxial BHEs with heat injection and extraction, respectively. Results for the single and double U - pipe BHEs are in Figures 45 and 46 with heat injection and extraction, respectively.

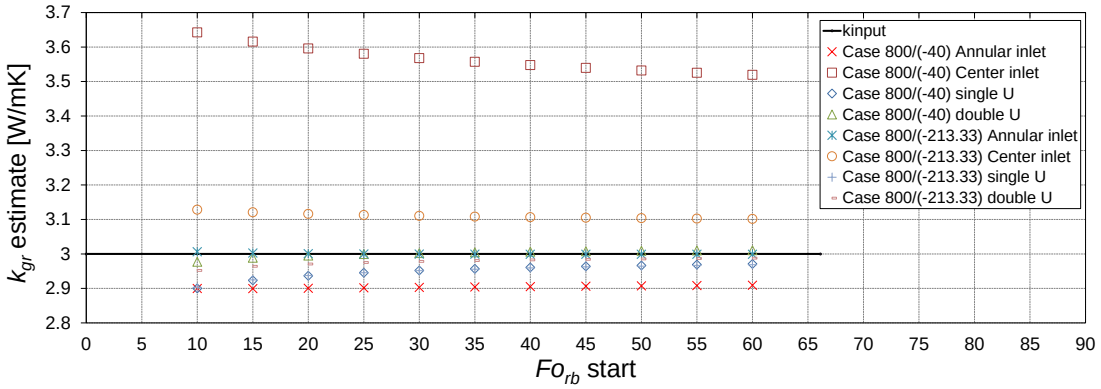

Figure 42 Ground conductivity estimates from classic TRT analysis as a function of the Fourier number window taken into consideration. BHE geometry and operating conditions are the parameters (heat extraction cases related to the 800m DBHEs).

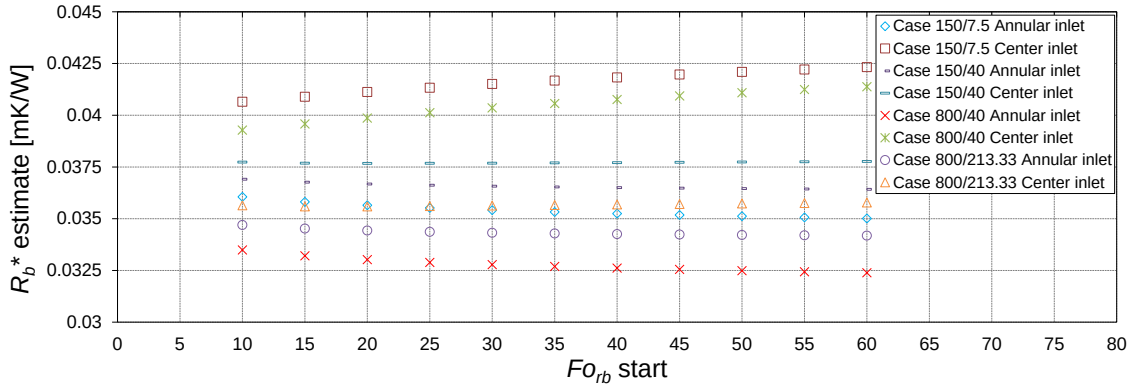

Figure 43 Effective borehole thermal resistance estimates from classic TRT analysis as a function of the Fourier number window taken into consideration. BHE length and operating conditions are the parameters (heat injection cases related to the coaxial BHEs).

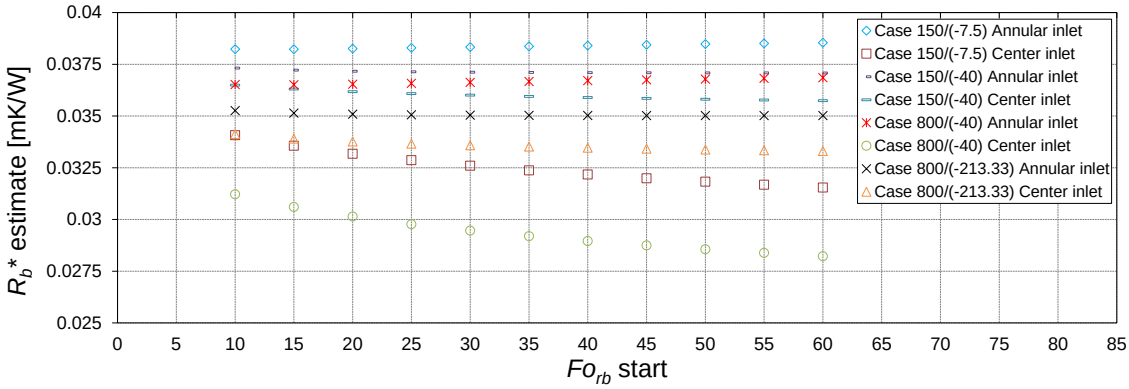

Figure 44 Effective borehole thermal resistance estimates from classic TRT analysis as a function of the Fourier number window taken into consideration. BHE length and operating conditions are the parameters (heat extraction cases related to the coaxial BHEs).

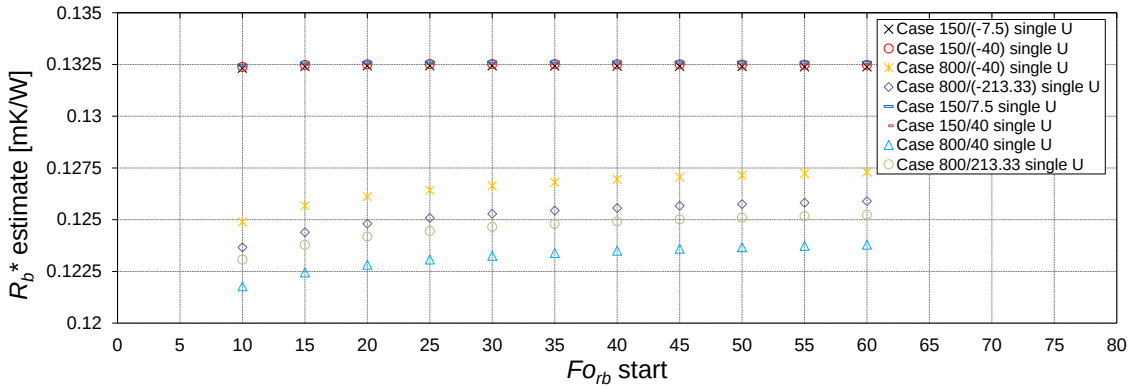

Figure 45 Effective borehole thermal resistance estimates from classic TRT analysis as a function of the Fourier number window taken into consideration. BHE length and operating conditions are the parameters (heat injection/extraction cases related to the single U-pipe BHEs).

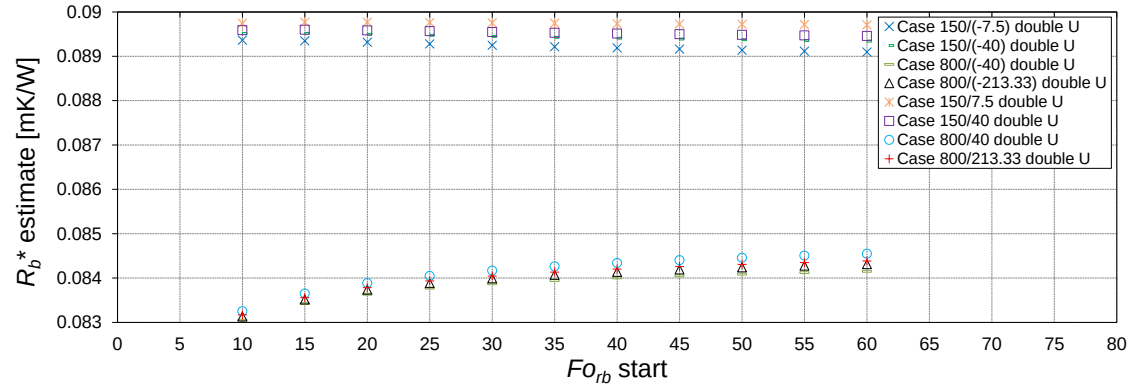

Figure 46 Effective borehole thermal resistance estimates from classic TRT analysis as a function of the Fourier number window taken into consideration. BHE length and operating conditions are the parameters (heat injection/extraction cases related to the double U-pipe BHEs).

Furthermore, the overall R^*_b value for the 150m and 800m BHE cases has been computed as the mean of the values assumed inside the $10 \leq Fo_{rb} \leq 66.12$ interval. The overall R^*_b mean value inside the $10 \leq Fo_{rb} \leq 66.12$ window ranges from -1.88% to -7.27% of the values reported in Figures 43 to 46.

From Figures 43 through 46 the coaxial BHE is characterized, especially for the DBHE cases, by a better performance in terms of $T_{f,ave}(\tau)$ and lower R^*_b than the U-BHE types (for the same $|q_{ratio}|$ value). This trend applies to both the "Heat injection" and the "Heat extraction" operation modes. This numerically confirms the findings reported by

(Acuña, 2013) and (Hellstrom, 2002).

For the coaxial BHE, it has to be noted that when the $|q_{ratio}|$ is lower than 1 (as for the cases denoted by $\left|q_{ratio,800/40}\right| = \left|q_{ratio,800/(-40)}\right| = 0.83$ and $\left|q_{ratio,150/7.5}\right| = \left|q_{ratio,150/(-7.5)}\right| = 0.83$) different R^*_b estimates occur since the different hydraulic configurations involve different k_{gr} estimates. In the case of heat injection mode, the k_{gr} has been underestimated for the "center inlet" cases of these types, while it is overestimated for the "annular inlet" cases of the same types. As a consequence, the coaxial BHE has greater R^*_b when the hydraulic configuration is "center inlet". On the other hand, the coaxial BHE has a lower R^*_b when the hydraulic configuration is "annular inlet", as shown by Figure 43. In heat extraction mode, the k_{gr} has been overestimated for the "center inlet" cases, while it is underestimated for the "annular inlet" cases of the same types. As a consequence, the coaxial BHE has a greater R^*_b when the hydraulic configuration is "annular inlet". The coaxial BHE has a lower R^*_b when the hydraulic configuration is "center inlet", as shown by Figure 44.

3.1.7 Explanation for different q_{ratio} effects on U-pipe and coaxial BHEs

The main findings from the simulation results related to the U-pipe cases are summarized here. The q_{ratio} has a smaller effect on the temperature profiles of the U pipes compared to the profiles of the coaxial BHEs. The temperature inversions between fluid and surrounding ground do not tend to occur for the U pipes when $|q_{ratio}|<1$. The temperature inversions for the U pipes apparently occur only for $|q_{ratio}|<<1$. The error in the k_{gr} estimation can be higher than ±10% only for $|q_{ratio}|<<1$ in the case of U-pipes, unlike the coaxial cases.

This section is aimed to provide a physical explanation for why the q_{ratio} effects are less for the U-tube boreholes than the coaxial boreholes. Picture an elemental fluid volume of thickness *dz* in one of the U-pipes. If the flow is downward through the pipe, then the q_{ratio} term (last term) in Eq. (93) acts as a heat sink, because the geothermal gradient tends to cause cooler fluid from above to enter the elemental volume. On the other hand, the term acts as a heat source under upward fluid flow, because the geothermal gradient tends to make warmer fluid enter the elemental volume from below.

The geothermal gradient influences the borehole fluid through radial heat conduction in the ground to or from the borehole wall. For the U-tube pipe arrangement, radial heat transfer follows similar pathways between the fluid in each pipe and the undisturbed ground with the geothermal gradient. Then, the effects (due to q_{ratio}) on the fluid in each pipe are more likely to have similar magnitudes but oppose each other (source/sink). They are more likely to cancel each other. In the coaxial BHE, the fluid in the annulus has a more direct pathway to heat exchange with the ground than the fluid in the center pipe. In order for the fluid in the center pipe to gain or lose heat with the ground, the heat must travel through the annular fluid. Thus, the heat transfer is indirect between the ground and the center-pipe fluid. Without the symmetry of the U-pipe arrangement, the effects of q_{ratio} are unbalanced on the two flow streams. Thus, the opposing effects (source/sink) are more likely to have different magnitudes and do not cancel. This unbalance makes the net effect of q_{ratio} larger in the coaxial borehole. These physical mechanisms can be linked to terms in the energy conservation equations for the circulating

fluid.

3.2 The influence of the q_{ratio} parameter and the g_0-transfer function on the ILS-based k_{gr} estimations in TRT with coaxial, single and double U BHE involving a single or multiple ground layers with different geothermal gradients

Among the different parameters investigated, the present section demonstrates that in TRT analyses the q_{ratio} is the dominant parameter that indicates when the ILS-based k_{gr} estimated value departs from the weighted-thickness average. The simulations' results highlight how the ILS-based k_{gr} estimated values are affected by the effect of the geothermal gradient when q_{ratio} is far from the condition q_{ratio} >>1. The effect of the q_{ratio} parameter on the TRT analyses is also related to a specific dimensionless *g*-transfer function called g_0 that is evaluated for performing the FFT spectral method. The g_0 function is obtained by performing a complete circulation test of the same duration of the TRT without conferring any heat input rate. The g_0 function incorporates the geothermal gradient. The study has been conducted considering shallow and deep BHEs, with and without geothermal gradient, and for homogeneous and stratified ground thermal conductivities.

The sizing of GCHP systems requires the most accurate knowledge of the ground thermal properties. In particular, the ground thermal conductivity k_{gr} and its variation along with depth are of primary importance for the correct sizing and selecting the most cost-effective depth for a borehole field. The TRT constitutes the usual experimental procedure to be performed by exploiting a pilot BHE already installed in order to estimate the ground thermal conductivity and borehole thermal resistance.

In the present study three Fortran90 programs implementing the finite-difference (FD) models related to coaxial, single and double U BHEs presented in previous investigations by the present research group (Morchio and Fossa, 2019, Morchio and Fossa, 2020) have been exploited for evaluating the influence of specific TRT parameters on the ground thermal conductivity estimation when the First Order Approximation (FOA) of the ILS model by (Carslaw and Jaeger, 1959) is applied in TRT analysis. The simulated cases reported in the present study are addressed to evaluate the influence of these parameters for shallow and Deep BHEs penetrating a single or multiple ground layers with different geothermal gradients imposed along the depth.

A previous study by (Liu et al., 2020) highlights how the layered subsurface and geothermal gradient have a great impact on the heat extraction performance of a medium-deep borehole heat exchanger. The weighting factors on individual-layer properties proper of the layer-factor method developed by (Beier et al., 2021) reveal how conventional 1D models determine the effective ground thermal conductivity in simulated DTRTs in deep boreholes. The weighting factors change with heat injection versus heat extraction, placement of the fluid inlet, and the direction of increasing ground thermal conductivity. The studies by (McDaniel et al., 2018, Luo et al., 2014, Signorelli et al., 2007, Lee, 2011) found that the ILS-based k_{gr} estimated value is near the weighted-thickness average. It has to be taken into account that these last studies together with those numerical and

experimental by (Lee and Lam, 2012, Raymond and Lamarche, 2013, Luo et al., 2015, Li et al., 2017, Hu, 2017, Erol and François, 2018) on TRT and DTRT analyses were focused on shallower boreholes (depth < 150 m).

(Beier, 2020) developed a 2D heat transfer model of coaxial DBHEs (depth > 350 m) able to highlight how the geothermal gradient affects TRT estimates of ground thermal conductivity. The study by (Beier et al., 2022) was focused on performing DTRT analyses through numerical models for coaxial DBHEs to study the effect of upward and downward increasing trends of thermal conductivity among ground layers on the estimate of the mean k_{gr} and the k_{gr} estimates for individual layer.

The present study extends the analyses of simulated TRT and DTRT involving single and multiple layers with a constant (or variable with depth) and positive geothermal gradient considering coaxial, single and double U DBHEs. Among the different parameters investigated, the present study highlights the effect of the q_{ratio} parameter introduced by (Morchio et al., 2022) on the ground thermal conductivity estimation when the conventional-1D ILS model is applied to interpret the TRT data. As the borehole depth increases, more importance is assumed by the q_{ratio} parameter. This implies that during the planning and the execution of a TRT, especially when DBHEs are involved, it should be highly recommended to have performed and made available the undisturbed ground temperature profile measurements, like those provided by (Holmberg et al., 2018) to have an estimate of the natural heat rate $\dot{Q}'_{geo}$. In this manner, the engineer can choose the more suitable heat transfer rate $\dot{Q}'$ to apply to the carrier fluid during the TRT, thus controlling and in case modifying q_{ratio}. The simulations' results reported in the present section verify that q_{ratio} is the dominant parameter that indicates when the ILS-based k_{gr} estimated value departs from the weighted-thickness average.

In addition, the present section is aimed to highlight how the effect of the q_{ratio} parameter on the TRT analyses is also related to a specific dimensionless g-transfer function called g_0 that is obtained by performing a complete circulation test of the same duration of the TRT. The dimensionless temperature transfer functions (Temperature Response Factor) and the related approach of the g-functions are credited to (Eskilson, 1987). Further developments for their convolutions performed in the spectral domain are due to (Marcotte and Pasquier, 2008, Pasquier and Marcotte, 2013, Pasquier and Marcotte, 2014). The g_0 function incorporates the geothermal gradient and in general, the disturbance effect (particularly prominent for DBHEs) related to the undisturbed ground temperature profile during the TRT. One of the aims of the present section is to demonstrate that when q_{ratio} is lower than 1 the $g_{0,j}(\tau)$ function is able to modify the slope of the general solution $T_{f,j}(\tau)$ for each fluid node.

3.2.1 Theory and insights on q_{ratio} parameter and the g-transfer functions in TRT analysis

The k_{gr} estimated value by applying the ILS model in the TRT analysis in cases of single and multiple layers is an effective value of the ground thermal conductivity. This value is near the weighted-thickness average, as confirmed by previous studies focused on shallower boreholes (depth < 150 m) by (McDaniel et al., 2018, Luo et al., 2014, Signorelli et al., 2007, Lee, 2011). For layered ground, the average is the effective ground thermal

conductivity for parallel heat conduction through layers with boundary conditions of uniform temperature at each end. Thus, the weighted average is a useful reference value. In the case of layers with equal thickness, the average is the simple arithmetic mean.

Except for the first 20 m of the substrate that is subjected to seasonal temperature oscillations, the ground temperature approximately increases linearly with depth, according to a geothermal gradient generally in the 0.02-0.03 K/m range. The ground temperature behavior can be well described by the (Lunardini, 1981) analytical solution. Quite rare "geothermal anomalies" (due to surface magma chambers) and the presence of deep water-saturated soils are the exceptions to the above rule. In TRT and GCHP applications, the importance assumed by the q_{ratio} parameter increases, according to its definition (Eq. 91), as the borehole active depth H increases.

The typical depth H reached by the DBHEs allows the exploitation of the natural heat $\dot{Q}'_{geo}$ made available at such depths. In particular, the thermal performance and the heat transfer rate that can be extracted by the DBHEs for GCHP applications are enhanced as the $\dot{Q}'_{geo}$ is higher, as shown by previous studies by (Mazzotti et al., 2018, Holmberg et al., 2016, Morchio et al., 2022). On the other hand, as highlighted by (Morchio et al., 2022) the k_{gr} estimated value from an ILS-based TRT analysis can be highly influenced by the q_{ratio} parameter. This is because as the borehole active depth H increases, the thermal interaction between the external injected/extracted $\dot{Q}/H$ and the natural $\dot{Q}'_{geo}$ increases. The numerical results related to the simulations reported in the present study for a single and a multilayered subsurface of different k_{gr} values lead to understanding and verifying that q_{ratio} is the dominant parameter that indicates when the ILS-based k_{gr} estimated value departs from the weighted-thickness average. One of the main assumptions of the ILS model is that a constant heat transfer rate in time and space is irradiated (or absorbed) from a linear source embedded into a medium of infinite extent. According to (Pasquier and Marcotte, 2013) if the heat flux signal is of step function type varying with time, the temporal superposition principle can be used to express the temperature variation at any time $\tau=\tau_{n_t}$, where n_t is the number of previous time steps:

$$T(r,\tau) - T_{gr,\infty} = \sum_{n=1}^{n_t} \frac{\dot{Q}'_n - \dot{Q}'_{n-1}}{4\pi k_{gr}} \int_{\frac{r^2}{4\alpha_{gr}}}^{\infty} \frac{e^{-\beta}}{\beta} d\beta; \qquad \tau_{n_t-1} < \tau \leq \tau_{n_t} \tag{100}$$

which can be rewritten, for each j_{th} node of the fluid domain, as:

$$T_{f,j}(\tau) - T_{gr,\infty} = \sum_{n=1}^{n_t} f(\tau_n) g_j(\tau - \tau_{n-1}) \tag{101}$$

where

$$f(\tau_n) = \dot{Q}'(\tau_n) - \dot{Q}'(\tau_{n-1}) \tag{102}$$

and

$$g_j(\tau - \tau_{n-1}) = \frac{1}{4\pi k_{gr}} \int_{\frac{r^2}{4\alpha_{gr}}}^{\infty} \frac{e^{-\beta}}{\beta} d\beta \tag{103}$$

Therefore, according to (Pasquier and Marcotte, 2013), the ILS model can be decomposed into an incremental heat flux function f and a model-specific integral g_j evaluated for a constant and unit heat pulse (Marcotte and Pasquier, 2008) for each j_{th} node, see Eqs. (101), (102), (103). Computing Eq. (101) in the time domain for a long heat flux signal $\dot{Q}'$ is computationally intensive. (Marcotte and Pasquier, 2008) noticed that the right-hand side of equation (101) corresponds to a convolution product, noted $(f*g_j)(\tau)$, and suggested solving it by using a spectral approach. This means that being the convolution in the time domain corresponding to multiplication in the frequency domain, $(f*g_j)(\tau)$ is connected to discrete Fourier transforms. Denoting with the letter F the Fast Fourier Transform (*FFT*) and F^{-1} the Inverse Fast Fourier Transform (the symbols "*" and "." in Eq. (104) are the symbols related to the convolution product and the Hadamard product respectively) any convolution $(f*g)(\tau)$ in the time domain can be computed exploiting the frequency domain according to the following general expression:

$$\left(f * g_j\right)(\tau) = F^{-1}(F(f)\,.\,F(g_j)) \tag{104}$$

According to (Pasquier and Marcotte, 2013), the spectral approach to solve a convolution product by *FFT* can be exploited under the following main assumptions:

- The heat flux signal is represented by a step function.
- All the heat pulses are of equal duration ($\Delta\tau=\tau_j-\tau_{j-1}$).
- f and g_j (f_0 and $g_{0,j}$) are both periodic functions.

In case one or both f and g_j (f_0 and $g_{0,j}$) are not periodic functions, the zero-padding technique can be adopted, as reported by (Pasquier and Marcotte, 2013). The zero-padding technique consists in adding n_t - 1 zeros at the end of vectors f and g_j, to evaluate $F^{-1}(F(f)\,.\,F(g))$ with these zero-padded vectors, and then to keep only the first n_t elements of the solution.

The solution provided by Eq. (104) gives the temperature change with respect to zero, as the ground (and the carrier fluid) is uniformly at 0°C as the initial condition. According to (Pasquier and Marcotte, 2013), to reconcile the real ground temperature with Eq. (104), the temperature at any node is simply given by Eq. (105):

$$T_{f,j}(\tau) = \left(f * g_j\right)(\tau) + T_0 \tag{105}$$

where T_0 is the mean initial undisturbed ground temperature. Eq. (105) assumes a uniform ground temperature profile over the domain's height. It is important to highlight that Eq. (105) assumes a uniform ground temperature profile T_0 over the domain's height (a zero geothermal gradient). The present study considers that a real vertical thermal profile data set is available and the geothermal gradient is taken into account. This generalization is provided by Eq. (106), where $T_{0,j}(\tau)=(f_0*g_{0,j})(\tau)$, contrary to T_0 in Eq. (105), is not necessarily constant in-depth and can vary in time. The present study highlights also that the effect on the TRT analyses due to the q_{ratio} parameter is directly correlated to the dimensionless g_0-transfer function evaluated from the numerical solution $S_j(\tau)$ by performing a complete circulation test of the same duration of the TRT without conferring any heat input rate. According to (Pasquier and Marcotte, 2013, Pasquier and Marcotte, 2014) the numerical (or experimental) temperature profiles $S_j(\tau)$ resulting from a series of

heat pulses can be reconstructed by the general solution $T_{f,j}(\tau)$ for each fluid node given by Eq. (106):

$$T_{f,j}(\tau) = \left(f * g_j\right)(\tau) + T_{0,j}(\tau) = \left(f * g_j\right)(\tau) + \left(f_0 * g_{0,j}\right)(\tau) \quad (106)$$

Eq.(106) denotes that the general solution $T_{f,j}(\tau)$ for each fluid node is given by superposing in time two different solutions (two different/separated convolutions). The k_{gr} that has to be estimated in the TRT is hidden inside both the $g_j(\tau)$ and $g_{0,j}(\tau)$ transfer functions. The external heat input rate is incorporated into the external excitation function $f(\tau)$ and expressed in terms of the fluid temperature difference imposed by the TRT machine at the BHE inlet and outlet sections. The excitation $f_0(\tau)$ is needed only in presence of non-zero $dT_{gr,\infty}/dz$. Both $f(\tau)$ and $f_0(\tau)$ have to be convolved with each $g_j(\tau)$ and $g_{0,j}(\tau)$ dimensionless functions respectively (for each j_{th} node, for any time τ). The $g_j(\tau)$ and $g_{0,j}(\tau)$ functions related to each j_{th} node of fluid volume are evaluated from the simulated (or experimental) temperature profiles $S_j(\tau)$ resulting from the complete numerical model (the three FD Models considered in the present study). The $g_{0,j}(\tau)$ functions take into account the effect related to the undisturbed ground temperature profile which is particularly important in the case of a non-zero geothermal gradient in the TRT analysis. The $g_{0,j}(\tau)$ functions are derived by simulating the TRT (or performing the real test) with no thermal inputs. This incorporates the effect on TRT of any specific non-uniform temperature distribution. When q_{ratio} is lower than 1, the effect of the geothermal gradient incorporated into the $g_{0,j}(\tau)$ function, is able to modify the slope of the general solution $T_{f,j}(\tau)$ for each fluid node, as graphically shown by Figure 47 (expressed in terms of $T_{f,ave}(\tau)$). The $T_{f,ave}(\tau)$ profiles computed by the FD Model and reconstructed by the $T_{f,j}(\tau)$ profiles from Eq. (106) are reported as an example in Figure 47. The simulated case has been performed according to the input data related to the 800 m cases reported in (Morchio et al., 2022); in particular, the one denoted with “Case 800/40” related to the center inlet configuration of the coaxial BHE, where 800 is the BHE depth and 40 is the average heat transfer rate per unit BHE length. As illustrated in Figure 47, the ILS-based k_{gr} estimation when the $g_{0,j}(\tau)$ function is taken into account differs by -14.3 % from the ILS-based k_{gr} estimation without taking into account the effect related to the geothermal gradient incorporated into the $g_{0,j}(\tau)$ function (the reference value for k_{gr} used in the FD model is 3 W/mK). The correct estimated k_{gr} value from the ILS-based TRT analysis can be obtained only by removing the $g_{0,j}(\tau)$ function from the real (in this case simulated) TRT data.

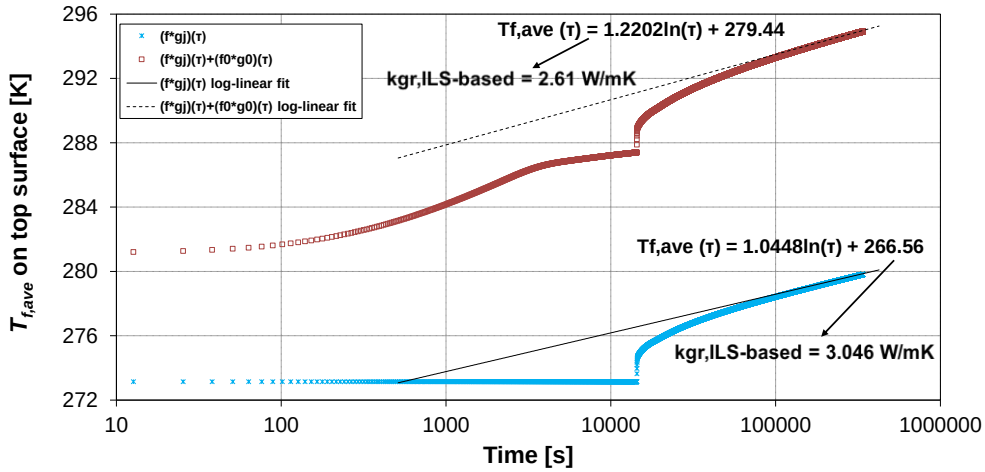

Figure 47: Fluid temperature profiles computed by FD Model as reconstructed by the $T_{f,j}(\tau)$ profiles from Eq. (106) (in terms of $T_{f,ave}(\tau)$ on top surface, geothermal gradient set to 0.02 K/m, q_{ratio} <1) related to the Center inlet case of Case 800/40 reported in (Morchio et al., 2022).

Figure 47 shows how the evaluation and removal of the g_0 function from any TRT data would be of great importance to remove the geothermal gradient influence (highlighted by q_{ratio} <1) and obtain the correct k_{gr} estimations from any TRT analysis based on the ILS model (for single and also for multiple ground layers).

The $T_{0,j}(\tau)=(f_0*g_{0,j})(\tau)$ functions related to the single and double U-pipes have been compared with those related to the coaxial BHEs (center-inlet and annular-inlet hydraulic configurations) in the case of the geothermal gradient is 0.02 K/m, as reported in Figure 48. These simulated cases reported as an example have been performed according to the input data of the 800 m cases reported in (Morchio et al., 2022); in particular, those denoted with "Case 800/40" related to coaxial, single and double U-BHE. Since 94 hours of circulation without any heat input rate are needed to compute the $T_{0,j}(\tau)=(f_0*g_{0,j})(\tau)$ functions, the profiles reported in Figure 48 for the inlet and outlet nodes necessarily overlap for each BHE-configuration type.

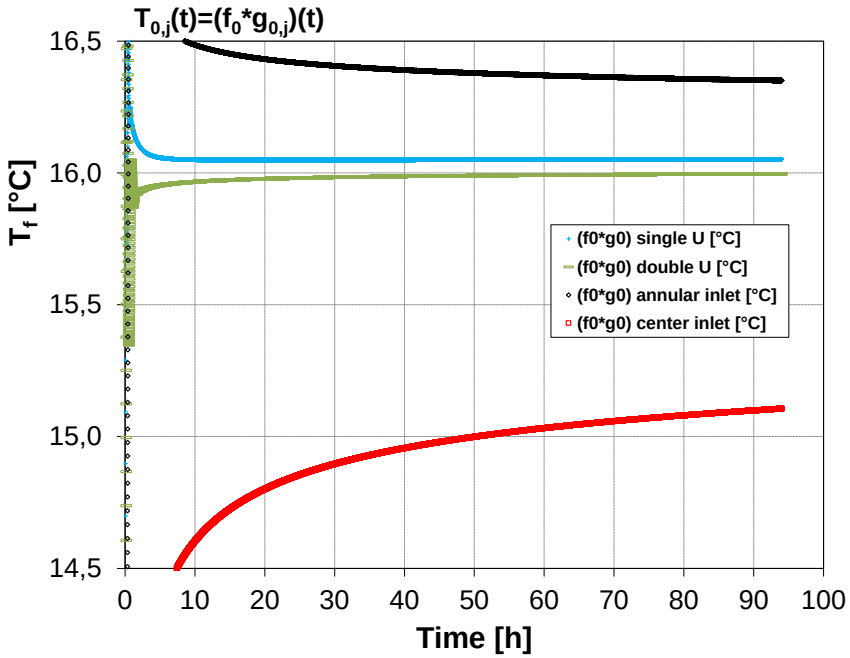

Figure 48: The comparison between the $T_{0,j}(\tau) = (f_0 * g_{0,j})(\tau)$ functions related to the coaxial, the single and double U-pipes (Case 800/40 reported in (Morchio et al., 2022), geothermal gradient set to 0.02 K/m).

The results reported in Figure 48 clearly show that the $T_{0,j}(\tau)$ profile related to the center inlet configuration of the coaxial case changes much more at late times than the $T_{0,j}(\tau)$ profiles related to the annular inlet, single and double U pipe (for the same borehole length of 800 m). While the $T_{0,j}(\tau)$ functions related to the inlet and outlet nodes assume a value close to being a constant for the single and double U pipes for almost the entire duration of a TRT, it can be noticed how the $T_{0,j}(\tau)$ functions related to the inlet and outlet nodes assume a slight slope in the case of the coaxial center inlet case. According to Table 3 reported in (Morchio et al., 2022) and contrary to what the ILS model assumes, for a DBHE in presence of a non-zero geothermal gradient, the thermal equilibrium temperature $T_{gr,\infty}$ between the fluid and the surrounding ground reached at the end of the circulation period does not correspond to the mean value along the BHE active depth H of the undisturbed ground temperature, especially for the coaxial center-inlet case. This is symptomatic of the almost nil contribution of additional heat input rate related to the available geothermal heat flux within the BHE length H in the case of the single and double U pipes, while a positive natural extra heat contribution in the case of the center inlet case. This confirms also that the $T_{0,j}(\tau)$ functions incorporate the contribution of an additional heat input rate related to the available geothermal heat flux within the BHE length H, then influencing the slope of the resulting $T_{f,j}(\tau)$ fluid profiles if not corrected through the proper choice of the best external heat transfer rate $\dot{Q}$. Also the Annular inlet case in Figure 48 shows a slight slope having a lower magnitude than the one of the center inlet case for the overall duration of the TRT. This represents another perspective that allows understanding why in the case of q_{ratio} <1, the annular inlet configuration confers better ILS-based k_{gr} estimation than the center inlet one (for both heat injection and heat extraction scenarios) as reported in (Morchio et al., 2022).

As an original contribution provided by the present thesis work, Figure 49 reports the $T_{f,ave}(\tau)$ profiles related to additional simulations characterized by complete "Case

800/40" tests of fluid circulation for two different k_{gr} values (2 and 3 W/mK) imposed all over the ground domain in the case of coaxial (center inlet and annular inlet), single U, double U BHE at the same undisturbed ground temperature profile characterized by a geothermal gradient of 0.02 K/m.

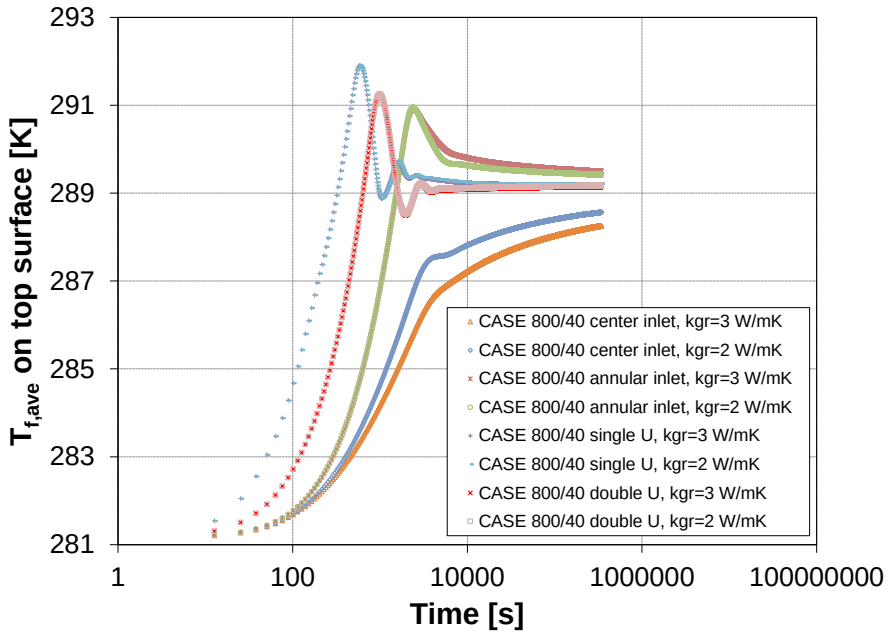

Figure 49: The comparison between the $T_{f,ave}(\tau)$ profiles related to complete "Case 800/40" tests of fluid circulation in the case of coaxial (center inlet and annular inlet), single U, double U BHE for two different k_{gr} values (2 and 3 W/mK) and a geothermal gradient set to 0.02 K/m.

As is clearly shown in Figure 49, for the single, double U BHEs and "annular inlet" configuration of the coaxial BHE the $T_{f,ave}(\tau)$ profile and the $T_{gr,\infty}$ value reached at the end of the test are not too much sensitive to the chosen k_{gr} value as an input of the simulation. For the "center inlet" configuration of the coaxial BHE the $T_{f,ave}(\tau)$ profile and the $T_{gr,\infty}$ value reached at the end of the test are significantly depending on the chosen k_{gr} value as an input of the simulation. This would demonstrate once more that the "center inlet" configuration is much more sensitive to the effect of the geothermal gradient incorporated into the q_{ratio} and the g_0-function that needs to be taken into account and removed to obtain the correct k_{gr} estimations from any TRT analysis based on the ILS model. On the other hand, this would demonstrate also that the circulation phase characterizing the "center inlet" configuration can be exploited since it provides useful and recognizable information aimed at the correct estimation of k_{gr} since each k_{gr} value differentiates and makes distinguishable each $T_{f,ave}(\tau)$ profile of the "center inlet" configuration of the coaxial BHE (especially in case of deep borehole and a significant geothermal gradient). Preliminary and new simulations, not reported for the sake of brevity, seem to demonstrate that the $T_{f,ave}(\tau)$ profile and the $T_{gr,\infty}$ value reached at the end of the circulation phase characterizing the coaxial BHE (for both the annular and center inlet configurations) are sensitive to the effect of the different k_{gr} values along the ground depth and the related order among the layers of equal thickness (especially in case of deep borehole and significant geothermal gradients related to the k_{gr} values among the layers through Eq. (92)).

The $g_{0,j}(\tau)$ functions have an effect during the entire TRT duration (also during the heat input phase). In the case of q_{ratio} lower than 1 the $g_{0,j}(\tau)$ functions can modify the slope of the fluid temperature profiles, especially for the coaxial BHE.

According to (Marcotte and Pasquier, 2008) and (Pasquier and Marcotte, 2013) the convolution products $(f*g_j)(\tau)$ and $(f_0*g_{0,j})(\tau)$ in Eq. (106) are computed in the frequency domain using the spectrum of f and g_j (f_0 and $g_{0,j}$); this is much faster than the standard convolution in the time domain. According to Eq. (104), the expressions $(f*g_j)(\tau)$ and $(f_0*g_{0,j})(\tau)$ in Eq. (106) are computed through Eqs. (107) and (108):

$$\left(f * g_j\right)(\tau) = F^{-1}(F(f)\,.\,F(g_j)) \tag{107}$$

$$\left(f_0 * g_{0,j}\right)(\tau) = F^{-1}(F(f_0)\,.\,F(g_{0,j})) \tag{108}$$

For more details on the *FFT* method, the Reader is addressed to read (Pasquier and Marcotte, 2013, Pasquier and Marcotte, 2014). The present approach exploiting the specific strengths of the *FFT* method in handling different types of boundary conditions (i.e. variable heat input rate above the ground and an undisturbed ground temperature profile which can be uniform or variable along the depth) saves a lot of the computation CPU time to run each simulation (provided that f, f_0, g_j and $g_{0,j}$ have been obtained). This is because any change of the external heat input rate involves only the external excitation function $f(\tau)$ that is convolved with each evaluated and invariant dimensionless $g_{,j}(\tau)$ function and superposed with the $(f_0*g_{0,j})(\tau)$ convolution product (for each node, for any time). On the other hand, the $g_{0,j}(\tau)$ functions are derived by simulating the model (or performing the real test) with no thermal inputs to properly take into account the effect related to the undisturbed ground temperature profile which is particularly important in the case of a non-zero geothermal gradient. The *FFT* method adopted in this work for computing the convolution products incorporates concepts based on the studies by (Marcotte and Pasquier, 2008, Pasquier and Marcotte, 2013, Pasquier and Marcotte, 2014, Nguyen et al., 2017).

3.2.2 Methodology

Three Fortran90 programs implementing the FD Models related to coaxial, single and double U-BHE geometries presented in (Morchio and Fossa, 2019, Morchio and Fossa, 2020) are exploited to evaluate the $g_j(\tau)$ and $g_{0,j}(\tau)$ functions related to each j_{th} node of fluid volume. These models have been proved and validated against available literature TRT measurements, showing very accurate thermal profiles which overlap those related to the experimental data as reported in (Morchio and Fossa, 2019, Morchio and Fossa, 2020). The Reader is directed to those papers for a complete model description. A dedicated Fortran90 program, whose results have been successfully cross-checked with those provided by an independent Matlab solver, implements the routine for performing the FFT computation used to reconstruct the $T_{f,j}(\tau)$ temperature profiles from the FD Models. The dedicated Fortran90 code allows the choice of subgroups of nodes for the reconstruction of the $T_{f,j}(\tau)$ for each j_{th}-node. The $g_{0,j}$-function in the term $(f_0*g_{0,j})(\tau)$ is the only term on the right-hand side of Eq. (106) with information about the geothermal gradient. The g_j-function in the term $(f*g_j)(\tau)$ is evaluated by ignoring the geothermal gradient. The evaluation of the g_j-function in the term $(f*g_j)(\tau)$ uses a uniform undisturbed ground temperature (constant with depth) profile whose value is imposed everywhere equal to 0

°C= 273.15 K (assumption proper of the method to evaluate the g_j for each node). To evaluate the values related to g_j for each fluid node, it is needed to run an entire numerical simulation with one of the three complete FD Models considered in the present study, with a 0 °C assigned to all the nodes. This is obtained by imposing a zero-geothermal gradient in the fluid and ground domain as the initial condition and applying the desired value of the external heat input rate (it is possible to adopt whatever value of the external heat input rate to evaluate the g_j function for each node because the boundary condition related to the external heat transfer rate is in any case handled by the $f(\tau)$ function). According to what is described in (Pasquier and Marcotte, 2013, Pasquier and Marcotte, 2014) the dimensionless g_j functions are derived using Eq.(109) reported hereafter:

$$g_j(\tau) = \frac{S_j(\tau)}{\beta} \tag{109}$$

The $S_j(\tau)$ term in the numerator is the solution computed by the complete FD numerical Model related to each node in the time domain ($S_j(\tau)$ in general can also represent the experimental temperature profile in a real test; in this last case, the $S_j(\tau)$ would already incorporate also the geothermal gradient effect, thus the $g_{0,j}(\tau)$ function) suitably converted in °C, according to the method described by (Pasquier and Marcotte, 2014), while β is the constant for which $g_j(\tau = \tau_{start\ heat\ input\ rate})=1$, then:

$$\beta = \frac{\dot{Q}_{start\ heat\ input\ rate}}{\dot{m}c_f} \quad [°C] \tag{110}$$

The value related to the constant β depends on the choice of the $\dot{Q}_{start\ heat\ input\ rate}$ value; therefore the choice of the value of external heat transfer to evaluate the g_j-functions can be arbitrary since the solution $S_j(\tau)$ is in any case affected by this choice and made dimensionless by dividing by the constant β.
The $f(\tau)$ excitation function incorporates the effect related to the external heat input rate in terms of the temperature difference between the BHE inlet and outlet sections, in particular:

$$f(\tau) = \frac{\dot{Q}(\tau) - \dot{Q}(\tau_{i-1})}{\dot{m}c_f} \qquad [°C] \tag{111}$$

In a standard TRT, since the external load $\dot{Q}$ should be typically kept constant (around 90-100 hours of heat injection at constant power) the $f(\tau)$ assumes the values (for each time step included in the defined τ window):

$$f(\tau) = [\frac{\dot{Q}_{start\ heat\ input\ rate}}{\dot{m}c_f}, 0, 0, 0, 0, \dots, 0] \ \forall \ \tau_{start\ heat\ input\ rate} \leq \tau \leq \tau_{end\ experiment} \tag{112}$$

To evaluate the values related to $g_{0,j}$ for each fluid node, in the present study the entire 94-h TRT simulated with the complete FD Model for coaxial BHE has been run taking into account the geothermal gradient thus the actual values of the undisturbed ground temperature profile imposed in the whole domain as the initial condition without considering any external heat input rate for all the entire duration of the experiment.

According to what is described in (Nguyen et al., 2017) the dimensionless $g_{0,j}$ functions are derived using the Eq.(113) reported hereafter:

$$g_{0,j}(\tau) = \frac{S_{0,j}(\tau)}{\beta=1°C} \quad (113)$$

$S_{0,j}(\tau)$ is the solution in the time domain computed by the complete FD Model without taking into account any external heat input rate for the entire duration of the experiment. $S_{0,j}(\tau)$ is related to each node ($S_{0,j}(\tau)$ can also represent the experimental temperature profiles in a real test of complete circulation) suitably converted in °C, while β is the constant that makes $g_{0,j}(\tau)$ dimensionless but numerically equivalent to the $S_{0,j}(\tau)$ solution, then β = 1 °C.

The $f_0(\tau)$ excitation function assumes the values reported in Eq.(114) so that the convolution product $T_{0,j}(\tau)=(f_0*g_{0,j})(\tau)$ coincides with the numerical solution $S_{0,j}(\tau)$ conferred by the FD Model (for each time step included in the defined τ window):

$$f_0(\tau) = [1, 0, 0, 0, 0, ...] \quad \forall \ 0 \leq \tau \leq \tau_{end\ experiment} \quad (114)$$

3.2.3 Validation of the method

As the validation of the FFT spectral method implemented in the dedicated Fortran90 program, it has been verified that the $T_{f,j}(\tau)$ solution provided by Eq. (106) coincides with the complete solution given by the FD Model run for the entire 94h simulated TRT related to the "Case 800/40" reported in (Morchio et al., 2022) (non-zero geothermal gradient characterizing the undisturbed ground temperature profile imposed in the whole domain as the initial condition and conferring the proper external heat input rate starting from the 4th hour of the experiment). The fluid temperature profiles related to the coaxial center-inlet case simulated by the FD Model and reconstructed by the FFT method have been reported in Figure 50. During the pre-circulation phase of 4 hours without any external heat input rate (and the geothermal effect during circulation) only the $(f_0*g_{0,j})(\tau)$ term in Eq. (106) provides a numerical contribution (the contribution related to the convolution product $(f*g_j)(\tau)$ is zero when the external heat input rate is 0 W). When the external heat input rate starts both the terms in Eq. (106) provide a numerical contribution. Under these assumptions, Eq. (106) produces the temperature profile reported in Figure 50 related to the inlet node of the 800 m coaxial center-inlet case whose input data are reported in (Morchio et al., 2022). In this case, q_{ratio} is lower than 1 and the geothermal gradient is 0.02 K/m.

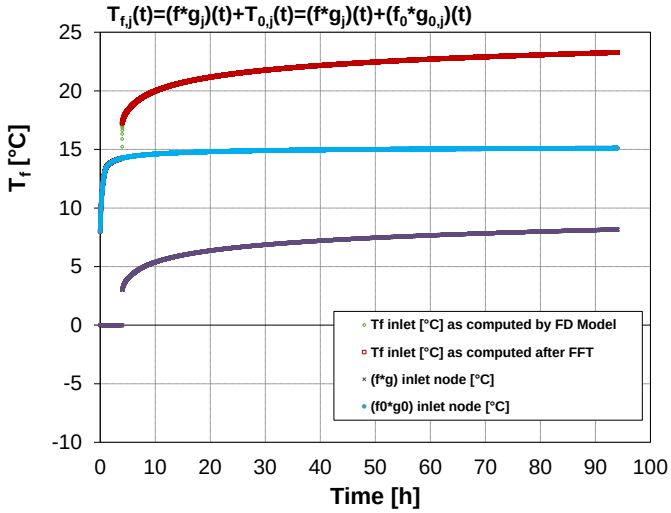

Figure 50: Fluid temperature computed by the FD Model as reconstructed by the superposition of the $(f*g_j)(\tau)$ and the $(f_0*g_{0,j})(\tau)$ profiles (for the inlet node, geothermal gradient set to 0.02 K/m, q_{ratio} <1) related to the Center inlet Coaxial DBHE of Case 800/40 reported in (Morchio et al., 2022).

From Figure 50 inspection, it is straightforward to notice that the profile related to the inlet node computed by the FD Model overlaps with the one obtained from Eq. (106) during the whole test of 94h.

3.2.4 Application of the method for TRT analysis in the case of single-layer subsurface for coaxial, single and double U BHEs

The numerical results plotted in the Figures of the present section are aimed to explain how the present method related to the *FFT* technique is applied to reconstruct the fluid temperature profiles computed by the complete FD Models. For the sake of clarity, only the temperatures resulting from the application of the *FFT* method have been reported in the Figures of the present section since are the same as the FD model. Furthermore, the profiles related to the convolution product $(f*g_j)(\tau)$ have been reported in the Figures of the present section (while the $T_{0,j}(\tau)$ profiles are those reported in Figure 48 of the present study). The results reported in the present section also graphically explain how the $g_{0,j}(\tau)$ function can influence the ground thermal conductivity estimation when the ILS model is employed in the TRT analysis. This is shown through simulations related to coaxial deep BHE of 800 m in presence of a single-layer subsurface with a non-zero geothermal gradient compared to the same case with an undisturbed ground temperature profile perfectly uniform along the depth.

According to Eq. (106), adding the convolution product $(f*g_j)(\tau)$ to the $T_{0,j}(\tau)$ profiles (those related to the Case 800/40 reported in Morchio et al., 2022, and in Figure 48 of the present study) produces the fluid temperature profiles shown in Figure 51. These temperature profiles are related to the inlet node of the 800 m coaxial (annular inlet and center inlet) and U-pipes (single and double U) BHEs in the case q_{ratio} is lower than 1, the geothermal gradient is 0.02 K/m, and a single layer subsurface having ground thermal conductivity value of 3 W/mK. The input data details related to these simulated cases are reported in (Morchio et al., 2022), those denoted with “Case 800/40”. For these cases, the

external heat input rate per unit length is 40 W/m competing against the available natural geothermal heat rate of 48 W/m along the BHE depth (q_{ratio} lower than 1).

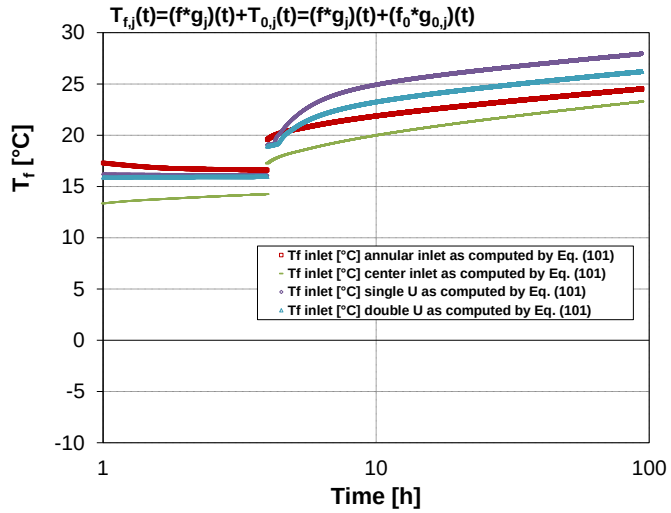

Figure 51: Fluid temperature from the superposition of the $(f^*g_j)(\tau)$ and the $(f_0^*g_{0,j})(\tau)$ profiles (for the inlet node, geothermal gradient set to 0.02 K/m, q_{ratio} <1) related to the coaxial and U - pipes of "Case 800/40" reported in (Morchio et al., 2022).

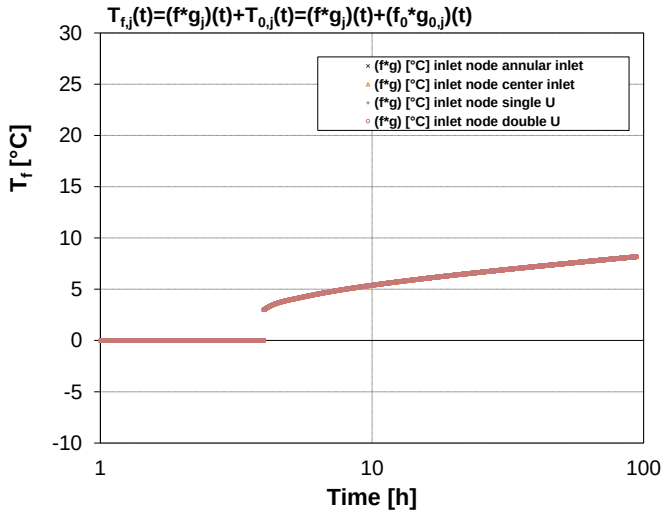

Figure 52: $(f^*g_j)(\tau)$ profiles (for the inlet node) related to the coaxial and U - pipes of "Case 800/40" reported in (Morchio et al., 2022).

The $(f^*g_j)(\tau)$ profiles related to the Case 800/40 have been reported in Figure 52. As it is easy to notice, the $(f^*g_j)(\tau)$ profiles reported in Figure 52 are almost overlapped for all the BHE types and hydraulic configurations. This is because the g_j-function in the term $(f^*g_j)(\tau)$ is evaluated by ignoring the geothermal gradient and a value equal to 0 °C= 273.15 K (constant with depth) is imposed in the fluid and ground domain as the initial condition. Figure 51 and Figure 52 are aimed to show the effect due to the $g_{0,j}(\tau)$ functions (that is the geothermal gradient effect) embedded into the $T_{0,j}(\tau)$ functions related to each BHE type and hydraulic configuration. In particular, Figure 51 confirms what is highlighted by Figure 48 on how the $T_{0,j}(\tau)$ functions and the $T_{gr,\infty}$ value reached at the end of the pre-circulation phase of 4 hours, prior to the start of heat injection (or extraction) of

a TRT, do not coincide among the coaxial and U-pipes cases when the geothermal gradient is 0.02 K/m. If the geothermal gradient would have been perfectly 0.0 K/m all the fluid temperature profiles shown in Figure 51 would almost coincide as they would differ from those shown in Figure 52 for a constant equal to T_0 that is the uniform ground temperature profile over the domain's height (zero geothermal gradient). The present investigation at q_{ratio} <1 (whose resulting profiles are shown in Figure 51) graphically confirms that, as opposed to both coaxial cases, the U-pipes are less influenced by the absolute value of q_{ratio} when the ILS model is used for the ground thermal conductivity estimation from TRT data. This is graphically shown by the almost equal slopes characterizing the late time of the test for the U-pipes and the different slopes assumed by the coaxial arrangements in Figure 51. As well as the $T_{gr,\infty}$ value reached at the end of the pre-circulation phase of 4 hours is almost equal for the U-pipes while differs between the coaxial configurations (as confirmed by Table 3 reported in Morchio et al., 2022). The $T_{0,j}(\tau)$ functions and in particular the $g_{0,j}(\tau)$ functions incorporate the main numerical reason for which the coaxial cases are more sensitive to the q_{ratio} parameter (to the geothermal gradient effect) than the U-pipes when the ILS model is used to estimate the ground thermal conductivity, as confirmed by the ILS-based k_{gr} estimation results reported in Table 4 of (Morchio et al., 2022).

The same numerical simulations have been performed in the case of a geothermal gradient of 0.0 K/m. For the sake of brevity, only the fluid temperature profiles related to coaxial cases have been presented and reported in Figure 53. In these cases, the $T_{gr,\infty}$ value reached at the end of the circulation phase corresponding to the previous simulations reported in Figure 51 for each coaxial case (annular inlet and center inlet) is directly imposed uniformly along the ground depth from the beginning of the test. As previously, these temperature profiles are related to the inlet node of the 800 m coaxial (annular inlet and center inlet). The profiles related to the convolution product $(f*g_j)(\tau)$ are the same reported in Figure 52 (in this case the $T_{0,j}(\tau)$ profiles are not plotted since they are related to a geothermal gradient of 0.0 K/m, thus invariant in time and equal to the $T_{gr,\infty}$ constant value corresponding to the uniform in-depth initial condition).

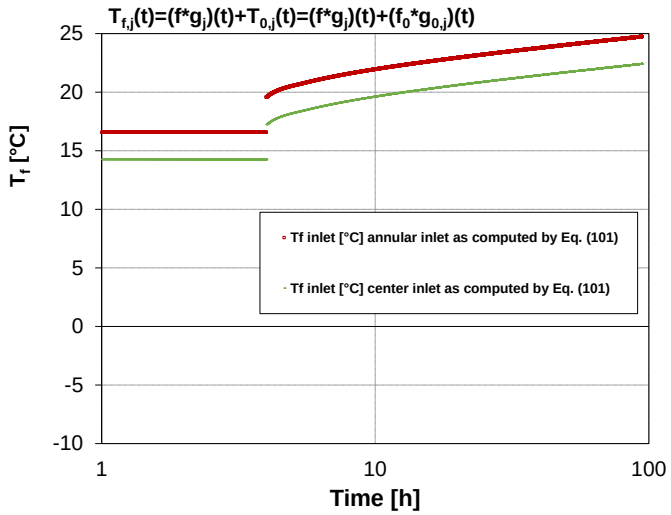

Figure 53: Fluid temperature from the superposition of the $(f*g_j)(\tau)$ and the $(f_0*g_{0,j})(\tau)$ profiles (for the inlet node, geothermal gradient set to 0.0 K/m) related to the coaxial DBHE of "Case 800/40" reported in (Morchio et al., 2022).

Since the geothermal gradient is 0.0 K/m all the fluid temperature profiles shown in Figure 53 differ from those shown in Figure 52 for a constant equal to T_0 which is the uniform ground temperature profile over the domain's height (zero geothermal gradient), a different constant between the coaxial cases. In this case, the $g_{0,j}(\tau)$ functions related to the inlet and outlet nodes do not influence the slope of the resulting $T_{f,j}(\tau)$ fluid profiles (nil contribution of additional heat input rate related to the available geothermal heat flux within the BHE length H since the geothermal gradient of 0.0 K/m). Therefore the corresponding ground thermal conductivity estimation from the ILS model will result very close to each other (regardless of the choice of the hydraulic configuration). This is also observed by similar fluid temperature profiles obtained from simulated TRTs with a zero geothermal gradient reported in (Morchio and Fossa, 2020) and the related k_{gr} ILS-based estimations.

According to the "800/213.33" coaxial case reported in (Morchio et al., 2022), Figure 54 graphically shows how in presence of the geothermal gradient of 0.02 K/m and q_{ratio} >>1, the fluid temperature profiles can assume the slope (in the semi-logarithmic time scale) compatible with the ground thermal conductivity value of 3 W/mK imposed in the program input file also in case the center inlet configuration is adopted. This case for which q_{ratio} is greater than 1 has been reconstructed by the FFT according to the present method synthetically represented by Eqs. (106), (107) and (108). The fluid temperature profiles related to q_{ratio} >>1 for the inlet node have been reported and compared with those related to q_{ratio} < 1 in Figure 54.

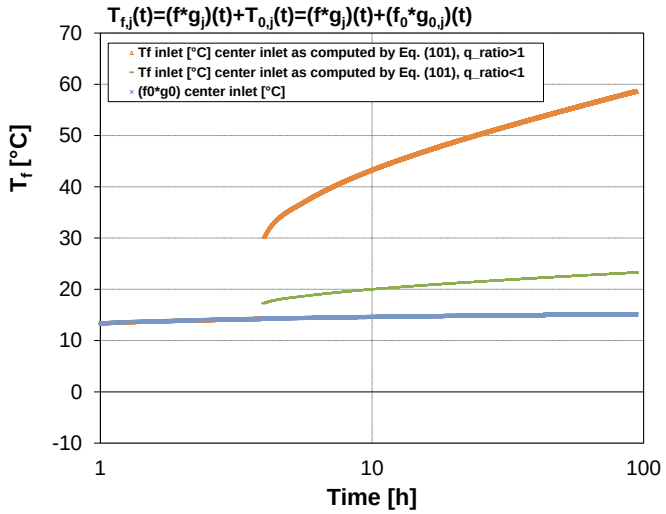

Figure 54: Fluid temperature from the superposition of the $(f*g_j)(\tau)$ and the $(f_0*g_{0,j})(\tau)$ profiles (for the inlet node, geothermal gradient set to 0.02 K/m, q_{ratio} >>1) compared with those obtained for q_{ratio} <1 related to the Center inlet case of Case 800/213.33 reported in (Morchio et al., 2022).

From Figure 54 inspection, it is straightforward to notice how in the case of q_{ratio} >>1 the contribution of heat input rate related to the $T_{0,j}(\tau)$ function is too lower compared to the one provided by the external heat input rate imposed (external heat input rate per unit length of 213.33 W/m against the available natural geothermal heat rate of 48 W/m along the BHE depth). In this case, the effect of the external heat input rate on the fluid temperature profiles greatly overrides the relatively small contribution related to the natural geothermal one. For the single-layer subsurface case, the condition related to q_{ratio} >>1 guarantees the correct ground thermal conductivity estimation for both the

hydraulic configurations when the ILS model is used in TRT analysis, as confirmed by the ILS-based k_{gr} estimation results reported in Table 4 of (Morchio et al., 2022).

3.2.5 Application of the method for TRT analysis in the case of multiple ground layers of equal thickness with geothermal gradient

A series of simulations has been carried out to investigate if the q_{ratio} is the dominant parameter when the ILS model is used to estimate the ground thermal conductivity, also in presence of different ground layers of equal thickness with different thermal conductivity values imposed along the depth. In particular, the numerical simulations reported in the present section aimed to demonstrate the influence of q_{ratio} along with the impact of other dimensionless parameters specific to TRTs. The results for ground with multiple layers are of particular interest because no previous research systematically studies these effects. The investigation reported in the present section is mainly focused on the coaxial case, which is the most likely configuration for deep boreholes and, as shown in the previous sections, the most affected by the effects due to q_{ratio}. Any changes in the r_b/H and $\dot{m}/H$ ratios are not able to mitigate the influence related to the q_{ratio} parameter on the ground thermal conductivity estimation when the ILS model is employed. The results reported in the present section have been graphically explained and clarified also in terms of $g_{0,j}(\tau)$ functions. The analysis considers different ground layers of equal thickness with different thermal conductivity values imposed along the depth and corresponding geothermal gradients. The condition related to q_{ratio} >>1 has to be satisfied in an ILS-based TRT analysis in order to override the additional heat input rate (particularly prominent for coaxial DBHEs) provided and incorporated into the $g_{0,j}(\tau)$ functions. The q_{ratio} >>1 condition guarantees the ILS-based k_{gr} estimation moving closer to the mean k_{gr} value among the layers.

The main input parameters are reported in Table 17 according to those reported in (Beier et al., 2021) while the grid properties characterizing the numerical simulations related to the 800 m coaxial DBHE case are reported in Table 18. The k_{gr} values and geothermal gradients for each layer follow the list in Table 19, also reported in (Beier et al., 2021). The k_{gr} values of the ground surrounding the simulated borehole are not specific to the geology related to any location but generically represent a range of possible physical values. In the DTRT simulations reported in the present study, the ground is made of four layers, each having a different k_{gr} value. The heat extraction rate per meter from the ground is kept at 40 W/m. The case 800/(-40) can serve as a base case (that is denoted with case 1 and case 2 in Beier et al., 2021, for the annular inlet and center pipe inlet configuration respectively, while in the present study is named “CASE 3A”) because the heat extraction rate (W/m) is in the typical range.

Table 17
Parameters used in CASE 3A simulations with the numerical model related to the 800 m coaxial DBHE (base case).

Parameter	***Value***

Borehole length	800 m
Borehole diameter	0.14 m
Center pipe inner radius	0.045 m
Center pipe wall thickness	0.008 m
Annular pipe inner radius	0.0695 m
Annular pipe wall thickness	0.0004 m
Internal and external pipe wall thermal conductivity	0.42 W/(m·K)
Ground surface temperature (z = 0)	281.15 K
Fluid mass flow rate	2.55 kg/s
Fluid density	1000 kg/m^3
Fluid specific heat capacity	4186 J/(kg·K)
Fluid thermal conductivity	0.60 W/(m·K)
Fluid viscosity	1.0 x 10^{-3} kg/(m·s)
Local borehole thermal resistance	0.00378 (m·K)/W
Heat extraction rate	32,000 W
Duration of fluid circulation prior to heat extraction	4 h
Duration of heat extraction	90 h

Table 18
Grid properties characterizing the numerical simulations related to the 800 m coaxial DBHE (base case).

Input type	Value
Domain end radial r-coordinate	3.2 m
Domain end axial z-coordinate	840 m
Number of partitions along the r-direction	30
Number of partitions along the z-direction	80
Finite increment Δz	10.5 m
Time step $\Delta\tau$	10.51 s

Table 19
Thickness, ground thermal properties and geothermal gradient of ground layers.

Layer	*Depth interval (m)*	$k_{gr,p}$ *(W/(m·K))*	$\alpha_{gr,p}$ *(m^2/s)*	$(\rho c)_{gr,p}$ *(J/m^3K)*	*Geothermal gradient (K/m)*
1	0 to 200	1	3.33×10^{-7}	3.0×10^{6}	0.04
2	201 to 400	1.7	5.66×10^{-7}	3.0×10^{6}	0.0235
3	401 to 600	2.4	8.0×10^{-7}	3.0×10^{6}	0.0167
4	601 to 800	3.1	1.03×10^{-6}	3.0×10^{6}	0.0129

A series of simulations for the coaxial pipe adopting the same main input data related to the 800 m base case (named "CASE 3A") has been performed by varying the borehole depth (100 m to 800 m, "CASE 3B" to "CASE 3A BIS") while keeping the thickness of each layer equal to ¼ of the total depth. The TRT simulations for both the hydraulic configurations of the coaxial BHE have been performed for each case. The main input and pre-processing data which distinguish and identify each case are summarized in Table 20. Note as the depth decreases the magnitude of q_{ratio} increases since the heat extraction rate per meter is kept at 40 W/m. It has to be specified that the values related to the natural heat rate per unit length reported in Table 20 have been computed according to Eq. (92) where the ground thermal conductivity is the arithmetic average value among the layers, in this case, equal to 2.05 [W/mK]. The product between the ground thermal conductivity k_{gr} and the geothermal gradient $dT_{gr,\infty}/dz$ is constant for each layer (this product was chosen equal to 0.04 W/m^2) and used in Eq. (92). For layered ground, the average is the effective ground thermal conductivity for parallel heat conduction through layers with boundary conditions of uniform temperature at each end. In the case of layers with equal thickness, the average is the simple mean.

Table 20
Main input and pre-processing data identifying the center inlet and annular inlet cases.

Case	$\dot{m}$ *[kg/s]*	$\dot{m}/H$ *[kg/ms]*	*H [m]*	*External heat extraction rate* $\dot{Q}$ *[W]*	*Natural heat rate per unit length [W/m]*	q_{ratio} *[-]*
3B	0.32	0.0032	100	4,000	4	10
3C	0.64	0.0032	200	8,000	8	5
3D	0.95	0.0032	300	12,000	12	3.33

3E	1.27	0.0032	400	16,000	16	2.5
3F	1.59	0.0032	500	20,000	20	2
3G	1.91	0.0032	600	24,000	24	1.66
3H	2.23	0.0032	700	28,000	28	1.43
3A	2.55	0.0032	800	32,000	32	1.25
3A BIS	2.55	0.0032	800	170,667	32	6.66

The mass flow rate varies among the cases in order to keep the fluid temperature difference $(T_{in}\text{-}T_{out})$ constant at the top of the BHE, while $\frac{\dot{Q}}{H}$ remains constant (except for the CASE 3A BIS). This case has been purposely simulated and reported to show the corrective effect provided by the q_{ratio} >>1 on the ILS-based k_{gr} estimation in comparison to CASE 3A. The simulations and analyses reported in the present section for multiple ground layers indicate that the ILS-based k_{gr} estimation changes with q_{ratio}. Figure 55 shows the results for cases as the borehole depth decreases (800 m to 100 m), which increases q_{ratio}.

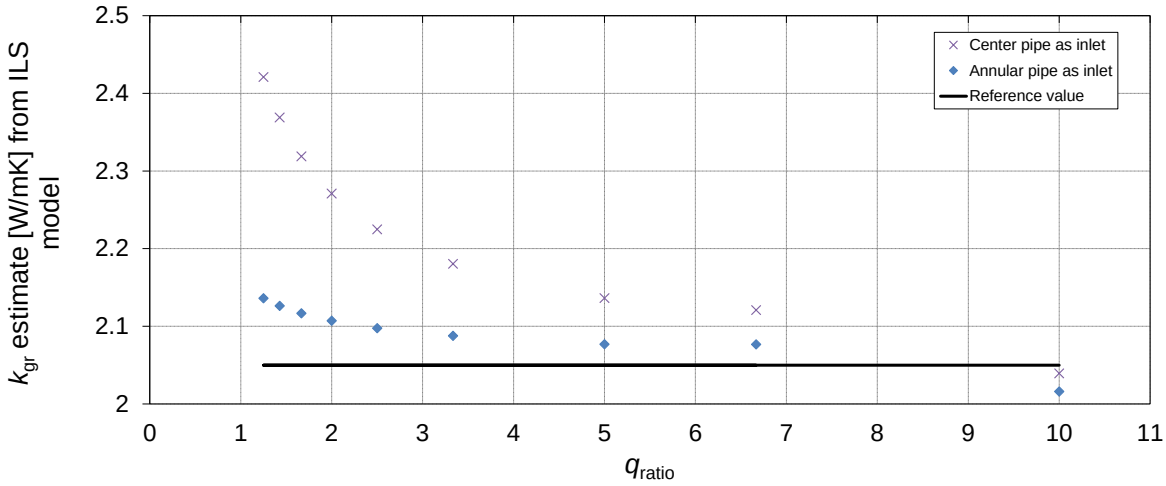

Figure 55: Effective ground thermal conductivity estimation from the FOA of the ILS model compared to the reference value (horizontal line).

Figure 55 compares the FOA-ILS-based k_{gr} estimation with the weighted-thickness average for the ground layers. In this case of layers with equal thickness, the average is the simple mean (the horizontal line is the reference value). The starting time of the time window for the ILS model is Fo_{rb}=10. The results indicate that as q_{ratio} decreases the ILS-based k_{gr} estimation departs from the arithmetic average. The same investigation has been carried out also considering different Fo_{rb} dimensionless time windows, producing the

graph reported in Figure 56 (for the center inlet) and Figure 57 (for the annular inlet) configurations. The Fourier number Fo_{rb} corresponds to the starting time for the ILS model fit.

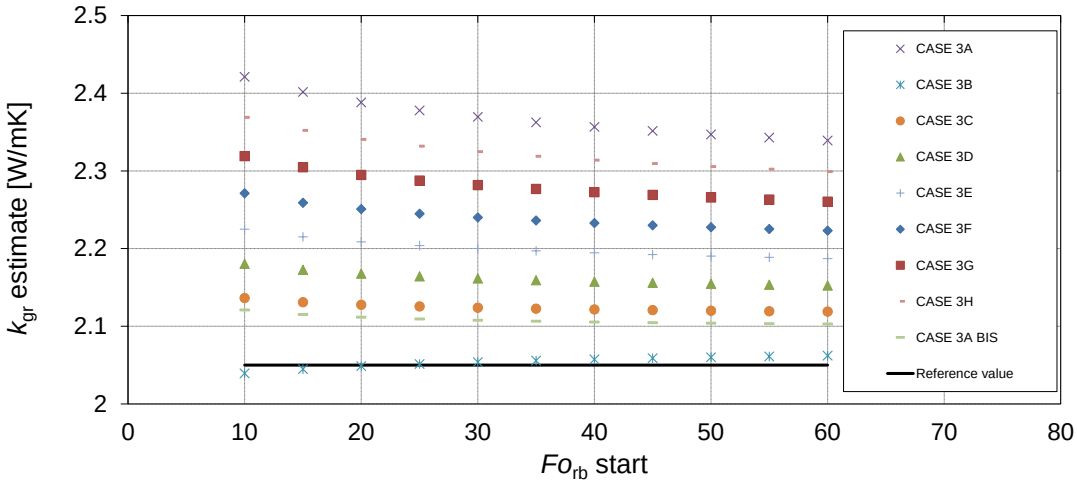

Figure 56: Effective ground thermal conductivity from the ILS model as estimated for different Fo_{rb} windows for the center inlet configuration.

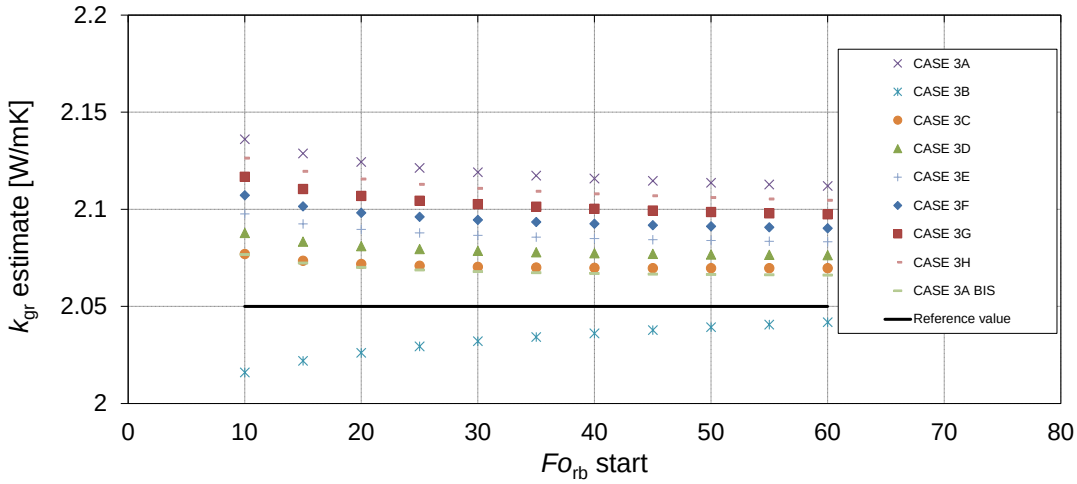

Figure 57: Effective ground thermal conductivity from the ILS model as estimated for different Fo_{rb} windows for the annular inlet configuration.

As in the previous papers by the Authors (Morchio et al., 2022, Beier et al., 2021), the ratio $\frac{\dot{m}}{H}$ has been kept constant among the cases by adjusting $\dot{m}$. The simulations demonstrate that when a strong geothermal gradient exists the difference between the FOA-ILS-based k_{gr} estimation and the mean k_{gr} tends to decrease as the total depth decreases. The parameter q_{ratio} is an indicator of this difference because as the total depth decreases, the q_{ratio} increases since the heat extraction rate per meter is kept at 40 W/m. The simulations demonstrate that as the depth decreases the estimated effective k_{gr} from the line-source model moves closer to the mean k_{gr}. This is due to the q_{ratio} parameter, as clearly demonstrated by the additional simulation (CASE 3A BIS) for the 800 m case with the heat extraction rate per meter from the ground set to 213.33 W/m. The additional

simulation (CASE 3A BIS) demonstrates that the estimated effective k_{gr} from the ILS model moves closer to the mean k_{gr} when q_{ratio} >>1. This demonstrates once more how q_{ratio} is the most relevant among the parameters characterizing the TRT analyses, also in presence of multiple ground layers of equal thickness with different thermal conductivity values imposed along the depth. For the coaxial BHEs, the estimated k_{gr} from the ILS model moves closer to the mean k_{gr} value among the layers only if q_{ratio} >>1 regardless of the k_{gr} variations among the layers. The simulations demonstrate also that the movement in the line-source estimates of the effective k_{gr} from the mean is less for the annulus inlet configuration. The corresponding cases with the annulus as the inlet have significantly smaller deviations from the average k_{gr} (compare Fig. 57 to Fig. 56). The movement in the line-source estimates from the mean k_{gr} are expected to be in general less also for single and double U-tube configurations for ground with layers of equal thickness.

Other parameters related to the coaxial geometry have been varied with the dimensionless groups listed in Table 5 reported in (Morchio et al., 2022) exploiting the cluster of simulations reported in the present study. The list includes the parameter N_1 related to the short-circuit thermal resistance, R_1, between each node placed in the center and annular pipe:

$$N_1 = \frac{H}{\dot{m}\, c_f\, R_1} \tag{115}$$

The N_2 and N_{gr} are the other dimensionless parameters in the list that include the $\frac{\dot{m}}{H}$ ratio:

$$N_2 = \frac{H}{\dot{m}\, c_f\, R_2} \tag{116}$$

$$N_{gr} = \frac{2\pi k_{gr} H}{\dot{m}\, c_f} \tag{117}$$

The parameter N_2 is related to the thermal resistance, R_2, between each node placed in the annular pipe and the borehole wall node. The parameter N_{gr} is the dimensionless conductance of ground, according to Table 5 reported in (Morchio et al., 2022). In the simulations whose results are reported in Figures 55, 56 and 57 of the present study the $\frac{\dot{m}}{H}$ ratio is constant. The parameters N_1, N_2 and N_{gr} remain almost constant among the cases since containing $\frac{\dot{m}}{H}$ (slight variations are due to R_1 and R_2 variations among the cases because of the fluid velocity variation caused by different mass flow rate values). The study has been expanded by varying $\frac{\dot{m}}{H}$ with respect to the previous cases while keeping the q_{ratio} values constant and equal to those corresponding to the cases reported in Table 20 of the present study. Cases in (Beier, 2020) for uniform k_{gr} indicate changes of $\frac{\dot{m}}{H}$ has little influence on the estimate of k_{gr} from a 1D radial model until $\frac{\dot{m}}{H}$ becomes small. In the present study, the effects of N_1, N_2 and N_{gr} have been studied by varying $\frac{\dot{m}}{H}$ for multi-layer ground. The other dimensionless parameters reported in Table 5 of (Morchio et al., 2022) are area ratios and thermal property ratios, which would tend not to change for a given borehole under various TRT conditions.

Additional simulations for the same cases reported in Table 20 of the present study have been performed adopting the half value of the $\frac{\dot{m}}{H}$ reported in Table 20 varying the mass flow rate among the cases in order to keep the $(T_{in}-T_{out})$ constant at the top of the BHE, while $\frac{\dot{Q}}{H}$ remains constant except for the CASE 3A BIS. For the sake of brevity, the graphs reporting the results of this simulations cluster have not been reported since the trends are not too dissimilar to those reported in Figures 55, 56, 57.

Another cluster of simulations has been performed at a third flow rate for each case in order to verify and consolidate if q_{ratio} is always the dominant parameter in the ILS estimation of the k_{gr} for more different $\frac{\dot{m}}{H}$ values (for both the center and annular inlet configuration of the coaxial cases). In particular, the mass flow rate related to the 200 m CASE 3C has been imposed on the 100 m and 300 m cases (3B and 3D respectively) while the cases from 400 m to 800 m (3E to 3A BIS respectively) adopt the mass flow rate related to the 600 m CASE 3G, as reported in Table 21. In this manner, 7 of the 9 cases are characterized by a different $\frac{\dot{m}}{H}$ value and the fluid temperature difference between the BHE inlet and outlet sections is kept included between 1.5°C and 4.5°C except for the CASE 3A BIS. The related results are reported in Figures 58, 59 and 60.

Table 21
Main input and pre-processing data related to the center inlet and annular inlet cases varying $\frac{\dot{m}}{H}$ among the cases.

Case	$\dot{m}$ *[kg/s]*	$\dot{m}/H_b$ *[kg/ms]*	H_b *[m]*	*External heat extraction rate* $\dot{Q}$ *[W]*	*Natural heat rate per unit length [W/m]*	q_{ratio} *[-]*
3B	0.64	0.0064	100	4,000	4	10
3C	0.64	0.0032	200	8,000	8	5
3D	0.64	0.0021	300	12,000	12	3.33
3E	1.91	0.0048	400	16,000	16	2.5
3F	1.91	0.0038	500	20,000	20	2
3G	1.91	0.0032	600	24,000	24	1.66
3H	1.91	0.0027	700	28,000	28	1.43
3A	1.91	0.0024	800	32,000	32	1.25
3A BIS	1.91	0.0024	800	170,667	32	6.66

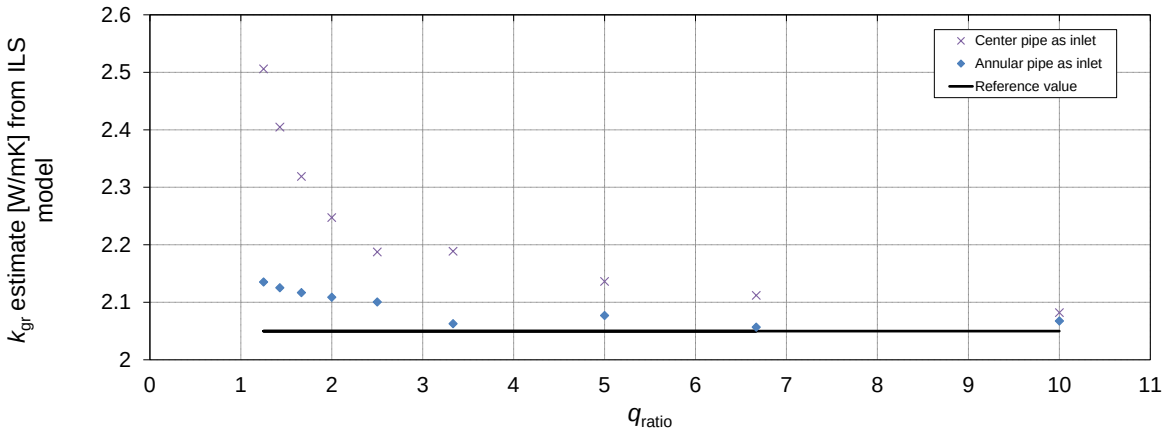

Figure 58: Effective ground thermal conductivity estimation from the FOA of the ILS model compared to the reference value (the results at a different $\frac{\dot{m}}{H}$ value for each case).

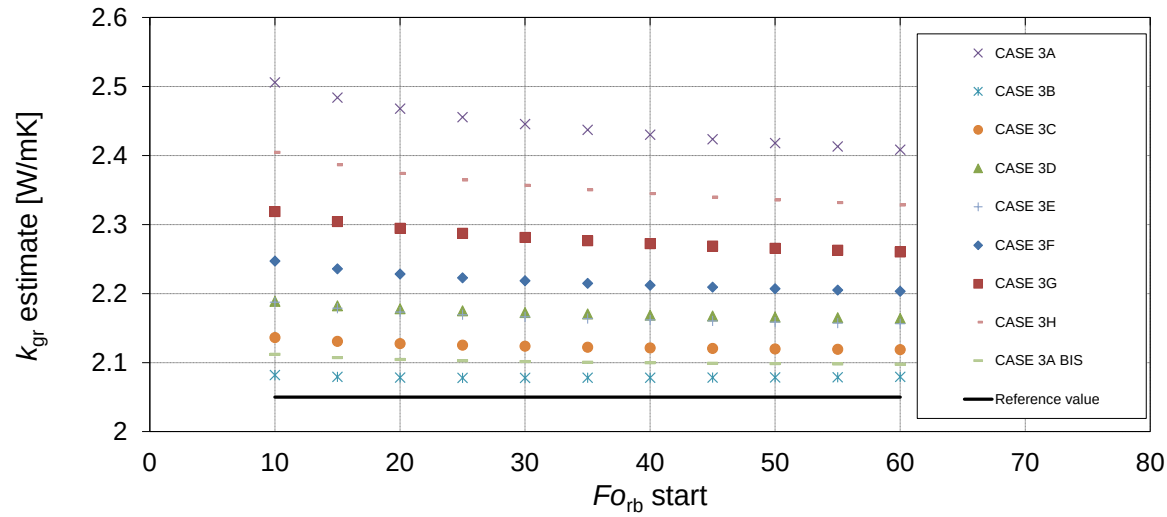

Figure 59: Effective ground thermal conductivity from the ILS model as estimated for different Fo_{rb} windows for the center inlet configuration (the results at a different $\frac{\dot{m}}{H}$ value for each case).

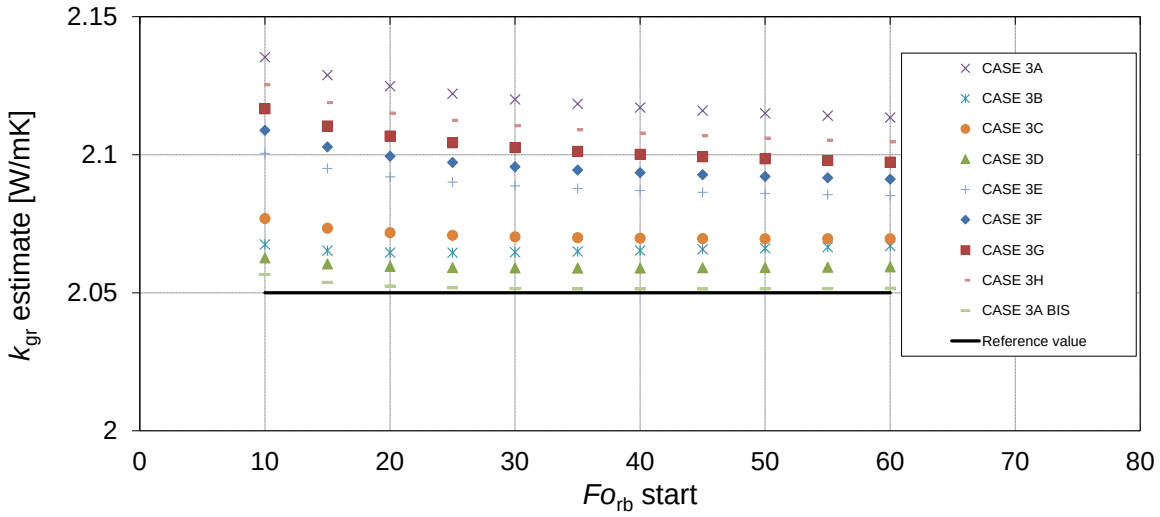

Figure 60: Effective ground thermal conductivity from the ILS model as estimated for different Fo_{rb} windows for the annular inlet configuration (the results at a different $\frac{\dot{m}}{H}$ value for each case).

Figures 55 and 58 show that the parameter q_{ratio} is an indicator of when the effective k_{gr} departs from the thickness-weighted average of the layers' k_{gr} values. For shallow boreholes and large q_{ratio} the ILS estimate is near the weighted average. As q_{ratio} decreases the departure increases as illustrated in Figures 55 to 60. For simplicity, the value of q_{ratio} = 1 is a tempting value to choose as the dividing value for when k_{gr} departs from the weighted-thickness average. Identifying an exact value of q_{ratio} for the transition may be difficult because the regions of transition change somewhat depending on the choice of the $\frac{\dot{m}}{H}$ and $\frac{r_b}{H}$ specific values. A departure of 10% is for q_{ratio} included between 2 and 2.5 for the coaxial center-pipe inlet cases considered and the departure increases with decreasing q_{ratio}. The original definition of q_{ratio} expressed by Eq. (91) proves that q_{ratio} is not sensitive of the $\frac{r_b}{H}$ variation. Additional simulations verify that varying $\frac{r_b}{H}$ has little influence on the k_{gr} ILS estimation.

A new cluster of simulations varying $\frac{r_b}{H}$ demonstrates that the influence of the value assumed by q_{ratio} on the ILS-based k_{gr} estimation has more weight than the one due to the specific value assumed by $\frac{r_b}{H}$. In the new cluster of simulations, the $\frac{r_b}{H}$ value has been varied from the value reported in Table 17 (r_b has increased from 0.07 m to 0.14 m). For the sake of brevity, the graphs reporting the results of this simulations cluster have not been reported since their trends are very similar, especially for what concerns Figures 55 and 58. The simulation results highlight that the ILS-based k_{gr} estimations are sensitive mainly to the value related to q_{ratio} regardless of the specific value assumed by the $\frac{r_b}{H}$ ratio. The $\frac{r_b}{H}$ is likely to have a minor influence on the ILS model estimate of the effective ground thermal conductivity. The $\frac{r_b}{H}$ ratio enters the problem when the borehole is treated with a finite length and/or multiple boreholes interacting with each other. The typical duration of TRTs is too short for axial heat conduction in the ground and the finite length to have significant effects. Therefore, any change of $\frac{r_b}{H}$ has little effect on the estimate of k_{gr}.

The results reported in the present section related to the coaxial cases have been graphically explained and clarified also in terms of $g_{0,j}(\tau)$ functions. The condition related to q_{ratio} >>1 has to be satisfied in an ILS-based TRT analysis in order to override the natural heat input rate related to the $g_{0,j}(\tau)$ functions. This makes the ILS-based k_{gr} estimation not sensitive to the effect related to the geothermal gradient incorporated into the $g_{0,j}(\tau)$ functions, therefore closer to the mean k_{gr} value regardless of the k_{gr} variations among the layers. The g_j - function approach of the present study has been applied in the case of a ground characterized by multiple layers of equal thickness with different thermal conductivity values imposed along the depth and corresponding geothermal gradients. Recall that the inlet and outlet temperature profiles in Figures 61 and 63 decrease with time because are related to TRTs in heat extraction mode. Figures 61, 62, 63 and 64 compare the $g_{0,j}$ curves related to two different cases of different H active depths (800 m and 100 m related to the center-inlet CASE 3A and 3B respectively), thus of extremely different q_{ratio} (respectively the lowest and the highest among the multilayered cases considered). In particular, the $g_{0,j}$ curves related to different nodes placed in the annulus at different depths have been compared while the ground thermal conductivity in the corresponding layer still follows the value reported in Table 19. This would make the approach related to the $g_{0,j}(\tau)$ functions analysis feasible also for DTRT analysis. The node numbered 87 is placed in the annulus and is related to the depth of 94.50 m and 11.81 m for CASE 3A and 3B respectively. The node numbered 107 is placed in the annulus and is related to the depth of 304.50 m and 38.06 m for CASE 3A and 3B respectively. The node numbered 127 is placed in the annulus and is related to the depth of 514.50 m and 64.31 m for CASE 3A and 3B respectively. The node numbered 147 is placed in the annulus and is related to the depth of 724.50 m and 90.56 m for CASE 3A and 3B respectively.

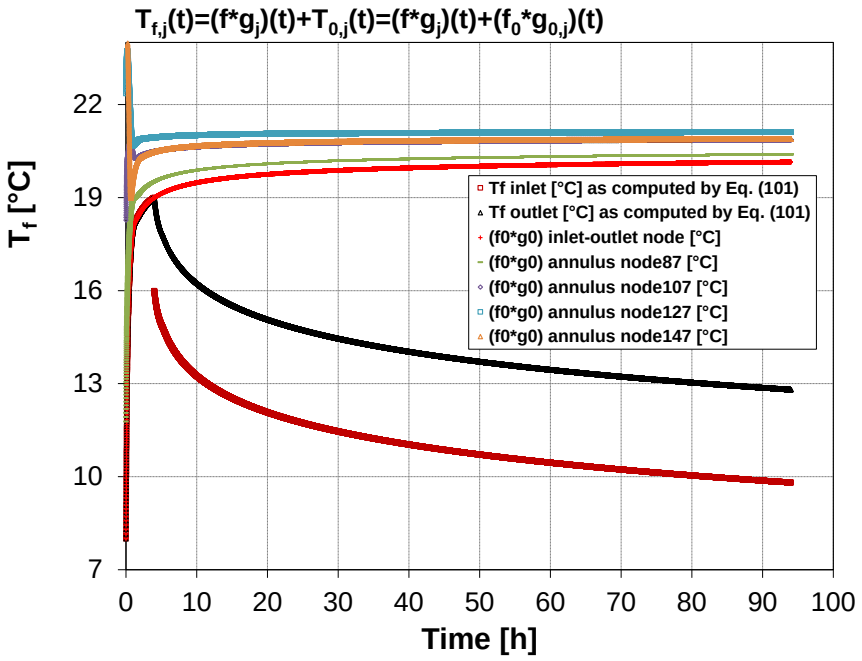

Figure 61: Fluid temperature inlet-outlet from the superposition of the $(f*g_j)(\tau)$ and the $(f_0*g_{0,j})(\tau)$ convolution products and the $T_{0,j}(\tau)$ profiles for the 4 nodes placed in the annulus at different depths related to the Center inlet Coaxial 800 m DBHE (CASE 3A).

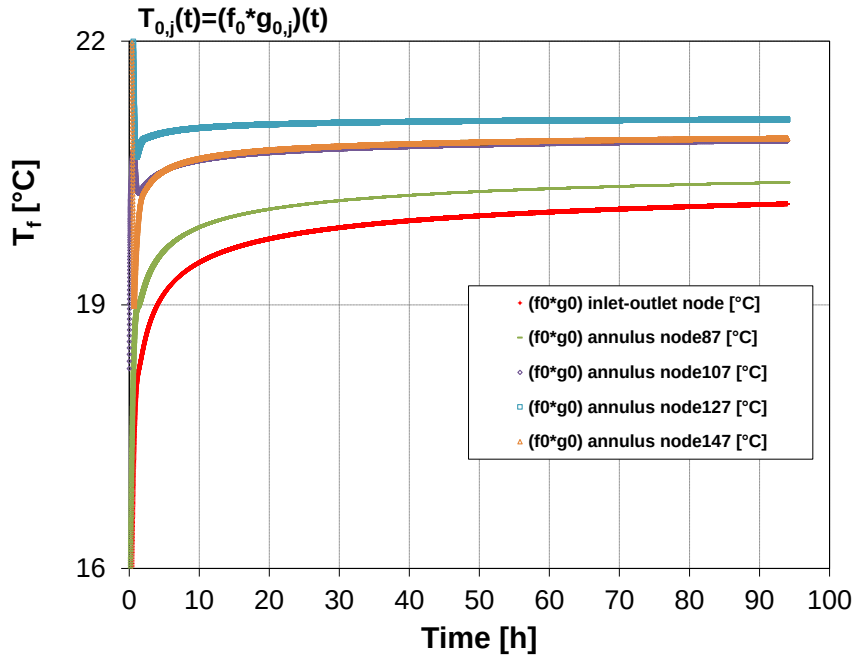

Figure 62: Focus on the $T_{0,j}(\tau)$ related to the inlet and outlet nodes and the 4 nodes placed in the annulus at different depths related to the Center inlet Coaxial 800 m DBHE (CASE 3A).

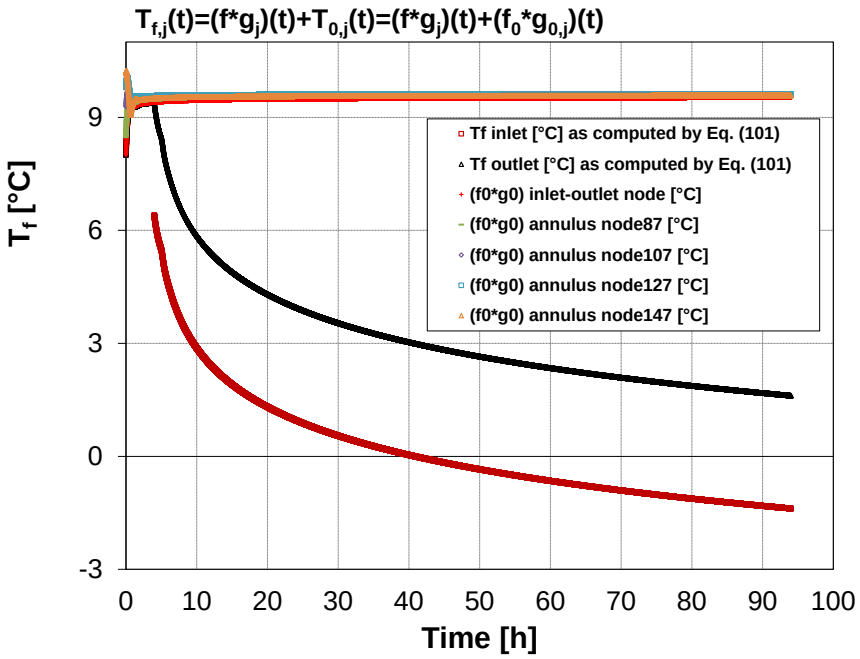

Figure 63: Fluid temperature inlet-outlet from the superposition of the $(f*g_j)(\tau)$ and the $(f_0*g_{0,j})(\tau)$ convolution products and the $T_{0,j}(\tau)$ profiles for the 4 nodes placed in the annulus at different depths related to the Center inlet Coaxial 100 m BHE (CASE 3B).

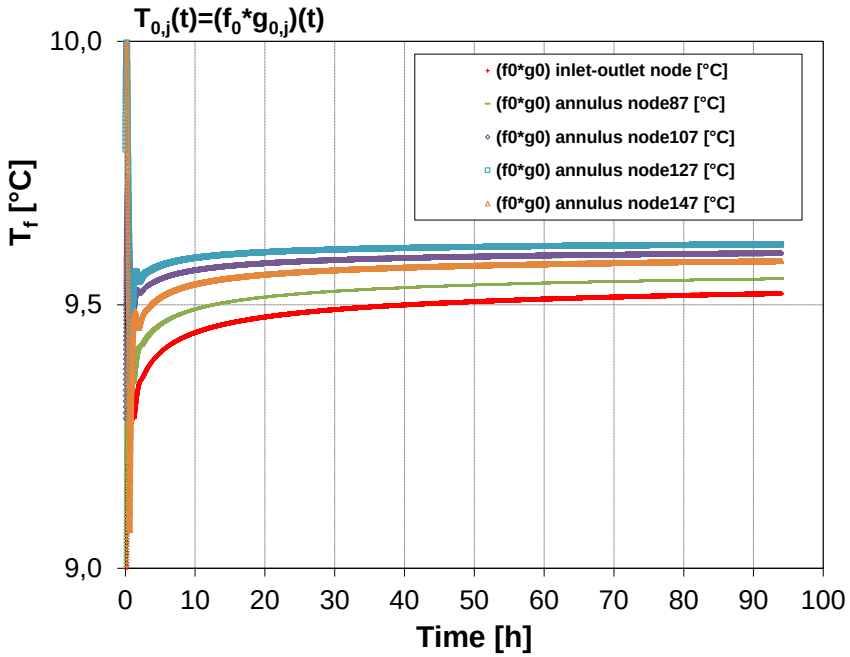

Figure 64: Focus on the $T_{0,j}(\tau)$ profiles related to the inlet and outlet nodes and the 4 nodes placed in the annulus at different depths related to the Center inlet Coaxial 100 m BHE (CASE 3B).

The graphs reported in Figures 61, 62, 63 and 64 compare the $g_{0,j}$ curves related to two different cases of different H active depths (extremely different q_{ratio}, 1.25 and 10 for the CASE 3A and CASE 3B respectively). The $g_{0,j}$ curves related to the inlet and outlet nodes are necessarily identical. Similarly to Figure 48 for the single-layer subsurface case, the results reported in Figures 61, 62, 63 and 64 for the multilayer case clearly show that the $T_{0,j}(\tau)$ profile related to the center inlet configuration of the coaxial 800 m (q_{ratio} = 1.25) center inlet CASE 3A changes much more at late times than the $T_{0,j}(\tau)$ profiles related to the coaxial 100 m (q_{ratio} = 10) center inlet CASE 3B. Therefore, especially for the coaxial BHE, the $g_{0,j}$ functions can be used as an indicator similar to the one represented by q_{ratio} also in the case of multiple ground layers ($g_{0,j}$ functions and q_{ratio} are directly linked, being affected both by the geothermal gradient $dT_{gr,\infty}/dz$). In particular, the condition related to q_{ratio} >>1 has to be satisfied in an ILS-based TRT and DTRT analysis in order to override the additional available heat input rate related to the $g_{0,j}$ (τ) functions. This makes the ILS-based k_{gr} estimation not sensitive to the effect related to the $g_{0,j}(\tau)$ functions, therefore closer to the mean k_{gr} value regardless of the k_{gr} variations among the layers.

4. The innovative Electric Depth Distributed Thermal Response Test (EDDTRT)

The present chapter reports the experimental setup related to a suitable reduced-scale prototype of the real BHE and the surrounding ground for innovative EDDTRT experiments. Measurement error analyses in estimating the grout and ground thermal conductivity are reported in the present chapter. Present measurements highlight the possibility of reliably performing a TRT experiment and estimating the slate/ground thermal conductivity with an agreement of about +12% with respect to measurements provided by a standard commercial conductivity meter on proper cylindrical samples of the same material and onto 10 different portions of the slate block. The thermal conductivity estimations of both the ground and grout constitute important input parameters for the BHE field sizing methods.

4.1 The experimental setup related to a suitable reduced-scale prototype of the real BHE and the surrounding ground for the innovative EDDTRT

The knowledge of the ground thermal conductivity is fundamental for the correct sizing of the GCHP plant. The present section is aimed to present an experimental setup constituted by a suitable scale prototype of the real BHE and the surrounding ground for developing innovative EDDTRT experiments. The measurements collected highlight the possibility of performing reliable TRT experiments and estimating the grout and ground thermal conductivities.

The experimental setup aimed to realize a suitable scale prototype of the real BHE and the surrounding ground for reduced-scale TRT experiments is described. Numerical analyses were carried out to correctly determine suitable geometric and operational parameters for the present setup. The scaled ground volume is realized with a slate block. The scaled heat exchanger, inserted into the block, is created with additive technology (3D printer) and equipped with a central electrical heater along its entire depth and with temperature sensors at different radial distances and depths. The all-in-one BHE equipped with the central electrical heater and with temperature sensors for the EDDTRT assures continuous BHE performance monitoring, test for correct grouting, and test for aquifer presence.

As reported by the International Energy Agency (IEA, 2020), Ground-Coupled Heat Pumps (GCHP) are indicated as the most effective system (in terms of energy savings and reductions in CO_2 and greenhouse gas emissions) for efficient heating, ventilation, and air conditioning of buildings for civil and industrial use. In most European countries, heating, and air conditioning of buildings accounts for nearly 50% of total primary energy consumption (Köhler et al., 2016). The market related to building air conditioning systems employing GCHP involves about one million installations in Europe. As reported by (IEA, 2020), Sweden and Germany are the two main European markets, with 20,000 up to 30,000 new installations every year in each country. More than half of GCHP in the world are installed in the United States. According to (IEA, 2020), electric heat pumps could supply more than 90% of air and water heating with lower CO_2 emissions than the

condensing gas boiler technology (92–95% efficiency), even when the primary carbon intensity of electricity consumption is taken into account. GCHP applications are composed of a heat pump coupled with the ground through multiple vertical or horizontal ground heat exchangers constituting a closed-loop system. Typically, vertical borehole heat exchangers (BHEs) are the most frequently adopted solution.

For the correct sizing of these closed-loop systems and their energy and economic sustainability, it is important to know the ground thermal parameters. One of the more simple to use and in any case reliable methods for sizing a BHE field is the Ashrae method improved with the Tp8 approach (Fossa and Rolando, 2015, Fossa, 2017). However, also in this case, the thermal conductivity of both the ground and the backfilling material (also known as grout) must be estimated (or similarly the couple ground thermal conductivity and BHE thermal resistance).

As it is known, ground thermal conductivity and BHE thermal resistance are typically evaluated through the TRT. The TRT experiment is based on constantly heating (or cooling) the carrier fluid flowing through a pilot BHE while continuously measuring the inlet and outlet fluid temperatures. The effective ground thermal conductivity together with the effective borehole thermal resistance can be estimated from the slope and the intercept of the average fluid temperature profile.

Dedicated experimental equipment, the so-called TRT machines (shown in Figure 65), are used to perform the measurement campaigns. The first moveable measurement devices were introduced by (Eklöf and Gehlin, 1996, Austin, 1998, and Gehlin, 2002). Unfortunately, these machines have a particularly high realization cost (EUR 20,000–60,000 from 2019 estimates).

Diffused literature about TRT and comprehensive analyses of the related methods are available (Zhang et al., 2014, Spitler and Gehlin, 2015). A general analysis of the various TRT types, including standard TRT, pulsated TRT (Fossa et al., 2018) and Distributed Thermal Response Test (DTRT) with fibre optics using the Raman effect is discussed by (Acuña et al., 2009); the theoretical basis of the method is, for example, reported by (Franco and Conti, 2020).

Among conventional 1D radial models that can be used for TRT analysis, a cylindrical-source model neglecting the thermal storage of the fluid (and the grout if present) within the borehole has been applied to boreholes by (Ingersoll et al., 1951, Ingersoll et al., 1955) and (Deerman and Kavanaugh, 1991). On the contrary, the cylindrical-source model derived by (Blackwell, 1954) includes the borehole storage.

A robust 3D numerical model by the present research group (Fossa et al., 2013) has been employed for performing simulations of a classical TRT in Comsol Multiphysics environment. The model accounted for the transient behaviour of ground, grout, and circulating fluid. In fact, the 3D Fourier heat conduction equation was solved in both the ground and the grout while a 1D (along the pipe axial coordinate) energy transient equation included in the analysis also the thermal effects related to the counter current fluids.

(**a**) (**b**)

Figure 65. (**a**) Traditional TRT machine (Photo: Geoenergi, Gehlin 2002), (**b**) the pulsated TRT machine developed at the University of Genova (Fossa et al., 2018).

Generally speaking, to analyze the BHE behaviour, also an experimental approach can be used, by realizing a scaled pilot BHE. (Cimmino and Bernier, 2015) built an experimental setup to obtain the *g*-function of a small-scale borehole (400 mm long inserted in a 2 m^3 sand tank with known thermal properties), and (Beier et al., 2011) obtained data from a "sandbox" containing a borehole with a U-tube. Other similar examples are those presented by (Gu and O'Neal, 1998, Eslami-nejad and Bernier, 2012, Kramer et al., 2015, Salim Shirazi and Bernier, 2014), and more recently by (Mazzotti et al., 2018).

In the present study, a reduced-scale experimental apparatus is designed and realized, with the aim of performing and analyzing an innovative one based on electric heating at the BHE axis. The scaled setup allows performing tests under more controlled conditions than those achievable in field tests. The scaled apparatus is constituted by a rock (slate) volume in which the scaled heat exchanger is inserted, realized with additive technology (3D printer). Some preliminary numerical simulations have been carried out to assess the reliability of the method and to correctly determine suitable geometric and operational parameters of the scale prototype. The proposed innovative TRT can be considered a reliable method to estimate the slate/ground thermal conductivity representing a cheaper solution with respect to the conventional TRT methods. The present reduced scale analysis and experimentation have to be intended as the initial demonstrator of the present application. The next step related to the present research is to establish its applicability in a real GCHP plant.

4.1.1 Scaling the Experiment

Preliminary numerical simulations aimed to correctly size the scaled prototype are reported in the present section.

As previously explained, the scaled experimental set-up is composed of a rock (slate) volume in which the scaled heat exchanger, realized with additive technology, is inserted. The correct size of the slate volume was determined through an accurate preliminary evaluation based on dimensionless analysis and numerical simulations with Comsol Multiphysics.

The 3D Comsol model includes the slate volume and the BHE volume. The equation to be solved in both domains is the unsteady Fourier equation without heat generation in cylindrical coordinates:

$$\rho c \frac{\partial T}{\partial \tau} = k \nabla^2 T = k \left(\frac{\partial^2 T}{\partial r^2} + \frac{1}{r} \frac{\partial T}{\partial r} + \frac{\partial^2 T}{\partial z^2} \right) \quad (118)$$

where ρ, c, and k are the density, the specific heat capacity, and the thermal conductivity, respectively, assumed as constants. In the preliminary simulations, the two domains have the same thermophysical properties, namely $(\rho \cdot c) = 2.1 \times 10^6$ J/m^3 K and $k = 2.5$ W/m·K. The slate domain is a parallelepiped with side L and high H, with adiabatic top and bottom surfaces. These boundary conditions are aimed to reproduce ideally the condition of infinite volume in the axial direction. The imposed initial condition is a uniform temperature distribution in the ground and BHE volumes, $T_{gr,\infty} = 20$ °C. For the sake of completeness, the Reader is directed to (Fossa et al., 2013) for more details about the model. The robust 3D numerical model by the present research group was validated against real TRT experiments, as reported in (Fossa et al., 2013).

The BHE volume has a depth equal to the slate whole thickness, namely $H = 0.4$ m. As previously specified, the geometry was scaled, with a BHE radius equal to $r_b = 0.02$ m, with a geometrical reduction with respect to actual cases at 1/2.5. In the middle of the BHE volume, a hole with radius $r_h = 0.002$ m and a boundary condition of constant heat transfer rate per unit length $\dot{Q}' = 40$ W/m represents the heater.

A period of operation $\tau = 150{,}000$ s (about 42 h) was considered and non-uniform time steps were adopted in the computations, starting from a time step equal to 0.001 s for $\tau < 0.01$ to a time step of 5000 s in the late period ($\tau > 15{,}000$).

A mesh independence analysis was carried out and, as a compromise between accuracy and computational effort, a mesh of nearly 136,000 elements was adopted for all simulations.

In the BHE domain, the temperature is evaluated as an average along three ideal vertical lines located at different radial distances from the heat source, namely $r = 0.25 \cdot r_b$, $r = 0.5 \cdot r_b$ and $r = r_b$.

In order to properly select the dimensions of the slate block and assure that the prototype may represent, for the analyzed time period, the behaviour of an infinite ground, a series of simulations were carried out by changing the side L of the parallelepiped. In particular, to verify that the results are unaffected by the slate domain size, two different boundary conditions were applied to the lateral surfaces of the block, namely adiabatic and isothermal surface $T_{gr,\infty}$. The sensitivity analysis is based on comparing the numerical results carried out by adopting the two different far-field boundary conditions according to the approach reported in different studies by the present research group (Fossa et al., 2013, Morchio and Fossa, 2019, Morchio and Fossa, 2020, Priarone and Fossa, 2015).

The results for the two cases were compared in terms of temperature profile vs. time for increasing values of L, up to reaching the profiles presented in Figure 66, for $L = 0.8$ m.

The curves for the two different boundary conditions overlap, with a difference of less than 0.01 °C, up to approximately ln(τ) = 10 which corresponds to τ = 15,000 s. This overlapping means that the temperature field at the boundary is still undisturbed, thus the domain size is enough to represent ideally the infinite ground.

For the rescaled geometry (r_b = 0.02 m), the period of τ = 15,000 s corresponds to about Fo_{rb} = 45, that, if referred to a not-scaled geometry (r_b = 0.05 m) with the same thermophysical properties, corresponds to about τ = 26 h, a reasonable time duration for that type of TRT.

From the point of view of the axial temperature behaviour in the slate block, interesting information can be deduced from some numerical simulations described in the following. In the newly analyzed cases, a different boundary condition is imposed all around the slate block, namely a convective one with a convective coefficient h = 10 W/m^2·K and an external fluid temperature equal to $T_f = T_{gr,\infty}$ = 20 °C. This boundary condition can better represent the actual situation of the scale prototype located in a laboratory. The temperature in the BHE domain is now calculated not only as an average along the three vertical ideal lines previously discussed, but also in specifically defined sample points, as sketched in Figure 67.

The radial distance of all the sample points is $r = 0.25\ r_b$, except for the point TK4 that is located at the heater surface, namely for $r = 0.1\ r_b$.

Figure 68 presents the results of this numerical analysis. As expected, the temperature profile for the sample point on the heater (TK4) is higher than the others, although it presents the same slope, related to the thermal conductivity value. The other profiles, associated to sample points located all at the same radial distance ($r = 0.25\ r_b$), almost overlap (with an error with respect to the nearly central point TK3 of less than 0.2 °C) in the previously discussed time range up to τ = 15,000 s (ln(τ) = 9.62), except for the point TK1n. In fact, the temperature of the point TK1n is influenced by the boundary effects in the axial direction and the slope of its profile seems not useful for a proper calculation of the thermal conductivity.

As a consequence, in the scaled prototype the axial position of the thermocouple TK1n was modified (TK1), as presented again in Figure 67, with a bigger distance from the boundary (0.07 m instead of 0.015 m).

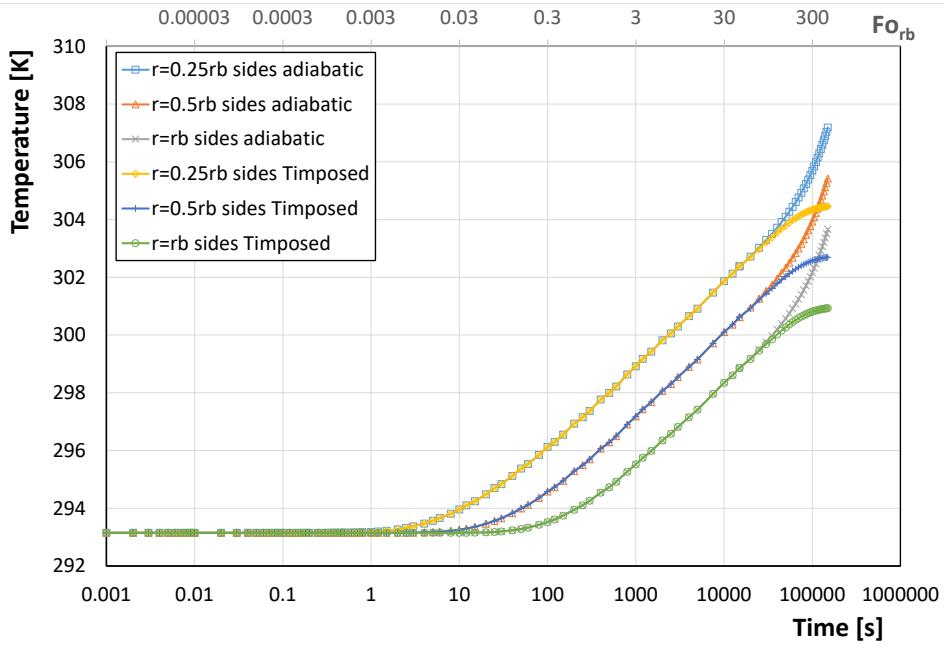

Figure 66. Simulation data analysis: axial average temperature in the slate volume at different radial distances from the heater. In abscissa the logarithm of time.

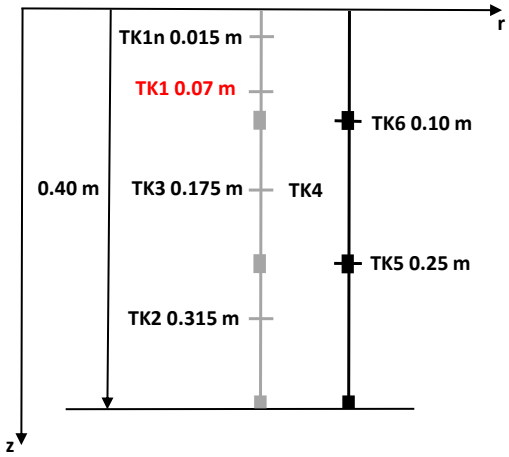

Figure 67. Sketch of the temperature samples axial position into the slate block.

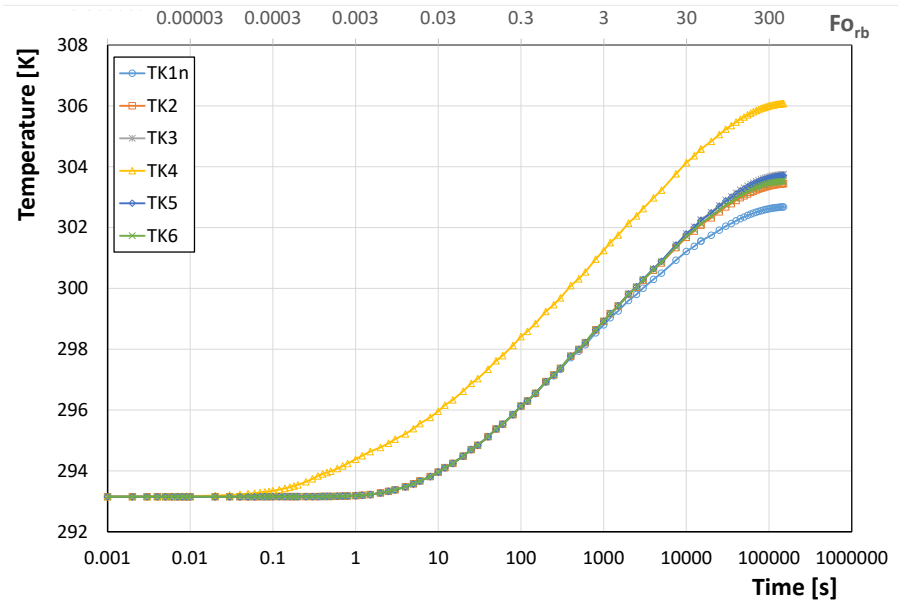

Figure 68. Simulation data analysis: temperature in the slate volume at different axial positions according to Figure 67. In abscissa the logarithm of time.

Finally, to have a more realistic idea of the actual behaviour of the scaled prototype, further simulations were carried out by imposing a different value of the grout thermal conductivity, namely k_{gt} = 0.8 W/m·K. Figure 69 shows the corresponding temperature profile for the reference sample point TK3.

The trend plotted in Figure 69 presents two different slopes: the first one, for approximately $5.5 < \ln(\tau) < 7$, takes into account the thermal response of the medium near the source, namely the simulated BHE; the second one, for $\ln(\tau) > 7.5$ and up to the suggested limiting value $\ln(\tau) = 9.62$ (τ = 15,000 s) allows to estimate the slate/ground thermal conductivity.

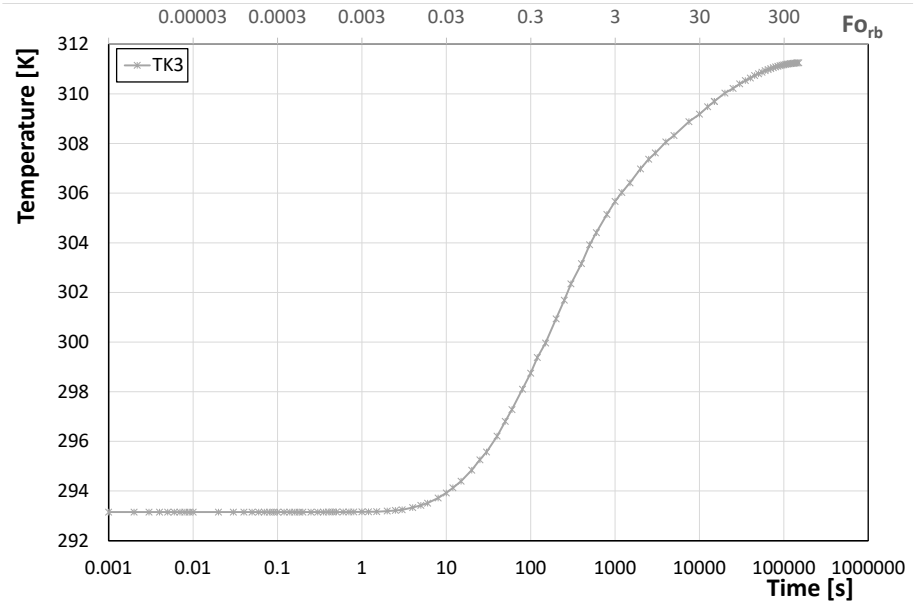

Figure 69. Simulation data analysis: temperature of the slate volume in sample point TK3 for k_{gt} = 0.8 W/m·K. In abscissa the logarithm of time.

4.1.2 Experimental Apparatus

The scaled experimental set-up is aimed to represent the BHE and the surrounding ground volume. In particular, the test section is made by a slate block having dimensions 0.8×0.8×0.4 m (Figure 70), axially perforated along the 0.4 m length (vertical direction). The cylindrical hole diameter is 40.5 mm. An aluminum tube, with external and internal diameters of 40 and 38 mm, respectively, was machined to fit the hole inside the rock block. The aluminum tube is aimed to simplify the disassembling of the test section, if necessary, when the hole is filled with grout. Tube thermal resistance was demonstrated to be negligible compared to the grout and slate counterparts, as checked during Comsol simulations not reported here for the sake of brevity. Its small thickness and high thermal conductivity ensure negligible effects on the thermal behaviour of the assembly.

Figure 70. The rock sample (slate) and the cart that is used to keep the block stably raised during the planned experimental activity.

The present prototype incorporates the scaled borehole heat exchanger that includes the pipes (single or double U-pipe type), the resistive heating cable placed in the middle of the BHE, and a plurality of temperature sensors which are placed at known depths along the vertical direction and radial positions with respect to the heating cable (according to Figure 67). The volume included among the plastic tubes, the heater, and the aluminium tube inside the borehole is filled by grout (Figure 71).

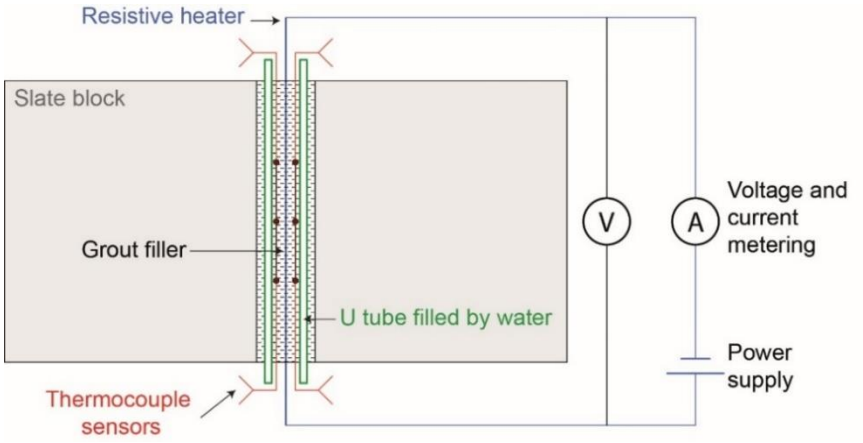

Figure 71. BHE assembly representing the "all-in-one" heat exchanger.

The described BHE assembly represents an "all-in-one" heat exchanger, as shown in Figure 72. To allow the positioning of the temperature probes at a known radial distance from the heater, the BHE plastic pipes are equipped with suitable ribbed parts. The electrical cable, that can provide the linear heating during the procedure, is maintained at the center of the BHE by means of a proper spacer, in the present investigation realized by means of 3D additive manufacturing. The heat transfer rate can be conferred to the carrier fluid at the top ground surface (standard TRT) as well as by employing the electrical wire maintained at the center of the BHE (innovative TRT experiment based on electric heating at the BHE axis). The carrier fluid circulation in the pipes can be guaranteed as well as the test can also be performed without any fluid circulation. The BHE pipes with suitable ribs (Figure 73) were realized with a Cartesian-type 3D printer.

In the reduced scale experiment, the heating cable is realized by a resistance copper wire (Ø0.8 mm, a length of 0.42 m and heat shrink tube, shrink ratio 3:1). The 0.8 mm diameter resistance wire is characterized by a 0.97 Ω/m resistance per unit length. A constant heat transfer rate per unit length of about $\dot{Q}'$ = 40 W/m has to be uniformly injected into the surrounding volume by the electrical wire. The cable is powered by means of a programmable, adjustable, switching, regulated DC 30 V/10 A power supply aimed to adapt the voltage and current parameters (model Rockseed RS310p, max voltage value 30 V, max current value 10 A DC).

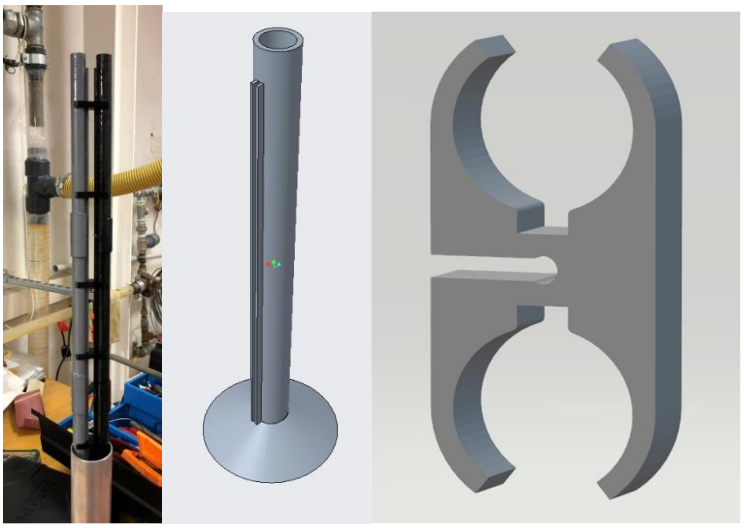

Figure 72. 3D representation of the reduced scale BHE assembly, including its 3D printer-manufactured prototype and its spacer.

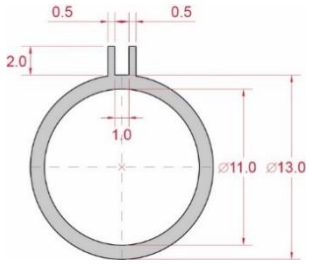

Figure 73. Dimensions (in mm) of the section of each pipe manufactured using the Cartesian 3D printer.

The temperature sensors are armored K-type thermocouples (Ø0.5 mm) and the temperature measurements are read and stored by a multi-channel and multi-function data logger 18bit acquisition board (model FieldLogger-Novus-HMI 512 K). The K-type thermocouples are accurately calibrated on 7 reference temperature values thanks to a thermostatic bath model Thermo Haake C25 and a reference PT100 class A thermometer inserted in the same calibration copper block. The sensor accuracy after calibration in the 5–60 °C range resulted in ±0.15 °C. Accuracy with respect to voltage and current at the power supply operating conditions (heat transfer rate per unit length of the heating cable ranging from 10 to 50 W/m) resulted to be within 0.5% of the readings.

Finally, the experimental apparatus, constituted by the slate block and all-in-one prototype heat exchanger, is located in a laboratory and maintained at a nearly constant temperature by means of an air conditioning system. The aim is to ideally realize, for the analyzed domain, the imposed convective boundary condition with constant external temperature.

The reference thermal conductivity and heat capacity values of the slate were preliminarily measured by means of a contact instrument, model Applied Precision Isomet 2114 conductivity meter, having an accuracy of 4%. Slate thermal properties were measured on 10 different portions of the slate block. In addition, the slate thermal conductivity was also independently measured with a steady-state meter realized at the University of Genova (Unige), working on the principle of the one-dimensional Fourier law. Steady-state measurements were carried out on proper cylindrical slate samples (“disks”) cut from the same original rock volume. Table 22 shows the thermal conductivity

and heat capacity values obtained according to the above reference measurements, together with the uncertainty (standard deviation σ (%)) due to instrument accuracy and repeated measurement differences.

Many factors can influence measurements performed on the same sample by different devices. Parameters such as the surface roughness of the sample face in contact with the probe, the size of the sample tested, possible fluctuations in ambient temperature and humidity, as well as possible non-homogeneities in the materials, can determine the non-uniformity of the same measurement. Exactly for this reason, it is advisable to repeat the analysis using measurement methods characterized by different approaches.

Before starting with the experimental campaign of the electrical TRT, some preliminary measurements were realized on the scaled prototype by means of an infrared camera, model Flir E6-XT. During the test, the heating cable located inside the scaled BHE was electrically powered and the surface temperature field was measured and corresponding images were captured.

Figure 74 shows an example of measurements of the temperature field at the top end of the heat exchanger as performed by the infrared camera. It is possible to visualize the circular shape of the temperature field around the heater due to the radial heat flux which confirms the assumptions on which the present analysis is based.

Table 22. Measured thermal conductivity and heat capacity of the slate.

Material	Measurement Method	Thermal Conductivity (W/m·K)	Heat Capacity ($MJ/m^3 \cdot K$)
Slate block	Applied Precision Isomet 2114 conductivity meter	2.85 σ = 0.18%	2 σ = 0.26%
Cylindrical slate samples	Applied Precision Isomet 2114 conductivity meter	2.85 σ = 0.12%	2.12 σ = 0.035%
Cylindrical slate samples	Unige Steady-state meter	2.48 σ = 0.023%	-

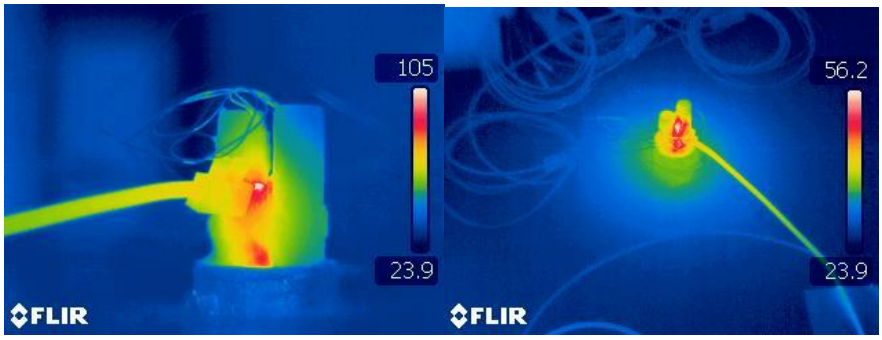

Figure 74. Infrared temperature map close to the top part of the scale prototype. On the right, the concentric temperature profiles can be observed.

4.1.3 Inner Borehole Temperature Evolution

This section presents the preliminary measurements on the scaled prototype, realized by providing electrical power to the central cable in order to heat the borehole and the surrounding slate volume. At the same time, temperature values were measured by the K-type thermocouples, located in the scaled BHE according to Figure 67. For each temperature sensor, a temperature vs. time profile can be obtained on a semi-logarithmic scale (Figure 75).

In particular, Figure 75 shows the temperature profiles for one of the experimental tests carried out, during which a constant in time heat transfer rate per unit length is provided to the block ($\dot{Q}'$ = 38.86 W/m). According to the sketch of Figure 67, the temperature sensor TK4 is located near the electrical heater and the other sensors on the surface of the pipes. As a consequence, the temperature of TK4 is higher than the other, although keeping the same slopes. The temperature trends reveal that probably also the thermocouple TK1 has moved from the planned radial position toward the heater.

The medium around the heat sources is not homogenous because it is composed of a small volume representing the BHE and a big volume of the slate block that simulates the ground, considered as semi-infinite. Thus, the perturbation in the temperature field reaches first the BHE domain (for low Fo_{rb}) and later the slate one (for higher Fo_{rb} values). As a consequence, the temperature profile measured by the thermocouples shows different slopes for different Fo_{rb} ranges, in agreement with the simulated behaviour presented in Figure 69. For this reason, two zones can be recognized on each graph, and only the second one can provide useful information to deduce the thermal conductivity of the slate/ground, namely for $7.5 < \ln(\tau) < 9.5$.

Figure 76 focuses on the "ground slope zone" and shows the linear temperature profiles recorded by the different sensors together with the trend lines, with their corresponding equations.

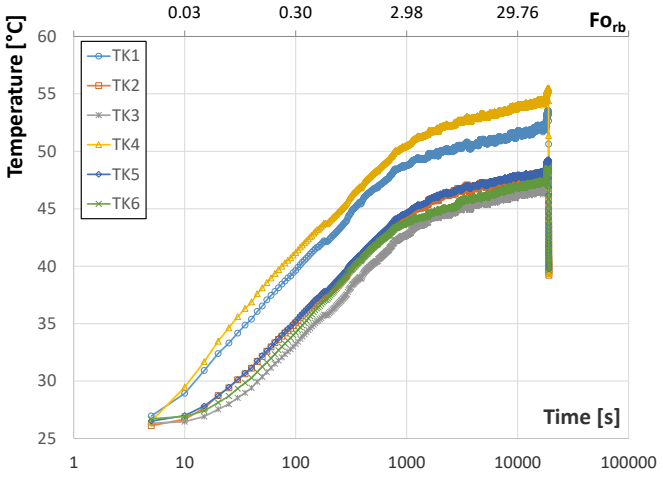

Figure 75. Temperature vs. time profiles for the different sensors inserted into the "all-in-one" heat exchanger.

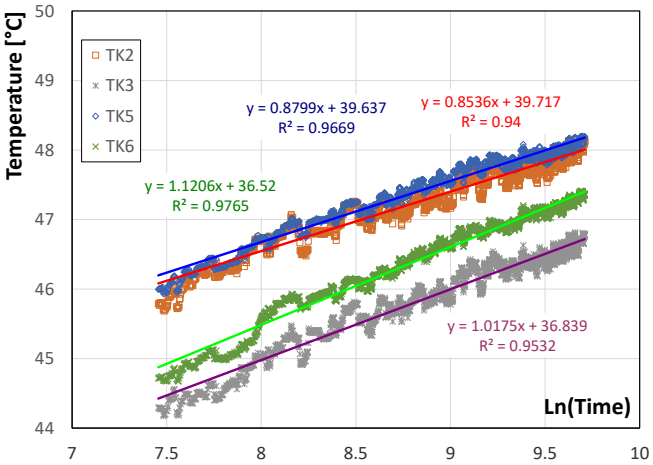

Figure 76. Temperature vs. time profiles: the "ground slope zone".

After estimating the slope of the linear profiles, according to $k_{gr} = \frac{\dot{Q}}{4\pi Hm}$ it is possible to calculate the corresponding values of the ground thermal conductivity.

Table 23 summarises the main results related to the experimental test carried out. The agreement with the preliminary measured thermal conductivity values presented in Table 22 is good, especially comparing the results related to the central thermocouple TK6.

Table 23. Thermal conductivities related to the experimental test.

Ground		
Thermocouple ID	**Slope**	**k_{gr} (W/m·K)**
TK2	0.854	3.58
TK3	1.017	3.01
TK5	0.880	3.48
TK6	1.121	2.73
	Average	3.20

The error deviations between the estimated ground thermal conductivity average values provided by different methods were computed in terms of relative percentage error, $\varepsilon_{i\%}$, which is defined by the following equation:

$$\varepsilon_{i\%} = \frac{k_{innovative\,TRT} - k_{meter}}{k_{meter}} \tag{119}$$

The percentage relative error on the estimated average ground thermal conductivity provided by the experimental test with respect to the value measured by the Applied Precision Isomet 2114 conductivity meter resulted in +12.3%. It can be specified that deviations in the measurements of the same thermophysical property are also because the operating principles and related measurement methods on which each device is based are deeply different. Exactly for this reason, it is advisable to repeat the analysis using measurement methods characterized by different principles in order to increase the confidence level on the estimated property.

4.2 Additional results related to the measurements of the grout thermal properties

As an original contribution, the present thesis work reports the measurements collected for estimating the grout thermal conductivity. It has to be specified that the measurements reported in the present study have been collected with the pipes of the reduced-scale heat exchanger filled with air. This would demonstrate how the innovative EDDTRT can be performed in a completely electrical (heating) way without needing any fluid circulation. Test results and related measurements in presence of water filling the pipes have been carried out but not reported for the sake of brevity. The results in the case of water filling the pipes and related analysis are expected not too dissimilar to those obtained in the case of air filling the pipes.

As mentioned above, the use of thermocouples required a dedicated preliminary calibration process in order to make accurate (and repeatable) temperature measurements.

Figure 77. Some steps of the thermocouple calibration process with a thermostatic bath and resistance thermometer.

Figure 77 presents some steps of the calibration process, which are briefly described hereafter:

- 8 armored K-type thermocouples (Ø0.5 mm, length 500 mm) are suitably placed into a thermostatic bath model Thermo Haake C25.

- Each hot junction is placed inside a perforated copper block placed inside the bath (at the same hole in the block). The center hole of that copper block is occupied by the PT100 resistance thermometer for having the reference of the absolute temperature measurement read through the Keithley 2700 precision multimeter.

- Each thermocouple is assigned to each of the 8 channels of the FieldLogger-Novus acquiring instrument (datalogger), thus being connected to the instrument terminal block (cold junction). The (analog type) temperature measurement provided by each of the 8 K-type thermocouples is read through each of the 8 channels of the Fieldlogger, which provides the A/D conversion. 7 reference temperature levels that can be set through the thermostatic bath have been chosen: 5, 10, 25, 30, 40, 50, 60 °C.

- Internally to the datalogger, through the specific configuration file, measurement values were entered through which to obtain the calibration curve to adjust and correct the signal being read from the data acquisition (Custom Calibration). Acquisitions were made by setting the appropriate value related to the Logging Interval and Scan Interval within the configuration file.

As previously, the reference thermal conductivity and heat capacity of grout were preliminarily measured by means of the contact instrument Applied Precision Isomet 2114 conductivity meter. In addition, the grout thermal conductivity was also independently measured with the steady-state meter realized at the University of Genova (Unige). Table 24 shows the thermal conductivity and heat capacity values obtained according to the above reference measurements, together with the uncertainty (standard deviation σ (%)) due to instrument accuracy and repeated measurement differences.

Table 24. Measured thermal conductivity and heat capacity of the grout.

Material	**Measurement Method**	**Thermal Conductivity (W/m·K)**	**Heat Capacity ($MJ/m^3 \cdot K$)**
Cylindrical grout samples	Applied Precision Isomet 2114 conductivity meter	0.89 σ = 0.25%	1.44 σ = 0.029%
Cylindrical grout samples	Unige Steady-state meter	0.77 σ = 0.003%	-

The experimental setup related to the steady-state meter realized ad hoc at Unige is shown in Figure 78. The DC 30 V/10 A power supply, the thermostatic bath, the insulated box and the related hydraulic circuit constituting the entire assembled system are shown in Figure 78.

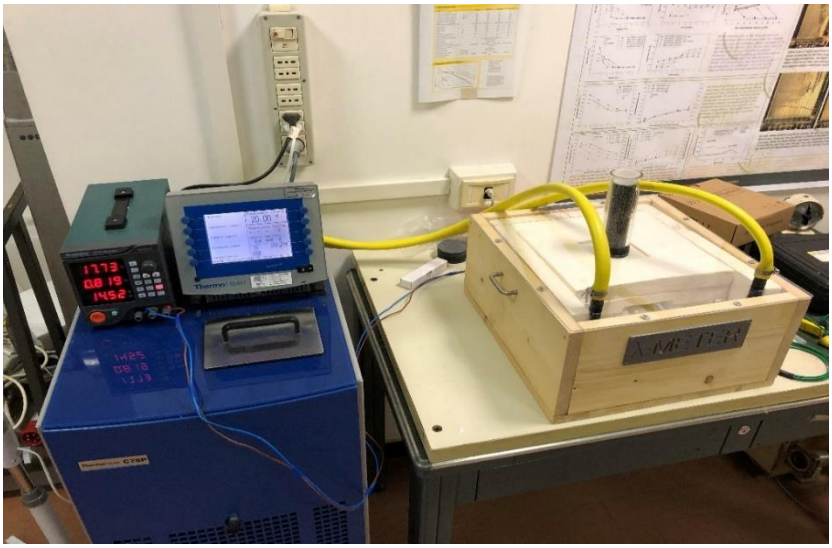

Figure 78. Final setup of the steady-state conductivity meter.

The measurement of the k_{gt} thermal conductivity of the grout specimens, placed inside the steady-state meter by means of special 3D printed cylindrical containers, was found to be 0.77 W/mK, in agreement with the value obtained through the use of the Isomet 2114 instrument. It is specified that during the preliminary operations, it had been opted to use the grout product TermoPlast Plus® di Laviosa Chimica Mineraria SPA. The product was found to have poor mechanical and thermal properties (poor consistency and low thermal conductivity) most likely due to a defect related to improper storage, so it was decided to use the grout product Creteo® Inject CC 854 from RÖFIX Spa. Such grout, which is much less liquid than the previous one, provides a shorter solidification time (in addition to a greater consistency inherent to the quality of the powder composition) and a thermal conductivity of about 2 W/mK (value reported on the related datasheet).

Figure 79. The aluminum tube containing the scaled instrumented heat exchanger.

Once the grout drying process was finished, the instrumented pipe (shown in Figure 79) was placed inside the slate block. Good thermal contact between the outer surface of the aluminum tube and slate was ensured by applying a layer of conductive paste. By connecting the thermocouples to the related extension cables and data acquisition, the innovative EDDTRT measurement campaign performed through the present reduced-scale system was carried out. As seen, it was therefore possible to derive, for example, the grout and slate thermal conductivity values and compare these with the values obtained through the different methods and devices (Isomet 2114 and the original thermal conductivity meter realized and reported in this study). Figure 80 focuses on the "grout slope zone" and shows the linear temperature profiles recorded by the different sensors together with the trend lines, with their corresponding equations, related to the first Fo_{rb} window, namely for approximately $5.5 < \ln(\tau) < 7$, to deduce the grout thermal conductivity used in each pipe of the reduced scale experiment.

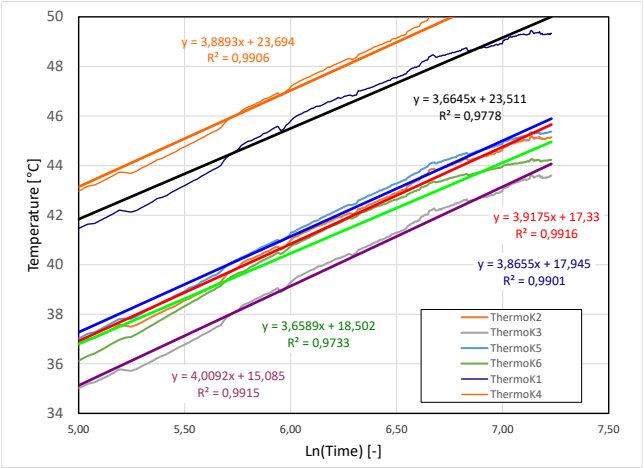

Figure 80. The "grout slope zone" and the linear temperature profiles recorded by the different sensors together with the trend lines equations related to $5.5 < \ln(\tau) < 7$.

These estimations are reported in Table 25 together with the slope and the percentage relative error on the estimated average grout thermal conductivity provided by the experimental test with respect to the value measured by the Applied Precision Isomet 2114 conductivity meter.

Table 25. Thermal conductivities related to the experimental test.

	Grout		
Thermocouple ID	**Slope**	k_{gt} **(W/m·K)**	$\varepsilon_{i\%}$
TK1	3.664	0.84	-5.62%
TK2	3.918	0.78	-12.36%
TK3	4.009	0.76	-14.61%
TK4	3.889	0.79	-11.23%
TK5	3.866	0.79	-11.23%
TK6	3.659	0.84	-5.62%
	Average	0.79	-11.23%

The same experiment has been repeated for testing the reproducibility of the results obtained on the grout of the reduced-scale experiment. Figure 81 shows the temperature profiles from thermocouples measurements related to the typical grout ($5.5 < \ln(\tau) < 7$) Fo_{rb} window together with the related trend lines and their corresponding equations to deduce the grout thermal conductivity. These estimations are reported in Table 26 together with the slope and the percentage relative error on the estimated average grout thermal conductivity provided by the experimental test with respect to the value measured by the Applied Precision Isomet 2114 conductivity meter.

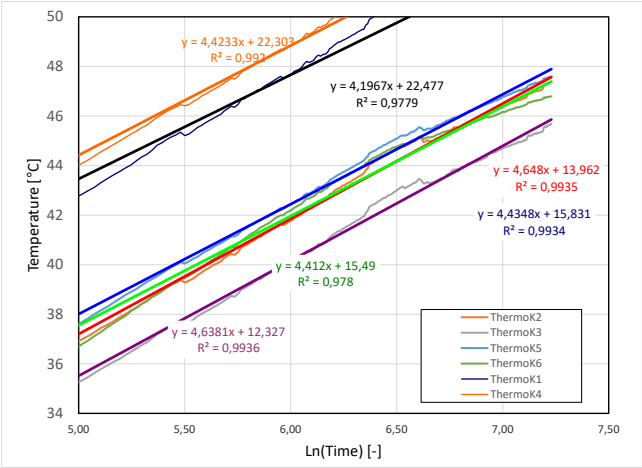

Figure 81. The "grout slope zone" and the linear temperature profiles recorded by the different sensors together with the trend lines equations related to $5.5 < \ln(\tau) < 7$.

Table 26. Thermal conductivities related to the repeated experimental test.

	Grout		
Thermocouple ID	**Slope**	k_{gt} **(W/m·K)**	$\varepsilon_{i\%}$
TK1	4.197	0.73	-18.0%
TK2	4.648	0.66	-25.84%
TK3	4.638	0.66	-25.84%
TK4	4.423	0.69	-22.47%
TK5	4.435	0.69	-22.47%
TK6	4.412	0.70	-21.35%
	Average	0.68	-23.60%

The range of values inherent to the thermal conductivity of the product TermoPlast Plus® by Laviosa Chimica Mineraria SPA, a geothermal filler mortar having a claimed thermal conductivity between 1.6 and 2.3 W/mK (depending on the powder-to-water mass ratio used), was analyzed through the procedures previously described, finding a thermal conductivity value between 0.71 and 1.3 W/mK (by Applied Precision Isomet 2114 conductivity meter).

Furthermore, the hydration heat release (Minchio et al., 2020) from the grout hydration reaction and the grout thermal behavior in response to an electrically scaled TRT (according to the theory related to the reference ILS model) were investigated. A specific test was carried out to measure the heat release during the mortar solidification reaction in a dedicated manner. For this purpose, the powder/water mixture in a ratio of 1.1 was poured inside a cylindrical and insulated container. Two thermocouples were embedded in the grout, one in an axial position (along the axis of the cylinder, at mid-height) and another one at a radial distance of 25 mm (at mid-height). A third thermocouple was used to measure the ambient air temperature.

Four tests were performed under the same conditions to verify the repeatability of the measurement. The temperature measurements shown in Figure 82 are those related to the third acquisition. Each test had a duration of about four days. This duration is necessary to ensure the complete exhaustion of the process related to hydration reaction heat release

(having an estimated duration of about 27 hours), as shown by the temperature trends in the grout (plotted in Figure 82).

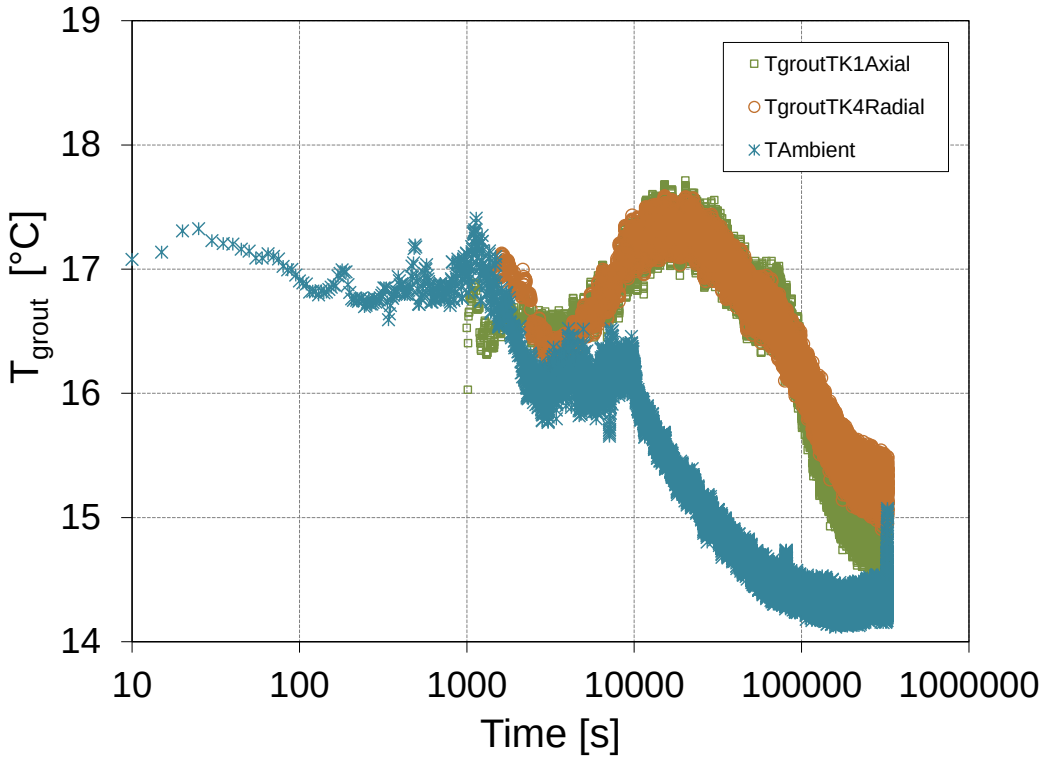

Figure 82. Temperature measurements aimed at estimating the grout hydration reaction heat release.

The collection of this kind of data allowed to inferring a reference time necessary for the reaction related to the hydration and formation process of the grout, in conjunction with the complete evaporation of the water present within the mortar, to be completed without external interference.

A further test based on the ILS interpretative model was performed to estimate the grout thermal conductivity. A heating cable (along the axis of the cylinder) and the two thermocouples (one on the cable at half height and one at a known radial distance, at half height) were placed in an insulated cylindrical container.

Subsequently, as previously described, the grout was poured and prepared to maintain a mass powder/water ratio of 1.1 to guarantee the achievement of the highest declared thermal conductivity value. Once the time required for its complete solidification had elapsed, the cable was powered and then a constant heat transfer per unit length was injected into the preparation.

The equation $k_{gt} = \frac{\dot{Q}}{4\pi H m}$ allows estimating the grout thermal conductivity based on the injected constant heat transfer per unit length $\frac{\dot{Q}}{H}$ and the slope *m* of the temperature profile.

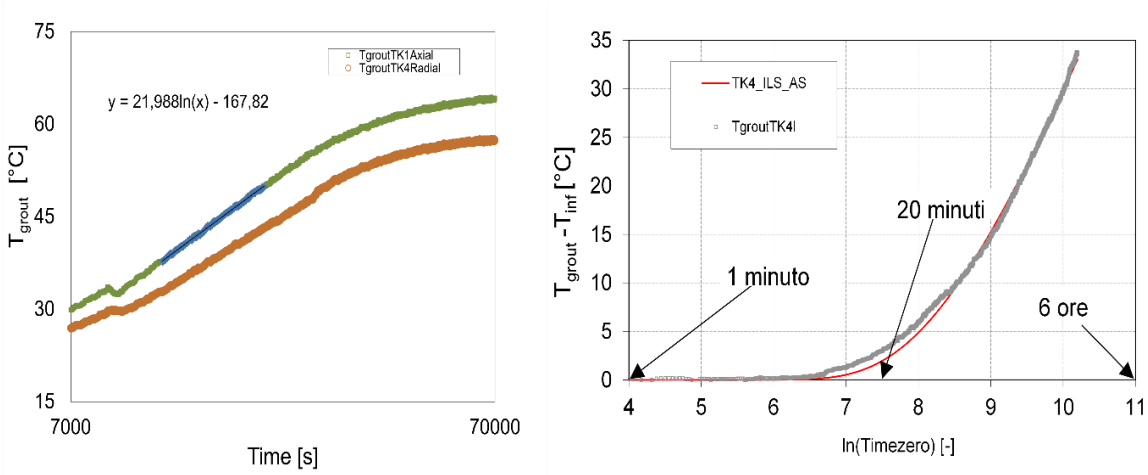

Figure 83. Temperature measurements aimed at estimating the grout thermal conductivity based on a reduced scale electrical TRT.

Time is plotted on the x-horizontal axis with an interval between 7000 and 70000 s to detect the constant slope section, which is useful for analysis.

The heat transfer per unit length injected corresponds to 40 W/m. Employing the bench power supply (programmable and adjustable), the necessary electrical power is supplied to the heating cable. This power is then injected in the form of thermal power, thus by the Joule effect, within the conductive medium (the grout). The equation $k_{gt} = \frac{\dot{Q}}{4\pi Hm}$ yields a thermal conductivity value of 0.144 W/mK. This value is highly unrealistic (it is well below the thermal conductivity value of water). This deviation from the expected value is attributable to the failure to wait for the time required for the complete completion of the chemical reaction associated with the formation of the grout itself. The test was activated without waiting for the complete evaporation of the water present within the grout. For this reason, any further scaled TRT aimed at estimating the grout thermal conductivity has to be carried out once the time associated with the completion of the reaction, which is recommended to be about 28 days, has elapsed.

5. The web app for the correct sizing of the BHE fields

As shown in the previous chapter, the thermal conductivity estimations of both the ground and grout constitute important input parameters for the BHE field sizing methods. The present chapter is dedicated to presenting the main input parameters and references related to the web calculation tool for the design of BHE fields based on a modified version of the Ashrae Method, also employed in the corresponding UNI Italian standard (see https://en.geosensingdesign.org/).

5.1 The proposed model for temperature penalty correct calculation

In this chapter, the Ashrae method for borehole heat exchanger field design is presented in order to trace its theory and physical meaning. A new version of the Temperature Penalty calculation procedure is described since it is able to maintain the ASHRAE formalism and simplicity while enhancing the accuracy of the design results (demonstrated by a comprehensive comparison with reference results pertaining to a vast number of borefield configurations).

The ASHRAE final formula, can be recast in a form first proposed by Bernier (2006) and it can be written as follows:

$$L = \frac{\left\{\dot{Q}_y R_y + \dot{Q}_m R_m + \dot{Q}_h \left(R_h + R_{bhe}\right)\right\}}{T_{gr,\infty} - T_{f,ave}(\tau_N) - T_p} \tag{120}$$

where $\dot{Q}_y, \dot{Q}_m$ and $\dot{Q}_h$ are the average heat transfer rates (heat loads) from (or to) the ground in a given period of 10 years ($\Delta\tau_y$), one month ($\Delta\tau_m$) and 6 hours ($\Delta\tau_h$), respectively. The overall period at which the analysis is addressed is τ_N, the summation of the above three subperiods. The far-field temperature is denoted $T_{gr,\infty,}$ while $T_{f,ave}$ is the target (inlet/outlet average) fluid temperature at the heat pump, R_{bhe} is the effective thermal resistance of the borehole, and remaining resistances R_y, R_m, R_h are ground resistances evaluated according to the ICS model at given time intervals. The ICS solution is known as the G function (Ingersoll et al. 1954, Ingersoll and Plass 1948) and it is in turn a function of the Fourier number Fo_{rb} based on the borehole radius r_b. The ASHRAE equation contains the Temperature Penalty T_p which accounts for "interference of adjacent borehole", as stated in the ASHRAE Handbook. In the following, a more detailed and physically based description of this quantity is given.

The ASHRAE formula is based on the assumption that the building's thermal history (and consequently the ground one) can be described by three basic thermal pulses (of constant strength), acting as a series of the duration of 10 years, 1 month and 6 hours ($\Delta\tau_h$) respectively (Bernier 2006).

Applying superposition in time (Eskilson 1987, Yavuzturk and Spitler 1999, Fossa 2011) demonstrated that Γ being the proper solution (temperature response factor) of the Fourier equation describing the thermal interaction between the ground and a system of buried heat exchangers when the series of three heat pulses of the ASHRAE model is considered, the following expression arises:

$$T_{gr,\infty} - T_{f,ave}(\tau_N) = \frac{\dot{Q}_h}{L} R_{bhe} + \frac{1}{Lk_{gr}} \left\{ \begin{array}{l} \dot{Q}_y \Gamma(\tau_N) - \dot{Q}_y \Gamma(\tau_2) + \\ + \dot{Q}_m \left[\Gamma(\tau_2) - \Gamma(\tau_3) \right] + \dot{Q}_h \Gamma(\tau_3) \end{array} \right\} \quad (121)$$

where k_{gr} is ground thermal conductivity, $\tau_N = (\Delta\tau_y + \Delta\tau_m + \Delta\tau_h)$, $\tau_2 = (\Delta\tau_m + \Delta\tau_h)$ and $\tau_3 = \Delta\tau_h$.

In the early to the medium period (say for $Fo_{rb}<10^4$ or $\ln(9Fo_H)<-6$) ILS practically coincides with any g-function: there is no need to refer to g-functions for calculating the ground response to sub-year thermal pulses. ICS and ILS cannot efficiently describe the long-term (say at τ_N period) ground behavior and a difference $\Delta\Gamma_G=(g/2\pi-G)$ always exists at τ_N time even when the borefield is constituted by a single BHE of finite length (Fossa 2011).

Hence the ICS model can be considered a good solution for describing the ground resistances R_h and R_m, but unfortunately, ICS is not suitable for calculating the "late" ground resistance R_y at time τ_N where the proper g-function for that BHE field should be employed.

Coming back to Eq. (121), it can be now rewritten in the following form:

$$T_{gr,\infty} - T_{f,ave}(\tau_N) - \frac{\dot{Q}_y \Delta\Gamma_G(\tau_N)}{Lk_{gr}} = \frac{1}{Lk_{gr}} \left\{ \begin{array}{l} \dot{Q}_y \left[G(\tau_N) - G(\tau_2) \right] + \\ + \dot{Q}_m \left[G(\tau_2) - G(\tau_3) \right] + \dot{Q}_h \left(G(\tau_3) + k_{gr} R_{bhe} \right) \end{array} \right\} \quad (122)$$

introducing a comprehensive correction term named T_p one obtains:

$$T_{gr,\infty} - T_{f,ave}(\tau_N) - T_P = \frac{1}{Lk_{gr}} \left\{ \begin{array}{l} \dot{Q}_y \left[G(\tau_N) - G(\tau_2) \right] + \\ + \dot{Q}_m \left[G(\tau_2) - G(\tau_3) \right] + \dot{Q}_h \left(\left[G(\tau_3) \right] + k_{gr} R_{bhe} \right) \end{array} \right\} \quad (123)$$

which is coincidental with Eq. (120) when the terms in brackets are assigned as thermal resistances (R_y, R_m and R_h respectively), and where the temperature penalty term is demonstrated to be equal to:

$$T_p(L) = \frac{\dot{Q}_y \left(\frac{g(\tau_N)}{2\pi} - G(\tau_N) \right)}{Lk_{gr}} \quad (124)$$

The ASHRAE method addresses the work by (Kavanaugh and Rafferty, 1997, K&R from here on) for calculating the temperature penalty. The ASHRAE Handbook also provides a table of T_p typical values, but at the same time, it warns against the reliability of such information. The K&R procedure is centered on the concept of the "heat diffused inside a square cylinder" according to an expression containing the "temperature change in the local earth surrounding the bore", T_{p1}. The related expression can be recast in the following way:

$$T_{p1} = \frac{\dot{Q}_y \sum_{i=1}^{n} (R_{i+1}^2 - R_i^2) E_{1,i}(\tau_N, \frac{R_{i+1} + R_i}{2})}{4 k_{gr} L B^2} \tag{125}$$

Here the *i-th* radius R_i is representative of a cylindrical shell around the borehole, R_1 is equal to half of the BHE interdistance (B/2), and R_n is the "maximum radius", "suggested to be around 25-30 feet.

T_p according to K&R (hereafter T_{pA}) is finally expressed as:

$$T_{pA} = T_{p1} \frac{N_4 + 0.5 N_3 + 0.25 N_2 + 0.1 N_1}{N_{tot}} \tag{126}$$

where N_4, N_3, N_2 and N_1 are the number of boreholes surrounded by only 4 other ones, only 3 other ones, and so on, respectively.

The present method was developed by Fossa and Rolando (2015).

It applies a superposition scheme for T_p calculation as done for building g-functions but the ILS solution is adopted for the sake of calculation simplicity. The reference geometry is a regular matrix where a single BHE is surrounded by other 8 BHEs arranged in a regular matrix. In this scheme, the active BHE is surrounded by 4 BHE at a distance of B from it and by other 4 at a distance $\sqrt{2}$ B. If spatial superposition is applied the excess temperature θ_8 at the central BHE as induced by the BHEs around it can be written (when referring to the yearly heat transfer rate) as:

$$\theta_8 = \dot{Q}_y \frac{E_1(\tau_N, B) + E_1(\tau_N, B\sqrt{2})}{\pi k_{gr} L} \tag{127}$$

The T_p according to the present model will hereafter be indicated as T_{p8} and it has been expressed in a form that deliberately mimics the original ASHRAE/K&R formulation.

$$T_{p8} = \theta_8 \frac{a N_4 + b N_3 + c N_2 + d N_1}{N_{tot}} \tag{128}$$

Constants a, b, c, d and their dependency on B/H (where it applies) have been calculated by optimum search by comparison of T_{p8} values with reference ones, as evaluated in terms of pertinent g-function (Eq. 124). The g-functions have been calculated starting from the FLS solution provided by Lamarche and Beauchamp (2007) as described in Fossa (2011).

The method has been refined taking into consideration several BHE geometries including square configurations (up to 10x10 BHEs), rectangular (up to 10x8), in-line (up to 12x1), L configurations (up to 10x10L), U configurations (up to 10x10U) and empty rectangles (O configurations, up to 10x10). Non-dimensional borehole spacings (B/H) have been varied in the range of 0.03÷0.125. Validity refers to $-2 < \ln(9Fo_H) < 0$ and r_b/H range (0.00025÷0.001).

The optimum search (Fossa and Rolando 2015) has been performed by tuning the heat loads in order to obtain reference depths H_{ref} equal to 100 m at a reference ground diffusivity $\alpha_{gr,\ ref}$ equal to 1.62e-6 m^2/s: according to such a choice, the $(Fo_H)_{ref}$ value resulted in 0.0515.

Optimized constants are reported in Fossa (2017).

The functions that best describe the variation of those constants with the dimensionless distance are reported below:

a(Rectangular configurations) = 1.95005+0.105215/(B/H)-55.6543 $(B/H)^2$ (129)

c(non-Rectangular configurations and slender rectangles) = -0.2817·ln(B/H)-0.2355 (130)

"Slender" rectangular configurations (namely 6x2, 7x2, 8x2 and so on) for accurate calculation demonstrated to belong to the in-line arrangements, and hence non-R constants have to be applied.

Further comparisons have been made with respect to the present model accuracy when the BHE depth and ground thermal properties are different from their reference values (e.g. H is different from H_{ref}). The analysis showed that the present model is able to efficiently estimate the borefield length for an extensive range of ground properties even if they affect the estimation of the g-function value through the related Fo_H number. This circumstance is related to the fact that the θ_8 parameter does include the ground properties. On the other hand, the different BHE depths (again affecting the Fo_H number but not Fo_{rb}) have to be managed by employing a corrected Fo* according to which the θ_8 parameter and its E_1 function have to be calculated:

$$Fo^* = Fo(\tau_N, R)\cdot\left(\frac{H_{ref}}{H}\right) \tag{131}$$

In the above expression, R can be either B or $B\sqrt{2}$. In such a way the model accuracies calculated at H_{ref} can be proved to be maintained in the wide H range of depth values 60-260 m.

Finally, an approximate but accurate (error below 1%) correlation for the ICS G function calculation is proposed according to the following expression:

$$G = \sum_{j=0}^{6} c_j \left[Log_{10}(Fo_{rb})\right]^j$$

c_0= 1.2777E-01 c_1= 1.0812E-01 c_2=3.0207E-02
c_3= -2.3037E-03.

c_4= -1.4459E-03 c_5= 3.6415E-04 c_6= -2.4889E-05

(132)

An overall comparison between the original K&R method and its present evolution (T_{p8} method) in terms of equation and constant sets is given in Fossa (2017), where the analogies and differences between the two procedures are made apparent.

5.2 The web calculation tool for the design of BHE fields based on a modified version of the Ashrae Method (see https://en.geosensingdesign.org/)

BHEDesigner8 is the tool for the design of BHE fields which incorporates the "Ashrae-Tp8" algorithm. The present tool carries out the sizing (overall length calculation) of the BHE field according to the "Ashrae-Tp8" algorithm. The algorithm requests the building's monthly heat loads (positive values in heating mode), the ground thermophysical properties and the expected performance of the heat pump in the tenth year of operation, as described by the heat carrier fluid (ground side) expected temperature which corresponds to the expected *COP* at the peak (target *COP* at 10 years for assigned expected fluid temperature, as required by the ASHRAE method and by the Italian Standard Uni 11466). The outputs of the calculation code are the total required length of the BHEs (the overall number of BHEs, depth H) and the related configuration (BHEs arrangement) provided that the 3 ground thermal resistances (as superposed in time) have been computed based on the G (ICS) solution. By ‘’its nature’’ the 10yrs resistance requires a correction, that can be written in terms of a Temperature Penalty T_p. No previously computed *g*-functions are needed. The user while inserting the data is in real-time addressed to the proper BHE field configuration (see Figures 77, 78) and BHE number. The algorithm and its parameters have been optimized by comparing the results related to 1200 borefield configurations as described by their "true" *g*-functions. The validation has been performed for dimensionless BHE distances in the range $0.03<B/H<0.125$. As in other known commercial codes for the sizing of the BHE field, the heat loads to the building are supplied as monthly values, together with the corresponding peak loads in heating and cooling modes. The paper by (Cullin and Spitler, 2011) explains well the definition and the concept related to what has to be considered a peak load. The thermal resistance of BHE (if its value is not already known) can be calculated through the web-app using Paul's semi-empirical model, adopted by the Italian Standard UNI11466.

BHEDesigner8, completely free, is currently available in the form of an Excel application transposed into a web environment via the SpreadsheetConverter interface. In the future, this web app may evolve into different programming languages.

A complete description of the model is available in the articles by (Fossa, 2011, Fossa, 2017, Fossa and Rolando, 2015, Fossa and Rolando, 2016, Fossa et al., 2017), in a series of Master's Theses of the University of Genoa (2012-2021) and in Davide Rolando's Ph.D. thesis (2015). The method is widely described and validated in a series of scientific papers in international journals (Fossa, 2017, Fossa, 2011, Rolando et al., 2015, Priarone and Fossa, 2016, see the https://en.geosensingdesign.org/ web page). The nomenclature of symbols is shown at the bottom of the page (see Figure 86). The BHE field configurations handled by the Web app are briefly shown in Figure 84.

Regarding the input related to the number of boreholes (N, M and hence N_{tot}), it is advisable to refer to the precalculated value available in cell $N_{tot,suggested}$ (Red Cell, see Figure 86). In such a way the iterative calculation (see Figure 85) performed by this app can be fast in leading to convergence results.

The correct functioning of the calculation code necessarily depends on the correctness and reasonableness of the input values (boxes in yellow, see Figure 86). The home page and the people in Unige who worked on the website are shown in Figures 87 and 88 respectively.

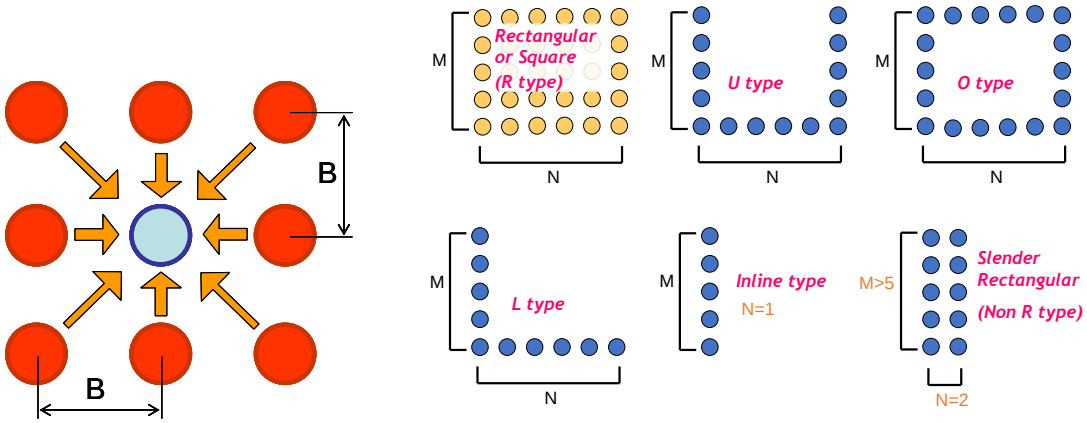

Figure 84. The BHE field configurations that can be handled by the BHEDesigner8 web app https://en.geosensingdesign.org/

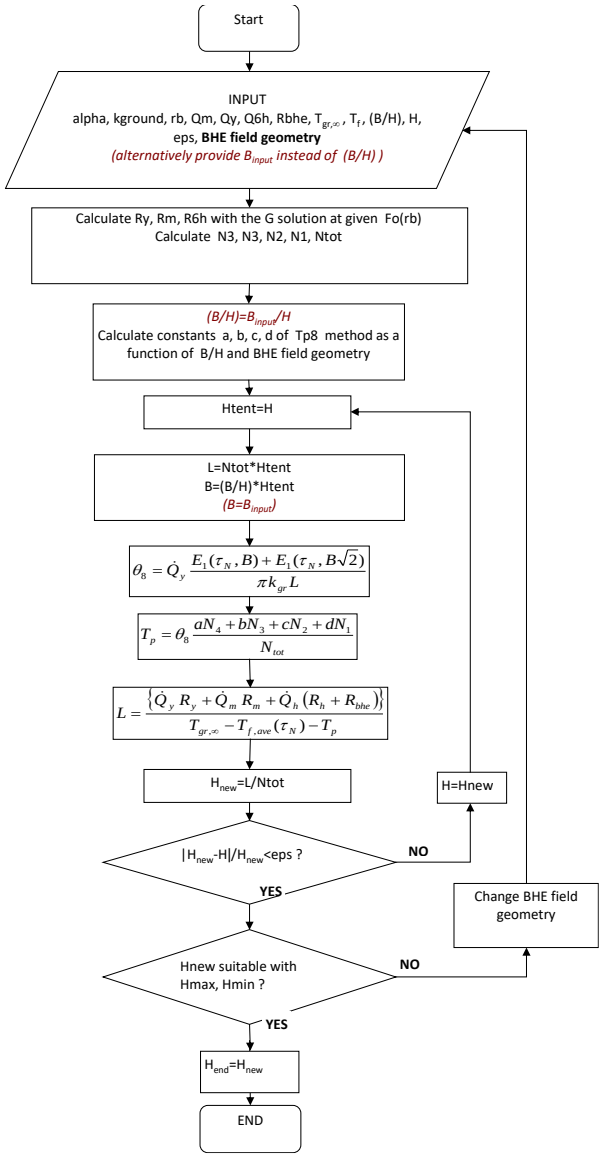

Figure 85. Iterative process proper of the Ashrae / Tp8 Method.

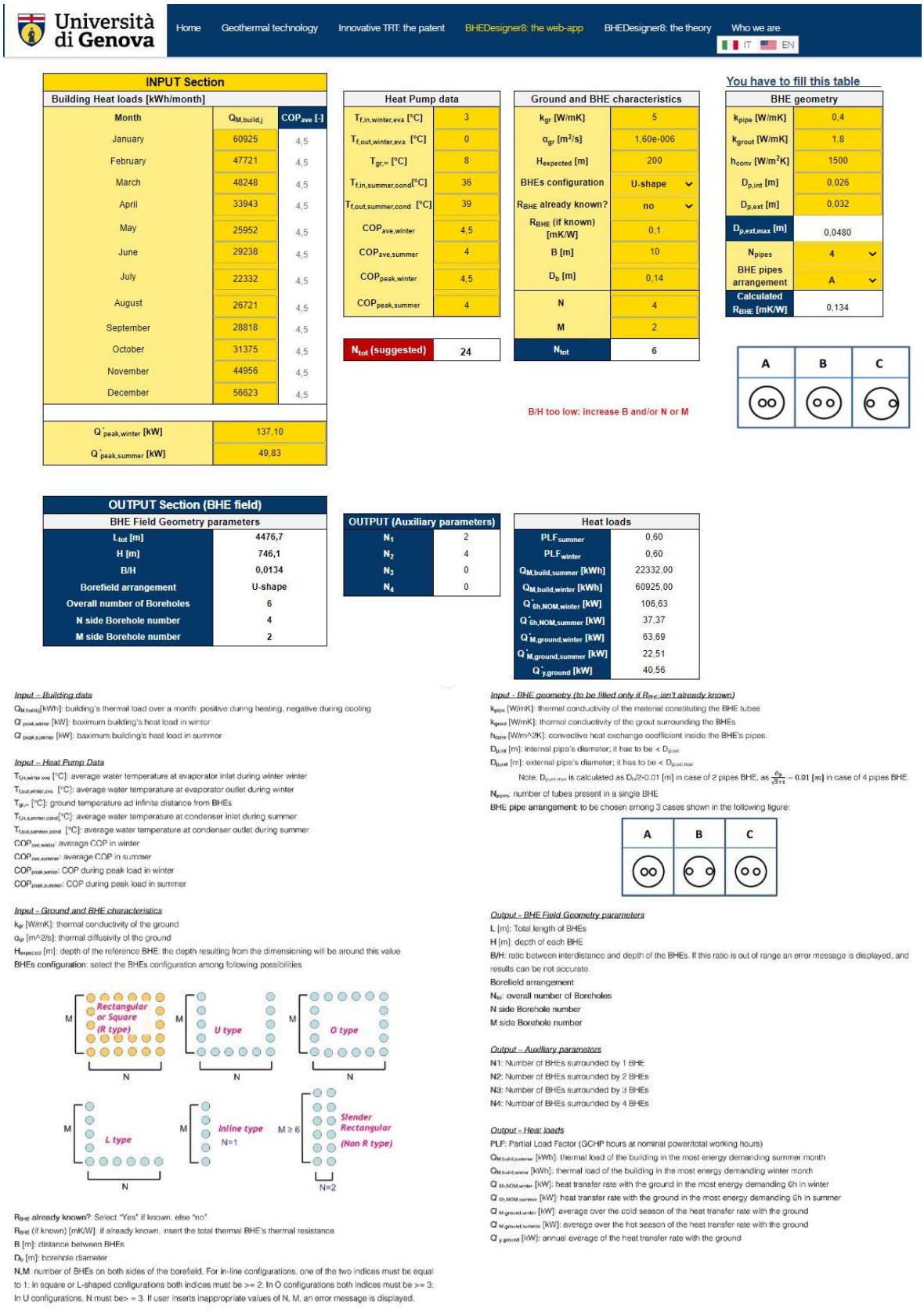

Figure 86. Nomenclature of symbols, inputs and outputs related to the BHEDesigner8 web app https://en.geosensingdesign.org/

Figure 87. The home page of the web site https://en.geosensingdesign.org/

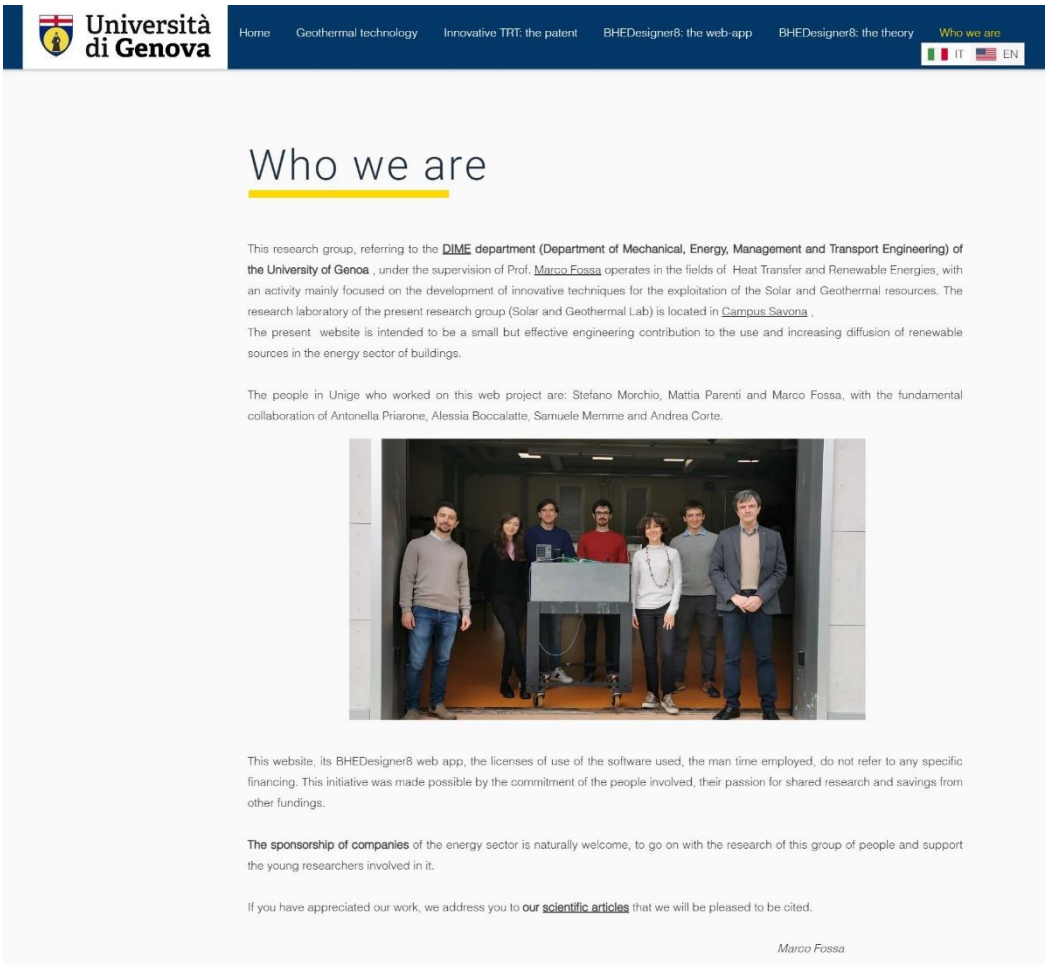

Figure 88. The people in Unige who worked on the web project https://en.geosensingdesign.org/

6. Conclusions

In this Ph.D. dissertation three finite difference numerical models related to coaxial, single and double U geometries, implemented in Fortran 90 calculation programs, have been developed for studying the hydrodynamic and thermal performance of conventional length BHEs and Deep BHE in densely built urban areas. These models serve as numerical references for the interpretation of TRTs in GCHP applications. These models have been coupled with the FFT spectral method. The models have been implemented in three in-house Fortran90 codes that have been optimized to cope with variable longitudinal and radial mesh distribution for simulating the BHE configurations at given geothermal gradients, resembling both standard conditions and geothermal anomalies. The models have been extensively validated through the comparison of the numerical results with experimental measurements. Criteria for both the Courant number and radial grid spacing have been proposed and validated. The attention was focused on the early period (100 hours) of heat exchanger response, the most important for describing the on/off cycles of the heat pump and its peak working conditions. Simulations have been performed for different pipe geometries of the coaxial case while maintaining the same borehole external diameter to assess the geometry effects on fluid friction losses and fluid temperature along the heat exchanger and the inlet and outlet sections at the heat pump side. Concerning the combined effect on pressure drop and best temperatures, an optimum diameter ratio (inner to annular pipe) belonging to the 0.5-0.6 range has been found for a given linear distribution of ground undisturbed temperatures.
Vertical temperature profiles of circulating fluid, grout and borehole wall are generated by the models. The simulation cases performed and reported in the present Ph.D. dissertation confirm that in a real-world installation, it is quite common that the thermal properties of the grout material given by the manufacturer are not those of the actual BHE. And also when the laboratory measurements are available, it is argued that the measured value cannot be representative of the real backfilling material conditions inside the BHE. The volumetric heat capacity of the grout material is often unknown and its influence on the numerical solution has been investigated in the present Ph.D. dissertation. The present study demonstrated that in most cases, the uncertainty related to the knowledge of the grout volumetric heat capacity has a similar influence on results as the value applied to the *Y* weighting factor. In this sense, the simulation program developed in the present thesis for modeling the single and double U-BHE can be considered a tool through which to evaluate how the grout thermal properties can be varied with respect to those given by the manufacturer in order to capture the real U-BHE thermal transient behavior.

The applicability of the ILS (two thermal resistance) model for the ground thermal conductivity estimation in TRT experiments has been extensively analyzed concerning coaxial, single U, double U BHEs and DBHEs. According to conventional borehole heat transfer models such as the ILS model, the magnitude of the steady heat injection/extraction heat rate during a TRT does not theoretically affect the estimated value of k_{gr}. Through analyses of TRT simulations, this Ph.D. dissertation demonstrates that the

magnitude of the heat rate can affect the k_{gr} estimation if the undisturbed ground temperature follows a constant and significant geothermal gradient uniform with depth. The main evidence from the present study is that the borehole length and the undisturbed ground temperature profile largely affect the fluid temperature evolution in time and space and in turn they provide different ground conductivity values if classic FOA-ILS-based TRT analysis is applied. The dimensionless parameter q_{ratio} has been identified as a useful indicator of when this effect occurs. The influence of the q_{ratio} parameter has been investigated for shallow and Deep BHEs with a geothermal gradient in cases of single and multiple layers of different ground thermal conductivities along the depth. A sensitivity analysis on how specific parameters (q_{ratio} included) affect the k_{gr} estimation when the ILS model is applied to interpret the TRT data has been conducted. To this aim, the three in-house built Fortran90 codes implementing the FD Models related to coaxial, single and double U-BHE geometries have been exploited to evaluate the dimensionless *g*-transfer functions related to each fluid volume. A suitable spectral method based on the use of the FFT technique and implemented in another dedicated Fortran90 program allows the reconstruction of the fluid temperature profiles computed by the FD Model. The reconstruction of the fluid temperature profiles is obtained by superposing two separated convolutions in the time domain for the entire simulated TRT and serves as the validation of the method. The present method verifies that q_{ratio} is the dominant parameter when the ILS model is used to estimate the effective k_{gr} in TRT data analysis (in cases of single and multiple layers of equal thickness with different ground thermal conductivities along the depth). The present study is the first that highlights the generalization provided by $T_{0,j}(\tau)=(f_0*g_{0,j})(\tau)$, where the term $T_{0,j}(\tau)$ is not necessarily constant and the geothermal gradient is taken into account. The main conclusions of this study are the following.

1. When q_{ratio} is lower than 1, the $g_{0,j}(\tau)$ function is able to modify the slope of the general solution $T_{f,j}(\tau)$ for each fluid node. The $g_{0,j}(\tau)$ function incorporates the geothermal gradient and can influence the k_{gr} estimation when the ILS model is employed in the TRT analysis.

2. The investigation at q_{ratio} <1 graphically confirms that, as opposed to the coaxial cases, the U-pipes are less influenced by the absolute value of q_{ratio} when the ILS model is used for the ground thermal conductivity estimation from TRT data.

3. In a single-layer subsurface when the geothermal gradient is 0.0 K/m, the nil contribution of additional heat input rate related to the available geothermal heat flux within the BHE length H assures that the k_{gr} can be correctly estimated from the ILS model. For the coaxial case and geothermal gradient 0.0 K/m, the ILS-based k_{gr} estimations are very close to each other (regardless of the choice of the hydraulic configuration).

4. In the case of a single-layered subsurface, the condition related to q_{ratio} >>1 assures the correct ILS-based k_{gr} estimation for any BHE geometry and hydraulic configuration.

5. An increasing external heat transfer rate tends to decrease this error in k_{gr} as the resulting absolute value of q_{ratio} exceeds 1. Then, the error caused by this simplifying assumption of the ILS model is reduced, allowing better estimates of ground thermal properties. However, in some cases a sufficiently large value of the external heat rate can not practically be delivered.

6. In the case of the coaxial center-pipe inlet case with a single-layered subsurface and q_{ratio}<1, the ILS-based k_{gr} estimation when the g_0-function is taken into account can differ by -14 % from the correct ILS-based k_{gr} estimation without taking into account the g_0-function.

7. The q_{ratio} is the dominant parameter when the ILS model is used to estimate the ground thermal conductivity, also in presence of different ground layers of equal thickness with different thermal conductivity values imposed along the depth. Any changes in the r_b/H and $\dot{m}/H$ ratios are not able to mitigate the influence related to the q_{ratio} parameter on the ground thermal conductivity estimation when the ILS model is employed.

8. In the case of a multilayered subsurface, the results for the coaxial BHEs indicate that as q_{ratio} decreases the ILS-based k_{gr} estimation departs from the arithmetic average. The simulations demonstrate that when a strong geothermal gradient exists the difference between the ILS-based k_{gr} estimation and the mean k_{gr} tends to decrease as the total depth decreases. The parameter q_{ratio} is an indicator of this difference. The q_{ratio} parameter indicates when the effective k_{gr} estimated by the ILS model departs from the weighted-thickness average. A departure of 10% is for q_{ratio} included between 2 and 2.5 for the coaxial center-pipe inlet cases considered and the departure increases with decreasing q_{ratio}.

9. In presence of different ground layers of equal thickness with different thermal conductivity values imposed along the depth and corresponding geothermal gradients, the condition related to q_{ratio} >>1 has to be satisfied in an ILS-based TRT analysis in order to override the additional heat input rate (particularly prominent for coaxial DBHEs) provided and incorporated into the $g_{0,j(\tau)}$ functions thus obtaining the ILS-based k_{gr} estimation moving closer to the mean k_{gr} value among the layers. For the coaxial BHEs, the estimated k_{gr} from the ILS model moves closer to the mean k_{gr} value among

the layers only if q_{ratio} >>1 regardless of the k_{gr} variations among the layers. The simulations demonstrate also that the cases with the annulus as the inlet have significantly smaller deviations from the average k_{gr}. The errors in the line-source estimates of the mean k_{gr} are expected to be in general less also for single and double U-tube configurations for ground with layers of equal thickness.

10. The g_j - function approach has been applied in the case of a ground characterized by multiple layers of equal thickness with different thermal conductivity values imposed along the depth and corresponding geothermal gradients. This would demonstrate how the approach related to the $g_{0,j}(\tau)$ functions analysis can be feasible also for DTRT analysis.

11. For the coaxial BHE, the $g_{0,j}$ functions can be used as an indicator similar to the one represented by q_{ratio} also in the case of multiple ground layers. In particular, the condition related to q_{ratio} >>1 has to be satisfied in an ILS-based TRT and DTRT analysis in order to override the additional available heat input rate related to the $g_{0,j}$ (τ) functions. This makes the ILS-based k_{gr} estimation not sensitive to the effect related to the $g_{0,j}(\tau)$ functions, therefore closer to the mean k_{gr} value regardless of the k_{gr} variations among the layers.

12. The fluid vertical and undisturbed ground temperature profiles provide additional insights into the coaxial borehole cases. Inversions between the fluid and the surrounding ground temperatures can occur in the bottom section of the coaxial BHE when $|q_{ratio}|<1$. These temperature inversions are accompanied by errors in the k_{gr} estimation when the ILS model is applied in TRT analysis.

13. Temperature inversions in the U-pipe configurations apparently occur only for $|q_{ratio}| \ll 1$, and $|q_{ratio}| \ll 1$ must occur for the error in the k_{gr} estimation to exceed ± 10%. Such low $|q_{ratio}|$ values correspond to thermal power values that are not usually employed in real-world TRTs. For this reason, the classic ILS approach has fewer limitations for the U-pipes.

14. For the coaxial configuration in deep boreholes, TRT guidelines at the national and international levels should consider the magnitude (the absolute value) of the external heat transfer rate per unit length through the dimensionless parameter q_{ratio}. The parameter affects the estimates of the ground thermal conductivity by the ILS model.

In the present Ph.D. dissertation, a suitable scale prototype of a real BHE and the surrounding ground has been realized to perform and analyze an innovative TRT procedure based on electric heating at the BHE axis, addressed to evaluate the ground thermal conductivity for the correct sizing of GCHPs. The analysis was first addressed at the correct sizing of the prototype through an accurate preliminary evaluation based on

dimensionless analysis and numerical simulations with Comsol Multiphysics. The suitable size was theoretically and numerically assessed in terms of the Fourier number time window of interest. The results highlight the possibility of reliably estimating the slate/ground thermal conductivity with an accuracy of about +10% with respect to the reference measured values. Based on the results obtained it can be concluded that the presented experimental apparatus related to the innovative TRT method can reliably estimate the slate/ground thermal conductivity without having to resort to expensive standard TRT methods.

The research group of the University of Genoa (Unige, Department of Mechanical Engineering, Dime) has been active for over 15 years in the dynamic modeling of geothermal systems using ground vertical exchangers and has developed, starting from the original ASHRAE method, a BHE field design algorithm named "Ashrae-Tp8", widely described and validated in a series of scientific papers in international journals. This method has been made available as free of charge sizing tool (BHEDesigner8 web-app https://en.geosensingdesign.org/).

6.1 Discussion and Future Work

Further investigations and applications of the present models will be related to the effects of different geothermal gradients (non-linear undisturbed ground temperatures) and the mass flow rate effects. Further analyses of the optimum mass flow rate and pipe dimensions will be made in terms of *COP* and COP_{total} (which includes the external work provided by the pump to cope with the pressure losses).

Other sources of uncertainty (not investigated in the present Ph.D. dissertation) on the correct reproduction of the experimental data that can be compensated by the suitable value assumed by the *Y* weighting factor are represented by the knowledge of the grout thermal conductivity k_{gt} and shank spacing *s* real values (that very often are unknown).

The present study could represent the basis for further studies on deconvolution techniques in the time domain aimed to evaluate the g_0 function from any TRT recorded data in order to understand how the g_0 function weights its influence on the ILS-based k_{gr} estimations from a TRT analysis for single and multiple ground layers. The evaluation and removal of the g_0 function from any TRT recorded data through deconvolution techniques (or simply by performing a real complete test of the same duration of the TRT with no heat input rate and only fluid circulation, recording the data, and then detracting these data from the heat injection/extraction TRT) will be of great importance in order to remove the geothermal gradient influence (that is particularly prominent when q_{ratio} <1) and obtain the correct k_{gr} estimations from any TRT analysis based on the ILS model (for single and multiple ground layers).

The reduced scale analysis and experimentation presented in this study have to be intended as the initial demonstrator of the present application. The next step related to the present research is to establish the applicability of the innovative TRT procedure also in a real GCHP plant. BHEDesigner8 is a tool that the "Solar and Geothermal Lab" research group active in the Dime Department of the University of Genoa has decided to develop and make available for free to researchers and designers from all over the world active in the field of geothermal heat pumps. To date (2022), BHEDesigner8 is the only (and completely "free") web-app on the entire internet. It will be constantly developed and updated free of charge, as a tool aimed at technicians, engineers and researchers involved in GCHP applications for the realization of heating/cooling systems with minimum environmental impact. Any suggestion and help from the users of BHEDesigner8 will be appreciated and profitably implemented. Among the future works that can be faced is the analysis of how the heat transfer models interpret the interaction between ground and geothermal probe in multi-probe configurations when time windows longer than the standard ones are considered. This is for the dynamic sizing of geothermal energy collection systems (an upgrade of the already mentioned "Ashrae-Tp8" Method). Furthermore, interface these models with the innovative method aimed at the accurate estimation of geothermal parameters, starting from the measurements carried out by the reduced-scale experimental setup, DTRT measurements and considerations on q_{ratio}.

REFERENCES

Abramovitz, M. and Stegun, I. 1964. Handbook of mathematical functions with formulas, graphs, and mathematical tables. Nat. Bureau of Standards 228-233.

Acuña, J., Mogensen, P., Palm, B., Distributed Thermal Response Test on a U-Pipe Borehole Heat Exchanger. In Proceedings of the Effstock 2009, 11th International Conference on Thermal Energy Storage, Stockholm, Sweden, 14–17 June 2009.

Acuña, J., 2010, Improvements of U-pipe Borehole Heat Exchanger, Licentiate Thesis in Energy Technology, KTH, Stockholm.

Acuña, J., B. Palm, A novel coaxial borehole heat exchanger: description and first distributed thermal response test measurements, in: Proceedings of the World Geothermal Conference, Bali, Indonesia. April 25-2, 2010.

Acuña, J., Palm, B., First experiences with coaxial borehole heat exchangers. In: Sources/sinks alternative to the outside air for heat pump and air-conditioning techniques, Padua, Italy; April 5-7, 2011.

Acuña, J., 2013, Distributed Thermal Response Tests- New Insights on U-tube and Coaxial Heat Exchangers in Groundwater-filled Boreholes (Doctoral thesis), KTH, Stockholm.

Acuña, J., Palm, B., Distributed thermal response tests on pipe-in-pipe borehole heat exchangers, Applied Energy 109 (2013) 312-320. https://doi.org/10.1016/j.apenergy.2013.01.024.

ASHRAE, Geothermal energy, in: ASHRAE Handbook - HVAC Applications, ASHRAE, Atlanta, Ch. 34, 2015.

Austin, WA., Development of an In Situ System for Measuring Ground Thermal Properties. Oklahoma State University, Stillwater, Oklahoma, 1998.

Austin, WA., Yavuzturk, C., Spitler, J.D., Development of an in situ system for measuring ground thermal properties. ASHRAE Transactions 106, 356–379, 2000.

Bae, SM, Nam, Y, Choi, JM, Ho Lee, K, Choi, JS. Analysis on thermal performance of ground heat exchanger according to design type based on thermal response test. Energies 2019. https://doi.org/10.3390/en12040651.

Bauer, D., Heidemann, W., Müller-Steinhagen, H., Diersch, H.-J.G., 2011, Thermal resistance and capacity models for borehole heat exchangers, Int. J. Energy Res. 35 312-320.

Bauer, D., Heidemann, W., Diersch, H.-J.G., Transient 3D analysis of borehole heat exchanger modeling, Geothermics, 2011. 10.1016/j.geothermics.2011.08.001

Beier, R.A., Smith, M., 2003. "Minimum Duration of In-Situ Tests on Vertical Boreholes". ASHRAE Transactions. 109(2):475-486.

Beier, R.A., Smith, M.D., Spitler, J.D. Reference data sets for vertical borehole ground heat exchanger models and thermal response test analysis. *Geothermics* 2011, *40*, 79–85.

Beier, R.A., Acuña, J., Mogensen, P., Palm, B., Vertical temperature profiles and borehole resistance in a U-tube borehole heat exchanger, Geothermics, Volume 44, 2012, https://doi.org/10.1016/j.geothermics.2012.06.001.

Beier, R.A., Acuña, J., Mogensen, P., Palm, B., 2013. Borehole resistance and vertical temperature profiles in coaxial borehole heat exchangers. Appl. Energy 102, 665–675.

Beier, R. A., Fossa, M., Morchio, S., Models of thermal response tests on deep coaxial borehole heat exchangers through multiple ground layers, Applied Thermal Engineering, 2020, https://doi.org/10.1016/j.applthermaleng.2020.116241.

Beier, R.A., Thermal response tests on deep borehole heat exchangers with geothermal gradient, Appl. Therm. Eng. 178 (2020) 115447, https://doi.org/10.1016/j.applthermaleng.2020.115447 .

Beier, R. A., “Transient heat transfer in a U-tube borehole heat exchanger,” Applied Thermal Engineering, vol. 62, no. 1, pp. 256–266, Jan. 2014.

Beier, R. A., Morchio, S., Fossa, M., Thermal response tests on deep boreholes through multiple ground layers, Geothermics 101 (2022), 102371.

Bernier, M. 2006. Closed-loop ground-coupled heat pump systems. ASHRAE Journal 48(9):12–19.

Blackwell, J.H., A transient-flow method for the determination of thermal constants of insulating materials in bulk. *J. Appl. Phys.* 1954, *25*, 137–144.

Carslaw, H.S., Jaeger, J.C., 1947.Conduction of heat in solids, Claremore Press, Oxford, U.K.

Carslaw, H.S., Jaeger, J.C., 1959. Conduction of Heat in Solids, 2nd ed. Oxford University Press, Oxford, pp. 261–263. 338-339.

Cimmino, M., Bernier, M., and F. Adams. 2013. A contribution towards the determination of g-functions using the finite line source. Appl. Therm. Eng. 51: 1–2.

Cimmino, M., Bernier, M., 2014 A semi-analytical method to generate g-functions for geothermal bore fields. Int. J. Heat and Mass Transfer 70: 641–650.

Cimmino, M., Bernier, M., Experimental determination of the g-functions of a small-scale geothermal borehole. *Geothermics* 2015, *56*, 60–71.

Claesson, J. and S. Javed. 2011. An analytical method to calculate borehole fluid temperatures for time-scales from minutes to decades. ASHRAE Trans. 117 (2): 279–288.

Clausen, H., Durchführung von Simulationsrechnungen zum Einfluss verschiedener Randbedingungen auf die Thermische Leistungsfähigkeit von Erdwärmesonden. Student research thesis, University of Stuttgart Institut für GebäudeEnergetik, 2008, Stuttgart, Germany, 80 pp.

Cullin, JR., Spitler, JD., A computationally efficient hybrid time step methodology for simulation of ground heat exchangers, Geothermics, Volume 40, Issue 2, 2011, Pages 144-156, ISSN 0375-6505, https://doi.org/10.1016/ j.geothermics.2011.01.001

Dalla Santa, G., Galgaro, A., Sassi, R., Cultrera, M., Scotton, P., Mueller, J., Bertermann, D., Mendrinos, D., Pasquali, R., Perego, R., Pera, S., Di Sipio, E., Cassiani, G., De Carli, M., Bernardi, A. An updated ground thermal properties database for GSHP applications, Geothermics, Volume 85, 2020, 101758. https://doi.org/10.1016/j.geothermics.2019.101758.

De Carli, M., Tonon, M., Zarrella, A., Zecchin, R., 2010, A computational capacity resistance model (CaRM) for vertical ground-coupled heat exchangers, Renewable Energy. 35: 1537-1550.

Deerman, J.D., Kavanaugh, S.P. Simulation of vertical U-tube ground-coupled heat pump systems using the cylindrical heat source solution. *ASHRAE Trans.* 1991, *97*, 287–295.

Della Vedova, B., Petronio, B., Poletto, F., Palmieri, F., Marcon, A., Farina, B., Cimolino, A., Bellezza C., 2015. The Geothermal District Heating System on the Grado Island (North-eastern Adriatic Sea), Proceedings World Geothermal Congress 2015, Melbourne, Australia, 19-25 April 2015, 1-12.

Deng, J.W., Wei, Q.P., He, S., Liang, M., Zhang, H. Simulation analysis on the heat performance of deep borehole heat exchangers in medium-depth geothermal heat pump systems, Energies 13 (Issue 3) (2020) 754. https://doi.org/10.3390/en13030754.

Deng, J.W., Wei, Q.P., Liang, M., He, S., Zhang, H. Field test on energy performance of medium-depth geothermal heat pump systems (MD-GHPs), Energy and Buildings 184 (2019) 289–299. https://doi.org/10.1016/j.enbuild.2018.12.006.

Eklöf, C., Gehlin, S. TED—A Mobile Equipment for Thermal Response Test. Master's Thesis, Lund University, Lund, Sweden, 1996.

Erol, S., François, B. 2018. Multilayer analytical model for vertical ground heat exchanger with groundwater flow. Geothermics 71, 294–305. https://doi.org/10.1016/j.geothermics.2017.09.008.S.A.

Eskilson, P. 1987. Thermal analysis of heat extraction boreholes. Ph.D. Thesis, Lund University of Technology, Sweden.

Eskilson, P., Claesson, J. Simulation model for thermally interacting heat extraction boreholes. Numerical Heat Transfer, 1988; 13:149–165.

Eslami-nejad, P., Bernier, M. Freezing of geothermal borehole surroundings: A numerical and experimental assessment with applications, Applied Energy, 98, 333-345 (2012) https://doi.org/10.1016/j.apenergy.2012.03.047

Fang, L., Diao, N., Shao, Z., P., Zhu, K., Fang, Z. 2018, A computationally efficient numerical model for heat transfer simulation of deep borehole heat exchangers, Energy and Buildings Volume 167, Pages 79-88.

Fang, L., Diao, N., Shao, Z., Cui, P., Zhu, K., Fang, Z. Thermal analysis models of deep borehole heat exchangers, 2018. https://doi.org/10.22488/okstate.18.000018.

Fossa, M. The Temperature Penalty Approach to the Design of Borehole Heat Exchangers for Heat Pump Applications, Energy and Buildings, vol. 43; p. 1473-1479, 2011.

Fossa, M., Rolando, D., Priarone, A., Vaccaro, J. Numerical evaluation of the Ground Response to a Thermal Response Test experiment, European Geothermal Congress 2013. In Proceedings of the EGC 2013 Pisa, Pisa, Italy, 3 June 2013.

Fossa, M., Rolando, D. Improving the Ashrae method for vertical geothermal borefield design. *Energy Build.* 2015, *93*, 315–323. https://doi.org/10.1016/j.enbuild.2015.02.008. Available online: https://www.sciencedirect.com/science/article/pii/S0378778815001036.

Fossa, M., Rolando, D. Improved Ashrae method for BHE field design at 10 year horizon, Energy and Buildings, 116, 114–121, 2016.

Fossa, M., Rolando, D., Priarone, A. An Investigation on the Effects of Different Time Resolutions in the Design and Simulation of BHE Fields. Proc. IGSHPA Conference, Denver (CO) March 14-16, 2017. https://shareok.org/handle/11244/49344.

Fossa, M. A fast method for evaluating the performance of complex arrangements of borehole heat exchangers, HVAC&R Research, 2011, 17:6, 948-958

http://dx.doi.org/10.1080/10789669.2011.599764

Fossa, M., Priarone, A, Rolando, D., Berti, F. Borefield Design and Enhanced Thermal Response Test for the Energy Building of the University of Genova, 4-6 July 2016, Ferrara, 34th Heat Transfer Conference.

Fossa, M., Correct design of vertical BHE systems through the improvement of the ASHRAE method, Science and Technology for the Built Environment, 23 (Issue 7) (2017) 1080-1089. https://doi.org/10.1080/23744731.2016.1208537.

Fossa, M., Rolando, D., Pasquier, P. Pulsated Thermal Response Test experiments and modelling for ground thermal property estimation. *IGSHPA Res. Track Stockh.* 2018. https://doi.org/10.22488/okstate.18.000021.

Franco, A., Conti, P. Clearing a Path for Ground Heat Exchange Systems: A Review on Thermal Response Test (TRT) Methods and a Geotechnical Routine Test for Estimating Soil Thermal Properties. *Energies* 2020, *13*, 2965. https://doi.org/10.3390/en13112965.

Fujii, H., Okubo, H., Nishi, K., Itoi, R., Ohyama, K., Shibata, K. An improved thermal response test for U-tube ground heat exchanger based on optical fiber thermometers, Geothermics 38 (2009) 399-406. http://www.sciencedirect.com/science/article/pii/S0375650509000340.

Galgaro, A., Pasquier, P., Schenato, L., Cultrera, M., Dalla Santa, G. (2018). Soil thermal conductivity from early TRT logs using an active hybrid optic fibre system. 1-9. 10.22488/okstate.18.000023.

Gao, L., Zhao, J., Tang, Z., 2015. A review on borehole seasonal solar thermal energy storage, International Conference on Solar Heating and Cooling for Buildings and Industry, SHC 2014, Energy Procedia 70 (2015) 209-218.

Gehlin, S., Thermal Response Test Method Development and Evaluation, Doctoral Thesis, Department of Environmental Engineering, Luleå University of Technology, Sweden, 2002. https://www.diva-portal.org/smash/get/diva2:991442/FULLTEXT01.pdf

Gnielinski, V., New equations for heat and mass transfer in turbulent pipe and channel flow, International Chemical Engineering 16 (1976) 359–368.

Gordon, D., Bolisetti, T., Ting, DSK., Reitsma, S. Short-term fluid temperature variations in either a coaxial or U-tube borehole heat exchanger. Geothermics 2017. https://doi.org/10.1016/j.geothermics.2016.12.001.

Ghoreishi-Madiseh, S.A., Kuyuk, A.F., Rodrigues de Brito, M.A. An analytical model for transient heat transfer in ground-coupled heat exchangers of closed-loop geothermal systems, Applied Thermal Engineering 150 (2019) 1359-4311. https://doi.org/10.1016/j.applthermaleng.2019.01.020

Gu, Y., O'Neal, D.L. Modelling the effect of backfills on U-tube ground coil performance. *ASHRAE Trans*. 1998, *104*, 356–365.

Gustafsson, A.M., Westerlund, L., Hellström, G. CFD-modelling of natural convection in a groundwater-filled borehole heat exchanger, Applied Thermal Engineering 30 (2010) 683-691. https://doi.org/10.1016/j.applthermaleng.2009.11.016

Gustafsson, A.M., Westerlund, L. Multi-injection rate thermal response test in groundwater filled borehole heat exchanger, Renewable Energy 35 (2010) 1061-1070. https://doi.org/10.1016/j.renene.2009.09.012

Hellström, G. Ground heat storage – thermal analyses of duct storage systems – theory PhD thesis. Sweden: University of Lund; 1991.

Hellström, G. Thermal performance of borehole heat exchangers. Department of Mathematical Physics, Lund Institute of Technology, (1991).

Hellström, G. Borehole Heat Exchangers: State of the Art 2001. Implementing Agreement on Energy Conservation through Energy Storage: Annex 13-Design, Construction and Maintenance of UTES Wells and Boreholes. Subtask 2, International Energy Agency (IEA), 2002.

He, M., Rees, S.J., Shao, L. Applications of a dynamic 3D numerical model for borehole heat exchangers. In: Proceedings of Effstock, the 11th International Conference on Thermal Energy Storage, Stockholm International Fairs, 2009, Stockholm, Sweden.

Holmberg, H., Acuña, J., Næss, E., Sønju, O.K., 2016. Thermal evaluation of coaxial deep borehole heat exchangers. Renew. Energy 97, 65–76.

Holmberg, H., Acuña, J., Næss, E., Sønju, O.K. Numerical model for non-grouted borehole heat exchangers, Part 2—Evaluation, Geothermics 59 (2016) 134-144. https://doi.org/10.1016/j.geothermics.2014.11.002

Holmberg H, Ramstad RK, Riise MH. Temperature profile measurements - easy, cheap and informative, 2018. https://doi.org/10.22488/okstate.18.000027.

Hu, J. 2017. An improved analytical model for vertical borehole ground heat exchanger with multiple-layer substrates and groundwater flow. Appl. Energy 202, 537–549. http://www.sciencedirect.com/science/article/pii/S0306261917307006.

IEA. Heat Pumps; IEA: Paris, France, 2020; Available online: https://www.iea.org/reports/heat-pumps .

Incropera, F. P. and DeWitt, D. P. Introduction to Heat Transfer, 4th edn, John Wiley & Sons, New York, 2002.

Ingersoll, L.R. and H.J. Plass. 1948. Theory of the ground pipe heat source for the heat pump. Heating, Piping and Air Conditioning 20(7):119 – 122.

Ingersoll, L., Adler, F., Plass, H., Ingersoll, A. Theory of earth heat exchangers for the heat pump. *Trans. ASHVE* 1951, 57, 167–188.

Ingersoll, L.R. Zobel, O.J. Ingersoll, A.C. Heat conduction with engineering, geological, and other applications, Physics Today (1955), https://doi.org/10.1063/1.3061951.

Iry, S., Rafee, R. 2018, Transient numerical simulation of the coaxial borehole heat exchanger with the different diameters ratio, Geothermics Volume 77, January 2019, Pages 158-165.

Javed, S. Nakos, H., Claesson, J. A method to evaluate thermal response tests on groundwater-filled boreholes. ASHRAE Transactions 118(1) (2012) 540-549.

Kavanaugh, S.P. and K. Rafferty. 1997. Ground source heat pumps design of geothermal system for commercial and institutional buildings. ASHRAE Hanbook, Atlanta, GA.

Kays, W., Crawford, M., Weigand, B. 2005, Convective Heat and Mass Transfer.

Kelvin, L. Mathematical and physical papers. (1882), https://doi.org/10.1017/CBO9780511996023

Köhler, B., Dengler, J., Dinkel, A., Azam, M., Kalz, D., Bonato, P., Tobias, F., Steinbach, J., Ragwitz, M., Arens, M., Aydemir, A., Elsland, R., Frassine, C., Herbst, A., Hirzel, S., Krail, M., Reuter, M., Toro, F., Rehfeldt, M., Jakob, M. (2016). Mapping and analyses of the current and future (2020-2030) heating/cooling fuel deployment (fossil/renewables) Work package 2: Assessment of the technologies for the year 2012. 10.13140/RG.2.2.28214.96329.

Kramer, C.A., Ghasemi-Fare, O., Basu, P. Laboratory thermal performance tests on a model heat exchanger pile in sand. *Geotech. Geol. Eng*. 2015,volume 33, 253–271. https://doi.org/10.1007/s10706-014-9786-z

Lamarche, L. and Beauchamp, B. 2007. A new contribution to the finite Line-source model for geothermal boreholes. Energy and Buildings 39:188-198.

Lamarche, L. Kajl, S., Beauchamp, B. A review of methods to evaluate borehole thermal resistances in geothermal heat-pump systems, Geothermics 39 (2), 187–200, 2010.

Le Lous, M., Larroque, F., Dupuy, A. and Moignard, A. "Thermal performance of a deep borehole heat exchanger: Insights from a synthetic coupled heat and flow model," Geothermics, vol. 57, pp. 157–172, Sep. 2015.

Lee, C.K. Effects of multiple ground layers on thermal response test analysis and ground-source heat pump simulation, Applied Energy 88 (Issue 12) (2011) 4405-4410. https://doi.org/10.1016/j.apenergy.2011.05.023.

Lee, C.K., Lam, H.N. 2012. A modified multi-ground-layer model for borehole ground heat exchangers with an inhomogeneous groundwater flow. Energy 47, 378–387.

Li, M., Zhang, L., Liu, G. Estimation of thermal properties of soil and backfilling material from thermal response tests (TRTs) for exploiting shallow geothermal energy: Sensitivity, identifiability, and uncertainty. Renew Energy 2019. https://doi.org/10.1016/j.renene.2018.09.022.

Li, Y., Han, X., Zhang, X., Geng, S., Li, C. 2017. Study the performance of borehole heat exchanger considering layered subsurface based on field investigations. Appl. Therm. Eng. 126, 296–304. http://www.sciencedirect.com/science/article/pii/S0360544212007359.

Liu, J., Wang, F., Cai, W., Wang, Z., Li, C. 2020. Numerical investigation on the effects of geological parameters and layered subsurface on the thermal performance of medium-deep borehole heat exchanger. Renew. Energy 149, 384–399. https://www.sciencedirect.com/science/article/pii/S0960148119318609

Luo, J., Rohn, J., Bayer, M., Priess, A., Xiang, W. Analysis on performance of borehole heat exchanger in a layered subsurface, Applied Energy 123 (2014) 55-65. https://doi.org/10.1016/j.apenergy.2014.02.044.

Lunardini, V.J. 1981. Heat Transfer in Cold Climates. Van Nostrand Reinhold Co.,Toronto, Canada.

Luo, J., Rohn, J. Xiang, W., Bayer, M., Priess, A., Wilkmann, L., Steger, H., Zorn, R., 2015. Experimental investigation of a borehole field by enhanced geothermal response test and numerical analysis of performance of the borehole heat exchangers. Energy 84, 473–484. http://www.sciencedirect.com/science/article/pii/S0360544215003035.

Marcotte, D., Pasquier, P. Fast fluid and ground temperature computation for geothermal ground-loop heat exchanger systems, Geothermics 37 (6) (2008) 651e665.

Mazzotti, W., Acuña, J., Lazzarotto, A., Palm, B., 2018, Deep Boreholes for Ground Source Heat Pump, Final Report Effsys Expand (Energimyndigheten), KTH (Sweden), 1-77.

McDaniel, A., Tinjum, J., Hart, D.J., Lin, Y.F., Stumpf, A., Thomas, L. Distributed thermal response test to analyze thermal properties in heterogeneous lithology, Geothermics 76 (2018) 116-124. https://doi.org/10.1016/j.geothermics.2018.07.003.

Minaei, A., Maerefat, M. Thermal resistance capacity model for short-term borehole heat exchanger simulation with non-stiff ordinary differential equations, Geothermics, 2017. http://dx.doi.org/10.1016/j.geothermics.2017.06.011

Minchio, F., Cesari, G., Pastore, C., Fossa, M. Experimental Hydration Temperature Increase in Borehole Heat Exchangers during Thermal Response Tests for Geothermal Heat Pump Design. Energies 2020, 13, 3461. https://doi.org/10.3390/en13133461

Mogensen, P. Fluid to duct wall heat transfer in duct system heat storages, in: Proceedings of the International Conference on Subsurface Heat Storage in Theory and Practice, Swedish Council for Building Research, Stockholm, Sweden, June 6-8, 1983, pp. 652-657.

Morchio, S., Fossa, M. Thermal modeling of deep borehole heat exchangers for geothermal applications in densely populated urban areas. Therm Sci Eng Prog 2019;13. https://doi.org/10.1016/j.tsep.2019.100363.

Morchio, S., Fossa, M. On the ground thermal conductivity estimation with coaxial borehole heat exchangers according to different undisturbed ground temperature profiles, Applied Thermal Engineering, 2020. https://doi.org/10.1016/j.applthermaleng.2020.115198.

Morchio, S., Fossa, M. Modelling and Validation of a New Hybrid Scheme for Predicting the Performance of U-pipe Borehole Heat Exchangers during Distributed Thermal Response Test Experiments, Applied Thermal Engineering, 2020, https://doi.org/10.1016/j.applthermaleng.2020.116514.

Morchio, S., Fossa, M. Corrigendum to "On the ground thermal conductivity estimation with coaxial borehole heat exchangers according to different undisturbed ground temperature profiles" [Appl. Therm. Eng. 173 (2020) 115198], Applied Thermal Engineering, Volume 193, 2021, 116981, ISSN 1359-4311, https://doi.org/10.1016/j.applthermaleng.2021.116981.

Morchio, S., Fossa, M., Beier, R. A. Study on the best heat transfer rate in Thermal Response Test experiments with coaxial and U-pipe Borehole Heat Exchangers. Appl. Therm. Eng. 2022, 200, 117621.

Morchio, S., Fossa, M., Priarone, A., Boccalatte, A. Reduced Scale Experimental Modeling of Distributed Thermal Response Tests for the Estimation of the Ground Thermal Conductivity. Energies 2021, 14, 6955. https://doi.org/10.3390/en14216955

Nguyen, A., Pasquier, P., Marcotte, D. Borehole thermal energy storage systems under the influence of groundwater flow and time-varying surface temperature, Geothermics, Volume 66, 2017, Pages 110-118, ISSN 0375-6505, https://doi.org/10.1016/j.geothermics.2016.11.002.

Pahud, D., Matthey, B. Comparison of the thermal performance of double U-pipe borehole heat exchangers measured in situ. Energy Build 2001. https://doi.org/10.1016/S0378-7788(00)00106-7.

Pasquier, P., Marcotte, D. Efficient computation of heat flux signals to ensure the reproduction of prescribed temperatures at several interacting heat sources, Applied Thermal Engineering, Volume 59, Issues 1–2, 2013, Pages 515-526, ISSN 1359-4311, https://doi.org/10.1016/j.applthermaleng.2013.06.018.

Pasquier, P., Marcotte, D. Joint use of quasi-3D response model and spectral method to simulate borehole heat exchanger, Geothermics, Volume 51, 2014, Pages 281-299, ISSN 0375-6505, https://doi.org/10.1016/j.geothermics.2014.02.001.

Priarone, A. and Fossa, M. 2015. Modeling the ground volume for numerically generating single borehole heat exchanger response factors according to the cylindrical source approach. Geothermics 58: 32–38.

Priarone, A., Fossa, M. Temperature Response Factors at Different Boundary Conditions for Modeling the Single Borehole Heat Exchanger, Applied Thermal Engineering, 2016.

Raymond, J., Lamarche, L. 2013. Simulation of thermal response tests in a layered subsurface. Appl. Energy 109, 293–301. http://www.sciencedirect.com/science/article/pii/S0306261913000421.

Rolando, D., Acuña, J., and Fossa M. A Web Application for Geothermal Borefield Design, Proceedings World Geothermal Congress 2015 Melbourne, Australia, 19-25 April 2015.

Ruiz-Calvo, F., De Rosa, M., Acuña, J., Corberán, J.M., Montagud, C. Experimental validation of a short-term Borehole-to-Ground (B2G) dynamic model, Applied Energy, 2015. http://dx.doi.org/10.1016/j.apenergy.2014.12.002

Sakata, Y., Katsura, T., Nagano, K. Multilayer-concept thermal response test: Measurement and analysis methodologies with a case study, Geothermics 71 (2018) 178–186. https://doi.org/10.1016/j.geothermics.2017.09.004.

Salim Shirazi, A., Bernier, M. A small-scale experimental apparatus to study heat transfer in the vicinity of geothermal boreholes. *HVACR Res*. 2014, *20*, 819–827.

Signorelli, S., Bassetti, S., Pahud, D., Kohl, T. Numerical evaluation of thermal response tests, Geothermics 36 (Issue 2) (2007) 141-166. https://doi.org/10.1016/j.geothermics.2006.10.006.

Spitler, J.D., Gehlin S. Thermal response testing for ground source heat pump systems - An historical review. Renew Sustain Energy Rev 2015. https://doi.org/10.1016/j.rser.2015.05.061.

Spitler, J.D., Javed, S., Ramstad, R.K. Natural convection in groundwater-filled boreholes used as ground heat exchangers, Applied Energy 164 (2016) 352-365. https://doi.org/10.1016/j.apenergy.2015.11.041

UNI 11466 - Heat pump geothermal systems Design and sizing requirements, page 107, Italian guidelines, 2012.

Yavuzturk, C. and Spitler, J. D. 1999. A short time step response factor model for vertical ground loop heat exchangers. Ashrae Transactions 105:475-485.

Yavuzturk, C., Spitler, J.D., Rees, S.J. A transient two-dimensional finite volume model for the simulation of vertical U-tube ground heat exchangers, ASHRAE Transactions 105 (2), 465–474, 1999.

Zanchini, E., Lazzari, S., Priarone, A., 2010a. Effects of flow direction and thermal shortcircuiting on the performance of small coaxial ground heat exchangers. Renew. Energy 35, 1255–1265.

Zarrella, A., Scarpa, M., De Carli, M., 2011. Short time step analysis of vertical ground-coupled heat exchangers: The approach of CaRM. Renewable Energy. 36: 2357-2367.

Zarrella, A., Emmi, G., Graci, S., De Carli, M., Cultrera, M., Dalla Santa, G., et al. Thermal response testing results of different types of borehole heat exchangers: An analysis and comparison of interpretation methods. Energies 2017. https://doi.org/10.3390/en10060801.

Zeng, H.Y., Diao, N.R. and Fang, Z.H. 2002. A finite line-source model for boreholes in geothermal heat exchangers. Heat Transfer-Asian Research, 31:558-567.

Zeng, H.Y., Diao, N.R. and Fang, Z.H. Heat transfer analysis of boreholes in vertical ground heat exchangers, International Journal of Heat and Mass Transfer, 2003.

Zhang, C., Guo, Z., Liu, Y., Cong, X., Peng, D. A review on thermal response test of ground-coupled heat pump systems. *Renew. Sustain. Energy Rev.* 2014, *40*, 851–867.

Zhang, X., Hu, Q., 2018. Development of Geothermal Resources in China: A Review, Article in Journal of Earth Science Vol.29 No.2 April 2018,p. 452–467.DOI: 10.1007/s12583-018-0838-9

Zhang, L., Luo, X., Huang, G., Zhang, Q. Comparative analysis of U-pipe location on the sizing of borehole heat exchangers, Applied Thermal Engineering, 2019. https://doi.org/10.1016/j.applthermaleng.2019.01.017

Zheng, K., Mo, Y., Chen, L., 2015. Twenty Years of Geothermal Heat Pumps in China, Proceedings World Geothermal Congress 2015, Melbourne, Australia, 19-25 April 2015.